UNIVERZA V MARIBORU

FAKULTETA ZA NARAVOSLOVJE IN MATEMATIKO

DOKTORSKA DISERTACIJA

VPLIV TOPOLOŠKIH LASTNOSTI KOMPLEKSNIH MREŽ IN DINAMIČNIH LASTNOSTI SKLOPLJENIH CELIČNIH OSCILATORJEV NA KOLEKTIVNO DINAMIKO

Rene Markovič

Mentor: red. prof. dr. Marko Marhl

Somentor: doc. dr. Marko Gosak

Februar, 2015

Zahvala

Iskreno se zahvaljujem mentorju in somentorju za vse strokovne napotke, vodenja, pomoč in usmeritve pri študiju ter raziskovalnem delu. Posebna zahvala gre tudi kolegom s Fiziološkega inštituta Medicinske fakultete Univerze v Mariboru.

Zahvala gre tudi vsem, ki ste me podpirali in mi kakorkoli pomagali pri nastajanju dela.

KAZALO

Povzetek

Doktorska disertacija zajema raziskave na področju kolektivne dinamike mrežno sklopljenih oscilatorjev. Razdeljena je na dva dela. V prvem delu analiziramo, kako dinamične lastnosti oscilatorjev in struktura mreže sovisno vplivata na kolektivno dinamiko. Pokažemo, da je kolektivna dinamika fleksibilnih oscilatorjev najbolje koordinirana, ko so oscilatorji povezani v primeru široko skalno mrežo. Oscilatorji z močno disipativno dinamiko, ki implicira rigidnost, pa dosežejo najvišjo raven sinhronizacije v skalno neodvisnih mrežah. Pojav analitično razložimo in rezultate ponazorimo z različnimi matematičnimi modeli, ki vključujejo tako zvezne kakor tudi diskretne oscilatorje, ter izkazujejo različne stopnje dinamične kompleksnosti. Pri analizi kolektivne dinamike upoštevamo tudi hitrost širjenja signalov med vozlišči v mreži. Ugotovimo, da obstaja tako optimalna mrežna topologija kakor tudi optimalna hitrost širjenja signalov med vozlišči mreže, pri kateri je raven kolektivne sinhronizacije najvišja. Ugotovitve in metodologijo iz naših teoretičnih študij v drugem delu disertacije apliciramo na sistem povezanih celic beta v Langerhansovih otočkih trebušne slinavke miši, ki predstavlja z vidika fiziologije metabolnih procesov izredno pomemben predmet preučevanja. Mrežno povezane celice beta, katerih poglavitna naloga je izločanje inzulina in s tem uravnavanje koncentracije glukoze v krvi, analiziramo ob podpori eksperimentalnih podatkov, izmerjenih pri različnih koncentracijah glukoze. Naši rezultati kažejo, da se celice beta povezujejo v lokalne funkcionalne skupnosti. Njihova segregiranost pa se v splošnem manjša z naraščajočo koncentracijo glukoze. S postopnim povečevanjem koncentracije glukoze postanejo v otočku tudi vse bolj izražene lastnosti široko skalnih mrež malega sveta. S tem rezultati doktorske disertacije prispevajo k razlagi fiziološkega pomena učinkovitost mrežne povezanosti celic beta in nakazujejo možnosti patoloških sprememb, ki so posledica sprememb v medcelični komunikaciji.

UDK: **530.182:517.17(043.3)**

THE INFLUENCE OF TOPOLOGICAL FEATURES OF COMPLEX NETWORKS AND DYNAMICAL PROPERTIES OF COUPLED CELLULAR OSCILLATORS ON COLLECTIVE DYNAMICS

Abstract

This doctor thesis is both theoretical and applicative. In the theoretical part of the thesis, we examine how the interplay of dynamical features of oscillators and structural properties of complex networks affect the collective behavior of the system. We show, that weakly dissipative and flexible oscillators synchronize best in a broad scale network topology, whereas on the other hand strongly dissipative and rigid oscillators exhibit maximal synchronization in a scale-free network topology. We provide an analytical explanation for this phenomenon and validate it by implementing various continuous as well as discrete mathematical models that exhibit different levels of dynamical complexity. In the continuation, we additionally investigate how speed of signal transmission in the network affects the collective dynamic of the system. Our results show that besides an optimal network topology, also an optimal information transmission speed exists, at which the system reaches the highest degree of global synchronization. In the second part we apply the findings and the methodology from our theoretical studies to the examination of the collective pancreatic beta cell activity in the islets of Langerhans, which represents the main mechanism for the regulation of blood glucose homeostasis by the secretion of the hormone insulin. We show that the beta cells dynamics is not synchronized on the global scale of the whole islets. Instead, the cells form local clusters of synchronized activity which tend to get less segregated under higher stimulatory glucose concentrations. Furthermore, higher glucose concentrations also lead to the presence of broad scale small world connectivity patterns in the functional beta cell network. The main findings thereby shed light on the physiology and collective behavior of the islets of Langerhans and point out the possibilities of pathological changes associated with changes in the intercellular communication pathways.

Seznam simbolov in kratic

$x_i(t)$	časovna vrsta *i*-tega oscilatorja
R	korelacijska matrika
R_{ij}	ij-ti element korelacijske matrike
$R_{ij}(t_n)$	vrednost korelacijskega koeficienta med i-to in j-to časovno vrsto v določenem časovnem intervalu
t_n	srednja vrednost časa n-tega časovnega okna
$\Delta\tau$	dolžina časovnega okna
R_{avg}	povprečna vrednost korelacijske matrike
N	število vozlišč v mreži
R^2_{avg}	koeficient determiniranosti
r_{avg}	povprečna fazna sinhronizacija
t	čas
n_i	*n*-ti lokalni ekstrem *i*-te časovne vrste
$t_i(n_i)$	čas pojava *n*-tega lokalnega ekstrema v *i*-ti časovni vrste
$\varphi_i(t)$	časovni potek faze *i*-te časovne vrste
Z_i	število zaznanih lokalnih ekstremov v *i*-ti časovni vrste
$r(t)$	trenutna vrednost fazne sinhronizacije
$\mathbf{z}$	vektor stanja
$\boldsymbol{z}^*$	fiksna točka dinamičnega sistema
J	Jacobijeva matrika
Tr(**J**)	sled Jacobijeve matrike
px, py	spremenljivki Poncaréjevega oscilatorja
γ	disipativnost Poincaréjevega oscilatorja
R_0	razdalja od izhodišča faznega prostora do trenutne lege Poincaréjeva oscilatorja
A	polmer limitnega cikla
ν	frekvenca periodične dinamike Poincaréjevega oscilatorja
ν_v	vsiljena frekvenca zunanjega periodičnega signala
ε	jakost sklopitve
a, b	parametri modela Brusselator

u, v	spremenljivki modela Brusselator
rx, ry	hitra in počasna spremenljivka Rulkove mape
α, β, σ	parametri Rulkove mape
kx, ky, kz	spremenljivke Rösslerjevega oscilatorja
a_r, b_r, c_r	parametri Rösslerjevega oscilatorja
$\mathbf{d}$	matrika sosednosti
d_{ij}	ij-ti element matrike sosednosti
$d_{ij}(t_n)$	ij-ti element matrike sosednosti znotraj časovnega okna t_n
k_i	povezanost i-tega vozlišča
K_i	število povezav med sosedi i-tega oscilatorja
k_{avg}	povprečna povezanost
$P(k)$	verjetnostna porazdelitev povezanosti
ϑ	skalirni eksponent potenčne porazdelitve povezav
E_{avg}	povprečna globalna učinkovitost mreže
l_{ij}	najkrajša geodetska razdalja med i-tim in j-tim vozliščem
C_{avg}	povprečnen koeficient gručavosti
C_i	gručavost i-tega vozlišča
c_i	i-ta skupnost
Q	modularnost
r_{as}	asortativnost
f_i	fitnes vrednost i-tega oscilatorja
Θ	prag za določanje povprečne povezanosti
g	števil vseh najkrajših poti med pari vozlišč
g_i	števil vseh posrednih najkrajših poti med pari vozlišč, ki potekajo čez i-to vozlišče
B_i	osrednjost i-tega vozlišča
δ	parameter mrežne topologije
I_{ij}	evklidska razdalja med i-tim in j-tim vozliščem
$\bar{\nu}$	povprečna frekvenca
ν_i	frekvenca i-tega oscilatorja mreže
$\lvert\overline{\Delta\nu}\rvert$	povprečna absolutna sprememba v frekvenci
M_i	število lokalnih maksimumov i-tega oscilatorja mreže

ν_i^m	frekvenca i-tega oscilatorja mreže v m-tem lokalnem ekstremu
E^*	normirana vrednost učinkovitosti
$\lvert\overline{\Delta\nu}\rvert^*$	normirano vrednost povprečne absolutne spremembe frekvence
$\gamma_{dyn,i}$	dinamična disipativnost i-tega oscilatorja mreže
Rk	povprečna jakost motenj direktnih sosedov
v	hitrost širjenja informacij med vozlišči mreže
τ_{ij}	zakasnitev v komunikaciji med i-tim in j-tim vozliščem
EEMD	empirična dekompozicija signala
$w_j(t)$	j-ta generacijo belega šuma ob času t
$x'_{i,j}(t)$	eksperimentalno dobljena časovna vrsta i-te celice ob j-ti generaciji belega šuma ob času t
$m_{j,k}$	povprečna vrednost med zgornjo in spodnjo ovojnico ob j-ti generaciji belega šuma in k-ti dekompoziciji signala
$IMF_{i,l}^j(t)$	l-ta enostavna funkcija i-tega oscilatorja ob j-ti generaciji belega šuma ob času t
$o_{i,j}(t)$	ostanek med $x'_{i,j}(t)$ in $IMF_{i,l}^j(t)$
L	število generacij belega šuma pri EEMD
$\bar{o}_i(t)$	povprečje ostankov $o_{i,j}(t)$, ki so bili določeni med L-timi generacijami belega šuma.
$\overline{IMF}_{i,l}(t)$	povprečna l-ta enostavna funkcija i-tega oscilatorja ob času t
F	zaznana intenziteta fluorescentnega barvila
F_0	bazalna intenziteta fluorescentnega barvila

1 UVOD

Raziskovalno področje kompleksnih mrež je od odkritja lastnosti mrež malega sveta in skalno neodvisnih mrež v številnih realnih sistemih deležno velike pozornosti raziskovalcev iz različnih znanstvenih disciplin [1, 2]. Značilnosti teh dveh mrežnih struktur so bile prepoznane v številnih mrežah, ki smo jih oblikovali ljudje, ali pa so se razvile v teku evolucije bioloških sistemov. Raziskovanje njihovih strukturnih lastnosti in pravil, ki so omogočila razvoj tako kompleksnih struktur, predstavlja trenutno paradigmo na tem raziskovalnem področju [3, 4]. Že dolgo je tako znano, da porazdeljenost števila povezav vozlišč v realnih mrežah odstopa od Poissonove porazdelitve, ki jo lahko zaznamo v modelih naključnih grafov. Amaral s sodelavci [5] natančno opredeli pojem mreže malega sveta in to mrežno topologijo razčleni na tri podtipe (skalno neodvisne mreže, široko skalne mreže in eno skalne mreže). Izkazalo se je, da so sistemom, kot so električna distribucijska mreža, mreža sodelovanja filmskih igralcev, nevronska mreža, WWW in citiranost znanstvenih objav, skupne lastnosti mrež malega sveta [6-9]. V številnih mrežah je prav tako možno zaslediti lastnosti skalno neodvisnih mrež, katerih porazdelitev povezav sledi potenčno padajoči funkciji. V takšnih mrežah se oblikuje malo število centralnih vozlišč (t.i. hubov), ki predstavljajo izredno povezana vozlišča. Po drugi strani pa ima večji del vozlišč mreže dokaj majhno povezanost. Za mreže malega sveta so značilne tudi daljnosežne povezave, ki močno prispevajo k bolj učinkoviti komunikaciji med vozlišči [10, 11]. V številnih realnih sistemih, ki so vpeti v prostor, pa obstajajo omejitve, ki preprečujejo vzpostavitve zelo dolgih povezav oz. prevelikega števila daljnosežnih povezav. Te omejitve posledično zavirajo oblikovanje izrazito centralnih vozlišč, kot jih je možno zaznati v skalno neodvisni mrežni topologiji. To se odraža v prelomu potenčno padajoče porazdeljenosti povezanosti vozlišč. Tovrstne mreže imenujemo široko skalne mreže. Ob teh dveh mrežnih topologijah pogosto srečamo še naključne mreže, katerih porazdeljenost povezav sledi Poissonovi porazdelitvi, ki ima maksimum pri povprečni povezanosti mreže [12], in regularno mrežo, kjer ima vsako vozlišče enako število povezav [13]. Tako naključne kakor tudi regularne mreže pa uvrščamo v skupino eno skalnih mrež. Za razliko od mrež malega sveta, so regularne mreže zelo neučinkovite pri prenosu informacij.

Z razvojem tega raziskovalnega področja se je pogled na vozlišča, kot zgolj transdukcijske točke v mreži, postopoma spremenil. Vozliščem je bila dodeljena dinamika, generirana z različnimi matematičnimi modeli, ki so bili med seboj sklopljeni, kot je to narekovala mrežna struktura. To pa ključno vpliva na kolektivno obnašanje sistema. Verjetno najbolj raziskan pojav v tem kontekstu je sinhronizacija kolektivne dinamike v mreži. S tem pojavom se pogosto srečamo v številnih realnih sistemih [14, 15]. Pokazano je bilo, da so sinhronizacijske lastnosti mrež močno pogojene z njihovimi strukturnimi lastnostmi. Heterogenost mreže tako do določene mere pozitivno vpliva na raven sinhronizacije kolektivne dinamike [16]. Negativen učinek heterogenosti mrežne strukture pa je možno uravnovesiti z obtežitvijo sklopitve med vozlišči [17]. Metodologija raziskovanja tovrstnih pojavov je napredovala tudi do te mere, da je bilo možno pokazati, da je pot do sinhroniziranega obnašanja v heterogenih mrežah različna od poti v homogenih mrežah [18, 19]. Dodatno je bilo pokazano tudi, da lahko skupnosti v mreži zavirajo kolektivno sinhronizacijo oscilatorjev v mreži [20, 21]. Iz preglednega članka o sinhronizaciji v kompleksnih mrežah [14] je razvidno, da so vplivi topoloških lastnosti mrež na raven kolektivne sinhronizacije dobro raziskane, kar pa ne drži tudi za dinamične lastnosti oscilatorjev, ki poseljujejo vozlišča mreže. Sovisen vpliv dinamičnih lastnosti vozlišč in strukture mreže še ni bil raziskan. Iz tega razloga se v tem delu podrobneje posvečamo prepletanju topoloških lastnosti mrež in dinamične narave oscilatorjev, ki krojijo njihovo lokalno dinamiko. Dinamična lastnost, za katero je znano, da znatno vpliva na sinhronizacijske lastnosti sklopljenih oscilatorjev, je disipativnost [22]. Ta lastnost dinamičnega sistema odraža, kako hitro se ta po manjši perturbaciji vrača v prostor atraktorja. V splošnem se dinamični sistemi, ki so močno disipativni, po perturbaciji hitro vrnejo nazaj k atraktorju, medtem ko šibko disipativni dinamični sistemi za to potrebujejo več časa. Eksperimentalno in teoretično je bilo pokazano, da na disipativnost dinamičnih elementov mreže vpliva tudi jakost sklopitve med njimi. Natančneje, pokazano je bilo, da šibkeje sklopljeni oscilatorji bolje sledijo zunanjemu periodičnemu signalu [23, 24]. Ključna zveza med strukturo sklopitvenih vzorcev v mreži in disipativnostjo pa je ostala neznanka. V luči tega smo se v naših raziskavah posvetili preučevanju mrežnih struktur, ki zagotavljajo najboljšo sinhronizacijo različnim tipom

oscilatorjev, t.j. močno in šibko disipativnim [25]. Izkaže se, da se močno disipativni sistemi najbolje sinhronizirajo v zelo heterogenih skalno neodvisnih mrežah, medtem ko šibko disipativni dosežejo največjo raven koherentnosti v manj heterogeni široko skalni mrežni topologiji. Fenomen smo dodatno raziskali in pokazali veljavnost za različne tipe modelov, ki krojijo dinamiko posameznih vozlišč. Matematični modeli so lahko tudi bolj kompleksni, tako da je njihova rešitev kaotična, ali pa tudi diskretni [10, 25]. Omenjen pojav smo uspeli razložiti in pokazati, na kakšen način mrežna topologija vpliva na dinamične lastnosti posameznih oscilatorjev, ter napovedati, kakšna mrežna struktura danih dinamičnih lastnosti oscilatorjev omogoča najvišjo raven sinhronizacije kolektivne dinamike [11].

Koncepti s področja kompleksnih mrež so se izkazali kot izredno uporabni za proučevanje delovanja živih organizmov na velikostnem redu posamezne celice [26] do velikostnega reda celotnega ekosistema [27]. Zelo pogosto se ti koncepti uporabljajo na področju nevroznanosti, tudi z vidika kliničnih aplikacij [28]. Sodobne tehnologije nevrološkega upodabljanja namreč omogočajo zajemanje obsežnih podatkov o anatomski ali funkcionalni povezanosti človeških možganov. Tovrstne študije dajejo nova spoznanja o strukturi in funkcionalnosti zdravih in obolelih možganov. Oslabljena in motena kompleksna možganska mreža je bila zaznana v primerih avtizma [29], shizofrenije [30, 31] in multiple skleroze [32].

Na nivoju tkiv pa je tovrstnih raziskav izredno malo, čeprav so številna tkiva organizirana v mreže, katerih celice lahko obravnavamo kot dinamični sistemi, ki so med seboj sklopljeni. Eden izmed glavnih razlogov je pomanjkanje ustreznih eksperimentalnih metod, ki bi omogočale neinvazivne in dolgotrajne meritve v intaktnih tkivih. V nekaterih najnovejših študijah pa je bila predstavljena tehnika, ki omogoča ekstrakcijo funkcionalne povezanosti na nivoju tkivnih rezin, s poudarkom na celicah beta iz Langerhansovih otočkov trebušne slinavke miši [33, 34]. Eksperimentalni preboj na tem področju je uspel tudi našim sodelavcem iz Inštituta za fiziologijo Medicinske fakultete Univerze v Mariboru [35]. Celice beta, katere predstavljajo prevladujoč tip celic v Langerhansovih otočkih, proizvajajo in izločajo inzulin, ki igra ključno vlogo pri uravnavanju koncentracije glukoze v krvi.

Funkcionalna povezanost med celicami je bila določena na podlagi korelacije med eksperimentalno izmerjenimi kalcijevimi signali v celicah beta, ki so bili posneti s konfokalnim mikroskopom z laserskim skenerjem [33, 35].

Doktorska disertacija temelji na nadgradnji in poglobitvi raziskav tako s področja sinhronizacijskih pojavov v kompleksnih mrežah kakor tudi analizi funkcionalne povezanosti v živih tkivih. V delu pokažemo, kako različne topološke lastnosti mrež, različne jakosti sklopitve med heterogenimi oscilatorji in njihova disipativnost, sovisno določajo raven sinhronizacije, ki jo dana kompleksna mreža lahko doseže. Teoretske pristope, ki smo jih razvili za določanje in preučevanje topoloških lastnosti mrež in določanje ravni sinhronizacije sklopljenih sistemov, uporabimo v nadaljevanju tudi za izgradnjo in analize funkcionalne mreže celic beta.

Teze doktorske disertacije so naslednje:

1. Intrinzično rigidni oscilatorji dosegajo maksimum usklajene kolektivne dinamike znotraj zelo učinkovitih in heterogenih skalno neodvisnih mrež, medtem ko intrinzično fleksibilni oscilatorji dosegajo največjo raven sinhronizacije v manj heterogenih široko skalnih mrežnih topologijah malega sveta.
2. Optimalno sinhronizacijo mrežno povezanih oscilatorjev glede na njihovo fleksibilnost lahko razložimo s stopnjo frekvenčne prilagodljivosti in globalno učinkovitostjo mrežne strukture.
3. V prostorsko vpetih mrežah obstajata tako optimalna mrežna topologija kakor tudi optimalna hitrost širjenja signala, pri kateri sistem sklopljenih oscilatorjev doseže maksimalno raven sinhronizacije.
4. V mreži funkcionalne povezanosti celic beta iniciatorske in mediatorske celice ohranjajo svojo vlogo pri različnih ravneh stimulacije celic z glukozo.
5. V tkivnih rezinah trebušne slinavke miši tvorijo celice beta lokalne skupnosti oziroma gosto povezane pod-enote, katerih pojavnost in porazdelitev je odvisna od koncentracije glukoze.

Disertacija je razdeljena na tri dele. Najprej je predstavljena metodologija, ki jo uporabljamo pri raziskovalnem delu. Tukaj predstavimo osnovne pojme s področja kompleksnih mrež in mere, ki jih uporabimo za karakterizacijo njihovih struktur. Predstavimo model prostorsko vpete mreže [36], ki ga uporabimo za generiranje različnih mrežnih struktur. Mrežni model analiziramo glede na njegove lokalne in globalne topološke lastnosti ter grafično prikažemo karakteristično prostorsko porazdeljenost vozlišč in povezav za različne izbrane mrežne topologije. Sledi predstavitev štirih matematičnih modelov, ki jih uporabimo za opis dinamike vozlišč v mrežah. Podrobneje predstavimo njihove dinamične lastnosti, za tri primere pa analiziramo tudi, kako se njihova vodljivost spreminja s stopnjo njihove disipativnosti. V ta namen naredimo stabilnostno analizo ter določimo disipativnost oscilatorja in izdelamo bifurkacijske diagrame. V primerih, kjer stabilnostne analize ni mogoče izvesti analitično, disipativnost dinamičnega sistema določimo numerično z izračunom spektra Ljapunovih eksponentov [20,21]. Glede na izračunano raven disipativnosti oscilatorje razdelimo na fleksibilne in rigidne. Obravnavamo tako zvezne kot tudi diskretne dinamične sisteme. V zadnjem delu poglavja vpeljemo še različne mere za določitev ravni sinhronizacije kolektivne dinamike.

Naslednje poglavje je namenjeno predstavitvi rezultatov naših raziskav [10, 11, 25, 37], s poudarkom na vpliv dinamičnih lastnosti oscilatorjev na raven kolektivne sinhronizacije v mrežah različnih topologij. Disipativnost neskloplјenih oscilatorjev poimenujemo intrinzična disipativnost. Pokažemo, da se intrinzično fleksibilni oscilatorji najbolje sinhronizirajo v široko skalni mreži malega sveta, medtem ko so intrinzično rigidni oscilatorji najbolje sinhronizirani v skalno neodvisni mreži. Na izbranem primeru izvedemo stabilnostno analizo, s katero pokažemo, v kolikšni meri lahko mrežna topologija spremeni disipativnost posameznih oscilatorjev. Za disipativnost mrežno vpetega oscilatorja vpeljemo pojem dinamične fleksibilnosti. Posebno pozornost namenimo tudi preučevanju vpliva hitrosti širjenja signala po mreži na sinhronizacijo sklopljenih oscilatorjev. Dobljene rezultate povežemo z določenimi patološkimi stanji v bioloških nevronskih mrežah.

Rezultate teoretičnih raziskav nato uporabimo za analizo funkcionalne povezanosti celic beta v Langerhansovih otočkih trebušne slinavke miši. Obstoječi protokol

konstrukcije funkcionalne mreže nadgradimo s predhodno obdelavo eksperimentalno dobljenih časovni sledi s t.i. EEMD dekompozicijo (*"Ensemble Empirical Mode Decomposition"*), ki temelji na Hilbert-Huangovi transformaciji [38]. Predhodna obdelava časovnih vrst nam omogoča zanesljivo ekstrakcijo dinamike na različnih časovnih skalah in posledično bolj natančno ter podrobno preučevanje evolucije medcelične komunikacije. Analiziramo vpliv različnih koncentracij glukoze na topološke lastnosti mrež celic beta, še posebej zgradbo skupnosti in globalno ter povprečno skupinsko sinhronizacijo v funkcionalni mreži. Pokažemo, da aktivnost celic beta v Langerhansovem otočku ni sinhrona na globalni ravni celega sincicija, temveč se celice združujejo v skupnosti, znotraj katerih je raven usklajenosti mnogo večja kot na ravni celotnega Langerhansovega otočka.

V sklepnem delu disertacije povzamemo in izpostavimo ključne ugotovitve naših raziskav. Na koncu nakažemo tudi smer nadaljnih raziskav ter možnosti nadaljnjih aplikacije naših rezultatov.

2 MATEMATIČNI MODELI IN METODE

V doktorski disertaciji obravnavamo pojav kolektivne sinhronizacije v kompleksnih mrežah. V ta namen so uporabljena različna matematična orodja, s katerimi lahko proučujemo strukturne lastnosti mrež, dinamične lastnosti oscilatorjev in raven sinhronizacije. Posamezna orodja, ki nam to omogočajo, so predstavljena v tem poglavju.

Vozlišča mreže obravnavamo sprva kot statične točke, brez lastne dinamike. Na primeru treh realnih mrež predstavimo tri tipe mrež malega sveta (skalno neodvisne, široko skalne in eno skalne), kot jih je opredelil Amaral s sodelavci [5]. Omenjenim mrežam izrišemo tudi pripadajoče verjetnostne porazdelitve povezav. Za potrebe nadaljnjih analiz pa predstavimo še druge mere, ki so pomembne za določanje lokalnih in globalnih lastnosti mrež. Kot osnova za izvedbo teoretičnih analiz kompleksnih mrež predstavimo algoritem za konstrukcijo prostorsko vpete mreže. Tipične mrežne strukture, generirane s tem algoritmom, primerjamo s tremi realnimi mrežami. Iz primerjave je razvidno, da lahko z numeričnim algoritmom prostorsko vpete mreže reproduciramo tri tipične mrežne strukture, zaznane v realnih sistemih. Velika prednost uporabljenega mrežnega modela je, da lahko s spreminjanjem enega parametra zvezno določamo tip mreže, ki ga želimo upodobiti. Odvisnost strukturnih lastnosti uporabljenega mrežnega modela od parametra topologije je tudi izračunana. Za posamezne celice, oz. v splošnem za posamezne oscilatorje, ki jih poselimo v vozlišča mrež, predstavimo matematične modele, s katerimi opišemo njihovo dinamiko. Dinamične lastnosti posameznih modelov so podrobneje predstavljene. Poseben poudarek je namenjen disipacijskim lastnostim teh matematičnih modelov. Za vsak model naredimo stabilnostno analizo. Pomen disipacije ponazorimo še z analizo, ki kaže, kako je vodljivost izbranih matematičnih modelov odvisna od nje. V zaključnem delu tega poglavja predstavimo še metode, s katerimi določamo raven sinhronizacije med časovnimi vrstami.

2.1 Kompleksne mreže

Osnovni gradniki mrež so vozlišča in povezave med njimi. Vozlišča lahko ponazarjajo poljubne elemente določenega sistema (celice, ljudi, letališča, transformatorske postaje …), povezave med vozlišči pa interakcije med temi elementi (presledkovni stiki med celicami, poznanstva, direktni leti, daljnovodi …). Strukturne lastnosti mreže so popolnoma odvisne od načina povezanosti vozlišč. Informacija o povezanosti mreže je navadno zajeta v matriki sosednosti **d**, ki predstavlja numerično upodobitev mreže. Razsežnost matrike **d** je enaka $N \times N$, kjer je N število vozlišč. Ker ne bomo upoštevali usmerjenosti in obteženosti povezav med vozlišči, bo ta matrika simetrična. Matrika **d** je binarna, saj njeni elementi zavzemajo le vrednost 0 ali 1. Kadar sta vozlišči i in j med seboj povezani, bosta ij-ti kot tudi ji-ti element matrike sosednosti enaka 1 $\left(d_{ij} = d_{ji} = 1\right)$. V nasprotnem primeru, ko i-ti in j-ti vozlišči nista povezani, pa sta ij-ti kot tudi ji-ti element matrike sosednosti enka 0 $\left(d_{ij} = d_{ji} = 0\right)$. Na sliki (2.1) je prikazana oblika zapisa matrike **d** in izrisana pripadajoča mreža.

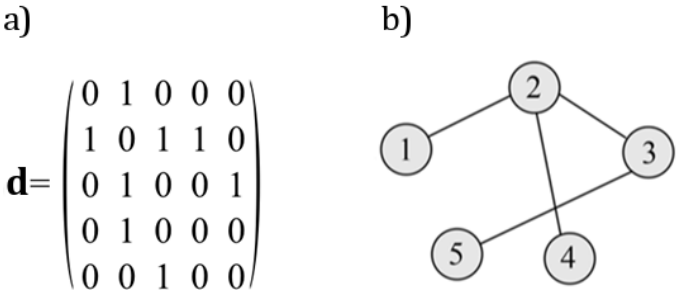

Slika 2.1: Upodobitev matrike sosednosti (a) in pripadajoča mreža (b).

Kot je razvidno iz slike (2.1), so vse informacije, ki jih potrebujemo za proučevanje lastnosti mrežene strukture, zajete v matriki sosednosti **d**. Kakršnakoli analiza mrežne strukture je pogojena z analizo te matrike. Ena izmed verjetno najpreprostejših, a hkrati izredno pomembnih lastnosti, je povezanost posameznih vozlišč mreže. Označujemo jo s k_i, kjer podpisani i ponazarja, da je to lastnost i-tega vozlišča. Večji kot je faktor k_i določenega vozlišča, več povezav ima in s tem se povečuje tudi njegova pomembnost v mreži [39]. Povezanost posameznih vozlišč pa določimo tako, da seštejemo vse pripadajoče vodoravne elemente v matriki sosednosti **d**:

$$k_i = \frac{1}{N}\sum_{i\neq j}^{N} d_{ij}. \tag{2.1}$$

Za globalni opis povezanosti mreže določimo povprečno povezanost mreže k_{avg}, kjer je povprečna povezanost mreže definirana z enačbo:

$$k_{\mathrm{avg}} = \frac{1}{N}\sum_{i}^{N} k_i. \tag{2.2}$$

Večji kot je k_{avg}, bolj gosto so vozlišča med seboj povezana. Omeniti je potrebno, da povprečna povezanost ne odraža nujno tudi karakteristične povezanosti posameznih vozlišč zaradi možne variabilnosti v povezanosti posameznih vozlišč. Tako podatek o povprečni povezanosti navadno uporabljamo skupaj z verjetnostno porazdelitvijo povezav, ki jo označujemo s $P(k)$ [40]. Za dano mrežo določimo $P(k)$ tako, da preštejemo, koliko vozlišč v mreži ima k povezav, in dobljeno porazdelitev delimo s skupnim številom vozlišč N. Porazdeljenost $P(k)$ predstavlja verjetnost, da bi naključno izbrano vozlišče mreže imelo k povezav. V splošnem lahko, glede na potek $P(k)$, mreže klasificiramo kot skalno neodvisne mreže, široko skalne mreže in eno skalne mreže [5].

Za skalno neodvisne mreže je značilno, da $P(k)$ sledi potenčno padajoči funkciji $P(k)\sim k^{-\vartheta}$, kjer so tipične vrednosti eksponenta v intervalu $\vartheta \in [2,3]$ [1]. Zaradi takšne porazdelitve povezav so prisotna velika odstopanja v povezanosti posameznih vozlišč glede na povprečno vrednost. V mreži se pojavi malo število vozlišč, ki imajo veliko povezanost (t.i. centralnih vozlišč), in vse več vozlišč, ki imajo malo povezav. Zaradi velikih razlik v povezanosti, ki se pogosto razpredajo čez več velikostnih redov, so skalno neodvisne mreže izredno heterogene. Primer takšne mreže je prikazan na sliki (2.2a), pripadajoča $P(k)$ pa na sliki (2.2d). Različne omejitve, ki so pogosto povezane s ceno povezav, v mnogo prostorsko vpetih mrežah preprečujejo nastajanje izrazitih centralnih vozlišč, kot jih opazimo v skalno neodvisnih mrežah. Ta omejitev se odraža v porazdelitvi $P(k)$, kjer od določene mejne vrednosti povezanosti dalje krivulja hitreje pada. Tovrstne mreže so manj heterogene od skalno neodvisnih mrež in jih imenujemo široko skalne mreže.

Primer široko skalne mreže je prikazan na sliki (2.2b), pripadajoč $P(k)$ pa s sliko (2.2e). Zadnji tip mreže so eno skalne mreže. V ta tip mrež sodijo tako naključne kot tudi regularne mreže, v katerih ima vsako vozlišče enako število povezav k. V primeru regularne mreže lahko $P(k)$ ponazorimo z delta funkcijo [13]. V primeru naključne mreže pa ima $P(k)$ obliko Poissonove porazdelitve, ki ima maksimum pri povprečni povezanosti mreže k_{avg}. Takšne mreže so homogene, saj ni velikih razlik v povezanosti posameznih vozlišč. Primer realne naključne mreže je prikazan na sliki (2.2c), pripadajoč $P(k)$ pa na sliki (2.2f). Podatki za izris mrež so vzeti s spletne strani SNAP [41]. Omeniti je potrebno, da večina tovrstnih podatkovnih baz še ne vsebuje informacij o geografskih lokacijah posameznih vozlišč. Za potrebe postavitve vozlišč smo v mreži uporabili pristop, ki sta ga opisala Fruchterma in Reingold [42]. Lokacije vozlišč v mreži tako ne odražajo njihove dejanske geografske lokacije.

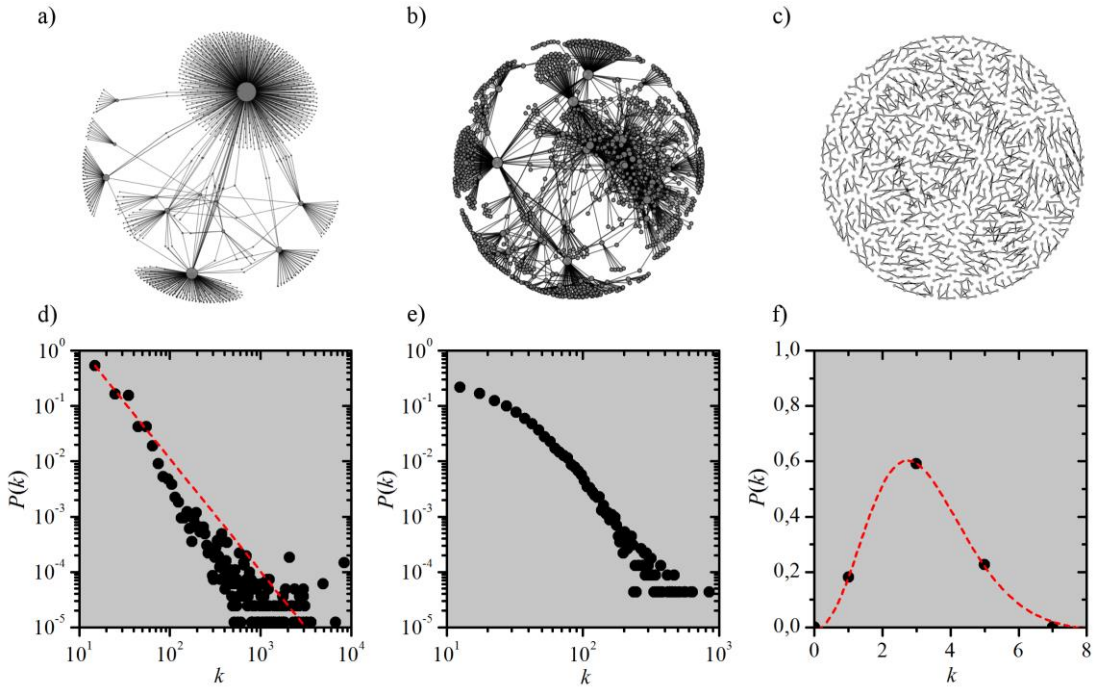

Slika 2.2: Upodobitev treh realnih mrež. a) spletnih strani Univerze v Stanfordu, b) citiranost člankov in c) cestne mreže Kalifornije v ZDA ter verjetnostne porazdelitve povezav za primere d) spletnih strani Univerze v Stanfordu, e) citiranost člankov in f) cestne mreže Kalifornije v ZDA.

Postavlja se vprašanje, kakšne so razlike med tipi mrež ob očitni razliki v obliki poteka $P(k)$. V ta namen so se znotraj področja teorije grafov in kompleksnih mrež razvile mere, s katerimi lahko podamo učinkovitost komunikacijskih lastnosti mreže, integriranost ali segregiranost vozlišč v mrežo, njihove ranljivosti, heterogenosti oz. homogenosti, itd. Podrobnejši pomen teh mer ter algoritme, s katerimi jih lahko izračunamo, predstavljamo v nadaljevanju.

2.1.1 Določanje strukturnih lastnost kompleksnih mrež

Kadar želimo ovrednoti komunikacijske lastnosti mreže, to podamo z učinkovitostjo, ki jo označujemo z E_{avg}. Ta mera podaja stopnjo vključenosti oz. integriranosti vozlišč v mreži [43]. Učinkovitost mreže določimo tako, da izračunamo vse najkrajše poti med vsemi pari vozlišč mreže. Tukaj se najkrajša pot, ki jo bomo označevali s l_{ij}, nanaša na najkrajšo geodetsko razdaljo med dvema vozliščema oz. na najmanjše število povezav, ki jih je potrebno prečkati med dvema poljubnima vozliščema. Za določanje najkrajše geodetske poti l_{ij} med vozliščema i in j bomo uporabili Dijkstratov algoritem [44]. V primeru, ko ne obstaja posredna ali neposredna pot, ki bi povezovala i-to in j-to vozlišče, upoštevamo, da je $l_{ij} = \infty$. Učinkovitost mreže je nato definirana kot vsota inverznih najkrajših poti v dani mreži:

$$E_{\text{avg}} = \frac{1}{N(N-1)} \sum_{i \neq j}^{N} \frac{1}{l_{ij}}. \tag{2.3}$$

Učinkovitost mreže E_{avg} zavzema vrednosti med 0 in 1. Večja učinkovitost pomeni, da je v povprečju potrebno prečkati manjše povezav, da pridemo od enega do drugega vozla. V posebnem primeru popolnega grafa, kjer je vsako vozlišče povezano z vsakim, je povprečna povezanost enaka 1.

Naslednja uporabljena mera, je povprečna gručavost mreže C_{avg}. Ta podaja verjetnost, da tri vozlišča tvorijo med seboj popoln podgraf [45]. Za določanje C_{avg} bomo uporabili pristop, ki sta ga vpeljala avtorja Watts in Strogatz [2]. V prvem koraku določimo lokalne koeficiente gručavosti C_i, ki so definirani kot razmerje

dejanskega števila povezav K_i med sosedi i-tega vozlišča in največjim možnim številom povezav. Omenjeno lahko zapišemo kot:

$$C_i = \frac{2K_i}{k_i(k_i - 1)}. \tag{2.4}$$

Povprečni koeficient gručavosti C_{avg} nato preprosto določimo z izračunom povprečja cele mreže:

$$C_{\text{avg}} = \frac{1}{N}\sum_{i=1}^{N} C_i. \tag{2.5}$$

Karakteristične konfiguracije in pripadajoče povprečne vrednosti koeficienta gručavosti so prikazane na sliki (2.3).

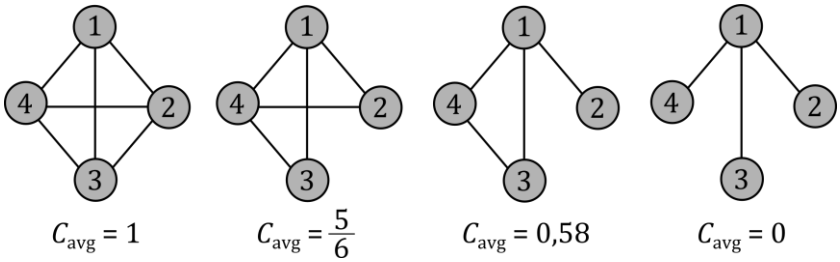

Slika 2.3: Shematski prikaz pomena povprečne gručavosti.

Gručavost odraža, kako gosto so med seboj povezani neposredni sosedje. Da bi prepoznali skupino vozlišč, ki so gosteje medsebojno povezani, razporedimo vozlišča v skupnosti. Beseda skupnost se v teoriji grafov nanaša na particijo mreže ali tudi podmreže, znotraj katere so vozlišča bolj gosto povezana kot v preostali mreži. Za prepoznavanje skupnosti v mrežah uporabimo algoritem, ki ga je predlagal Blondel s sodelavci [46]. V nadaljevanju bomo i-to skupnost vozlišč označevali s c_i. Da lahko vozlišča razporejamo po skupnostih, skušamo maksimizirati mero, ki jo imenujemo modularnost Q. Njena vrednost podaja, kako uspešno lahko mrežo razdelimo na skupnosti [47, 48] in je definirana kot:

$$Q = \frac{1}{2m}\sum_{i,j}\left(d_{ij} - \frac{k_i k_i}{2m}\right)\delta(c_i, c_j), \tag{2.6}$$

kjer je člen $\delta(c_i, c_j)$ enak 1, kadar je $c_i = c_j$ in 0 v nasprotnem primeru. Namen algoritma je maksimirati modularnost mreže z zveznim preoblikovanjem strukture skupnosti. Nova oblika skupnosti vozlišč je sprejeta le, če je sprememba v modularnosti ΔQ med trenutno in predhodno konfiguracijo pozitivna. Proces prerazporejanja vozlišč med skupnostmi ponavljamo toliko časa, dokler ne postanejo spremembe v ΔQ neznatne in smo posledično oblikovali najverjetnejšo porazdelitev vozlišč v skupnosti. Omenjen algoritem smo uporabili na primeru lastne spletne socialne mreže. Rezultati so prikazani na sliki (2.4). Obarvanost vozlišč ponazarja njihovo pripadnost določeni skupnosti. Tako so rdeča vozlišča osebe, s katerimi smo navezali stike v času študija, v zeleni skupnosti pa so osebe iz časov šolanja v srednji šoli ipd.

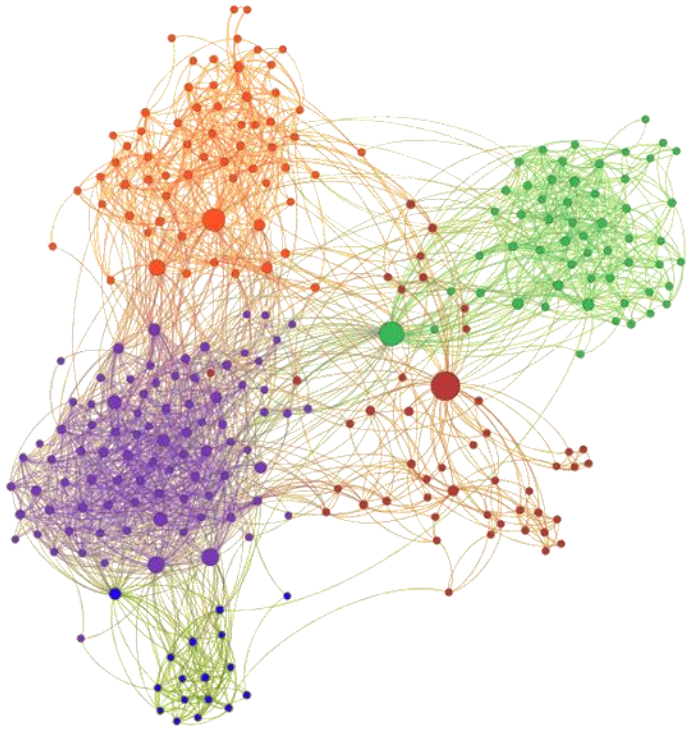

Slika 2.4: Mrežni prikaz spletnega socialnega omrežja. Barve vozlišč ponazarjajo pripadnost določeni skupnosti in njihova velikost odraža povezanost posameznega vozlišča.

Določena vozlišča mreže predstavljajo osrednje enote, preko katerih poljubni pari posredno povezanih vozlišč učinkovito izmenjujejo informacije. V modularnih mrežah se lahko zgodi, da vozlišča ene skupnosti komunicirajo z vozlišči druge skupnosti zgolj preko enega vozlišča. Takšna vozlišča imajo zelo veliko osrednjost, ki jo za i-to vozlišče označujemo kot B_i. Osrednjost vozlišča določimo na podlagi vsote najkrajših poti med poljubnima dvema posredno povezanima vozliščema mreže, ki potekajo preko i-tega vozlišča. Število najkrajših povezav, ki potekajo preko i-tega vozlišča, označimo s g_i. To število nato delimo s številom vseh najkrajših poti v mreži g:

$$B_i = \frac{g_i}{g}. \tag{2.7}$$

Za bolj nazorno predstavitev te lokalne mere, je v sliki (2.5) prikaz mreže šestih vozlišč ter upodobitev 3 najkrajših poti preko izbranega vozlišč.

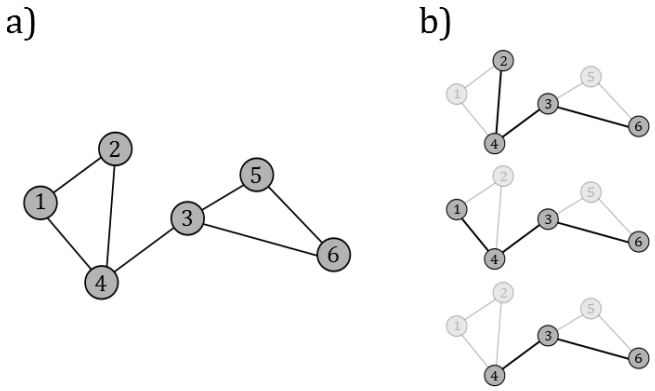

Slika 2.5: Prikaz osrednjosti vozlišč. Mreža šestih vozlišč (a) in prikaz najkrajših poti med posredno povezanimi pari vozlišč (b). Vidimo lahko, da ima vozlišče, označeno s številko 3, največjo osrednjost.

Kot zadnjo mero omenimo še asortativnost mreže r_{as}. Ta odraža, v kolikšni meri se vozlišča preferenčno povezujejo s seboj podobnimi oz. drugačnimi [49]. Vrednosti tega parametra se nahajajo v razponu od -1 (vozlišča z nizko povezanostjo so pogosto povezana z vozlišči, ki imajo veliko število povezav) do 1 (vozlišča, ki imajo enako ali podobno število povezav so pogosto povezana med seboj). Mreže, katerih asortativnost je močno negativna, so pogosto hierarhično organizirane, kjer je malo

število močno povezanih vozlišč povezano z velikim številom vozlišč, ki imajo zgolj malo povezav. Močno pozitivna vrednost parametra r_{as} pa je značilna za regularne mreže, kjer imajo vozlišča v povprečju podobno število povezav. Asortativnost mreže je v primeru neusmerjenega grafa definira kot:

$$r_{\mathrm{as}} = \frac{\sum_{i=1}^{N} e_{ii} - \sum_{i=1}^{N} a_i^2}{1 - \sum_{i=1}^{N} a_i^2}, \tag{2.8}$$

kjer e_{ii} ponazarja delež povezav mreže, ki povezujejo vozlišče tipa i z vozliščem tipa j. Tukaj se v splošnem tip nanaša na poljubno skalarno količino, ki jo lahko pripišemo vozliščem mreže [50]. Parameter a_i pa predstavlja, kolikšen delež direktnih sosedov i-tega vozlišča ima enako število povezav kot vozlišče i.

2.1.2 Model prostorsko vpete mreže

Različne tipe mrež generiramo z algoritmom prostorsko vpete mreže [36]. Model je primeren za modeliranje mrežnih sistemov, pri katerih obstaja omejitev pri kreiranju daljnosežnih povezav. Uporabljen je na primer bil za model tkiva gladkih mišičnih celic pljučne arterije [51]. V prvem koraku tega algoritma naključno porazdelimo N vozlišč v prostoru, ki ima obliko kvadrata s stranicami dolžine 1. Vsakemu od vozlišč dodelimo tudi naravno število i. V naslednjem koraku vozliščem predpišemo pomembnosti (t.i. fitnes vrednosti) f_i. Te porazdelimo v skladu s potenčno funkcijo $P(f) \sim f^{-\vartheta}$, kjer je bil skalni parameter $\vartheta = 2{,}5$. Povezava med i-tim in j-tim vozliščem je ustvarjena, če je izpolnjen naslednji pogoj:

$$\frac{f_i f_j}{I_{ij}^{\delta}} > \theta, \tag{2.9}$$

kjer je θ prag, s katerim nastavimo povprečno povezanost mreže k_{avg}, ki jo v nadaljevanju postavimo na $k_{\mathrm{avg}} = 5$. Faktor I_{ij}^{δ} predstavlja evklidsko razdaljo med i-tim in j-tim vozliščem. Ključni člen, s katerim lahko zvezno spreminjamo tip generirane mreže, je parameter δ. V primeru, ko ta zavzema majhne vrednosti ($\delta \ll 1$) to izzove, da je faktor $I_{ij}^{\delta} \sim 1$. Pogoj, s katerim sprejemamo povezave med

vozlišči in je zapisan v enačbi (2.9), postane neodvisen od evklidske razdalje med vozlišči mreže. Povezave se sprejemajo zgolj na podlagi predpisanih pomembnostih posameznih vozlišč f_i. Ker pa te sledijo potenčno padajoči funkciji, ima le malo število vozlišč, ki vzpostavijo v mreži veliko povezav, velik f_i. Večji del vozlišč v mreži, ki pa ima majhno vrednost f_i, vzpostavi zgolj par povezav. Ker v primeru $\delta \ll 1$ ni nobenih prostorskih omejitev, je mreža prekomerno sestavljena iz dolgih povezav in je izredno heterogena. Prednost tovrstnih mrež je predvsem njihova učinkovitost, ki je posledica izredno kratke geodetske razdalje. V drugi skrajnosti, ko je $\delta \gg 1$, je ključni člen pri vzpostavitvi povezav med vozlišči dolžina povezav. Povezave, ki se sprejemajo, so kratkega dosega. Pomanjkanje daljnosežnih povezav ima za posledico izredno neučinkovito mrežo. Ker so povezani bolj ali manj le bližnji sosedi, je mreža homogena. Porazdelitev števila povezav posameznih vozlišč $P(k)$ ima v tem primeru obliko Poissonove porazdelitve, kar je značilnost tudi naključnih geometričnih mrež. Pri srednjih vrednostih topološkega parametra δ ima mreža značilnosti široko skalne mreže. Povezave med oscilatorji se tvorijo tako med bližnjimi kot tudi med oddaljenimi oscilatorji. Bližnje povezave so posledica večjega vpliva parametra evklidske razdalje. Slednja ima za posledico tudi preprečitev nastanka zelo izrazitih centralnih vozlišč. Porazdelitev števila povezav $P(k)$ pri teh mrežah se več ne ujema s potenčno padajočo obliko $P(k)$ skalno neodvisnih mrež. Če primerjamo sliki (2.5d in 2.5e), lahko opazimo razliko med položnim vrhom za široko skalno mrežo in linearno padajočo krivuljo v log-log grafu za skalno neodvisno mrežo. Za tovrstne mrežne tipe je značilna manjša učinkovitost kot v skalno neodvisnih mrežah, relativno velik koeficient gručavosti ter sestava mreže tako iz kratkih kot tudi dolgih povezav.

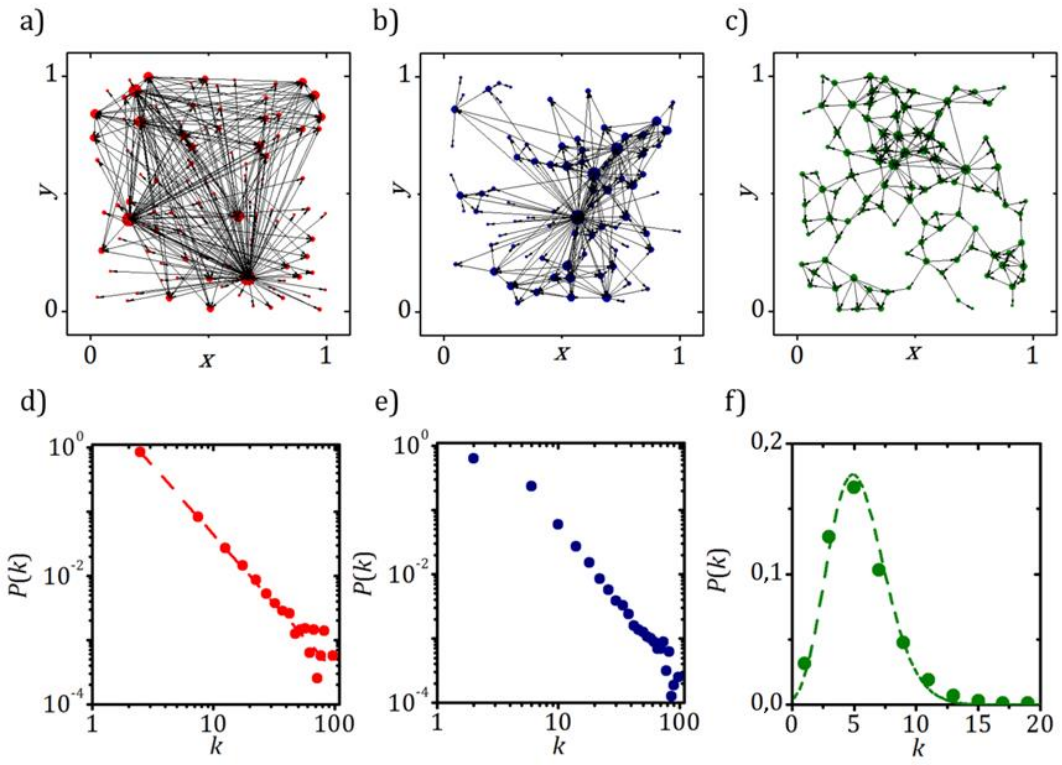

Slika 2.6: Karakteristične numerično generirane mrežne strukture, za vrednosti parametrov a) $\delta = 0{,}1$, b) $\delta = 1{,}3$ in c) $\delta = 5{,}1$ ter ustrezne verjetnostne porazdelitve povezav d) – f). Za $\delta = 0{,}1$ je točkam prilagojena najbližja potenčna funkcija, prikazana z rdečo črtkano črto. Za $\delta = 5{,}1$ je točkam prilagojena funkcija, ki ustreza najbližji Poissonovi porazdelitvi (zelena črtkasta črta).

Iz rezultatov, ki so prikazani na sliki (2.6), lahko vidimo, da je možno s tem mrežnim modelom zelo dobro posnemati spekter realnih mrežnih struktur (glej sliko 2.2).

Za dan mrežni model izračunamo učinkovitost, povprečno gručavost, povprečno evklidsko dolžino povezav, asortativnost, modularnost in število skupnosti v odvisnosti od topološkega parametra δ. Rezultati, prikazani na sliki (2.7), so dobljeni na podlagi 1000 realizacij algoritma prostorsko vpete mreže, sestavljene iz 100 vozlišč. V vsaki realizaciji smo topološki parameter δ povečevali za 0,2 v intervalu od 0,1 do 5,1.

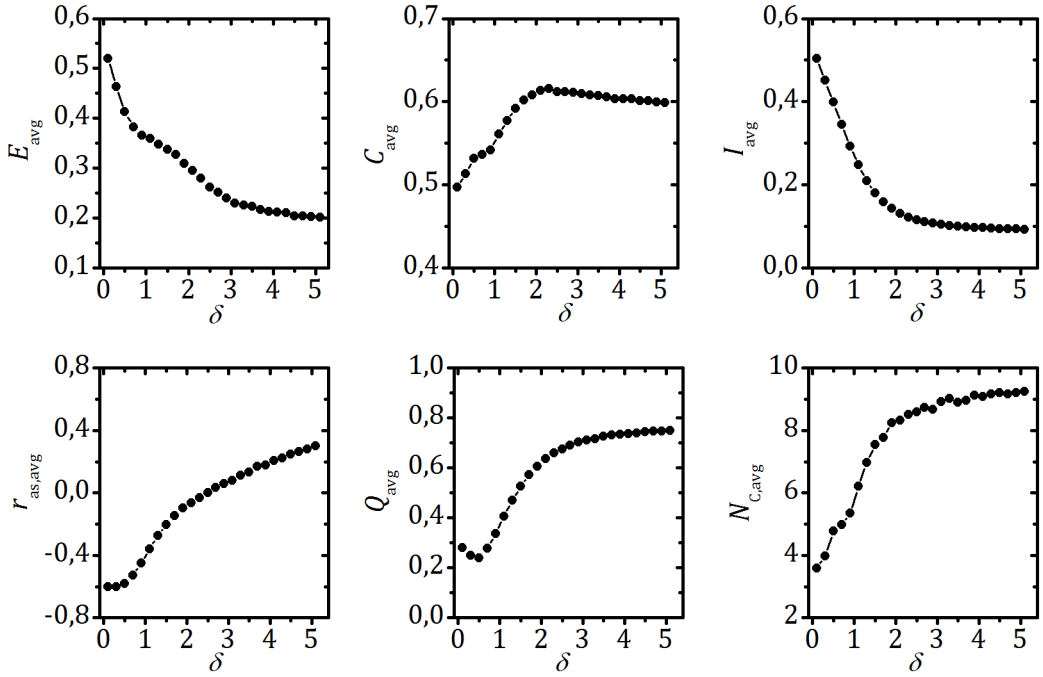

Slika 2.7: Karakterizacije mrežnih lastnsoti numeričnega modela. Odvisnost učinkovitosti (a), povprečne gučavosti (b), povprečne evklidske razdalje (c), povprečne asortativnosti (d), povprečne modularnosti (e) in števila skupnosti (f) od topološkega parametra δ.

Vidimo lahko, da se učinkovitost mreže monotono zmanjšuje z večanjem topološkega parametra δ (slika 2.7a). Povprečni koeficient gručavosti sprva narašča za manjše vrednosti topološkega parametra δ. Nato doseže najvišjo vrednost in od te vrednosti dalje zelo položno pada (slika 2.7b). Z večanjem topološkega parametra, kakor smo napovedali, se v splošnem dolžina povezav v mreži manjša (slika 2.7c). Vidimo lahko, da so v območju nizkih vrednostih topološkega parametra δ preferenčno povezana vozlišča, ki imajo izrazito različno povezanost. Ta preferenca se z večanjem parametra δ tudi znižuje in je pri srednjih vrednosti parametra δ tudi pozitivna (glej sliko 2.7d). Oglejmo si še odvisnost modularnosti in števila skupnosti mreže od topološkega parametra. Modulatnost Q generiranih mrež v splošnem monotono narašča v odvisnosti od parametra δ (glej sliko 2.7e). Nizka vrednost modularnosti odraža manj uspešno razvrstitev vozlišč v skupnosti oz. manjšo razliko v gostoti povezav med vozlišči znotraj ene skupnosti v primerjavi s celotno mrežo. Tudi število N_c skupnosti (glej sliko 2.7f), v katere so razvrščeni oscilatorji, narašča. V primeru nizkih vrednosti topoškega parametra imamo izredno heterogene mreže, ki

omogočajo izredno učinkovito komikacijo in so ne-segregirane. Z višanjem topološkega parametra pa postajajo mreže vse bolj homogene, manj učinkovite in segregirane.

Vozlišča v splošnem niso zgolj statične točke, ki so med seboj povezane, temveč imajo svojo lastno dinamiko. V naših analizah nas še posebej zanima, kako različne mrežne stukture in dinamične lastnosti oscilatorjev, ki vozlišča poseljujejo, vplivajo na raven kolektivne sinhronizacije v mreži. Za opis dinamike posameznih vozlišč uporabimo matematične modele, ki so predstavljeni v nadaljevanju.

2.2 Matematični modeli dinamike posameznih vozlišč

Lastnosti določenega sistema se odražajo tudi v njegovi dinamiki. V splošnem so vsi sistemi do določenega velikostnega reda vedno sestavljeni iz večjega števila elementov, ki vzajemno delujejo drug na drugega. Z namenom bolj poglobljenega razumevanja njihovega delovanja pogosto pričnemo z raziskovanjem lastnosti njihovih osnovnih gradnikov. V ta namen so se in se še zmeraj oblikujejo matematični modeli, ki tako na kvalitativni kot tudi na kvantitativni ravni dobro posnemajo dinamiko posameznih gradnikov. Običajno zapišemo dinamičen model v obliki diferencialne enačbe, ki ima obliko:

$$\frac{d}{dt}\mathbf{z} = \dot{\mathbf{z}} = f(\mathbf{z}), \tag{2.10}$$

kjer je $\mathbf{z}$ v splošnem l dimenzionalni vektor stanja in $\dot{\mathbf{z}}$ pripadajoči časovni odvod. V mnogih primerih ni možno podati eksplicitne rešitve takšnega sistema. S slednjo bi podali časovni razvoj trajektorije v faznem prostoru pri danih začetnih pogojih $\boldsymbol{z_0}$. Vendar v današnjih časih to ni ovira, saj lahko z zmogljivimi računalniki v zmernem času numerično izračunamo časovni razvoj sistema z več tisočimi diferencialnimi enačbami.

Poseben poudarek bomo namenili lokalni disipaciji danega matematičnega sistema, ki odraža, kako močno njegov atraktor privlači svojo okolico v faznem prostoru [22].

Zaradi disipacije se namreč fazni prostor krči v množico točk, ki predstavljajo atraktor faznega prostora. Trajektorija disipativnega dinamičnega sistema se tako za poljuben izbor začetnih pogojev približuje atraktorju. Lokalno disipacijo lahko po analitični poti določimo le v primeru, ko lahko podamo tudi eksplicitni zapis atraktorja. Tako je v prvi vrsti potrebno določiti fiksne točke $\mathbf{z}^*$ matematičnega sistema, kjer velja:

$$\frac{\partial}{\partial t}\mathbf{z}|_{z=z*} = f(\mathbf{z}^*) = 0. \qquad 2.11$$

Rešitev $\mathbf{z}^*$ predstavlja točke v faznem prostoru, kjer je časovni odvod funkcije enak 0 oz. se stanje sistema s časom ne spreminja. Ker je lahko to stanje stabilno oz. nestabilno, analiziramo obnašanje sistema v bližini ravnovesnega staja $\mathbf{z}^* + \delta\mathbf{z}$. V splošnem se lahko sistem v takšnem primeru odzove na dva načina, kot je to prikazano na sliki (2.8). Ob manjši motnji $\delta\mathbf{z}$, se lahko sistem ali vrne k rešitvi $\mathbf{z}^*$, ali pa se prične od nje oddaljevati. V kolikor se dinamični sistem vrne k rešitvi, rešitev predstavlja množico točk, ki oblikujejo atraktor faznega prostora, je rešitev stabilna. V nasprotnem primeru pa rešitev predstavlja nestabilno fiksno točko faznega prostora.

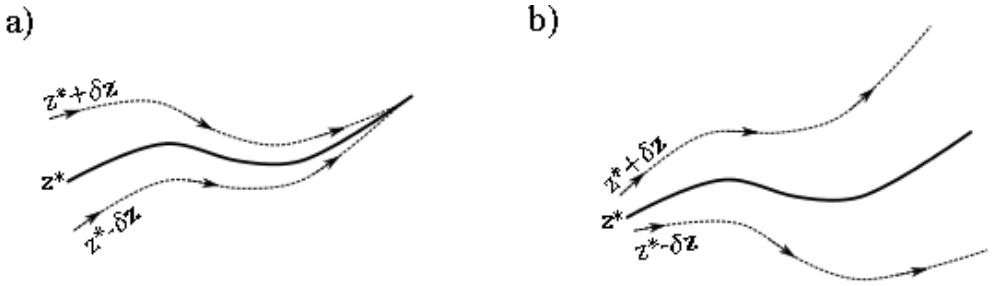

Slika 2.8: Možni odzivi dinamičnega sistema na perturbacijo $\delta\mathbf{z}$**:** a) primer privlačnega atraktorja. Bližnje trajektorije se po perturbaciji približujejo atraktorju. Slika b) pa prikazuje primer nestabilnega atraktorja, kjer se bližnje trajektorije oddaljujejo od njega.

Obnašanje dinamičnega sistema v bližini fiksne točke analiziramo tako, da sistem lineariziramo v majhni okolici $\delta\mathbf{z}$ okoli točke $\mathbf{z}^*$. To naredimo tako, da zapišemo Jacobijevo matriko sistema za stanje $\mathbf{z}^*$:

$$\mathbf{J}|_{\mathbf{z}=\mathbf{z}^*} = \begin{bmatrix} \frac{\partial \dot{z}_1}{\partial z_1} & \cdots & \frac{\partial \dot{z}_1}{\partial z_l} \\ \vdots & \ddots & \vdots \\ \frac{\partial \dot{z}_l}{\partial z_1} & \cdots & \frac{\partial \dot{z}_l}{\partial z_1} \end{bmatrix}. \tag{2.12}$$

Stabilnost stacionarnega stanja je pogojena s sledjo Jacobijeve matrike. Če je le ta negativna, je stacionarno stanje stabilno. Tovrstne matematične sisteme imenujemo tudi disipativni sistemi. V nasprotnem primeru, če je sled matrike pozitivna, pa se trajektorije v bližnji okolici stacionarnega stanja od njega oddaljujejo. Sled Jacobijeve matrike označujemo s Tr(**J**). Pogosto je ta imenovana tudi divergenca. Zapišemo jo lahko kot vsoto diagonalnih elementov Jacobijeve matrike:

$$\mathrm{Tr}(\mathbf{J}|_{\mathbf{z}=\mathbf{z}^*}) = \sum_{i=0}^{l} \frac{\partial \dot{z}_l}{\partial z_l}. \tag{2.13}$$

Tako lahko obnašanje trajektorije v bližini fiksne točke zapišemo kot:

$$\mathbf{z}(t) = \mathbf{C}e^{\mathrm{Tr}(\mathbf{J}|_{\mathbf{z}=\mathbf{z}^*})t}. \tag{2.14}$$

Kadar tovrstne analize ne moremo narediti analitično, za določanje lokalne disipativnosti atraktorja uporabimo numerične pristope. V nadaljevanju so predstavljeni štirje matematični modeli, ki krojijo dinamiko posameznih vozlišč. Prvi model je preprost, kar omogoča analitično analizo. Ostali trije so bolj zapleteni in predvidevajo tudi bolj kompleksno dinamiko. Eden izmed njih je diskreten. Za vsak oscilator bomo napravili stabilnostno analizo in tako podali, kako se njegova povprečna lokalna disipativnost spreminja v odvisnosti od izbranega parametra. Samo disipativnost danega matematičnega modela bomo določali tako analitično kot tudi numerično.

2.2.1 Poincaréjev oscilator

Za številne biološke sisteme je značilna oscilirajoča dinamika, ki je do določene mere robustna na zunanje dražljaje [52]. Kot preprost model, s katerim lahko matematično simuliramo tovrstno dinamiko, se pogosto uporablja Poincaréjev oscilator [24, 53]. V matematični obliki ga zapišemo kot:

$$\dot{px} = -\gamma(R_0 - A)px - 2\pi\nu py, \tag{2.15}$$

$$\dot{py} = -\gamma(R_0 - A)py + 2\pi\nu px. \tag{2.16}$$

Člena $\dot{px}$ in $\dot{py}$ ponazarjata časovni odvod dinamičnih spremenljivk px in py, ki predstavljata koordinati v kartezičnem koordinatnem sistemu, A je polmer limitnega cikla v faznem prostoru in $R_0 = \sqrt{px^2 + py^2}$, razdalja od izhodišča faznega prostora do točke trenutnega položaja v faznem prostoru. Parameter ν je enak frekvenci periodične dinamike. Vidimo lahko, da je matematični model relativno enostaven in nam kot takšen omogoča izvedbo stabilnostne analize po analitični poti. Sled Jacobijeve matrike za Poincaréjev oscilator ima sledečo obliko:

$$\mathrm{Tr}(\mathbf{J}) = -\gamma(3R_0 - 2A). \tag{2.17}$$

Sistem enačb (2.15 in 2.16) ima dve rešitvi. Prva rešitev je (0,0). Če vstavimo to rešitev v enačbo (2.17), dobimo, da je $\mathrm{Tr}(\mathbf{J})_{(0,0)} = 2A\gamma$. Vrednost sledi Jacobijeve matrike je tako pozitivna in se posledično bližnje trajektorije oddaljujejo od te nestabilne točke. Izpeljava druge rešitve pa vrne izraz $\sqrt{px^2 + py^2} = A$ oz. krožnico. Sled Jacobijeve matrike je posledično enaka $\mathrm{Tr}(\mathbf{J})_{(R_0)} = -\gamma$. Tako parameter γ poda hitrost približevanja bližnjih trajektorij k atraktorju. Na slikah (2.9a, 2.9b in 2.9c) so prikazane trajektorije za tri različne vrednosti parametra γ. Vidimo lahko, kako se v primeru, ko je $\gamma = 1$, trajektorije počasi približujejo limitnemu ciklu, v primerjavi s primerom, ko je $\gamma = 1000$, in se trajektorije zelo hitro vrnejo k atraktorju. Privlak atraktorja oz. lokalna disipativnost vpliva tudi na rigidnost sistema oz. njegovo vodljivost. Da bi prikazali ta koncept, smo Poincaréjev oscilator vzbujali s periodično funkcijo $\varepsilon \sin(2\pi\nu_v t)$, kjer ε ponazarja amplitudo zunanjega vzbujanja in ν_v

frekvenco, ki jo želimo sistemu vsiliti. Dinamiko oscilatorja obravnavamo kot sinhrono z zunanjim vzbujanjem, ko pade razlika med frekvenco oscilatorja in frekvenco zunanjega vzbujanja pod vrednost 10^{-3}. Rezultati simulacije za primera $\gamma = 1$ in $\gamma = 1000$ so prikazani s slikama (2.9d in 2.9e).

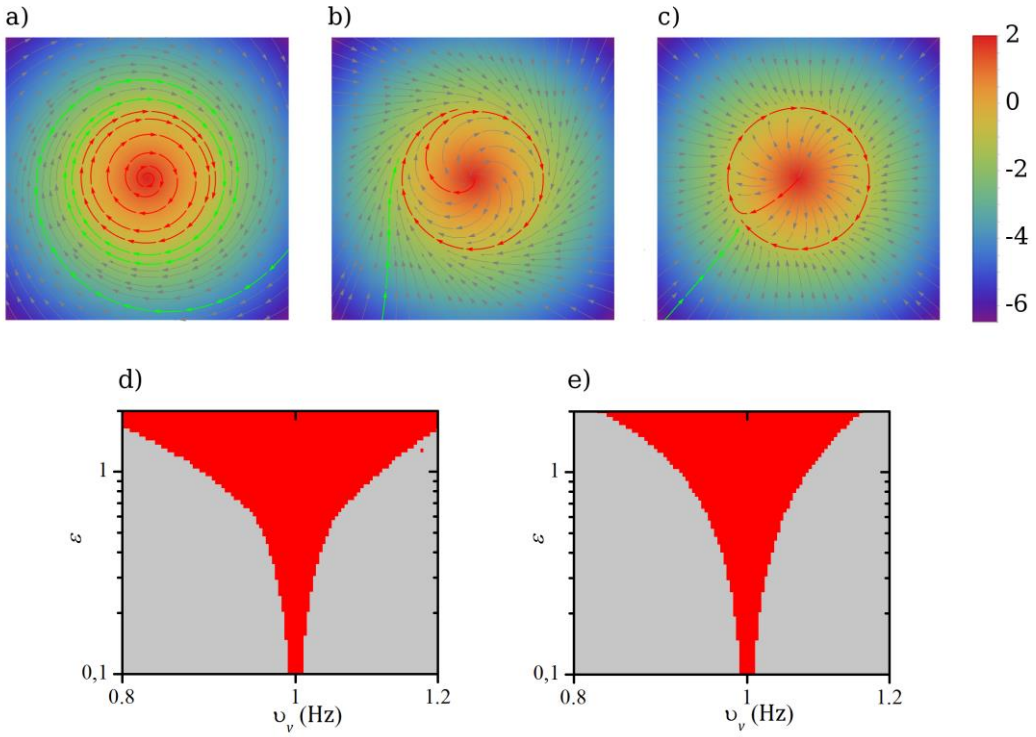

Slika 2.9: Prikaz trajektorij Poincaréjevega oscilatorja in lokalne disipativnosti faznega prostora za primere a) $\gamma = 1$, b) $\gamma = 10$ in c) $\gamma = 1000$ ter prikaz območja frekvenčne prilagojenosti oscilatorja z zunanjim vzbujanjem v od frekvence ν_v in amplitude ε zunanjega vzbujanja za primera d) $\gamma = 1$ in e) $\gamma = 1000$. Rdeče obarvano območje v d) in e) ponazarja območje, kjer je razlika med frekvenco oscilatorja in frekvenco zunanjega vzbujanja manjša od 10^{-3}.

Iz prikazanega na sliki (2.9) je zelo nazorno razvidno, kako parameter γ, ki odraža stopnjo disipativnosti sistema, vpliva na odzivanje sistema na določeno zunanje vzbujanje. V primeru, ko je vrednost parametra γ velika in je sistem tudi bolj disipativen, bo zunanja perturbacija hitro izzvenela (glej sliko 2.9c). V primeru majhne vrednosti parametra γ pa potrebuje sistem daljši čas, da se po zunanji motnji vrne k atraktorju (glej sliko 2.9a). Vidimo, da so šibko disipativni sistemi bolj dovzetni na zunanje vplive in so zato tudi bolj vodljivi [24].

2.2.2 Model Brusselator

Naslednji matematični model, ki ga bomo kasneje uporabili v naših simulacijah, je Brusselator. Ta model se pogosto uporablja kot paradigmatični teoretični model za avtokatalitične reakcije [54, 55]. Matematičen zapis modela ima obliko:

$$\dot{u} = a + u^2 v - u(b+1), \tag{2.18}$$

$$\dot{v} = bu - u^2 v, \tag{2.19}$$

kjer sta u in v dinamični spremenljivki sistema, a ter b pa parametra, ki določata dinamične lastnosti tega matematičnega modela. V vseh nadaljnjih simulacijah bomo vrednost drugega parametra postavili na $b = 2{,}5$. V nasprotju s Poincaréjevim oscilatorjem, katerega dinamika se zmeraj ujame v limitni cikel, se lahko Brusselator nahaja v dveh dinamičnih režimih. Zaradi relativno preproste oblike modela lahko tudi v tem primeru napravimo stabilnostno analizo sistema z analitičnimi pristopi. Sistem ima eno fiksno točko, ki je enaka $(a, b/a)$. Da določimo stabilnost le-te, izrazimo sled Jacobijeve matrike $\mathrm{Tr}(\mathbf{J})$, ki ima obliko:

$$\mathrm{Tr}(\mathbf{J}) = -u^2 + 2uv - (b+1). \tag{2.20}$$

Če upoštevamo fiksno točko sistema $(a, b/a)$ v izrazu za sled Jacobijeve matrike, zapišemo $\mathrm{Tr}(\mathbf{J})_{(a,b/a)} = -a^2 + b - 1$. Iz zapisanega lahko v nadaljevanju napovemo, da je fiksna točka nestabilna tako dolgo, dokler velja $a < \sqrt{b-1}$. V tem primeru je atraktor limitni cikel. Ko pa parameter a preseže mejno vrednost $a < \sqrt{b-1}$, postane fiksna točka $(a, b/a)$ stabilna. Ker točke, ki sestavljajo atraktor, ne moremo podati eksplicitno, odvisnost lokalne disipativnosti od parametra a določimo numerično. Z numerično simulacijo tako rešimo sistem enačb (2.18) in (2.19). V teku simulacije sistemu dovolimo, da se relaksira k atraktorju, in sprotno računamo vrednost sledi Jacobijeve matrike, zapisane v enačbi (2.20), stacionarne točke u^* spremenljivke u. Bifurkacijski diagram je skupaj s potekom lokalne disipativnosti prikazan na sliki (2.10a). Opazimo lahko, da zavzema povprečna lokalna disipativnost najvišjo vrednost v bližini točke bifurkacije, kjer je $a = \sqrt{b-1}$. Kadar je parameter manjši od te mejne vrednosti, se sistem ujame v limitni cikel, kjer

sistem oscilira okoli fiksne točke $(a, b/a)$. Za večje vrednosti parametra a pa postane fiksna točka $(a, b/a)$ stabilna. Trajektorija, ki bi izvirala iz poljubne točke v faznem prostoru, bi tako konvergirala k stacionarni točki $(a, b/a)$, ki predstavlja tudi atraktor. Karakteristična dinamika za ta dva dinamična režima je prikazana na slikah (2.10 b in c). Opazimo lahko, da je približevanje atraktorju mnogo počasnejše v primeru majhne disipacije (slika 2.10c).

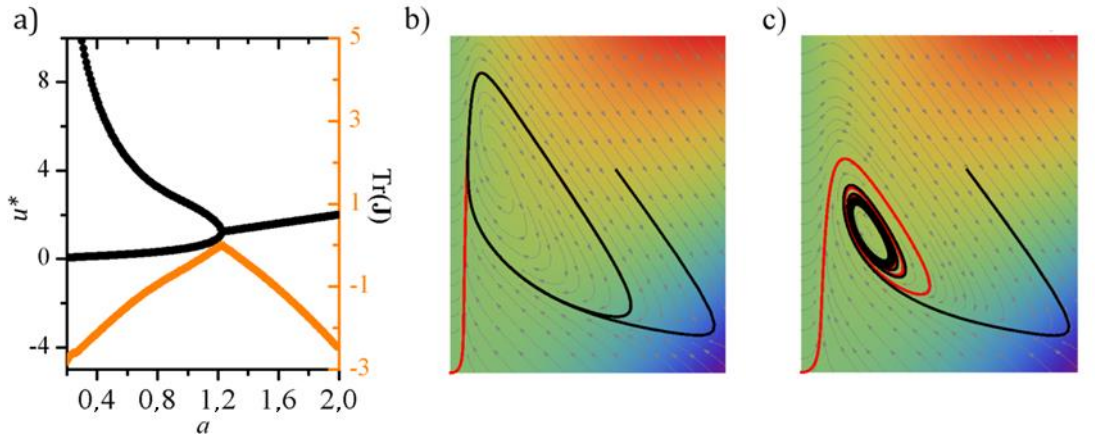

Slika 2.10: Predstavitev dinamičnih lastnosti Brusselatroja: a) bifurkacijskega diagrama skupaj s povprečno lokalno divergenco v odvisnosti od parametra a ter prikaz dveh karakterističnih trajektorij za primera b) $a = 0{,}8$ in c) $a = 1{,}2$.

Da proučimo frekvenčno prilagodljivost sistema v odvisnosti od njegove disipativnosti, tudi v tem primeru sistem vzbujamo z zunanjo funkcijo $\varepsilon \sin(2\pi\nu_v t)$. Dinamiko oscilatorja obravnavamo kot sinhrono z zunanjim vzbujanjem, ko pade razlika med frekvenco oscilatorja in frekvenco zunanjega vzbujanja pod vrednost 10^{-3}. Rezultati simulacije za dve izbrani vrednosti parametra a so prikazani na slikah (2.11a in 2.11b).

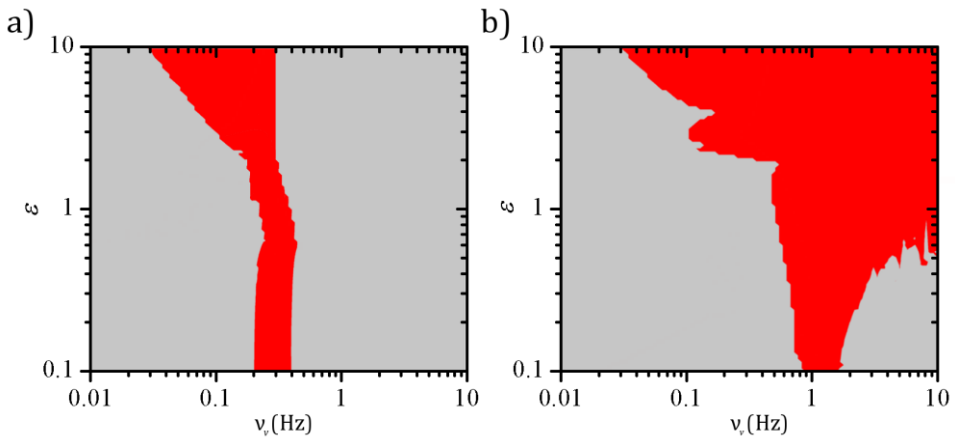

Slika 2.11: Karakterizacija prilagodljivosti Brusselatorja na zunanje vzbujanje. Barvno kodirana odvisnost vrednosti korelacije od kotne hitrosti ω in amplitude ε zunanjega vzbujanja za primera a) $a = 0{,}8$ ter b) $a = 1{,}2$.

Tudi v tem primeru lahko opazimo, da je sistem, ki ima manj negativno lokalno disipativnost, lažje vodljiv oz. vodljiv v širšem frekvenčnem območju tudi pri manjši amplitudi zunanjega signala.

2.2.3 Rulkova mapa

Leta 2001 je N. F. Rulkov predstavil dvodimenzionalni diskretni sistem, imenovan Rulkova mapa [56]. Ta matematičen model ima zelo bogato dinamiko in omogoča generiranje brstičnih oscilacij, ki so med drugim značilne za nekatere živčne celice [10]. Mapa je bila večkrat uporabljena za fenomenološki opis nevronske dinamike [56-59]. Prednost uporabe tega diskretnega sistema je predvsem v numerični učinkovitosti, kar omogoča računalniške simulacije na večjih sistemih v relativno kratkem času. Rulkova mapa ima obliko:

$$rx(t+1) = \frac{\alpha}{1+rx(t)^2} + ry(t), \tag{2.21}$$

$$ry(t+1) = ry(t) - \sigma rx(t) - \beta, \tag{2.22}$$

kjer je $rx(t)$ hitra in $ry(t)$ počasna spremenljivka ter t diskreten čas. Parametra β in σ vplivata na frekvenco oscilacij in stacionarna stanja sistema [60]. Za ta dva parametra se navadno uporabljajo majhne vrednosti reda 10^{-3}. Vlogo kontrolnega

parametra ima α, ki se v simulacijah giblje v intervalu $\alpha \in [0,5]$. Celotno dinamiko sistema v tem intervalu ponazorimo z bifurkacijkim diagramom, ki je prikazan na sliki (2.12).

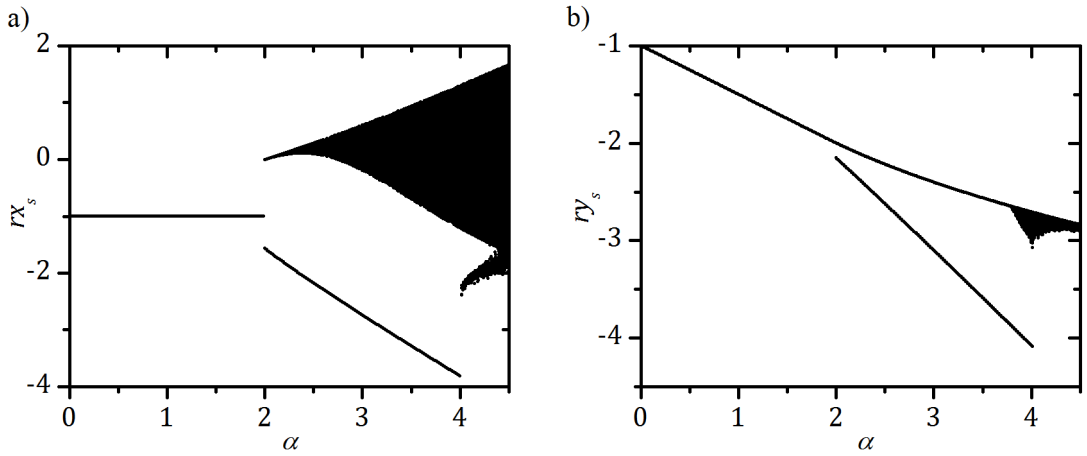

Slika 2.12: Dinamične lastnosti Rulkove mape: bifurkacijski diagram a) hitre in b) počasne spremenljivke Rulkove mape.

Kot je razvidno iz bifurkacijskega diagrama, prikazanega na sliki (2.11), se lahko sistem nahaja v treh dinamičnih režimih glede na parameter α. V primeru, ko je vrednost kontrolnega parametra v intervalu $\alpha \in [0,2]$, je ravnovesno stanje ena sama točka $\left(-1{,}1 - \frac{\alpha}{2}\right)$, h kateri sistem konvergira po zadostnem številu iteracij. Tako v intervalu $\alpha \in [2,4]$ sistem periodično oscilira. Omeniti je potrebno, da lahko pri tem prihaja do neregularnih brstičnih vrhov, ki predstavljajo visokofrekvenčno dušeno nihanje okoli stabilne veje rešitev med največjo in najmanjšo vrednostjo hitre spremenljivke. Zadnji interval v bifurkacijskem diagramu je območje kontrolnega parametra $\alpha \in [4,5]$. V tem dinamičnem območju so oscilacije kaotične. Dolžina trajanja teh brstov je pogojena s pojavom bifurkacije zaradi zunanje krize [37]. Lastnosti atraktorja pri določeni vrednosti kontrolnega parametra α lahko analiziramo z uporabo Jacobijeve matrike. V ta namen potrebujemo fiksne točke sistema. Te so v diskretnih sistemih definirane z izrazom $rx(t+m) = rx(t)$ in $ry(t+m) = ry(t)$, kjer je m zaporedno število iteracij od t-te iteracije. Če je atraktor ena točka v faznem prostoru, bo v stacionarnem stanju veljajo, da je vrednost vsake nadaljnje iteracije enaka prejšnji. V tem primeru je $m = 1$. V primerih, ko je stacionarnih stanj več, pa postane njihova določitev izredno

zapletena in mnogokrat tudi nemogoča. Stabilnostna analiza sistema z analitičnimi pristopi tako ni izvedljiva. V ta namen uporabimo primerni numerični pristop, ki nam omogoča izvedbo stabilnostne analize tudi v analitično nerešljivih sistemih. Numerični algoritmi, s katerimi lahko izvedeno takšno analizo, temeljijo na merjenem simuliranju časovnega razvoja trajektorij, ki se nahajajo v bližini atraktorja.

Ena od osnovnih lastnosti stabilnih atraktorjev je namreč ta, da privlačijo trajektorije v svoji bližini. Za kvalitativno oceno stabilnosti atraktorja uporabimo dve Rulkovi mapi. Oba sistema imata enake začetne pogoje in vrednosti parametrov. Eno od dveh map uporabimo kot referenčni sistem, ki podaja lokacijo trajektorije v faznem prostoru. Trajektorijo druge Rulkove mape pa periodično izmikamo glede na referenčni sistem za določeno majhno vrednost ϵ glede na referenčno trajetorijo in opazujemo, kako se oddaljenost med trajektorijama spreminja s časom $|x_r(t) - x_i(t)|$. Vsoto vseh absolutnih razlik v teku simulacije na koncu normiramo s številom iteracij in tako dobimo povprečno absolutno rast napake. Razlika je lahko le večja ali enaka 0. Iz tega lahko sklepamo:

1. Če je $|x_r(t) - x_i(t)| > 0$, se izmaknjen sistem oddaljuje od referenčnega atraktorja (sistem ni disipativen in atraktor ni stabilen).

2. Če je $|x_r(t) - x_i(t)| = \epsilon$, izmaknjen sistem ostaja v teku simulacije na isti oddaljenosti od referenčnega (sistem je konservativen in atraktor je navidezno stabilen).

3. Če je $|x_r(t) - x_i(t)| = 0$, se je izmaknjen sistem vrnil k referenčnemu atraktorju (sistem je disipativen in atraktor je stabilen).

Kot je razvidno iz slike (2.13a), se hitra spremenljivka po motnji vrača k referenčnemu sistemu, dokler za kontrolni parameter velja $\alpha < 3$. Od te točke naprej se hitra spremenljivka v povprečju oddaljuje od referenčnega sistema. Podrobnejšo analizo stabilnosti sistema lahko izvedemo z določitvijo njegovih Ljapunovih eksponentov, katerih število je zmeraj enako dimenziji sistema. V primeru diskretne Rulkove mape lahko sistemu določimo dva Ljapunova eksponenta. Ti eksponenti, ki jih lahko določimo numerično, predstavljajo realne dele lastnih vrednosti ustrezne Jacobijeve matrike v primeru zveznih sistemov. Označujemo jih z grško črtko λ_i, kjer

podpisan i simbolizira i-ti Ljapunov eksponent. V primeru diskretnih sistemov je dinamika bližnjih trajektorij sorazmerna z naravnim eksponentom posameznih Ljapunovih eksponentov λ_i [61]. S celotnim spektrom Ljapunovih eksponentov lahko napovemo, kakšno dinamiko ima sistem pri določeni vrednosti bifurkacijskega parametra in tudi, če je sistem disipativen ter kako močno je disipativen [62]. Algoritem za numerično določitev Ljapunovega spektra temelji na Wolfovem algoritmu [63]. Pri tem algoritmu uporabimo dva enaka matematična modela (tj. iste vrednosti parametrov in vrednosti začetnih pogojev). Enega od teh dveh modelov uporabimo za referenčnega, drugega pa v konstantnih časovnih intervalih izmikamo glede na lego referenčnega sistema v faznem prostoru. Sprotno računamo, kako se razdalja med tema trajektorijama spreminja s časom. Ob vsakem izmiku uporabimo tudi Gram-Schmidtov algoritem, s katerim sprotno generiramo ortogonalizirane vektorje v smeri razvoja dinamičnih spremenljivk ter sprotno beležimo velikosti posameznih komponent. Rezultati za naravne eksponente Ljapunovih eksponentov Λ_i so prikazani na sliki (2.13b). Vidimo lahko, da ima Λ_1 (glej sliko 2.13b) podobno obliko kot povprečna rast napake (glej sliko 2.13a). Iz poteka posameznih krivulj Λ_1 in Λ_2 lahko še dodatno razberemo dve informaciji, in sicer: atraktor počasne spremenljivke je v teku celotne simulacije zmeraj disipativen in sistem ima stabilen atraktor dokler $\alpha < 3$. V periodičnem oknu pa lahko še napovemo, da so brstični vrhovi regularni za $\alpha < 3$ in neregularni za $\alpha > 3$.

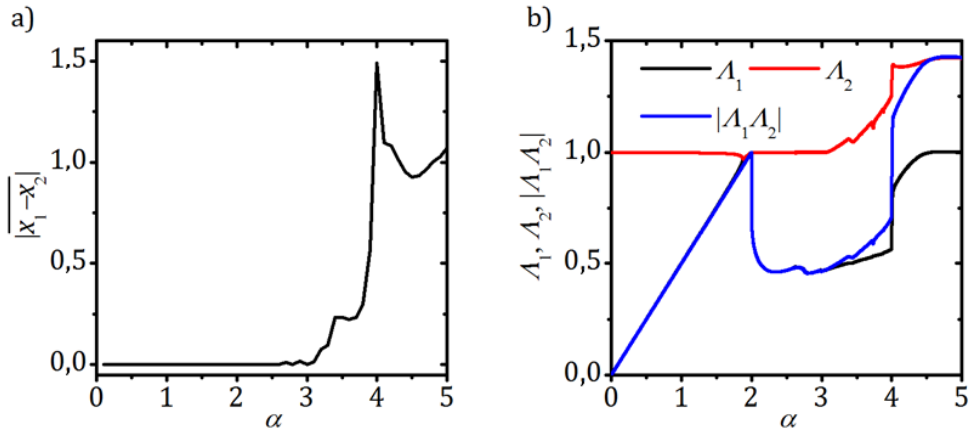

Slika 2.13: Rezultati numerične stabilnostne analize. Potek a) povprečne rasti napake in b) Ljapunovega spektra ter absolutnega produkta naravnih eksponentov Ljapunovega spektra v odvisnosti od kontrolnega parametra α.

Podobno kot sled Tr(J) odraža disipacijske lastnosti v zveznih zvezni sistemih, v primeru diskretnega sistema to odraža člen $|\Lambda_1\Lambda_2|$. Ker so posamezni členi določeni kot naravni eksponenti, velja [64]:

- $|\Lambda_1\Lambda_2| < 1$ – sistem je disipativen,
- $|\Lambda_1\Lambda_2| = 1$ – sistem je konzervativen,
- $|\Lambda_1\Lambda_2| > 1$ – sistem je kaotičen.

Tudi v tem primeru lahko opazimo, da se disipativnost v bližini bifurkacij v splošnem manjša. Podobno, kot smo to napravili do sedaj, bomo tudi v tem primeru preverili frekvenčno prilagodljivost tega modela v različnih dinamičnih režimih. Hitro spremenljivko vzbujamo s periodičnim signalom $\varepsilon \sin(2\pi\nu_v t)$, kjer je ε jakost sklopitve in ω kotna hitrost zunanjega vzbujanja. V teku simulacije računamo, kako se spreminja povprečne frekvence ν_{avg} Rulkove mape v odvisnosti od bifurkacijskega parametra α in frekvence zunanjega vzbujanja ν_v. Rezultati numerične simulacije so prikazani na sliki (2.14).

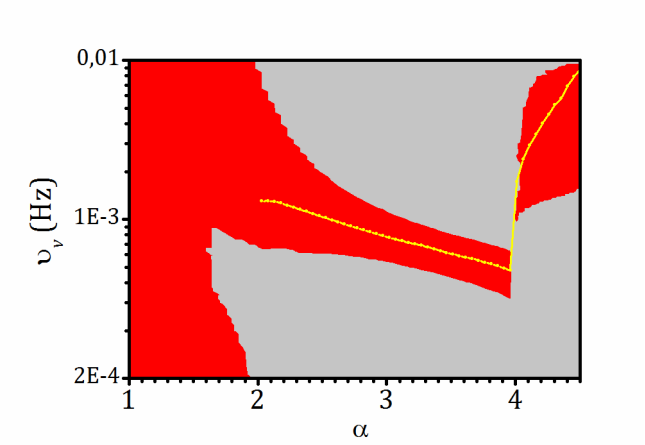

Slika 2.14: Frekvenčna prilagodljivost Rulkove mape. Območje, kjer je ν_{avg} Rulkove mapa prilagojena s frekvenco zunanjega vzbujanja, je prikazano z rdečo barvo. Rumena vrisana krivulja v grafu, ponazarja odvisnost povprečne frekvence ν_{avg} ne-sklopljene Rulkove mape.

V prvem delu, ko je $\alpha < 2$, se Rulkova mapa prilagodi poljubni frekvenci zunanjega vzbujanja. Manjše motnje v tem dinamičnem območju povzročijo, da se tako hitri

kakor tudi počasni spremenljivki poveča oz. zmanjša vrednost sorazmerno z jakostjo zunanjega signala. Zaradi stabilne fiksne točke sistem teži k njej in tako se vrhovi počasne spremenljivke pojavljajo usklajeno z zunanjim vzbujanjem vse dokler ni frekvenca zunanjega vzbujanja prevelika glede na čas, v katerem se lahko sistem vrne k stacionarnemu stanju. Ta relaksacijski čas je pogojen s produktom $|\Lambda_1\Lambda_2|$. V drugem delu, ko je $2 < \alpha < 4$, je območje frekvenčne sinhronizacije omejeno na bližnjo okolico lastne povprečne frekvence neskloplјene Rulkove mape. To območje postaja tudi ožje z večanjem bifurkacijskega parametra. V tretjem območju, ko je $\alpha > 4$, se sistem ponovno sinhronizira v okolici lastne frekvence neskloplјene Rulkove mape, vendar bolj nesimetrično. Razlago za obliko sinhroniziranega območja za periodično in kaotično območje lahko povežemo z bifurkacijskim diagramom počasne spremenljivke na sliki (2.12). Vrednosti, ki so zajete v tem diagramu, predstavljajo stacionarne točke, pri katerih v splošnem sistem preide iz ene veje stabilnih rešitev v drugo. Opazimo lahko, da se razpon vrednosti veča z bifurkacijskim parametrom v intervalu $2 < \alpha < 4$ in manjša v intervalu $\alpha > 4$. Širina območja je tesno povezana z verjetnostjo, da lahko sistem z manjšo motnjo vržemo v drugo vejo stabilnih rešitev in s tem uskladimo njegovo dinamiko z zunanjo motnjo. Širši kot je torej ta interval, manj je verjetno, da lahko z malimi motnjami dosežemo večjo spremembo v odzivu sistema. Tudi v tem primeru lahko opazimo, da je v frekvenčna prilagodljivost skladna s potekom produkta $|\Lambda_1\Lambda_2|$.

2.2.4 Rösslerjev oscilator

Zadnji matematični model, ki ga bomo predstavili v tem poglavju, je Rösslerjev oscilator. Ta dinamičen sistem je sestavljen iz treh med seboj sklopljenih diferencialnih enačb in se v splošnem uporablja v primerih, kjer želimo v numeričnih simulacijah generirati kaotično dinamiko. Matematičen zapis tega modela ima sledečo obliko:

$$\dot{kx} = -ky - kz, \tag{2.23}$$

$$\dot{ky} = kx + a_r ky, \tag{2.24}$$

$$\dot{kz} = b_r + kz(kx - c_r). \tag{2.25}$$

Zaradi kompleksnosti modela za analizo dinamičnih lastnosti tudi tokrat uporabimo numerični pristop. Povprečno lokalno disipativnost atraktorja določimo z enačbo:

$$\mathrm{Tr}(\mathbf{J}) = a_r + kx - c_r. \qquad 2.26$$

Ker ne poznamo fiksnih točk sistema in tudi ne eksplicitnega zapisa aktraktorja, v tem koraku ne moremo napraviti analitične stabilnostne analize.

Ponovno določimo spekter Ljapunovih eksponentov in preko njih definiramo dinamična območja in disipativnost oscilatorja v odvisnosti od bifurkacijskega parametra, ki bo v tem primeru enak a_r. Ljapunove eksponente določimo na podoben način, ko smo jih določili v prejšnjem poglavju (2.2.3), in sicer z uporabo Wolfovega algoritma [63]. Spekter Ljapunovih eksponentov in bifurkacijski diagram sta skupaj s povprečno lokalno divergenco, določeno kot vsoto Ljapunovih eksponentov prikazana na sliki prikazana na sliki (2.15).

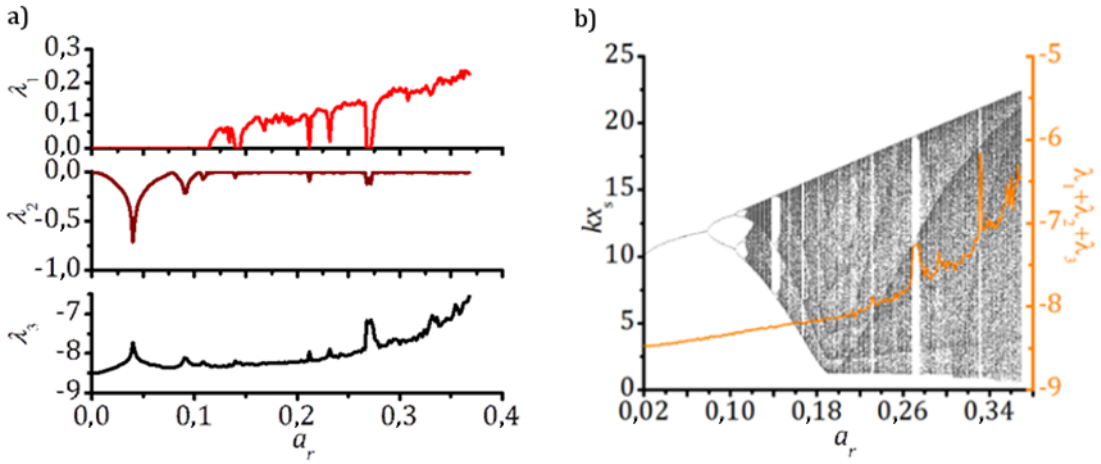

Slika 2.15: Predstavitev dinamičnih lastnosti Rösslerjevega oscilatorja: a) prikazuje odvisnost Ljapunovih eksponentov od bifurkacijskega parametra a_r in b) bifurkacijski diagram in odvisnost vsote Ljapunovih eksponentov od bifurkacijskega parametra a_r. Na bifurkacijskem diagramu so prikazani zaznani lokalni maksimumi za dano vrednost parametra a_r.

Celotni spekter Ljapunovih eksponentov nam veliko pove o dinamičnih lastnostih tega matematičnega modela. Tako lahko vidimo, da je prvi Ljapunov eksponent enak 0, dokler je za vrednosti bifurkacijskega parametra $a_r < 0{,}12$. Ker sta v tem območju preostala dva Ljapunova eksponenta manjša od 0, je atraktor limitni cikel. Za vrednosti bifurkacijskega parametra, ki so večje od $a_r > 0{,}12$, pa lahko opazimo, da postane prvi Ljapunov eksponent izmenično večji od 0. V teh intervalih, kjer je $\lambda_1 > 0$, je drugi Ljapunov eksponent $\lambda_2 = 0$. Tretji Ljapunov eksponent pa je zmeraj negativen. Wolf in sodelavci so v članku tudi klasificirali oblike atraktorjev, ki pripadajo določenemu spektru Ljapunovih eksponentov $(\lambda_1, \lambda_2, \lambda_3)$ [63]. Ti so: (+,0,0), kaotičen atraktor; (0,0,-), dvojni torus; (0,-,-), limitni cikel; in (-,-,-) fiksna točka. Iz prikazanega spektra Ljapunovih eksponentov na sliki (2.15a) je razvidna bogata dinamika, ki jo je možno generirati s tem matematičnim modelom. Sama disipativnost matematičnega modela, ki smo jo določili kot vsoto Ljapunovih eksponentov, pa v splošnem pada z večanjem bifurkacijskega parametra a_r. V kaotičnem dinamičnem režimu ($\lambda_1 > 0$) lahko tudi vidimo, da se disipativnost naglo poveča v območjih, ko postane vrednost $\lambda_1 = 0$. Pokazano je že bilo, da se lahko tudi ta matematičen modeli prilagodi frekvenci zunanjega periodičnega signala v okolici njegove lastne frekvence. To območje je možno tudi do določene mere razširiti s povečanjem amplitude zunanjega signala [65].

Omenjene štiri matematične modele oscilirajoče dinamike uporabimo za proučevanje vpliva mrežne strukture in dinamičnih lastnosti oscilatorjev na raven sinhronizacije kolektivne dinamike. V nadaljevanju zato vpeljimo še mere za kvantifikacijo sinhronizacije.

2.3 Orodja za določanje ravni sinhronizacije

Kooperativno sodelovanje znotraj sistemov, sestavljenih iz velikega števila dinamičnih elementov, zahteva medsebojno usklajenost gradnikov [14, 40, 66]. Zato ni presenetljivo, da se v številnih znanstvenih člankih raziskujejo s teoretičnega vidika sinhronizacijske lastnosti kompleksnih mrež, z aplikativnega vidika pa, kakšne lastnosti imajo realne mreže. V primerih realnih mrež, kjer imajo vozlišča mreže svojo dinamiko, se pogosto uporablja za upodobitev mreže raven

sinhronizacije med izmerjenimi odzivi posameznih elementov sistema [6, 33, 67]. Izhajamo iz primera, kjer poznamo časovne sledi vseh N elementov obravnavanega sistema. Časovno sled, ki ponazarja dinamiko i-tega elementa, označimo z $x_i(t)$.

V nadaljevanju predstavimo pristope, ki se uporabljajo za opredelitev ravni sinhronizacije kolektivne dinamike na podlagi individualnih časovnih vrst $x_i(t)$. Posebej izpostavimo tri različne mere ter za vsako od njih predstavimo in opredelimo njihove prednosti in slabosti.

2.3.1 Korelacija in koeficient determiniranosti

Korelacijski koeficient R_{ij} med i-to in j-to časovno vrsto določimo po enačbi:

$$R_{ij} = \frac{\sum_{t=1}^{T}\left[(x_i(t) - \overline{x_i})((x_j(t) - \overline{x_j})\right]}{S_{xi}S_{xj}}, \tag{2.27}$$

kjer $\overline{x_\iota}$ in $\overline{x_J}$ ponazarjata povprečno vrednost i-te in j-te časovne vrste, S_{x_i} in S_{x_j} pa njuni standardni deviaciji. Da lahko podamo kvantitativno oceno o sinhronizacije kolektivne dinamike, izračunamo korelacijske koeficiente med vsemi pari časovnih vrst in ustvarimo korelacijsko matriko **R**. V tej matriki njen ij-ti element ponazarja raven sinhronizacije med poljubnim parom časovnih vrst. Globalno stopnjo sinhronizacije kolektivne dinamike lahko izrazimo s povprečno vrednostjo korelacijskih elementov matrike **R**, kot:

$$R_{\text{avg}} = \frac{1}{N(N-1)}\sum_{i\neq j}^{N} R_{ij}. \tag{2.28}$$

Velika prednost tega pristopa je, da lahko določamo raven sinhronizacije med časovnimi vrstami, ki so si lahko tako po obliki kot tudi amplitudi različni. S to mero namreč podamo stopnjo relativne podobnosti med i-to in j-to časovno vrsto, saj primerjamo njune relativne trende. Razpon vrednosti povprečne korelacije R_{avg} je v intervalu $R_{\text{avg}} \in [-1,1]$. V primeru $R_{\text{avg}} = 1$ vse časovne vrste sledijo enakim

trendom. Kadar je $R_{\text{avg}} = 0$, med časovnimi vrstami ni možno zaznati nobene podobnosti. V takšnih primerih kolektivna dinamika ni sinhronizirana. V drugi skrajnosti, ko je $R_{\text{avg}} = -1$, imajo v povprečju pari časovnih vrst popolnoma nasprotne lastnosti (porast vrednosti v eni časovni vrsti izzove padec v drugi). Kvadratno vrednost povprečne korelacije R^2_{avg} imenujemo koeficient determiniranosti, ki predstavlja manj strogi pogoj za sinhronizacijo. Koeficient determiniranosti zavzema vrednosti v intervalu $R^2_{\text{avg}} \in [0,1]$. Da nam informacijo o ravni kavzalnosti trendov, torej, kolikokrat je določeni trend v i-ti časovni vrsti izzval zmeraj enaki trend v j-ti časovni vrsti. Vrednost R^2_{avg} lahko opišemo tudi kot vrednost, ki podaja, kolikšen odstotek variacij v i-ti časovni vrsti lahko razložimo s potekom j-te časovne vrste.

2.3.2 Fazna sinhronizacija

Naslednji pristop, uporabljen za določanje ravni sinhronizacije, je povprečna fazna sinhronizacija, ki jo označimo z r_{avg}. Ta mera predstavlja še šibkejši pogoj sinhroniziranosti kot R^2_{avg}. Pri tej meri sinhronizacije je potrebno najprej prečesati posamezne časovne vrste po lokalnih maksimumih ali minimumih ter zabeležiti čase n_i-tih lokalnih ekstremov $t_i(n_i)$, in to za vse časovne vrste. Med dvema zaporednima lokalnima ekstremoma i-te časovne sledi nato interpoliramo potek faze, ki se med njima linearno povečuje. To narekuje naslednja enačba:

$$\varphi_i(t) = 2\pi\left([n_i - 1] + \frac{t - t_i(n_i)}{t_i(n_i) - t_i(n_i - 1)}\right), \qquad 2.29$$

kjer je $\varphi_i(t)$ faza i-te časovne sledi ob času t, n_i zaporedni lokalni maksimum $(n_i = 0,1,2, \dots, Z_i)$ pri čemer je Z_i največje število lokalnih maksimumov i-te časovne sledi. Čas, ob katerem je bil zaznan posamezen lokalni maksimum v i-ti časovni vrsti, je označen s $t_i(n_i)$. Na sliki (2.16) je ponazorjeno, kako na podlagi časovne vrste določimo potek faze.

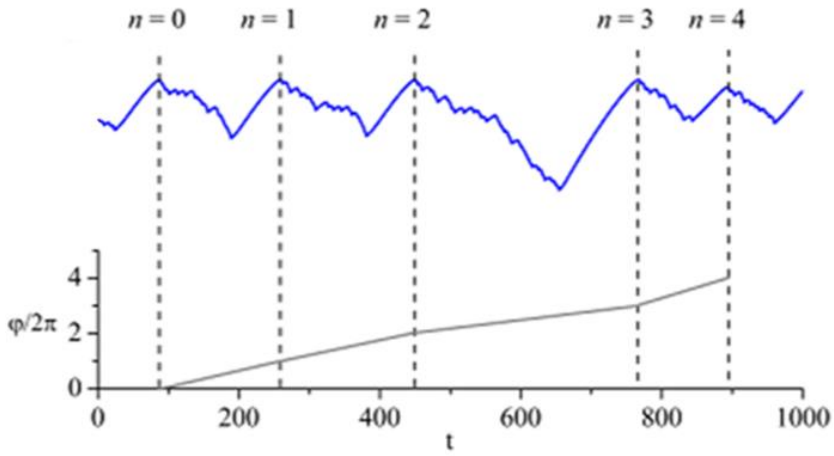

Slika 2.16: Shematski prikaz določanja poteka faze časovne vrste. Modra krivulja ponazarja časovno vrsto, ki smo ji določili lokalne maksimume. Zaporedni lokalni maksimumi so pripisani nad modro krivuljo. Pod njo je prikazan pripadajoči potek faze, ki se med dvema zaporednima lokalnima maksimumoma linearno povečuje.

Po določitvi poteka posameznih faz $\varphi_i(t)$ v naslednjem koraku izračunamo trenutne vrednosti fazne sinhroniziranosti $r(t)$, ki jo določimo kot.

$$r(t) = \frac{1}{N}\sum_{i=1}^{N} e^{i\varphi(t)} . \qquad 2.30$$

Nazornejši pomen zveze med spremenljivkama $\varphi_i(t)$ in $r(t)$ je prikazan na sliki (2.17), ki predstavlja geometrično interpretacijo trenutne vrednosti fazne sinhronizacije $r(t)$.

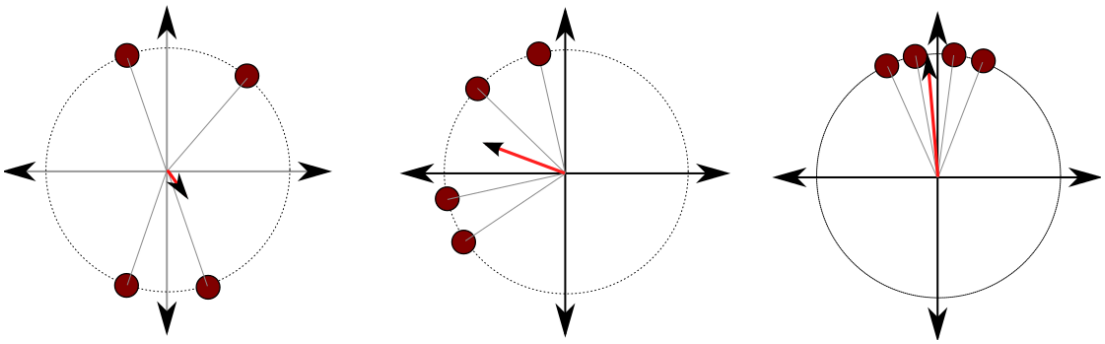

Slika 2.17: Prikaz geometrične interpretacije trenutne vrednosti fazne sinhronizacije $r(t)$. Velikost rdeče puščice predstavlja stopnjo fazne sinhronizacije v posameznih primerih.

Raven kolektivne fazne sinhronizacije r_{avg} nato določimo tako, da seštejemo vse trenutne vrednosti fazne sinhronizacije in vsoto delimo z dolžino časovnih vrst:

$$r_{\text{avg}} = \frac{1}{T}\sum_{t=1}^{T} r(t). \qquad 2.31$$

Bistvena razlika med povprečno korelacijo R_{avg} in povprečno fazno sinhronizacijo r_{avg} je v tem, da R_{avg} podaja raven usklajenosti dveh časovnih vrst v smislu, kako sta si le-ti podobni. Mera povprečne fazne sinhronizacije pa odraža stopnjo sočasnega nastopanja lokalnih ekstremov v časovnih vrstah. Vrednosti povprečne fazne sinhronizacije se enako kot v primeru R^2_{avg} nahajajo v intervalu $r_{\text{avg}} \in [0,1]$. V primeru, ko je vrednost $r_{\text{avg}} = 1$, se lokalni ekstremi v vseh časovnih sledeh pojavljajo sočasno. Vrednost $r_{\text{avg}} = 0$ za povprečno fazno sinhronizacijo pa ponazarja popolnoma neusklajeno nastopanje lokalnih ekstremom v časovnih vrstah.

3 ANALIZA KOLEKTIVNE DINAMIKE DIFUZIVNO SKLOPLJENIH OSCILATORJEV V MREŽI

V naravi obstaja veliko sistemov, t.i. mnogodelčnih sistemov, v katerih množica interakcij med delci določa pojavno (emergentno) globalno obnašanje sistema. Pri tem je pomembno, da je zagotovljena usklajena oz. sinhronizirana kolektivna dinamika [14]. Da lahko tovrstne naravne pojave proučujemo, moramo preiti iz statičnega modela kompleksnih mrež, ki je bil predstavljen v poglavju (2.1), na model, kjer imajo vozlišča lastno dinamiko. V ta namen vozlišča mreže poselimo z matematičnimi modeli, katerih dinamika kvalitativno opisuje obnašanje določenega realnega sistema in so interakcije med vozlišči kompleksne mreže, določene z matriko sosednosti. Danes se s takšnim pristopom proučujejo biološki [37], ekonomski [68], socialni [9] in tudi tehnični sistemi [3]. Izkaže se, da se kljub heterogenim dinamičnim lastnostim posameznih elementov določenega sistema v njem pojavi določena usklajena oz. sinhronizirana kolektivna dinamika. V nadaljevanju predstavljamo naše ugotovitve, ki pojasnjujejo, kako mrežna struktura in dinamične lastnosti vozlišč vplivajo na raven kolektivne sinhronizacije. S predstavljenimi metodami lahko napovemo, kakšna mrežna topologija zagotavlja najvišjo raven sinhronizacije kolektivne dinamike pri danih dinamičnih pogojih vozlišč [10, 11, 25, 37].

3.1 Vpliv dinamičnih lastnosti vozlišč in topoloških lastnosti mreže na globalno raven sinhronizacije

Podrobnejšo analizo vplivov dinamičnih lastnosti vozlišč in topoloških lastnosti kompleksne mreže na raven kolektivne sinhronizacije naredimo na izbranem primeru Poincarejevega oscilatorja (poglavje 2.2.1). Prednost tega matematičnega modela je predvsem njegova preprostost, ki nam omogoča analitičen pristop. Enačba sklopljenega Poincaréjeva oscilatorja ima obliko:

$$\dot{px}_i = -\gamma\left(R_{0,i} - A\right)px_i - 2\pi\nu_i py_i + \varepsilon\sum_{j=1}^{N} d_{ij}(px_j - px_i)\,, \tag{3.1}$$

$$\dot{py}_i = -\gamma\left(R_{0,i} - A\right)py_i + 2\pi\nu_i px_i + \varepsilon\sum_{j=1}^{N} d_{ij}(py_j - py_i), \tag{3.2}$$

kjer sta $\dot{px}_i$ in $\dot{py}_i$ časovna odvoda spremenljivk px_i ter py_i i-tega oscilatorja, faktor ε ponazarja jakost sklopitve med povezanimi oscilatorji, d_{ij} je ij-ti element matrike sosednosti z vrednostjo 1, če sta oscilatorja povezana, ter 0 v nasprotnem primeru in ν_i ponazarja frekvenco i-tega oscilatorja. Heterogenost v dinamičnih lastnostih posameznih oscilatorjev vpeljemo s Gaussovo porazdelitvijo posameznih frekvenc oscilatorjev, pri čemer je povprečna frekvenca sistema zmeraj enaka $\bar{\nu} = 1{,}0\ \mathrm{s}^{-1}$, relativna standardna deviacija v porazdelitvi frekvenc pa $0.2\bar{\nu}$. Jakost sklopitve med oscilatorji je $\varepsilon = 0{,}25$. Vsi rezultati v nadaljevanju temeljijo na povprečju 300 neodvisnih numeričnih simulacij omenjenega sistema. S tolikšnim vzorcem smo zagotovili statistično relevantnost dobljenih podatkov.

Odvisnost povprečne korelacije sistema R_{avg} od rigidnosti, ki jo za ta model podajamo s parametrom γ in parametra mrežne topologije δ, je prikazan na sliki (3.1). Opazimo, da je raven sinhronizacije kolektivne dinamike oscilatorjev na netrivialen način odvisna od mrežne topologije. Opazno je tudi, da se ta odvisnost razlikuje med rigidnimi in fleksibilni oscilatorji.

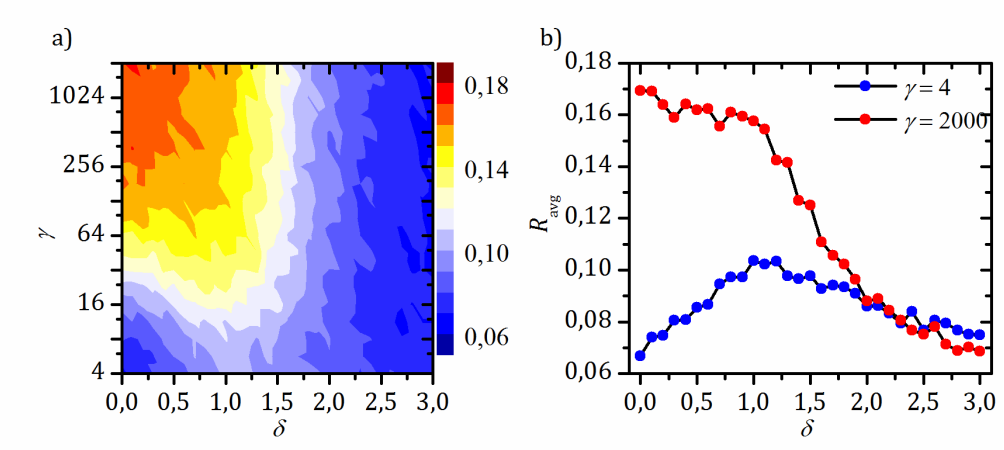

Slika 3.1: Odvisnost kolektivne sinhronizacije od mrežne topologije in disipativnosti oscilatorje. (a) Barvno kodirana vrednost povprečne korelacije R_{avg} v odvisnosti od mrežne topologije δ in rigidnosti oscilatorjev γ. (b) Odvisnost povprečne korelacije R_{avg} od mrežen topologije δ za primer $\gamma = 4$ (modri krogi) in $\gamma = 2000$ (rdeči krogi).

Rigidni oscilatorji ($\gamma = 2000$) se torej najbolje sinhronizirajo v skalno neodvisni mrežni topologiji. Ta rezultat sam po sebi ni presenetljiv, saj je bilo že v drugih študijah pokazano, da je raven sinhronizacije v pozitivnem smislu pogojena tako z učinkovitostjo mrežne topologije kakor tudi z njeno heterogenostjo [69-72]. Odvisnost učinkovitosti generiranih mrež od mrežne topologije je prikazana na sliki (2.16a). Presenetljiva je ugotovitev, da fleksibilni oscilatorji dosežejo najvišjo raven kolektivne sinhronizacije v manj heterogeni in tudi manj učinkoviti široko skalni mrežni topologiji. Ti rezultati tako kažejo, da je sinhronizacija kolektivne dinamike pogojena z vsaj dvema faktorjema, in sicer z mrežno topologijo, ki narekuje strukturno interakcijsko sliko elementov sistema, in dinamičnimi lastnostmi posameznih elementov, ki določajo, kako se posamezni elementi sistema odzivajo na dražljaje iz okolice.

Poudariti velja, da so v začetku simulacij frekvence posameznih oscilatorjev določene naključno v skladu z Gaussovo porazdelitvijo. Visoko raven sinhronizacije kolektivne dinamike lahko sistem doseže le v primeru, če se frekvence posameznih oscilatorjev dovolj prilagodijo med seboj. Z namenom ovrednotenja stopnje

frekvenčne prilagodljivosti sistema tako izračunamo povprečno absolutno spremembo frekvence sistema kot $|\overline{\Delta\nu}|$:

$$\overline{|\Delta\upsilon|} = \frac{1}{N}\sum_{i=1}^{N}\frac{1}{M_i}\sum_{m=1}^{M}\left|\upsilon_i - \upsilon_i^m\right|, \qquad 3.3$$

kjer je M_i število lokalnih maksimumov i-tega oscilatorja, člen $|\nu_i - \nu_i^m|$ ponazarja absolutno razliko med lastno frekvenco i-tega oscilatorja ν_i in njegovo dejansko frekvenco v m-tem lokalnem maksimumu ν_i^m. Vrednost ν_i^m se v teku simulacije določa kot recipročna vrednost časovnega intervala med m-tim lokalnim maksimumom in njegovim prvim predhodnikom. Rezultati frekvenčne prilagodljivosti sistema v odvisnosti od topološkega parametra δ za primer rigidnih ($\gamma = 2000$) in fleksibilnih ($\gamma = 4$) oscilatorjev je prikazana na sliki (3.2a). Vidimo, da rigidni oscilatorji dosegajo najvišjo raven frekvenčne prilagodljivosti v območju parametra δ, kjer se tipično generirajo heterogene in učinkovite mreže. Drugačno obnašanje pa opazimo v primeru fleksibilnih oscilatorjev, ki najvišjo raven frekvenčne prilagodljivosti dosegajo pri večjih vrednostih parametra δ, torej v območju mnogo bolj homogenih mrežnih struktur. Potek frekvenčne prilagodljivosti v primeru rigidnih oscilatorjev sovpada s potekom krivulje R_{avg}, prikazane na sliki (3.1b), in učinkovitosti mrežene strukture v odvisnosti od parametra δ (slika (2.16a)). Iz rezultatov sklepamo, da je raven sinhronizacije kolektivne dinamike rigidnih oscilatorjev določena z učinkovitostjo mreže oz. stopnjo integriranosti vozlišč mreže. V primeru fleksibilnih oscilatorjev pa opazimo močno podobnost med mrežnimi merami, ki odražajo stopnjo njene segregiranosti, kot so C_{avg}, r_{as}, Q in N_{c} in potekom frekvenčne prilagodljivosti, prikazane na sliki (3.2). Vendar ravno zaradi velike segregiranosti vozlišč je onemogočena visoka raven sinhronizacije kolektivne dinamike. V primeru fleksibilnih oscilatorjev se raven sinhronizacije kolektivne dinamike uravnava na podlagi kompromisa med učinkovitostjo dane mrežne strukture in zmožnostjo frekvenčne prilagodljivosti sistema v danih topoloških pogojih. To vzajemno odvisnost kvantificiramo s produktom med normirano vrednostjo učinkovitosti E^* in normirano vrednostjo povprečne absolutne spremembe frekvence $|\overline{\Delta\nu}|^*$. Rezultati, prikazani na sliki (3.2b), kažejo, da

maksimum produkta $E^*|\overline{\Delta\nu}|^*$ sovpada s točko, kjer naš sistem tudi dosega najvišjo vrednost R_{avg} (slika 3.1).

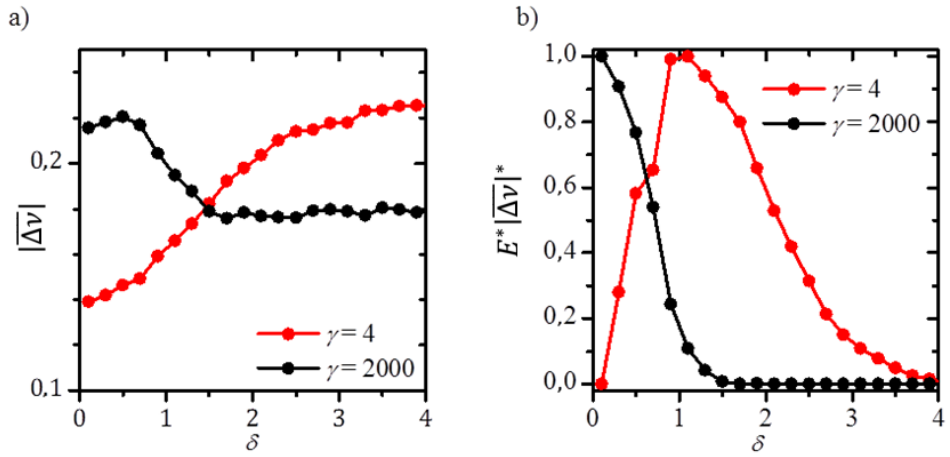

Slika 3.2: Povprečne absolutne spremembe frekvence sistema $|\overline{\Delta\nu}|$ v odvisnosti od parametra topologije δ (a) in b) potek normiranega produkta $E^*|\overline{\Delta\nu}|^*$ od parametra δ.

Za bolj poglobljen vpogled v izvor razlik med frekvenčno prilagodljivostjo rigidnih in fleksibilnih oscilatorjev v odvisnosti od mrežne strukture, izračunajmo še relativne spremembe povprečnih frekvenc posameznih oscilatorjev. Izračun napravimo ločeno za rigidne ($\gamma = 2000$) in fleksibilne ($\gamma = 4$) oscilatorje. Rezultat prilagodljivosti posameznih oscilatorjev v različnih mrežnih strukturah je prikazan na sliki (3.3).

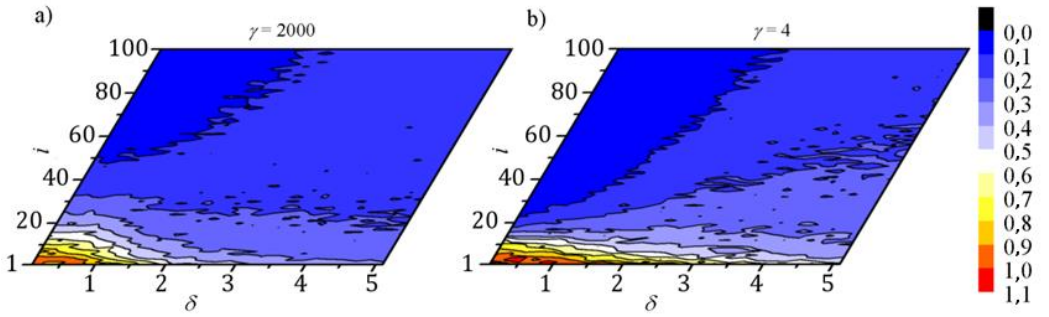

Slika 3.3: Barvno kodirane vrednosti relativne spremembe povprečne frekvence posameznih oscilatorjev v odvisnosti od mrežne topologije za primer a) rigidni in b) fleksibilni oscilatorjev.

Iz prikazanega lahko opazimo, da je frekvenčno najprilagodljiveših prvih 30 oscilatorjev pri nizkih vrednostih parametra δ. To lahko zaznamo tako v primeru fleksibilnih kakor tudi rigidnih oscilatorjev. Očitna razlika pa nastopi pri višjih vrednostih topološkega parametra δ, kjer v primeru rigidnih oscilatorjev le-ti postajajo vse manj frekvenčno prilagodljivi, medtem ko je v primeru fleksibilnih oscilatorjev to ravno obratno. V poglavju 2.2.1 smo predstavili vpliv parametera disipativnosti na frekvenčno prilagodljivost enega Poincarejevega oscilatorja. Večji kot je parameter γ in s tem rigidnost enega oscilatorja, večja mora biti amplituda zunanjega vzbujanja, da se dinamika oscilator prilagodi frekvenci zunanjega vzbujanja. Zato je po svoje presenetljivo, da najbolj heterogena mreža ne zagotavlja hkrati tudi najbolj koordinirano kolektivno dinamiko tudi v primeru fleksibilnih oscilatorjev. Na parameter γ se bomo v nadaljevanju sklicevali kot na intrinzično fleksibilnost. Predstavili bomo naše rezultate, s katerimi je možno razložiti to različno obnašanje sklopljenih rigidnih in fleksibilnih oscilatorjev. V ta namen bomo enačbi (3.1) in (3.2) zapisali v drugačni obliki:

$$\dot{px}_i = -\gamma\left(R_{0,i} - A\right)px_i - 2\pi\nu_i py_i - \varepsilon k_i px_i + \varepsilon \sum_{j=1}^{N} d_{ij} px_j \,, \tag{3.4}$$

$$\dot{py}_i = -\gamma\left(R_{0,i} - A\right)py_i + 2\pi\nu_i px_i - \varepsilon k_i py_i + \varepsilon \sum_{j=1}^{N} d_{ij} py_j. \tag{3.5}$$

Jacobijeva matrika za i-ti oscilator mreže ima obliko:

$$\mathbf{J}_i = \begin{bmatrix} -\gamma(R_{0,i} - A) - \gamma\dfrac{px_i^2}{R_{0,i}} - \varepsilon k_i & -\omega_i - \gamma\dfrac{px_i py_i}{R_{0,i}} \\ -\omega_i - \gamma\dfrac{px_i py_i}{R_{0,i}} & -\gamma(R_{0,i} - A) - \gamma\dfrac{py_i^2}{R_{0,i}} - \varepsilon k_i \end{bmatrix}. \tag{3.6}$$

Zaradi sklopitve se v sledi Jacobijeve matrike i-tega oscilatoraja pojavi novi člen: $-\varepsilon k_i$, ki vpliva na njegovo disipativnost. Dejanska disipativnost sklopljenega oscilatorja je v tem primeru odvisna tako od mrežne strukture kot od dinamičnih lastnosti drugih oscilatorjev. Disipativnost sklopljenega oscilatorja poimenujmo dinamična disipativnost $\gamma_{dyn,i}$, ki jo zapišemo kot:

$$\gamma_{dyn,i} = \mathrm{Tr}(\mathbf{J}_i) = -3\gamma R_{0,i} + 2\gamma A - 2\varepsilon k_i. \qquad 3.7$$

Dobljen rezultat kaže na to, da je zaradi sklopitev med oscilatorji njihova dinamična disipativnost $\gamma_{dyn,i}$ v splošnem večja od njihove intrinzične disipativnosti γ in jih posledično naredi bolj rigidne. V tem konkretnem primeru se tako rigidnost posameznega oscilatorja poveča sorazmerno s členom $-2\varepsilon k_i$.

Z razumevanjem dinamične disipativnosti, lahko razložimo rezultate na sliki (3.3). Vseh 100 oscilatorjev, ki so prikazani na sliki (3.3), razdelimo v 5 skupin. V prvo skupinino so zajeti oscilatorji, označeni z indeksi $i \in [1,20]$, v drugo skupino $i \in [21,40]$, v tretjo skupino $i \in [41,60]$, v četrto skupino $i \in [61,80]$ in zadnjo peto skupino $i \in [81,100]$. Za teh 5 skupin oscilatorjev si oglejmo, kako se spreminja njihova povprečna povezanost $k_{\mathrm{avg},i-j}$ in relativna sprememba v rigidnosti posameznih oscilatorjev v odvisnosti od parametra δ. Relativna sprememba v rigidnosti je določema kot razmerje med dinamično $\gamma_{dyn,i}$ in intrinzično disipativnostjo i-tega oscilatorja. Rezultati so prikazani na sliki (3.4).

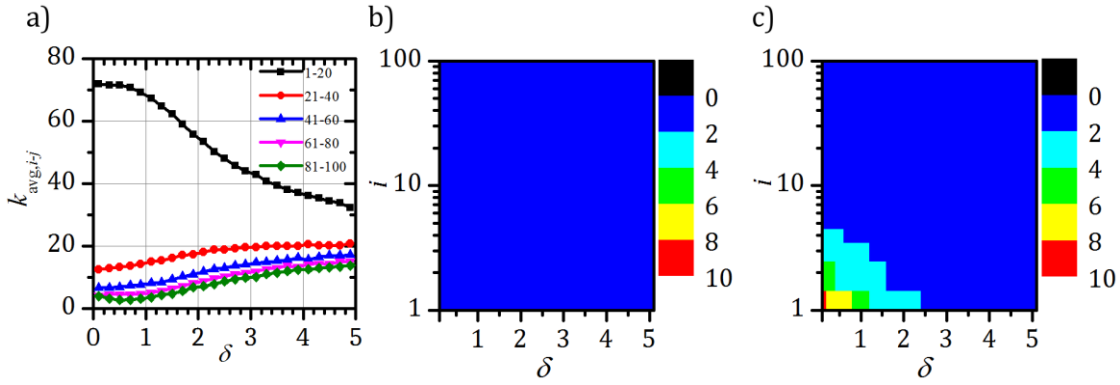

Slika 3.4: Povprečna povezanost petih skupin vozlišč (a) ter barvno kodiran graf relativne spremembe rigidnosti posameznih oscilatojev ($\gamma_{dyn,i}/\gamma$) za intrinzično rigidne (b) in intrinzično fleksibilne oscilatoje (c).

V območju $\delta < 2$ je povezanost oscilatorjev prve skupine ($i \in [1,20]$) mnogo večja od povezanosti oscilatorjev v preostalih štirih skupinah. Veliko število sosednjih vozlišč tako močno vpliva na njihovo dinamiko. Hkrati iz enačbe (3.7) vidimo, da je

dinamična disipativnost $\gamma_{dyn,i}$ oscilatorjev prve skupine, zaradi njihove velike povezanosti večja in so posledično bolj rigidni. Relativno povečanje rigidnosti je bolj izraženo v primeru oscilatorjev, ki imajo manjšo intrinzično disipativnost ($\gamma = 4$), kot pri oscilatorjih, ki so intrinzično bolj rigidni ($\gamma = 2000$). Na sliki (3.4b) vidimo, da so relativne spremembe dinamične disipativnosti $\gamma_{dyn,i}$ rigidnih oscilatorjev zanemarljive. V primeru fleksibilnih oscilatorjev, pa se njihova rigidnost poveča tudi za faktor 10 (glej sliko 3.4c). V procesu frekvenčnega prilagajanja posameznega oscilatorja je tako prisotno tekmovanje med dvema dejavnikoma. Na eni strani so številčno povezani oscilatorji mnogo bolj rigidni in s tem bolj rezistentni na zunanje motnje. Istočasno, pa jih veliko število zunanjih motenj, ki delujejo na te močno povezane oscilatorje, silijo k spremembi svoje frekvence. Prevlada enega dejavnika, pa je pogojena z intrinzično disipativnostjo. Tako so v primeru rigidnih oscilatorjev ($\gamma = 2000$), spremembe v relativni dinamični disipativnosti posameznih oscilatorjev zanemarljive in praktično neodvisne od mrežene topologije (glej sliko 3.4b). Prevladujoča gonilna sila frekvenčne prilagodljivosti rigidnih oscilatorjev je tako zunanje vsiljevanje frekvence sosednjih oscilatorjev. Ta pojav opazimo tako v primeru rigidnih kakor tudi v primeru fleksibilnih oscilatorjev (glej sliko 3.3 a in b). Vendar je v mreži, poseljeni s fleksibilnimi oscilatorji ($\gamma = 4$), relativna sprememba njihove dinamične disipativnosti bistveno večja v območju heterogenih mrežnih struktur ($\delta < 2$). Efekt povečanja rigidnosti posameznih oscilatorjev je večji od zunanjega vsiljevanja frekvence sosednjih oscilatorjev. Tako se fleksibilni oscilatorji bolje frekvenčno prilagodijo v bolj homogenih mrežnih strukturah ($\delta > 2$), kjer je dinamična disipativnost posameznih oscilatorjev primerljiva. Vendar, močno segregirana mrežna struktura v tem primeru preprečuje visoko raven sinhronizacije kolektivne dinamike. Najvišjo raven sinhronizacije kolektivne dinamike sistem doseže pri srednjih vrednostih mrežne topologije, kjer je mreža manj heterogena a še zmeraj dovolj učinkovita (glej sliko 3.2).

Omeniti velja, da lahko preveliko povečanje disipativnost oscilatorja izzove t.i. zamrtje amplitude. Znano je, da lahko do tega pojava pride v primeru prevelike jakosti sklopitve [73]. Ta pojav nastopi, ko postane sled Jacobijeve matrike za fiksno točko (0,0) negativna in postane fiksna točka stabilna. To se zgodi, ko je izpolnjen pogoj ($\varepsilon k_i > \gamma A$), kar implicira zamrtje amplitude zaradi sklopitve. V bližini pogoja $\varepsilon k_i > \gamma A$ se prične polmer limitnega cikla zmanjševati. Izpeljemo je izraz, ki podaja

odvisnost polmera limitnega cikla R_0^* od jakosti sklopitve, števila povezav in intrinzične disipativnosti oscilatorja:

$$R_0^* = A - \frac{\varepsilon k_i}{\gamma} + Rk, \qquad 3.8$$

kjer Rk odraža povprečno jakost prilivov sosedov, ki oscilator izmikajo od njegovega atraktorja. V bližini mejne vrednosti $\varepsilon k_i > \gamma A$ se prične amplituda oscilacij zmanjševati, dokler slednje popolnoma ne izzvenijo. Z namenom prikaza tega pojava lahko v teku simulacije sprotno beležimo polmere limitnih ciklov posameznih oscilatorjev in jih na koncu povprečimo ($R_{0,\mathrm{avg}}^*$). Pri tej analizi se osredotočimo zgolj na skalno neodvisno mrežno topologijo, znotraj katere pride do največjih razhajanj v povezanosti posameznih vozlišč. Za primer najbolj povezanega vozlišča in vozlišča, ki ima zgolj eno povezavo, je vrednost $R_{0,\mathrm{avg}}^*$ za dano jakost sklopitve v odvisnosti od parametra γ določena numerično in analitično. Rezultati so prikazana na sliki (3.5).

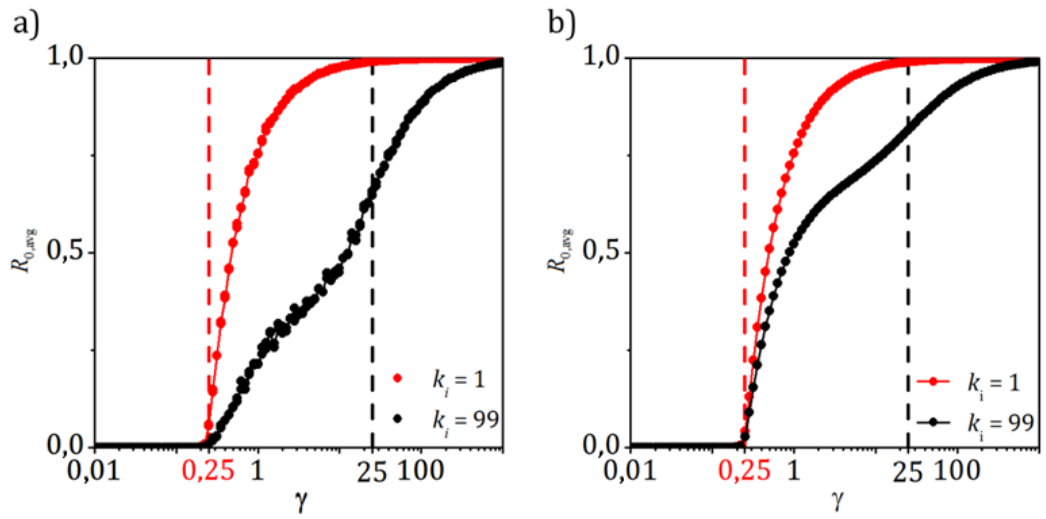

Slika 3.5: Povprečne vrednosti polmera limitnega cikla $R_{0,\mathrm{avg}}^*$, določene a) z numerično simulacijo in b) na osnovi teoretične napovedi. Prikazane so vrednosti za oscilator s povezanostjo $k_i = 1$ (rdeči krogi) in oscilator s povezanostjo $k_i = 99$ (črni krogi) v skalno neodvisni mreži. Jakost sklopitve je $\varepsilon = 0{,}25$.

Rezultati, prikazani na sliki (3.5), potrjuejo napoved, zapisano v enačbi (3.8). Amplitude oscilatojev v fleksibilnem dinamičnem sistemu lahko močno variirajo glede na disipacijski parameter γ. Vidimo lahko, da je najmanjša vrednost disipacijskega parametra, pri kateri pride do zamrtja amplitude, enaka $\gamma = 0{,}25$ in velja za oscilatorje z zgolj eno povezavo. Od te vrednosti naprej pa se prične polmer limitnih ciklov oscilatorjev z eno povezavo hitro povečevati. Pri vrednosti $\gamma = 4$ je tako polmer limitnih ciklov oscilatorjev z eno povezavo enak 0,93. Do odmrtja oscilacij pa pride v vozliščih, ki imajo več kot 16 povezav. Vendar zaradi velikega števila vozlišč, ki imajo le nekaj povezav, tudi ta vozlišča oscilirajo zaradi kumulativnega prispevka Rk.

Univerzalno spoznanje, da se rigidni dinamični sistemi najbolje sinhronizirajo v skalno neodvisni mreži in fleksibilni dinamični sistemi v široko skalni mreži, ~~si bomo~~ v nadaljevanju prezentirajmo še na treh primerih oscilatorjev.

3.1.1 Difuzivno sklopljen Brusselator

Ugotovitve prejšnjega poglavja (3.1) preverimo na primeru modela Brusselator, ki predstavlja paradigmatičen teoretičen model za oscilarujoče avtokatalitične kemijske reakcije [54, 55]. Enačba Brusselatorja, ki je podana v poglavju (2.2.2), ima s sklopitvenim členom obliko:

$$\dot{u}_i = a_i + u_i^2 v_i - u_i(b+1) + \varepsilon \sum_{j=1}^{N} d_{ij}(u_j - u_i), \tag{3.9}$$

$$\dot{v}_i = b u_i - u_i^2 v_i + \varepsilon \sum_{j=1}^{N} d_{ij}(v_j - v_i), \tag{3.10}$$

V simulacijah postavimo jakost sklopitve na $\varepsilon = 0{,}05$ in parameter $b = 2{,}5$. Heterogenost v dinamiki posameznih oscilatorjev mreže vpeljemo z distribucijo parametra a_i, ki je med oscilatorji razporejen naključno v skladu z Gaussovo distribucijo z relativno standardno deviacijo 3 %. Obravnavamo dva primera; pri prvem, ki ponazarja rigidne oscilatorje, povprečna vrednost parametrov a_i zavzema

vrednosti 0,2. V drugem primeru, ko simuliramo fleksibilne oscilatorje, pa je povprečna vrednost parametra enaka 1,16 (glej sliko 2.5). Tudi v primeru Brusselatorja (podobno kot smo to pokazali za Poincaréjev oscilator (enačba 3.7)) se posameznemu oscilatorju rigidnost poveča sorazmerno s členom εk_i (sklopitveni členi so enaki kot v primeru Poincarejevega oscilatorja), ki je v povprečju enak $\varepsilon k_{\mathrm{avg}} \approx 0{,}25$, saj je povprečna povezanost v mreži enaka 5. V primeru rigidnih oscilatorjev velja, da je sprememba v rigidnosti posameznih oscilatorjev zaradi sklopitvenega člena zanemarljiva v primerjavi z njihovo intrinzično disipativnost $\mathrm{Tr}(\mathbf{J}) \gg \varepsilon k_{\mathrm{avg}}$. V fleksibilnem dinamičnem režimu pa je intrinzična disipativnost primerljiva s povprečno spremembo v rigidnosti. Na sliki (3.6) je prikazano, kako se povprečna korelacija sistema spreminja v odvisnosti od mrežne topologije v primeru poselitve vozlišč s fleksibilnimi in rigidnimi oscilatorji. Ponovno se izkaže, da maksimalno korelacijo rigidni oscilatorji dosežejo v skalno neodvisni mreži, medtem ko so fleksibilni oscilatorji najboljše sinhronizirani v manj heterogeni in manj učinkoviti široko skalni mreži, ko je vrednost mrežnega parametra okoli 1,3.

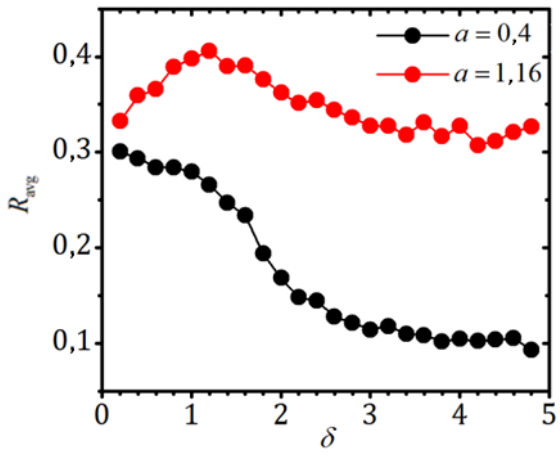

Slika 3.6: Povprečna korelacija R_{avg} v odvisnosti od parametra δ za primera dveh mrež: poseljena z rigidnimi (črna krivulja) in fleksibilnimi oscilatorji (rdeča krivulja).

3.1.2 Difuzivno sklopljene Rulkove mape

Splošnost naših ugotovitev dodatno podkrepimo na primeru mrež poseljenimi z Rulkovimi mapami, kar ponazarja prehod na diskreten oscilatorni sistem. Podrobnejša analiza tega diskretnega matematičnega modela je bila narejena v poglavju 2.2.3. Rulkova mapa s sklopitvenim členom ima obliko:

$$x(t+1) = \frac{\alpha_i}{1+x(t)^2} + y(t) + \varepsilon \sum_{j=1}^{N} d_{ij}(x_j - x_i) \ , \qquad 3.10$$

$$y(t+1) = y(t) - \sigma x(t) - \beta. \qquad 3.11$$

S tem matematičnim modelom poselimo vozlišča mreže različnih topologij. Za jakost sklopitve vzemimo $\varepsilon = 0{,}005$. Analiziramo dinamiko mrežnega sistema za dve vrednosti kontrolnega parametra α_i, kjer je dinamika nesklopljenih oscilatorjev v enem primeru rigidna in v drugem primeru fleksibilna. Za primer rigidnih oscilatorjev vzemimo $\alpha_i = 2{,}5$ in za primer fleksibilnih $\alpha_i = 4{,}1$, kjer je dinamika brstična. Rezultati simulacije so prikazani na sliki (3.7).

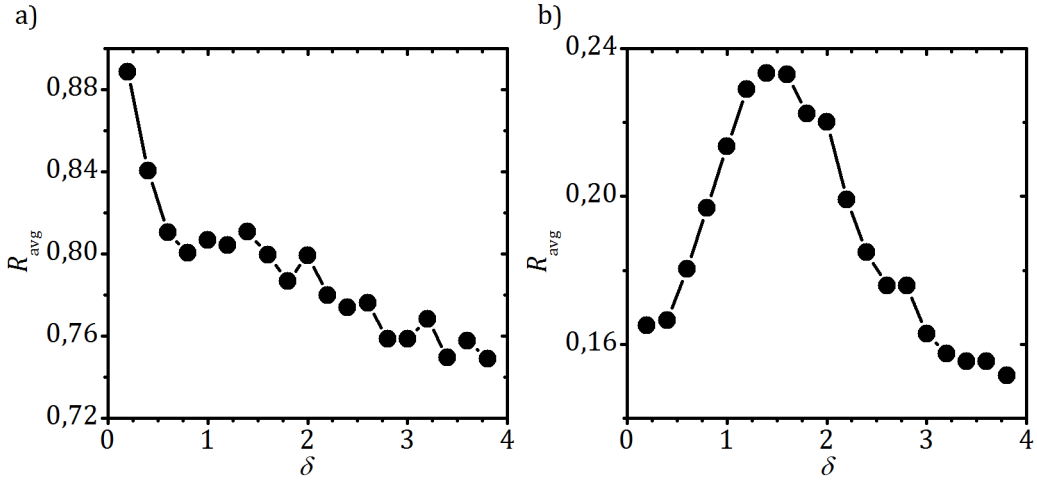

Slika 3.7: Stopnja sinhronizacije kolektivne dinamike R_{avg} v odvisnosti od mrežne topologije δ v mreži vozlišč, poseljenih z Rulkovimi mapami v a) rigidnem ($\alpha_i = 2{,}5$) in b) fleksibilnem ($\alpha_i = 4{,}1$) dinamičnem območju.

Kot napoveduje naša teorija, se v primeru rigidnih periodičnih oscilacij sistem najbolje sinhronizira v skalno neodvisni mreži, ko je vrednosti topološkega parametra $\delta = 0{,}1$ (glej sliko 3.6a). V primeru fleksibilnih oscilacij pa zagotavlja široko skalna mrežna topologija ($\delta \approx 1{,}5$) optimalno interakcijsko strukturo, pri kateri pride do največje stopnje sinhronizacije kolektivne dinamike (glej sliko 3.6b). Kljub temu, da je v tem matematičnem modelu prisotna bolj kompleksna dinamika, lahko zasledimo podoben kolektiven odziv sistema, kot v primeru Poncaréjevega oscilatorje in Brusselatorja. Neodvisno od kompleksnosti oscilacij, se izkaže fleksibilnost oz. rigidnost njihove dinamike kot univerzalna lastnost, s katero je pogojena mrežna topologija, ki zagotavlja najvišjo raven sinhronizacije.

3.1.3 Difuzivno sklopljeni Rösslerjevi oscilatorji

Kot zadnji primer obravnavajmo še en zvezni sistem, ki je tridimenzionalen, in nudi tudi kaotične dinamične vzorce. Dinamika Rösslerjevega oscilatorja, ki je bil podrobneje predstavljen v poglavju (2.2.4), je izredno bogata, kot je to tudi razvidno iz spektra Ljapunovih eksponentov (glej sliko 2.14a). Rösslerjev oscilator s sklopitvenim členom ima obliko:

$$\dot{kx_i} = -ky_i - kz_i + \varepsilon \sum_{j=1}^{N} d_{ij}(kx_j - kx_i), \tag{3.12}$$

$$\dot{ky_i} = kx_i + a_{r,i}ky_i + \varepsilon \sum_{j=1}^{N} d_{ij}(ky_j - ky_i), \tag{3.13}$$

$$\dot{kz_\iota} = b_r + kz_i(kx_i - c_r) + \varepsilon \sum_{j=1}^{N} d_{ij}(kz_j - kz_i), \tag{3.14}$$

Enačbe (3.12)-(3.14) določajo dinamiko posameznih vozlišč. Jakost sklopitve v tem primeru je $\varepsilon = 0{,}06$. Vzemimo dve vrednosti kontrolnega parametra $a_{r,i}$, kjer je dinamika v obeh primerih kaotična. Podobno kot v vseh dosedanjih primerih je rigidnost pogojena s stopnjo disipativnosti nesklopljenih oscilatorjev.

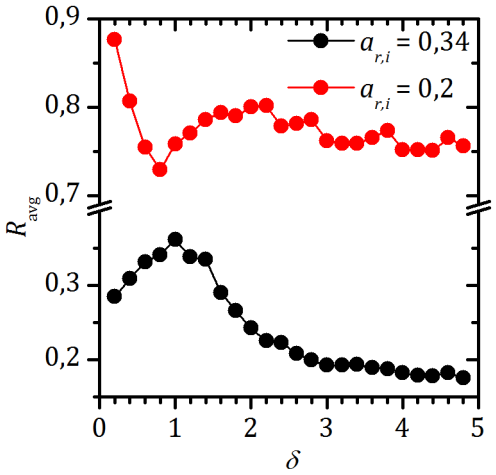

Slika 3.8: Odvisnost stopnje sinhronizacije kolektivne dinamike R_{avg} od mrežne topologije δ v primeru vozlišč, poseljenih z a) rigidnimi Rösslerjevimi oscilatorji $a_{r,i} = 0{,}2$ in b) fleksibilnimi Rösslerjevimi oscilatorji $a_{r,i} = 0{,}34$.

Tudi v tem primeru opazimo enak pojav. Kadar je mreža poseljena z rigidnimi Rösslerjevmi oscilatorji, je sinhronizacija kolektivna dinamika najvišja v sklano neodvisni mrežni topologiji. V nasprotnem primeru, ko dinamiko vozlišč mreže vodijo fleksibilni Rösslerjevi oscilatorji, pa sistem doseže najvišjo vrednost R_{avg} v široko skalni mreži.

V naše analize smo zajeli 4 različne matematične modele, ki so tako zvezni kot tudi diskretni in imajo zelo raznoliko lastno dinamiko. V vseh primerih je opažen pojav, ki smo ga napovedali in tudi razložili v poglavju (3.1). Kadar lahko dinamiko vozlišč mreže opredelimo kot fleksibilno, je raven sinhronizacije kolektivne dinamike najvišja v široko skalni topologiji mrež malega sveta. Kadar pa je dinamika vozlišč rigidna, pa predstavlja skalno neodvisna mrežna topologija interakcijsko strukturo, ki zagotavlja najvišjo raven sinhronizacije kolektivne dinamike. Dodatno težo tem spoznanjem pa deje dejstvo, da je bilo za številne biološke sisteme pokazano, da so le-ti funkcionalno povezani v široko skalno mrežno topologijo [7, 8, 28, 33, 74]. Opažanja zato implicirajo, da so številni biološki sistemi sestavljeni iz fleksibilnih celičnih oscilatorjev. V nadaljevanju tega poglavja se opremo na to predpostavko in za primer mrež nevronov analizirali vlogo hitrosti širjenja signala na raven sinhronizacije kolektivne dinamike v različnih mrežnih topologijah [10].

3.2 Vpliv hitrosti širjenja signala na raven sinhronizacije kolektivne dinamike fleksibilnih oscilatorjev v prostorsko vpeti mreži

Sinhrona aktivnost živčnih celic je tema številnih teoretičnih kot tudi eksperimentalnih študij [75, 76]. Znano je, da pretok informacij v teh mrežah ne poteka neskončno hitro. Tako se v splošnem signali prevajajo po aksonih z neko končno hitrostjo, kar pa ima za posledico, da v splošnem prispe signal s časovno zakasnitvijo do ciljnih živčnih celic. Velikostni red, s katerim se širijo signali po aksonih, je reda nekaj m/s in tako privede do zakasnitev nekaj milisekund [77]. Raziskave so pokazale, da lahko zakasnitve v komunikaciji med nevroni znatno vplivajo na njihovo časovno-prostorsko koordinacijo dinamike [78, 79]. V naši študiji uporabimo algoritem prostorsko vpete mreže (poglavje 2.1.2) za generiranje različnih tipov mrežnih struktur, kjer so vozlišča mreže porazdeljena v tridimenzionalni kocki.

Številne raziskave kažejo, da ima funkcionalna mreža možganov izražene lastnosti široko skalnih mrež [6, 29, 46, 80]. V prejšnjih poglavjih smo pokazali, da takšna mrežna topologija zagotavlja najvišjo raven sinhronizacije kolektivne dinamike, kadar so oscilatorji fleksibilni. Tako bomo mrežo poselili z oscilatorji, ki imajo fleksibilno dinamiko. Zakasnitev v komunikaciji med oscilatorji mreže pa vpeljemo kot posledico končne hitrosti širjenja signala po mreži in študirali bomo, kakšen vpliv ima ta hitrost na kolektivno sinhronizacijo.

Tipično brstično aktivnost živčnih celic simuliramo z Rulkovo mapo (glej poglavje 2.2.4). V poglavju 3.1.2 je sicer že zapisana matematična oblika sklopljenih Rulkovih map, a brez upoštevanja zakasnitve pri prenosu informacij. Ob vključitvi še tega učinka, se enačba (3.10) ustrezno spremeni:

$$x(t+1) = \frac{\alpha_i}{1+x(t)^2} + y(t) + \varepsilon \sum_{j=1}^{N} d_{ij}(x_j(t+\tau_{ij}) - x_i(t)) \ . \qquad 3.15$$

V sklopitvenem členu v enačbi (3.15) je upoštevano, da signal iz vozlišča i prispe do vozlišča j s časovnim zamikom τ_{ij}. Heterogenost v dinamiki vozlišč vpeljemo z distribucijo vrednosti kontrolnega parametra α_i, ki sledi potenčni funkciji oblike $P(\alpha) \sim \alpha^{-\beta}$, kjer je eksponent enak $\beta = 2{,}5$. Vrednosti kontrolnih parametrov α_i posameznih oscilatorjev je razporejen znotraj območja $\alpha_i \in [4.1, 4.4]$, kar zagotovi brstično dinamiko celega ansambla nevronov. Rezultati, prikazani v poglavju 2.2.3, kažejo, da je povprečna frekvenca večja pri večjih vrednostih parametra α. Takšna porazdelitev dinamičnih lastnosti oscilatorjev je vpeljana, ker posnema eksperimentalno izmerjeno aktivnost živčnih celih. Namreč, pokazano je, da v nevronski mreži obstaja majhno število t.i. vodilnih celic (»pacemaker-jev«), katerih namen bi naj bil sprožiti odziv njegovih sosednjih celic, ki delujejo kot globalni pobudniki nevronske aktivnosti [81].

Sklopitveni člen v enačbi (3.15) vsebuje faktor τ_{ij}, ki ponazarja zakasnitev, s katero prispe signal od i-tega do j-tega oscilatorja. To je posledica končne hitrosti, s katero se signal širi med vozlišči mreže. Zakasnitev τ_{ij}, s katero bo signal prispel do ciljnega vozlišča, določimo z enačbo:

$$\tau_{ij} = \frac{I_{ij}}{v}, \tag{3.16}$$

kjer je v je hitrost širjenja signala med vozlišči. Ker je uporabljen matematičen model diskreten, izračunane zakasnitve obravnavamo kot celo število, ki ga zaokrožimo navzdol. Vozlišča mreže so naključno razporejena v kocki, s stranicami dolžine 1. Največja možna razdalja med dvema vozliščema je tako lahko $\sqrt{3}$. Hitrost $v = 2$ tako ponazarja neskončno hiter prenos signalov med vozlišči, saj implicira $\tau_{ij} = 0$. Hitrosti manjše od $v = 2$ pa posledično izzovejo končno zakasnitev signala τ_{ij}, ki je pogojen z dolžino povezav med vozlišči. Z variacijo hitrosti tako lahko simuliramo zakasnitve, ki bi nastopile v nevronskih mrežah.

Zaradi uporabe diskretnega sistema, ki je časovno manj potraten, lahko v tej simulaciji uporabimo 200 vozlišč in tako tudi povečamo statistično relevantnost rezultatov. Ostale vrednosti parametrov so enake kot predhodno opisano v poglavju

2.2.2 in 3.1.2. Raven kolektivne sinhronizacije v kolektivni dinamiki podamo s povprečno vrednostjo fazne sinhronizacije, ki je podrobneje opisana v poglavju 2.3.2. Ta mera je implementirana, ker želimo ugotoviti, kako koordinirano prehajajo posamezni oscilatorji mreže v območje brstične dinamike. Rezultati numerične simulacije so prikazani na sliki (3.9).

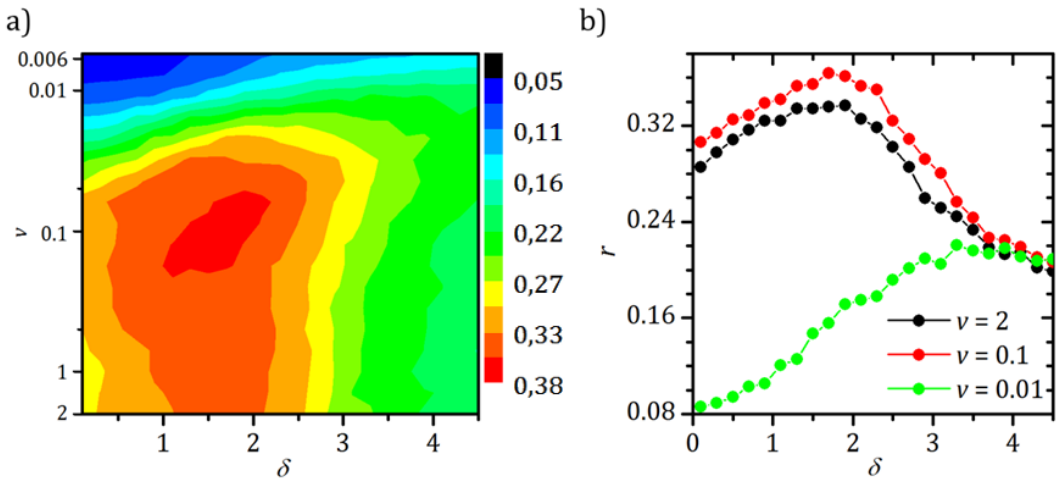

Slika 3.9: Vpliv hitrosti širjenja signala na sinhronizacijo oscilatorjev v mreži: (a) barvno kodirana površina grafa odraža vrednost fazne sinhronizacije v dani mrežni topologiji pri dani hitrosti širjenja signala, (b) odvisnost fazne sinhronizacije od parametra mrežne topologije za tri izbrane preseke barvnega grafa.

Na sliki 3.9 vidimo, da je za hitrosti $v > 0{,}02$, kolektivna dinamika najbolj koherentna za srednje vrednosti topološkega parametra δ. Pri manjših vrednostih hitrostih je kolektivna dinamika bolj sinhronizirana pri večjih vrednostnih parametra δ, kjer so vozlišča mreže povezana v bolj regularno mrežo. Iz rezultatov je tudi razvidno, da poleg optimalne mrežne konfiguracije obstaja tudi optimalna hitrost širjenja signala, ki je približno enaka $v \approx 0{,}1$. Pri tej hitrosti tako sistem doseže najvišjo raven fazne sinhronizacije.

Do sedaj smo predstavili rezultate teoretičnih dognanj o sinhronizacijskih lastnosti kompleksnih mrež, katerih vozlišča so poseljena z različnimi oscilatorji. Pokazano je, da se v primeru rigidnih celičnih oscilatorjev mreže najbolje sinhronizirajo v heterogeni skalno neodvisni mreži. V primerih fleksibilnih celičnih oscilatorjev pa se

najvišja raven sinhronizacije kolektivne dinamike doseže v manj heterogeni široko skalni mreži. Omenjeno je veljavno neodvisno od kompleksnosti uporabljenega matematičnega modela. Poleg optimalne topologije mreže pa smo ugotovili, da na sinhronizacijske lastnosti kompleksnih mrež, pomembno vpliva tudi hitrost potovanja signalov med vozlišči mrež. V nadaljevanju bomo naše ugotovitve aplicirali na realne mreže – funkcionalne povezanosti celic beta v tkivnih rezinah trebušne slinavke miši.

4 ANALIZA TOPOLOŠKIH LASTNOSTI FUNKCIONALNIH MREŽ CELIC BETA

Teoretska orodja, ki so bila predstavljena in uporabljena v prejšnjih poglavjih, bomo v nadaljevanju uporabili za preučevanje kolektivne dinamike celic beta v tkivnih rezinah trebušne slinavke miši. Pristop in sledeče analize temeljijo na ekstrakciji vzorcev funkcionalne povezanosti celic beta. Primarna naloga teh celic je, da z izločanjem inzulina uravnavajo raven glukoze v krvi in tako skrbijo za energijsko homeostazo celotnega telesa [82]. V primerjavi z drugimi študijami [34, 83] se v naših raziskavah osredotočimo na preučevanje strukture funkcionalne povezanosti teh celic znotraj fiziološko relevantnih koncentracij glukoze. Obstoječo metodologijo za konstrukcijo funkcionalne povezanosti celice beta [33] ustrezno nadgradimo, kar omogoči natančno vrednotenje sinhronosti dinamiki znotrajceličnega kalcija. Sistematično analiziramo mrežne lastnosti tkivnih vzorcev pri različnih koncentracijah glukoze, in sicer v mejah od 6 mM do 12 mM. Analiza ekstrahiranih funkcionalnih mrež razkriva, da so topološke lastnosti mreže in doseg interakcij močno odvisne od stimulacijske koncentracije glukoze. Eksperimenti, pri katerih se koncentracija korakoma zvišuje, nam omogočajo tudi preučevanje dinamične evolucije mrež. Naši rezultati pričajo o obstoju jasno izraženih lokalnih skupnosti v strukturi funkcionalne povezanosti, kar kaže na razdrobljeno organiziranost sincicija celic beta v Langerhansovem otočku trebušne slinavke. Uporabljeni teoretični pristopi omogočajo detekcijo najbolj pomembnih celic v smislu iniciatorjev in mediatorjev signalov. Predstavljeni rezultati vodijo do novih in poglobljenih spoznanj s področij mehanizma delovanja in funkcionalne organiziranosti sincicija celic beta, ki s konvencionalnimi metodološkimi orodij ne bi bila mogoča.

4.1 Postopek konstruiranja funkcionalne mreže

Ekstrakcija funkcionalne povezanosti celic beta temelji na ustaljeni metodi, pri kateri se povezanost določi na podlagi stopnje koreliranosti med izmerjenimi časovnimi vrstami znotrajceličnih kalcijevih signalov [33]. Slednji so bili posneti na Inštitutu za fiziologijo Medicinske fakultete, Univerze v Mariboru s konfokalnim

mikroskopom z laserskim skenerjem. Ta eksperimentalna tehnika omogoča hkratne in dolgotrajne meritve dinamike v velikem številu celic, in to v intaktni tkivni rezini. Surovi izmerjeni podatki vsebujejo šum, artefakte kot so fotodestrukcija, ter spremembe bazalnih vrednosti kalcija, ki niso predmet zanimanja. Iz tega razloga je za natančno analizo potrebno izmerjene časovne vrste prehodno še dodatno obdelati. V naših analizah uporabimo Huang-Hilbertovo dekompozicijo [84], ki omogoča zelo natančno izločanje dinamičnih komponent iz časovnih vrst, ob tem pa vsebuje relativno malo prostih parametrov, kar omogoča avtomatizirano obdelavo.

4.1.1 Obdelava časovnih vrst z EEMD metodo

Z namenom izključevanja artefaktov in šuma iz časovne vrste predhodno uporabimo posodobljeno obliko Huang-Hilbertove dekompozicije, imenovane tudi empirična dekompozicija signala (ang. »Empirical Ensemble Mode Decomposition – EEMD«) [84]. Pri tej metodi eksperimentalno dobljene časovne vrste i-te celice $x_i(t)$ numerično razstavimo na t.i. enostavne lastne funkcije (ang. »Intrinsic Mode Functions – IMFs"). V prvem koraku dekompozicije generiramo beli šum $w_j(t)$, kjer j ponazarja j-to generacijo belega šuma ob času t. Vrednost generiranega šuma se nahaja v intervalu $w_j(t) \in [-0{,}1, 0{,}1]$ in ga prištejemo vsaki eksperimentalno dobljeni časovni vrsti $x'_{i,j}(t) = x_i(t) + w_j(t)$. Signal $x'_i(t)$ prečešemo po lokalnih ekstremih in nato ločeno interpoliramo zgornjo ovojnico, ki objema točke lokalnih maksimumov in spodnjo ovojnico, ki objema točke lokalnih minimumov. Povprečna vrednost med zgornjo in spodnjo ovojnico ob času t označimo z $m_{j,1}(t)$ in odštejemo od $x'_{i,j}(t)$. Tako dobimo razliko $h_{j,1}(t)$. V naslednjem ciklu uporabimo $h_{j,1}(t)$ kot vhodni signal in ponovimo prej opisani postopek. Nato izračunamo razliko med $m_{j,2}(t)$ in $h_{j,1}(t)$ ter dobimo razliko $h_{j,2}(t)$. V splošnem lahko ta postopek zapišemo kot :

$$h_{j,k}(t) = m_{j,k} - h_{j,(k-1)}\,. \qquad 4.1$$

V enačbi (4.1) k ponazarja k-to ponovitev procedure, ki se ponavlja, dokler ni standardna deviacija med signaloma $h_{j,k}(t)$ in $h_{j,(k-1)}$ manjša od definirane meje

(10^{-5}). Ko je ta pogoj izpolnjen, postane razlika $h_{j,k}(t)$ prva enostavna lastna funkcija i-te časovne vrste $IMF_{i,1}^{j}(t)$ med j-to generacijo belega šuma. V prvi enostavni lastni funkciji je zajeta dinamika z najvišjo frekvenco. Naslednjo enostavno lastno funkcijo vhodnega signala $x_i(t)$ določimo tako, da iz njega izločimo $IMF_{i,1}^{j}(t)$. V tako izračunanem ostanku $o_{i,j}(t) = x'_{i,j}(t) - IMF_{i,1}^{j}(t)$ ni zajeta dinamika prve enostavne lastne funkcije. Ostanek $o_{i,j}(t)$ sedaj uporabimo kot vhodno časovno vrsto, za katerega določimo $IMF_{i,2}^{j}(t)$. Ta postopek ponavljamo, dokler ostanek $o_{i,j}(t)$ ne predstavlja monotone funkcije. Ko dekompoziramo vse vhodne signale na vse osnovne lastne funkcije in njihove trende, celoten cikel določanja IMF-jev in trendov ponovimo $L = 500$ krat. S tem izboljšamo kvaliteto dekomponiranih signalov. Povprečna vrednost posameznega IMF-ja in karakterističnih trendov signalov tako lahko zapišemo kot:

$$\overline{IMF}_{i,l}(t) = \frac{1}{L}\sum_{j=1}^{L} IMF_{i,l}^{j}(t), \tag{4.2}$$

$$\bar{o}_i(t) = \frac{1}{L}\sum_{j=1}^{L} o_{i,j}(t)\,. \tag{4.3}$$

Ko so vsi povprečni IMF-ji in trendi vseh vhodnih signalov določeni, iz njih izključimo vse enostavne lastne funkcije, ki ne vsebujejo relevantnih dinamičnih informacij. Zapišemo lahko:

$$x_i(t) = x'_i(t) - o_i(t) - \sum \overline{IMF}_{i,l}(t)\,. \tag{4.4}$$

Na sliki (4.1) je shematski prikaz algoritma empirične dekompozicije izmerjenega signala. Prikazana je tudi tipična oblika vhodnega signala, ki ga eksperimentalno določimo in končni dekompozirani signal, ki ga v nadaljevanju uporabimo za konstrukcijo funkcionalne mreže.

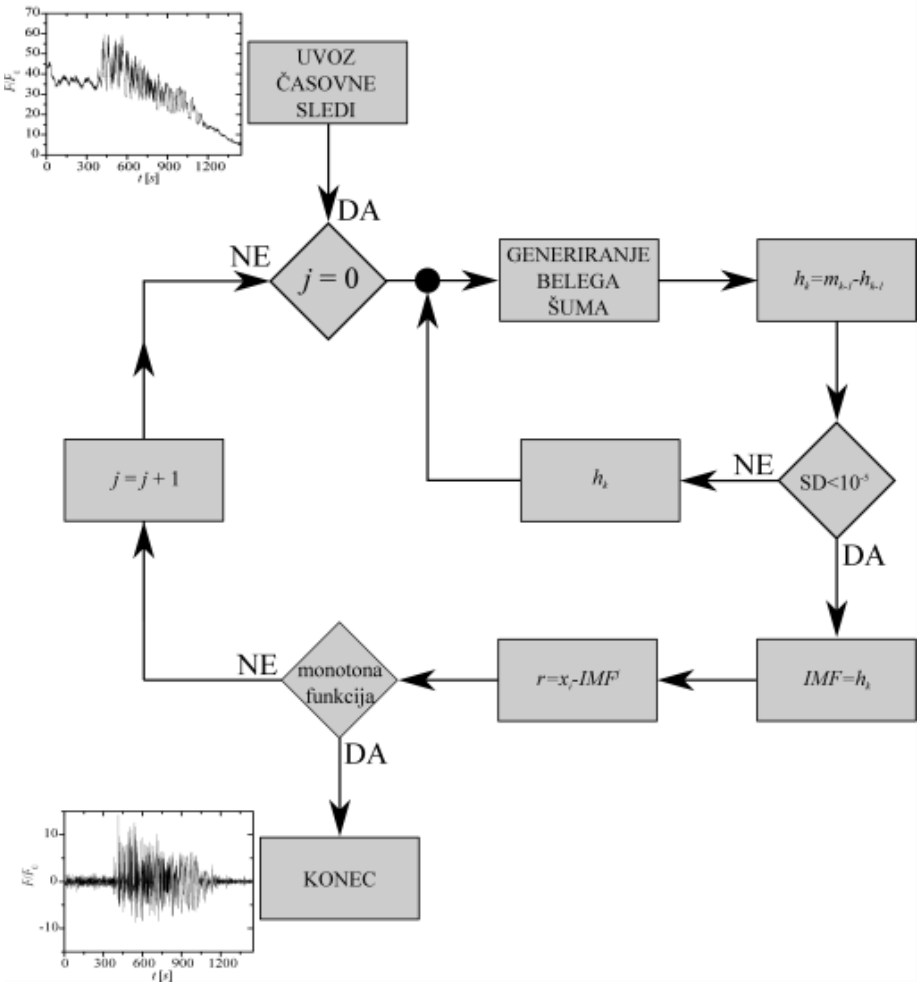

Slika 4.1: Shematski prikaz algoritma za posodobljeno obliko Huang-Hilbertove dekompozicije.

Za nazornejši prikaz prednosti uporabljene metode pred drugimi konvencionalnimi in bolj preprostimi pristopi, je na sliki (4.2) prikaz poteka neobdelanega signala in končna oblike obdelanega signala za tri različne metode glajenja. V prvem primeru (slika 4.2b) je signalu prilagojena linearno-eksponentno funkcija, ki ponazarja trend upadanja intenzitete zaradi bledenja barvila. V drugem primeru (slika 4.2c) so nizkofrekvenčne in visokofrekvenčne motnje v posameznih signalih izločene z uporabo pasovno-prepustnega frekvenčnega filtra. V tretjem primeru (slika 4.2d) pa je signal obdelan z uporabo EEMD dekompozicije. Vidimo, da prilagajanje izloči globalni trend bledenja, ne pa nihanj bazalnih vrednosti kalcija. Filtracija signala te trende sicer odstrani, vendar postanejo signali proti koncu, kjer je bolj izražen šum, slabo izraženi. Slednje je posledica slabšega razmerja signal šum. Filtracija prav tako

povzroči fazne zamike, ki si jih pri analizi korelacij, v kateri je zajeta tudi sočasnost dogodkov, ne moremo privoščiti. EEMD teh slabosti nima.

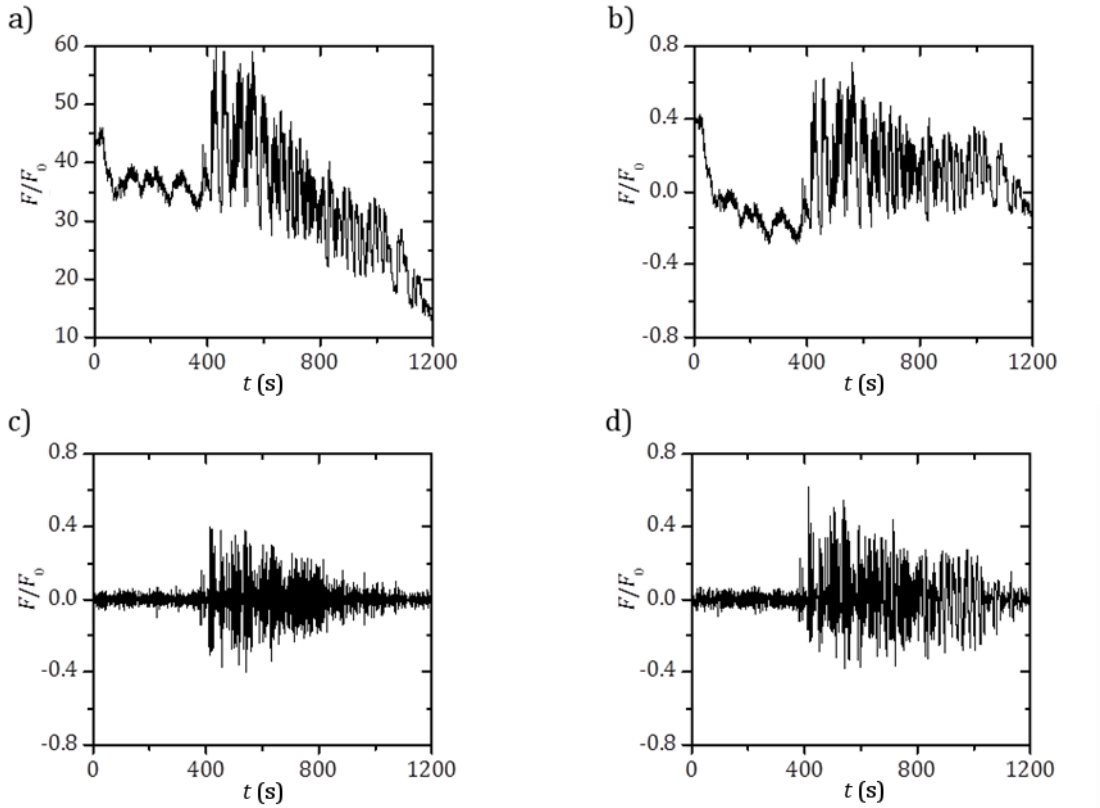

Slika 4.2: Vpliv obdelave signala na kvaliteto izločenega signala. Grafi prikazujejo a) tipično eksperimentalno izmerjeno dinamiko znotrajceličnega Ca^{2+} v celice beta, b) obdelano časovno vrsto z linearno-eksponentno prilagojeno funkcijo, c) obdelano časovno vrsto s pasovno-prepustnim filtrom in d) obdelano časovno vrsto z EEMD dekompozicijskim algoritmom.

4.1.2 Izgradnja funkcionalne mreže

Funkcionalna povezanost med celicami zgradimo na osnovi začasnih korelacijskih koeficientov med pari časovnih vrst $R_{ij}(t_n)$. V ta namen časovne vrste razdelimo na manjša časovna okna dolžine $\Delta\tau = 32$ s, ki so med seboj oddaljene za čas $t_n = \Delta\tau\left(1/2 + n\right)$, kjer je t_n srednja vrednost časa n-tega časovnega okna. Povprečno koreliranost kolektivne dinamike R_{avg} v tem časovnem oknu pa določimo kot povprečneno vsoto ne-diagonalnih elementov $R_{ij}(t_n)$. Na sliki (4.3) je narejena primerjava, ki prikazuje potek povprečne korelacije v primeru, neobdelane časovne

vrste in časovne vrste, obdelane z EEMD dekompozicijskim pristopom. V teku eksperimenta je bil vzorec izpostavljen stopničasto naraščajoči koncentraciji glukoze. V obeh primerih lahko opazimo, da se R_{avg} v splošnem veča z večanjem koncentracije glukoze.

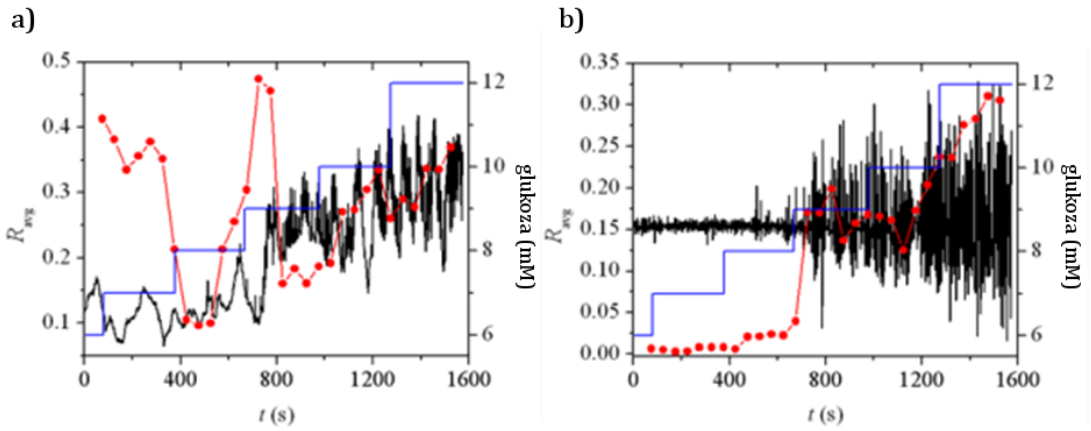

Slika 4.3: Povprečna korelacija R_{avg} (rdeča črta s krogi) in stimulatorne vrdnosti glukoze (modra črta) v odvisnosti od časa v primeru a) neobdelanih časovnih vrst in b) dekompoziranih časovnih vrst. Črne črte ponazarjajo povprečen signal.

Iz izvedene primerjave, prikazane na sliki (4.3), je razvidna dodana vrednost obdelave posameznih signalov. V splošnem povečanje stimulacijske koncentracije glukoze povzroči, da postanejo vse celice bolj aktivne. To se odraža v večji intenziteti zaznanega barvila in posledično v večji numerični vrednosti časovne vrste. Večja povprečna sinhronizacije sistema ob določenih časih (glej sliko 4.3a) tako ni posledica večje koreliranosti v dinamiki celic temveč je posledica skupnih trendov. Ko tovrstne pojave izključimo iz časovnih vrst, podobnega obnašanja ne zaznamo. Tako lahko z večjo gotovostjo trdimo, da bodo upodobljene funkcionalne povezave bolj natančno odražale celice, ki imajo podobno znotrajcelično dinamiko kalcija Ca^{2+}.

Ko določimo korelacijske koeficiente med vsemi pari časovnih vrst za vsa časovna okna, pričnemo z določanjem trenutne matrike sosednosti $\mathbf{d}(t_n)$. V primeru, ko je korelacijski koeficient $R_{ij}(t_n)$ v časovnem oknu $t_n \pm {}^{\Delta\tau}/_{2}$ večji od določene mejne vrednosti R_{th}, smatramo dinamiki i-te in j-te celice kot funkcionalno povezani. Tako postane ij-ti element matrike sosednosti za to časovno okno enak $d_{ij}(t_n) = 1$. V

nasprotnem primeru, ko je $R_{ij}(t_n)$ manjši od mejne vrednosti R_{th}, pa smatramo celici v tem časovnem oknu kot funkcionalno neskloplјeni in postavimo ij-ti element matrike sosednosti za to časovno okno na $d_{ij}(t_n) = 0$. Prag za povezanost smo določili v skladu s pogojem $R^2_{\mathrm{avg}} > 0{,}5$, kar zagotovi dovolj visoko stopnjo kavzalnosti med zaznanimi funkcionalnimi povezavami. Princip je shematsko ponazorjen na sliki 4.4.

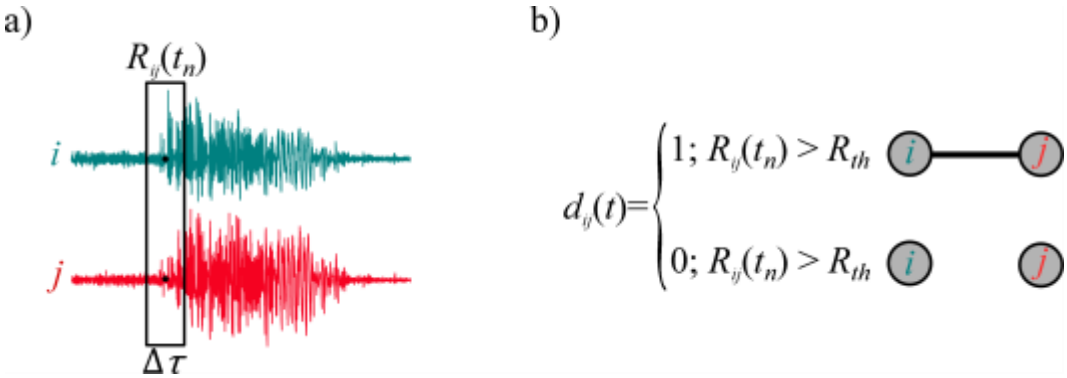

Slika 4.4: Upodobitev ključnih korakov pri konstrukciji funkcionalne povezanosti: a) prikaz dveh karakterističnih obdelanih časovnih vrst, ki jima znotraj časovnega okna določimo vrednost trenutne korelacije in b) pogoja za vzpostavitev funkcionalne povezanosti med tema dvema celicama.

4.2 Topološke lastnosti funkcionalnih mrež celic beta

Za preučevanje narave funkcionalnih vzorcev povezanosti uporabimo teoretska orodja vpeljana v poglavju 2.1. Takšen pristop nam omogoča, da z uveljavljenimi topološkimi merami kvantificiramo medcelično povezanost med celicami beta in tudi, da sledimo njenemu časovnemu razvoju tekom spreminjajoče stimulacije.

4.2.1 Struktura funkcionalnih skupnosti celic beta znotraj fizioloških koncentracij glukoze

Funkcionalno povezanost med celicami beta je določena v skladu z metodologijo opisano v poglavju (4.1). Pari celic, pri katerih korelacija med njunima Ca^{2+} signaloma presega mejno vrednosti R_{th}, se tretirajo kot funkcionalno sklopljene. Slika (4.5) prikazuje organiziranost funkcionalne povezanosti med celicami beta za

različne stimulacijske vrednosti glukoze. Opazimo, da se v primerih nižje koncentracije glukoze (≤8 mM) pojavi izredno malo število celic, ki imajo vzajemno dobro sinhronizirano dinamiko. Višja stimulacijska raven glukoze pa v splošnem izzove, da se število povezav v mreži povečuje, kar je posledica večje stopnje sinhronizacije kolektivne dinamike (glej sliko 4.3b). Iz rezultatov je razvidno, da so celice beta organizirane v funkcionalne skupnosti, ki so prostorsko urejene in lokalizirane. Pri nizkih koncentracijah glukoze so te podmreže močno segregirane. Z višanjem koncentracije glukoze pa se stopnja segregiranosti med skupnostmi v splošnem manjša. Neodvisno od koncentracije glukoze pa ostajajo skupnosti prostorsko urejene, saj je povsod močno izražen trend, da so bližnje celice med seboj bolj povezane kot oddaljene.

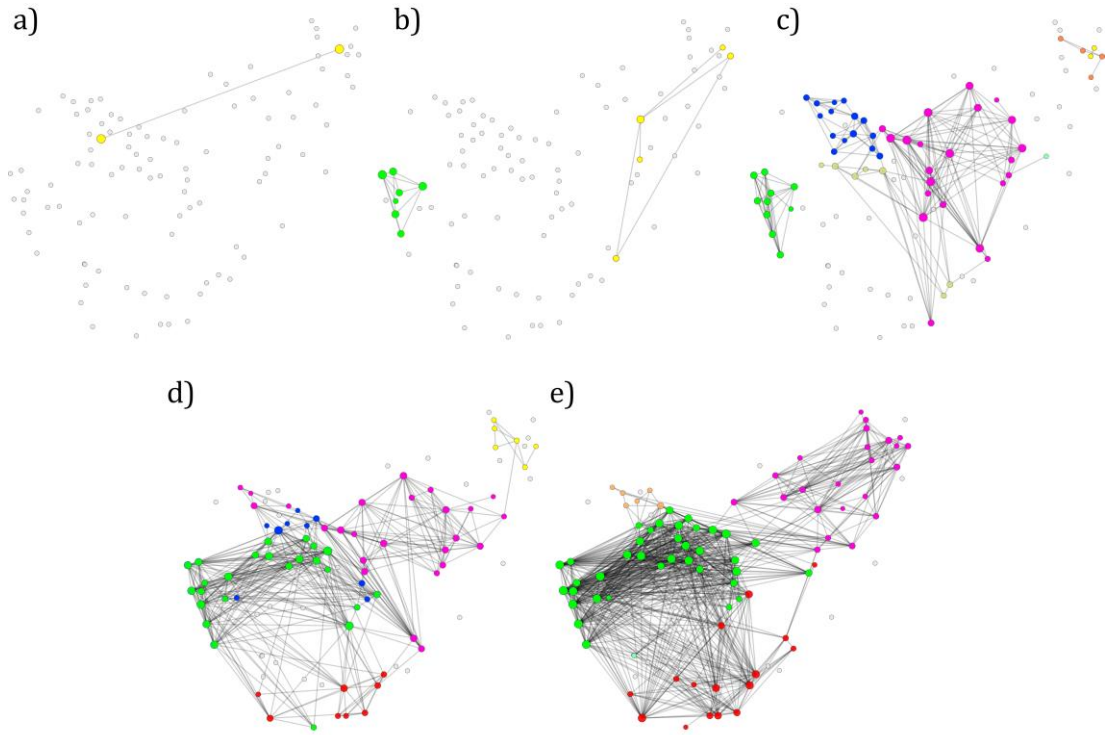

Slika 4.5: Funkcionalna povezanost celic beta pri različnih koncentracijah glukoze: a) 6 mM, b) 7 mM, c) 8 mM, d) 9 mM in e) 12 mM. Prostorska ureditev vozlišč mreže odraža dejansko lego posameznih celic v uporabljenem vzorcu. Vozlišča mreže so barvno kodirana glede na skupnost, kateri pripadajo. Nepovezana vozlišča so obarvana sivo. V vseh primerih je $R_{\mathrm{th}} = 0{,}7$. Vzorec sestavlja 100 celic.

Da podkrepimo omenjene ugotovitve, smo podobno analizo napravili še za 2 druga vzorca rezin trebušne slinavke miši, ki sta bila deležna identičnega eksperimentalnega protokola kot vzorec, uporabljen na sliki (4.5). V obeh dodatnih primerih lahko opazimo, da so funkcionalne mreže, ki so izpostavljene nizki vrednosti glukoze (slika 4.5 (a in b)), redke in močno segregirane. Kadar pa so izpostavljene visokim koncentracijam glukoze, pa je upodobljena mreža gosta in prepletena (slika 4.5 (c in d)). V obeh stimulacijskih režimih lahko opazimo jasno izražene in lokalizirane skupnosti.

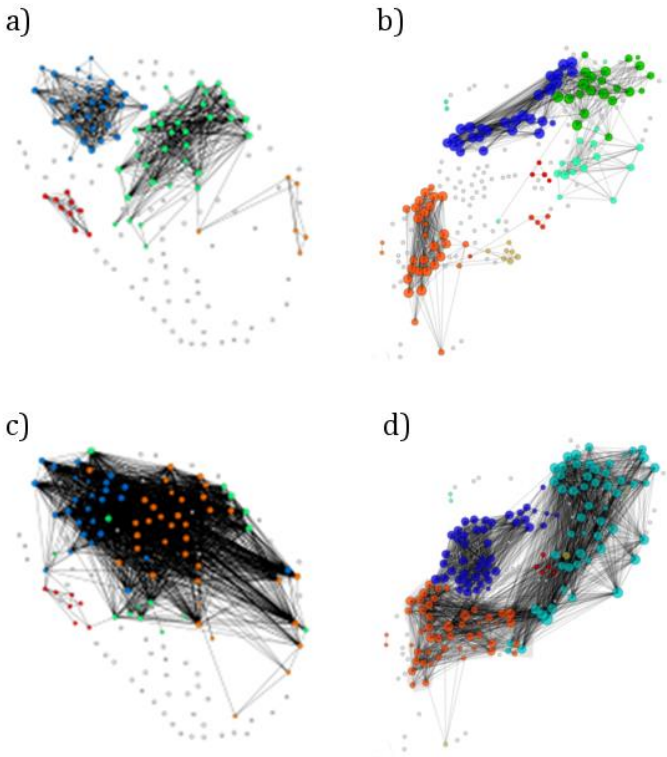

Slika 4.6: Funkcionalna povezanost celic beta v primeru 8mM (a in b) in 12 mM (c in d) koncentracije glukoze za tri dodatne otočke, ki so bile sestavljene iz 152 (a,c) in 200 (b,d) celic. Prostorska ureditev vozlišč mreže odraža dejansko lego posameznih celic v uporabljenem vzorcu. Celice so obarvane glede na skupnost, kateri pripadajo. Nepovezane celice so obarvane sivo. V vseh primerih je $R_{\mathrm{th}} = 0{,}7$.

Celice beta, ki pripadajo isti skupnosti, kažejo znake bolj sočasne aktivnosti, ki je znotraj ene skupnosti tudi bolje fazno sinhronizirana. Omenjeno empirično ugotovitev podkrepimo z izračunom povprečne korelacije med pari celic, ki pripadajo določeni skupnosti $R_{\mathrm{avg}}^{c_i}$ za vse skupnosti v mreži. S podatki $R_{\mathrm{avg}}^{c_i}$ posameznih skupnosti pa podamo povprečno vrednost sinhronizacije med celicami iste skupnosti $R_{\mathrm{avg}}^{\mathrm{cum}}$. Sprotno računamo tudi spreminjanje povprečne korelacije $R_{\mathrm{avg}}^{\mathrm{net}}$ med vsemi pari celic funkcionalne mreže, ki imajo vsaj eno povezavo. Vrednosti $R_{\mathrm{avg}}^{\mathrm{cum}}$ in $R_{\mathrm{avg}}^{\mathrm{net}}$ predstavljajo povprečje vzorca, uporabljenega v sliki (4.5). Rezultati so prikazani na sliki (4.7). Vidimo, da je $R_{\mathrm{avg}}^{\mathrm{cum}}$ v območju višje stimulacijske ravni glukoze znatno višji od $R_{\mathrm{avg}}^{\mathrm{net}}$. Ti rezultati še dodatno potrjujejo ugotovitev o segregirani organiziranosti v Langerhansovem otočku.

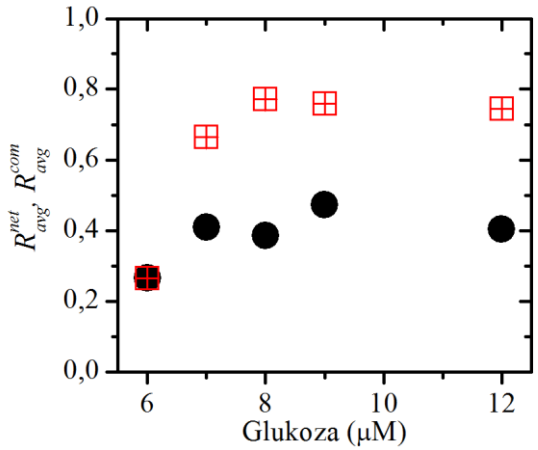

Slika 4.7: Povprečna korelacija med pari celic, ki pripadajo isti skupnosti $R_{\mathrm{avg}}^{\mathrm{cum}}$ (rdeči kvadrati) in povprečna korelacija med vsemi pari celic funkcionalne mreže $R_{\mathrm{avg}}^{\mathrm{net}}$ (črne pike) v odvisnosti od stimulacijske vrednosti glukoze. Mejna vrednost korelacije pri izgradnji funkcionalne povezanosti je bila $R_{th} = 0{,}7$. Vrednosti so dobljene za vzorec, prikazan na sliki (4.5)

V nadaljevanju še podrobneje preverimo, kako se topološke lastnosti funkcionalnih mrež spreminjajo v odvisnosti od koncentracije glukoze. Najprej preučimo, če obstajajo v tkivu celice, ki izstopajo v njihovem delovanju in imajo v mreži posebno vlogo. Izvedimo izračun, pri katerem preverimo, kako se je povezanost posameznih celic in njihova osrednjost spreminjata s časom. Ker nam povezanost celice pove, s kolikšnimi celicami ima izbrana celica visoko korelirano znotrajcelično dinamiko,

močno povezane celice klasificiramo kot iniciatorske celice. Celice, ki pa imajo veliko osrednjost, so ključne za učinkovit prenos informacij. Najpogosteje se te celice nahajajo na stičišču dveh lokalnih skupnosti. V kolikor teh celic ne bi bilo, bi bila onemogočena močneje koordinirana globalna aktivnost v tkivu. Celice z veliko osrednjostjo zato poimenujemo mediatorske celice. Rezultati časovnega razvoja povezanosti in osrednosti posameznih celic so prikazani na sliki (4.8).

Iz rezultata je razvidno, da močno povezane celice ostajajo močno povezane pri različnih koncentracijah glukoze. Tako lahko sklepamo, da se njihova vloga ohranja v tkivnih vzorcih. Slika (4.8b) pa prikazuje normirano osrednjost celic. Ponovno lahko opazimo, da celice, ki imajo veliko osrednjost, le-to tudi ohranjajo. Slika (4.8c) dodatno prikazuje potek normiranega produkta med povezanostjo in osrednjostjo posamezne celice. Rezultati tako kažejo, da obstajajo iniciatorske celice, ki so močno povezane in imajo tako velik doseg v smislu celic, na katere lahko vplivajo, in mediatorske celice. Slednje predstavljajo celice, ki so ključne za ohranjanje integriranosti komunikacijske mreže.

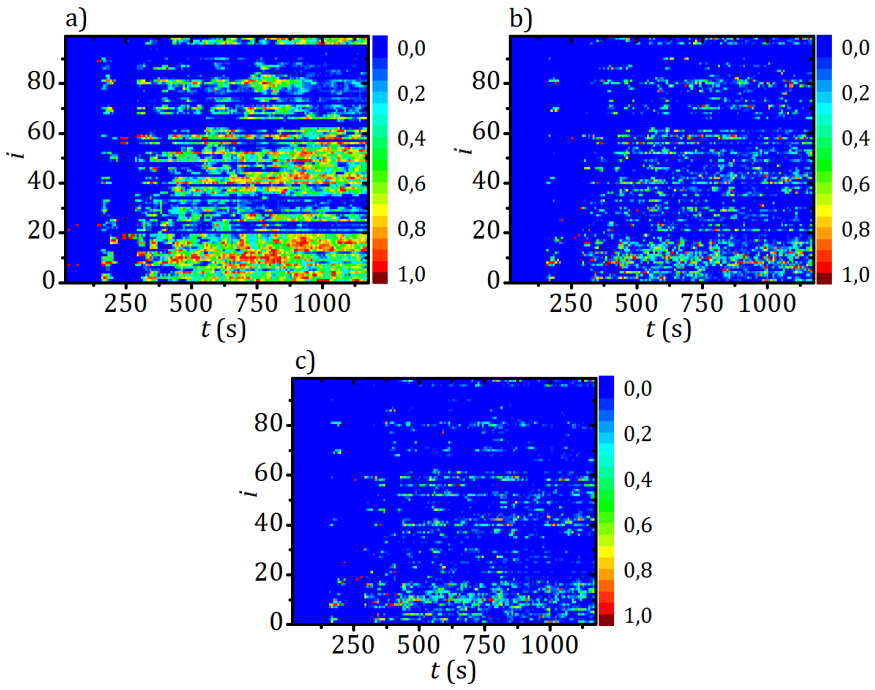

Slika 4.8: Prepoznavanje celic iniciatork in mediatork. Odvisnost a) normirane povezanosti, b) osrednjosti in c) produkt med normirano povezanostjo ter osrednjostjo posamezne celice od časa.

4.2.2 Funkcionalna povezanosti celic beta znotraj fizioloških koncentracij glukoze

Za pridobitev bolj poglobljene slike o spreminjanju funkcionalne povezanosti v tkivu tekom eksperimenta, izračunajmo več različnih topoloških mer, katerih pomen in tudi postopek računanja je bil podrobneje predstavljen v poglavju 2.1.1. Mere, ki so relevantne tudi z vidika fiziologije, so povprečna povezanost k_{avg}, povprečen koeficient gručavosti C_{avg}, povprečna globalna učinkovitost E_{avg}, število skupnosti N_{c}, povprečno število celic v skupnostih n_{c} in povprečna dolžina funkcionalnih povezav I_{avg}. Glavni predmet zanimanje je spreminanje teh mer v odvisnosti od stimulacijske vrednosti glukoze. Rezultat je prikazan na sliki (4.9). Odebeljena črna črta odraža povprečno vrednost določene mrežne mere pri dani koncentraciji glukoze. Na sliki (4.9a) je prikazana odvisnost povprečne povezanosti celic k_{avg} od koncentracije glukoze. Vidimo, da višja kot je koncentracija glukoze, gosteje povezane postajajo celice. Povečanje k_{avg} tudi naznanja, da postaja aktivnost celic bolj koordinirana (glej sliko 4.3b). Možna razlaga za ta pojav je, da postaja komunikacija med celicami, ki poteka preko električnih sinaps in drugih načinov daljnosežnega komuniciranja, bolj izrazita. Povprečna gručavost sistema C_{avg} (glej sliko 4.9b) je med drugim tudi mera funkcionalne segregiranosti in eden izmed indikatorjev topoloških lastnosti mrež malega sveta [40]. Vidimo lahko, da se celice beta kot odziv na povišanje koncentracije glukoze preferenčno povezujejo v lokalne gruče celic. Tako se C_{avg} v odvisnosti od glukoze povečuje do koncentracije glukoze 9 mM. Od te mejne vrednosti pa se vrednost C_{avg} saturira. Odvisnost povprečne učinkovitost mreže E_{avg}, ki odraža tudi stopnjo vključenosti vozlišč v mrežo od koncentracije glukoze, je prikazana na sliki (4.9c). Ponovno lahko opazimo, da postaja funkcionalna mreža celic beta z višanjem koncentracije glukoze tudi vse bolj učinkovita, dokler se vrednost E_{avg} ne zasiči pri višjih vrednostih glukoze ($\geq$10 mM). Na slikah (4.9d in 4.9e) je predstavljena analiza o modularni naravi funkcionalnih mrež v odvisnosti od glukoze. Slika (4.9d) tako prikazuje, kako se spreminja število skupnosti N_{c}, slika (4.9e) pa iz kolikšnega števila celic so te skupnosti v povprečju sestavljene. Vidimo, da se celice beta pri višjih koncentracijah glukoze ($>$8 mM) razporedijo v povprečju v sedem skupnosti. Tudi število celic v

skupnosti je močno odvisno od glukoze in se v splošnem veča z večanjem koncentracije glukoze ter doseže določeno končno vrednost pri 10 mM koncentraciji glukoze. Zadnji rezultat, prikazan na sliki (4.9f), pa odraža odvisnost povprečne dolžine funkcionalnih povezav I_{avg} v odvisnosti od glukoze. Hkrati ta mera odraža tudi, kolikšen je doseg direktne medcelične komunikacije znotraj otočka. Podobno kot smo že opazili pri ostalih merah, lahko največje spremembe v vrednostih I_{avg} zaznamo med 7 mM in 10 mM koncentracijo glukoze. Večje vrednosti glukoze pa imajo za posledico le manjšo spremembo v I_{avg}, ki se saturira pri razdalji 45 μm.

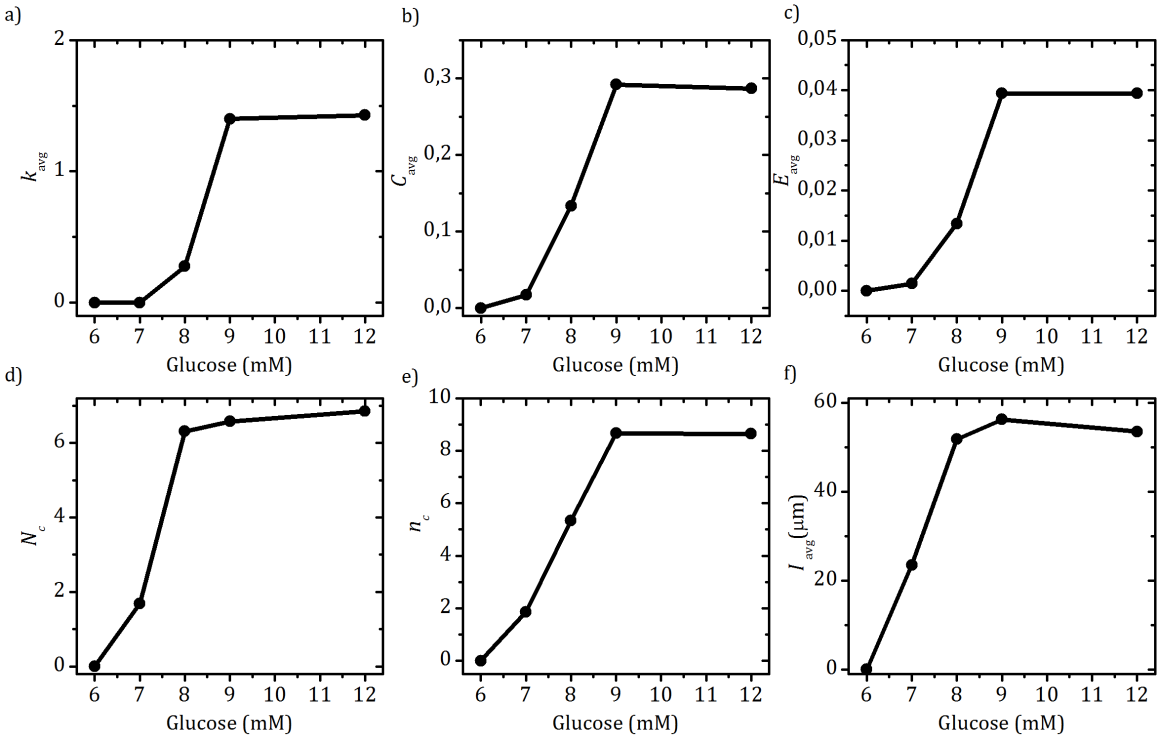

Slika 4.9: Vrednosti topoloških mer funkcionalnih mrež beta celica za štiri otočke: a) povprečna povezanost, b) povprečni koeficient gručavosti, c) globalna učinkovitost, d) povprečno število skupnosti, e) povprečna velikost skupnosti in f) povprečna dolžina funkcionalnih povezav. Mejna vrednost korelacije pri izgradnji funkcionalne povezanosti je $R_{\mathrm{th}} = 0{,}7$.

Ker smo hoteli potrditi, da so spremembe v mrežnih merah izključno posledica zviševanj koncentracije glukoze, smo v našo analizo vključili še štiri dodatne otočke. Dva otočka (skupaj 556 celic) sta bila po določenem času stimulirana s stalno koncentracijo 8 mM, druga dva (skupaj 540 celic) pa s 12 mM glukoze. Za vse vzorce

smo izračunali, kako so se mrežne mere, spreminjajo s časom. S to analizo lahko preverimo, ali se pri konstantni stimulaciji pojavljajo kakršnekoli časovno odvisne spremembe v topoloških lastnostih funkcionalnih mrež, ki so posledica dolgotrajne izpostavljenosti stimula. Rezultati analize so prikazani na sliki (4.10). Vrednosti topoloških mer med 8 mM in 12 mM stimulacijo vzorcev so primerljive z rezultati, prikazanimi na sliki (4.10). Vse topološke mere , razen N_c, so v splošnem manjše pri 8 mM koncentraciji glukoze, če jih primerjamo z vrednostmi topoloških mer v primeru 12 mM stimulacije glukoze. Pri vzorcih, ki so bili daljši čas stimulirani z 12 mM koncentracijo glukoze, lahko opazimo, da je skupni trend upadanje topoloških mer, za kar pa bi lahko bila odgovorna t.i. glukotoksičnost [85].

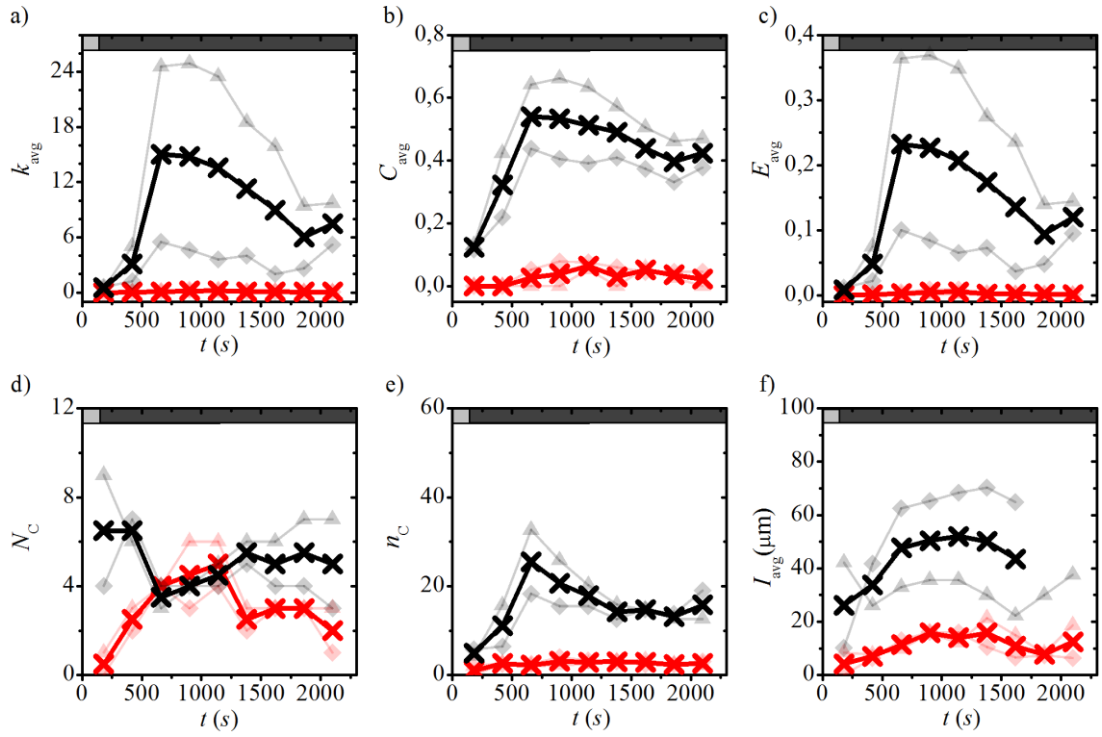

Slika 4.10: Časovni razvoj različnih topoloških mer v primeru konstantne stimulacije z 8 mM (rdeče črte) in 12 mM (črne črte) koncentracije glukoze: a) povprečna povezanost, b) povprečni koeficient gručavosti, c) globalna učinkovitost, d) povprečno število skupnosti, e) povprečna velikost skupnosti in f) povprečna dolžina funkcionalnih povezav. Mejna vrednost korelacije pri izgradnji funkcionalne povezanosti je bila $R_{th} = 0{,}7$. Sivo obarvan predel na vrhu grafov (a−f) ponazarja območje 6 mM glukoze in črno obarvan predel območje, kjer so bili vzorci simulirani z 8 mM ali 12 mM glukoze. Odebeljene črke s križci odražajo povprečno

vrednost za določeno koncentracijo glukoze.

Predstavljeni rezultati potrjujejo tezo o modularni naravi funkcionalnih mrež, kar pomeni, da celice beta v Langerhansovih otočkih tvorijo funkcionalne podenote. Celice, ki pripadajo eni skupnosti, so med seboj bolj gosto povezane in imajo bolje koordinirano aktivnost v primerjavi s celicami v drugih skupnostih oz. celostno funkcionalno mrežo. Funkcionalna povezanost celic beta se tako kaže kot izredno prilagodljiva in zmožna zveznega preoblikovanja iz močno segregirane v bolj integrirano funkcionalno mrežo. Ker medcelična komunikacija koordinira aktivnost posameznih celic, bi lahko prikazana modularna narava Langerhansovih otočkov predstavljala dodaten prostorsko regulacijski mehanizem izločanja inzulina. Podobni regulacijski pojavi, so opaženi tudi v nevronskih mrežah. Za ta biološki sistem je znano, da je uravnovešena kombinacija med segregiranim in integriranim procesiranjem informacij, ki jo je možno doseči v učinkoviti mrežni topologiji malega sveta, nujna za njegovo normalno delovanje [80]. Motnje v tej uravnovešenosti pa lahko vodijo do avtizma, ki je posledica prekomerno segregirane mreže ali shizofrenije, v primeru prekomerno integrirane mrežne strukture [30]. Pomembnost medcelične komunikacije je tudi izpostavljena na primeru gladkih mišičnih celic pljučnih arterij. Tako je pokazano, da v primeru zdravega tkiva celice tvorijo učinkovito mrežo. V primeru kronične hipoksije, pa je mrežna struktura medcelične sklopljenosti naključna [86]. Tako je tudi smotrno napovedovati, da so lahko nepravilnosti v funkcionalni povezanosti Langerhansovega otočka povezane s sladkorno boleznijo. Dodatne eksperimentalne in teoretične raziskave so tako nujno potrebne, da bi lahko razumeli, kako ta večcelični sistem regulira svoje delovanje z medcelično komunikacijo v patološkem stanju.

5 ZAKLJUČEK

V doktorski disertaciji je obravnavan pojav sinhronizacije kolektivne dinamike sistema, ki je sestavljen iz velikega števila oscilarujočih vozlišč. Sistemi, kjer dinamični elementi interagirajo med seboj na netrivialen način ter tvorijo globalno obnašanje, so v naravi, družbi in tehniki zelo pogosti [3, 9, 10, 68]. V disertaciji je posebna pozornost bila namenjena preučevanju vlog interakcijske topologije in dinamičnih lastnosti oscilatorjev pri zagotavljanju najboljše sinhronizabilnosti. Pokazali smo, da fleksibilni in rigidni oscilatorji dosegajo najvišjo raven kolektivne sinhronizacije v različnih mrežnih topologijah. Sistem sklopljenih rigidnih oscilatorjev doseže najvišjo raven kolektivne sinhronizacije v skalno neodvisni mrežni topologiji. Kadar pa so vozlišča mreže poseljena s fleksibilnimi oscilatorji, zagotavlja široko skalna mrežna struktura interakcijsko sliko, pri kateri sistem doseže najvišjo raven sinhronizacije kolektivne dinamike. Slednja mrežna struktura je bila zazna tudi v številnih realnih sistemih [6-9, 29, 46, 80]. V primeru bioloških nevronskih mrež so odstopanja od takšne sklopitvene strukture pogosto povezana z različnimi nevrološkimi obolenji [29-32]. Omenimo še, da je skalno neodvisna mrežna topologija izredno učinkovita ter tudi heterogena, medtem ko sta učinkovitost in razpršenost v povezanosti vozlišč v široko skalni mreži manjši. Razlika med tema dvema mrežnima tipoma je tudi njuna segegiranost; široko skalna mrežna topologija je bolj mudularna od skalno neodvisne mreže. To se odraža v formaciji izrazitih skupnostih, znotraj katerih so vozlišča gosteje povezana. Takšna organiziranost pa v splošnem zavira visoko ranve globalne sinhronizacije in spodbuja bolje sinhronizirano dinamiko med gosteje povezanimi vozlišči [20]. Kot zanimivo se izkaže tudi, da so široko skalne mrežne topologije manj občutljive na izpade njenih najbolj povezanih vozlišč, v primerjavi s skalno neodvisnimi mrežami [87]. V evolucijskem smislu je tako sistem bolj odporen na mutacije, ki se lahko pojavijo v teku njenega razvoja.

Iz naših rezultatov sledi, da je v primerih, kjer je sistem organiziran v široko skalno mrežno topologijo, dinamika vozlišč fleksibilna. Z analitičnim pristopom je izpeljan izraz, ki razkriva, da se rigidnost oscilatorjev mreže spremeni zaradi medsebojne sklopljenosti. Iskaže se, da je porast v disipativnosti, ki odraža stopnjo rigidnosti

oscilatorja zanemarljiva, kadar je intrinzična disipativnost mnogo večja od karakterističnega doprinosa sklopitvenega člena k rigidnost. To velja za rigidne oscilatorje. Zaradi neodvisnosti njihovih dinamičnih lastnosti od mrežne strukture, dosegajo najvišjo raven fekvenčne prilagodljivosti v heterogeni skalno neodvisni mrežni topologiji. V primeru fleksibilnih oscilatorjev pa je povečanje njihove disipativnsoti znatno. Izrazito heterogene mreže, ki so hkrati tudi zelo učinkovite, tako inducirajo velika razhajanja med dinamičnimi disipativnostmi posameznih oscilatorjev. Slednje zavira dobre sledilne lasnosti močno rigidnih oscilatorjev. Fleksibilni oscilatorji tako dosegajo najvišjo raven frekvenčne prilagodljivosti v segregiranih mrežnih strukturah, ki so tudi bolj homogene. Vendar, ker so slednje tudi mnogo bolj neučinkovite, je visoka raven kolektivne sinronizacije onemogočena. Mreže poseljene s fleksibilnimi oscilatorji tako dosegajo najvišjo raven sinhronizacije v vmesnih mrežnih strukturah, ki imajo zadostno učinkovist in hkrati tudi segregiranost, kot je to v primeru široko skalne mrežna topologije. To univerzalno veljavno spoznanje, je tudi prikazano še na treh dodatnih matematičnih modelih, ki so bili tako zvezni kot diskretni, katerih dinamika je bila tako regularna kot kaotična in ki so bili tako dvodimenzionalni kot tudi tridimenzionalni. Dodatno je pokazano tudi, da ob optimalni topologiji mreže obstaja tudi optimalna hitrost širjenja informacij med vozlišči mreže. Odstopanja od te optimalne hitrosti pa izzovejo znižane ravni sinhronizacije kolektivne dinamike. Ugotovitve, ki so bile predstavljene v teoretičnem delu lahko povzamemo v naslednjih točkah:

1. Intrinzično rigidni oscilatorji dosegajo maksimum usklajene kolektivne dinamike znotraj zelo učinkovitih in heterogenih skalno neodvisnih mrež, medtem ko intrinzično fleksibilni oscilatorji dosegajo največjo raven sinhronizacije v manj heterogenih široko skalnih mrežnih topologijah malega sveta ([11, 25, 37]; priloge 2, 3 in 4).

2. Optimalno sinhronizacijo mrežno povezanih oscilatorjev glede na njihovo fleksibilnost lahko razložimo s stopnjo frekvenčne prilagodljivosti in globalno učinkovitostjo mrežne strukture ([11]; priloge 4).

3. V prostorsko vpetih mrežah obstajata tako optimalna mrežna topologija kakor tudi optimalna hitrost širjenja signala, pri kateri sistem sklopljenih oscilatorjev doseže maksimalno raven sinhronizacije ([10]; priloga 1).

V aplikativnem delu doktorske naloge, ki je zajeto v poglavju 4, so teoretična orodja s področja kompleksnih mrež uporabljena za raziskavo narave medcelične komunikacije v tkivu. Predmet preučevanja je kolektivna dinamika celic beta v tkivnih rezinah trebušne slinavke miši. Osredinili smo se na fiziološko relevantne stimulacijske koncentracije glukoze. Obstoječo metodologijo izgradnje funkcionalne povezanosti celic beta smo nadgradili s predhodno obdelavo časovnih vrst z empirično dekompozicijo signala, s katero izločamo visokofrekvenčne in nizkofrekvenčne motnje v posameznih eksperimentalno dobljenih signalov. Rezultati analiz kažejo, da so celice beta organizirane v lokalne skupnosti, znotraj katerih so celice gosteje povezane in tudi bolje sinhronizirane. V območju nizkih stimulacijskih vrednostih glukoze, je funkcionalna mreža izredno neučinkovita in segregirana. Največje spremembe v funkcionalni povezanosti celic so zaznane v intervalu koncentracije glukoze od 7 mM do 9 mM. Stimulacija sistema z višjo koncentracijo glukoze pa v splošnem izzove zgolj manjše spremembe v lastnosti funkcionalne povezanosti. Pokazan je tudi obstoj celic, ki vzdržujejo integriteto funkcionalne povezanosti (mediatorske celice) ter celic iniciatork, ki imajo veliko povezanost. Vloga omenjenih tipov celic se med postopnim povečevanjem koncentraciji glukoze ohranjala. Te celice bi lahko tako bi lahko imele ključno vlogo pri zagotavljanju normalnega delovanja regulacije glukoze. Zanimivo je, da odvisnosti topoloških mer od koncentracije glukoze, sovpada z eksperimentalno izmerjenim potekom koncentracije izločenega inzulina [88]. Omenjeno nakazuje, da bi lahko bila izločena količina inzulina celotnega tkiva regulirana s strani medcelične komunikacije. Rezultati aplikativnega dela disertacije tako potrjujejo naslednje teze:

4. V mreži funkcionalne povezanosti celic beta iniciatorske in mediatorske celice ohranjajo svojo vlogo pri različnih ravneh stimulacije celic z glukozo (poglavje 4).

5. V tkivnih rezinah trebušne slinavke miši tvorijo celice beta lokalne skupnosti oziroma gosto povezane pod-enote, katerih pojavnost in porazdelitev je odvisna od koncentracije glukoze (poglavje 4, priloga 5).

S prikazanimi rezultati v doktorski disertaciji smo pokrili vse zastavljene teze. Sami rezultati so izvirni in bili deloma objavljeni v uglednih mednarodnih revijah. V nadaljnih raziskavah bi bilo smotrno ekperimentalno preveriti, kako se rigidnost celic spreminja v odvisnosti od njihove povezansosti. V kolikor bi zaznali koreliranost med tema dvema spremenljivkama, bi to krepilo dognanja naše teoretične raziskave. Široko skalno mrežno organiziranost številnih bioloških sistemov, kot je tudi Langerhansov otoček, bi tako lahko razložili s tukaj predstavljenimi rezultati. Dodatno analizo, ki je bila narejena v aplikativnem delu, bi bilo tudi nujno napraviti na vzorcu tkiv, kjer je regulacijski proces uravnavanja koncetracije glukoze moten. To bi omogočilo direktno primerjavo med funckionalno povezanostjo celic v zdravem ter bolanem vzorcu. Z rezultati takšnih raziskav bi producirali nova spoznanja o odelovanju tega sincicija in posledično tudi k razvoju metod, s katermi bi lahko možne nepravilnosti v njegovem delovanju tudi odpravili.

LITERATURA

[1] A.-L. Barabási, R. Albert, Science, 286 (1999) 509-12.

[2] D. J. Watts, S.H. Strogatz, nature, 393 (1998) 440-442.

[3] R. Albert, A.-L. Barabási, Rev. Mod. Phys. 74 (2002) 47-97.

[4] A.-L. Barabási, Nat. Phys. 8 (2012) 14-16.

[5] L. A. N. Amaral, A. Scala, M. Barthélémy, H. E. Stanley, Proc. Natl. Acad. Sci. U S A 97 **(**2000) 11149-52.

[6] J. D. Power1, A. L. Cohen, S. M. Nelson, G. S. Wig, K. A. Barnes, J. A. Church, A. C. Vogel, T. O. Laumann, F. M. Miezin, B. L. Schlaggar, S. E. Petersen, Neuron 72 (2011) 665-678.

[7] H. Jeong, B. Tombor, R. Albert, Z. N. Oltvai, A.-L. Barabási, Nature, 407 (2000) 651-654.

[8] R. Albert, J. Cell Sci. 118 (2005) 4947-4957.

[9] L. Weng, F. Menczer, Y. Y. Ahn, Sci. Rep. 3 (2013) 2522.

[10] M. Gosak, R. Markovic, M. Marhl, Physica A 391 (2012) 2764-2770.

[11] R. Markovič, M. Gosak, M. Marhl, Chaos Soliton. Fract. 69 (2014) 14-21.

[12] P. Erdős, A. Rényi, Bull. Inst. Internat. Statist. 38 (1961) 482-525.

[13] F. M. Atay, T. Biyikoglu, J. Jost, Trans. Circuits Syst. I, Reg. Papers1 53 (2006) 92-98.

[14] A. Arenas, A. Diaz-Guilera, J. Kurths, Y. Moreno, C. S. Zhou, Phys. Rep., 469 (2008) 93-153.

[15] J. J. Tyson, K. Chen, B. Novak, Nat. Rev. Mol. Cell. Biol. 2 (2001) 908-16.

[16] T. Nishikawa, A. E. Motter, Y. C. Lai, F. C. Hoppensteadt, Phys. Rev. Lett. 91 (2003) 014101.

[17] A. E. Motter, C. Zhou, J. Kurths, Phys. Rev. E 71 (2005) 016116.

[18] J. Gomez-Gardenes, Y. Moreno, A. Arenas, Phys. Rev. Lett. 98 (2007) 034101.

[19] J. Gomez-Gardenes, Y. Moreno, A. Arenas, Phys. Rev. E 75 (2007) 066106.

[20] P. N. McGraw, M. Menzinger, Phys. Rev. E 72 (2005) 015101.

[21] P. N. McGraw, M. Menzinger, Phys. Rev. E 75 (2007) 027104.

[22] M. Perc, M. Marhl, Bioelectrochemistry 62 (2004) 1-10.

[23] U. Abraham, A. E. Granada, P. O. Westermark, M. Heine, A. Kramer, H. Herzel, Mol. Syst. Biol. 6 (2010) 438.

[24] G. Bordyugov, A. Granada, Herzel, Eur. Phys. J. B 82 (2011) 227-234.

[25] R. Markovič, M. Gosak, M. Marhl, Journal of Physics: Conference Series 410 (2013) 012044.

[26] A.-L. Barabási, Z. N. Oltvai, Nat. Rev. Gen. 5 (2004) 101-113.

[27] D. G. Green, D.G., S. Sadedin, Ecol. Complex. 2 (2005) 117-130.

[28] E. Bullmore, O. Sporns, Nat. Rev. Neurosci. 10 (2009) 186-198.

[29] M. K. Belmonte, G. Allen, A. Beckel-Mitchener, L. M. Boulanger, R. A. Carper, S. J. Webb, J. Neurosci. 24 (2004) 9228-31.

[30] Y. Liu, M. Liang, Y. Zhou, Y. He, Y. Hao, M. Song, C. Yu, H. Liu, Z. Liu, T. Jiang, Brain, 131 (2008) 945-961.

[31] Q. Wang, T. P. Su, Y. Zhou, K. H. Chou, I. Y. Chen, T. Jiang, C. P. Lin, Neuroimage 59 (2012) 1085-1093.

[32] Y. He, A. Dagher, Z. Chen, A. Charil, A. Zijdenbos, K. Worsley, A. Evans, Brain 132 (2009) 3366-79.

[33] A. Stožer, M. Gosak, J. Dolenšek, M. Perc, M. Marhl, M. Slak Rupnik, D. Korošak, PLoS Comput. Biol. 9 (2013) e1002923.

[34] G. A. Rutter, D. J. Hodson, Mol. Endocrinol. 27 (2013) 1984-95.

[35] A. Stožer, J. Dolenšek, M. Slal Rupnik, PLoS One 8 (2013) e54638.

[36] S. Morita, Phys. Rev. E 73 (2006) 035104.

[37] R. Markovič, M. Gosak, M. Marhl, AIP Conference Proceedings, New York, USA 1468 (2012) 256-267.

[38] Y. Huang, L. Wu, S. Q. Zhu, Eur. Phys. J. B 69 (2009) 431-438.

[39] X. F. Wang, G. Chen, IEEE Circuits Sys. Mag. 69 (2003) 6-20.

[40] S. Boccaletti, V. Latora, Y. Moreno, M. Chavez, D. U. Hwang, Phys. Rep. 424 (2006) 175-308.

[41] J. Leskovec, R. Sosič, *SNAP: A general purpose network analysis and graph mining library in C++*. 2014. Pridobljeno 20. 11. 2014, iz http://snap.stanford.edu/snap.

[42] T. M. J. Fruchterman, E. M. Reingold, Software Pract. Exper. 21 (1991) 1129-1164.

[43] M. Rubinov, O. Sporns, Neuroimage 52 (2010) 1059-1069.

[44] E. W. Dijkstra, Numer. Math. 1 (1959) 269-271.

[45] P. Holme, B. J. Kim, Phys. Rev. E 65 (2002) 026107.

[46] V. D. Blondel, J. L. Guillaume, R. Lambiotte, E. Lefebvre, J. of Stat. Mech.-Theory E. 10 (2008) P10008.

[47] M. Girvan, M. E. Newman, Proc. Natl. Acad. Sci. U S A 99 (2002) 7821-6.

[48] M. E. J. Newman, Phys. Rev. E 74 (2006) 036104.

[49] M. E. J. Newman, Phys. Rev. Lett. 89 (2002) 208701.

[50] M. E. J. Newman, Phys. Rev. E 67 (2003) 026126.

[51] M. Gosak, doktorska disertacija, 2011.

[52] I. C. Baianu, Math. Mod. 7 (1986) 1513-1577.

[53] C. Bodenstein, M. Gosak, S. Schuster, M. Marhl, M .Perc, PLoS Comput. Biol. 8 (2012) e1002697.

[54] J. Auchmuty, J. G. Nicolis, B. Math. Biol. 37 (1975) 323-365.

[55] Y. C. You, Dynam. Part. Differ. Eq. 4 (2007) 167-196.

[56] N. F. Rulkov, Phys. Rev. Lett. 86 (2001) 183-6.

[57] C. A. Batista, A. M. Batista, J. A. de Pontes, R. L. Viana, S. R. Lopes, Phys. Rev. E 76 (2007) 016218.

[58] G. Schmidt, G. Zamora-Lopez, J. Kurths, Int. J. Bifurcat. Chaos 20 (2010) 859-867.

[59] Q. Y. Wang, G. R. Chen, M. Perc, Plos One, 6 (2011) e15851.

[60] B. Ibarz, J. M. Casado, M. A. F. Sanjuan, Phys. Rep. 501 (2011) 1-74.

[61] E. Aurell, G. Boffetta, A. Crisanti, G. Paladin, A. Vulpiani, J. Phys. A: Math. Gen. 30 (1997)

[62] L. Dieci, R. D. Russell, E. S. Van Vleck, SIAM J. Numer. Anal. 34 (1997) 402-423.

[63] A. Wolf, J. B. Swift, H. L. Swinney, J. A. Vastano, Physica D 16 (1985) 285-317.

[64] B. H. Wang, Commun. Theor. Phys. 21 (1994) 289-298.

[65] E. F. Stone, Phys. Lett. A 163 (1992) 367-374.

[66] M. S. Baptista, H. P. Ren, J. C. M. Swarts, R. Carareto, H. Nijmeijer, C. Grebogi, Plos One 7 (2012) e48118.

[67] K. A. Schindler, S. Bialonski, K. T. Horstmann, C. E. Elger, K. Lehnertz, Chaos 18 (2008) 033119.

[68] P. E. Vertes, R. M. Nicol, S. C. Chapman, N. W. Watkins, D. A. Robertson, E. T. Bullmore, Front. Syst. Neurosci. 5 (2011) 75.

[69] L. F. Lago-Fernandez, R. Huerta, F. Corbacho, J. A. Siguenza, Phys. Rev. Lett. 84 (2000) 2758-2761.

[70] H. Hong, B. J. Kim, M. Y. Choi, H. Park, Phys. Rev. E 69 (2004) 067105.

[71] X. F. Wang, G.R. Chen, Int. J. Bifurcat. Chaos, 12 (2002) 187-192.

[72] M. Barahona, L. M. Pecora, Phys. Rev. Lett. 86 (2002) 054101.

[73] W. Zou, X. Zheng, M. Zhan, Chaos 21 (2011) 023130.

[74] M. A. Henson, Chaos Soliton. Fract. 50 (2013) 48-64.

[75] F. Varela, J. P. Lachaux, E. Rodriguez, E., J. Martinerie, Nat. Rev. Neurosci. 2 (2001) 229-239.

[76] T. Nowotny, R. Huerta, M. I. Rabinovich, Chaos 18 (2008) 037119.

[77] E. R. Kandel, J. H. Schwartz, T. M. Jessell, *Principles of neural science*. Vol. 4. 2000: McGraw-Hill New York.

[78] A. Roxin, N. Brunel, D. Hansel, Phys. Rev. Lett. 94 (2005) 238103.

[79] M. Dhamala, V. K. Jirsa, M. Ding, Phys. Rev. Lett. 92 (2004) 074104.

[80] R. Russo, H. J. Herrmann, L. de Arcangelis, Sci. Rep. 4 (2014).

[81] J. P. Eckmann, S. Jacobi, S. Marom, E. Moses, C. Zbinden, New J. Phys 10 (2008) 015011.

[82] J. C. Henquin, Diabetologia 52 (2009) 739-51.

[83] D. J. Hodson, R. K. Mitchell, E. A. Bellomo, G. Sun, L. Vinet, P. Meda, D. Li, W. H. Li, M. Bugliani, P. Marchetti, D. Bosco, L. Piemonti, P. Johnson, S. J. Hughes, G. A. Rutter, J. Clin. Invest. 123 (2013) 4182-94.

[84] N. E. Huang, Z. Shen, S. T. Long, C. W. Manli, H. H. Shih, Q. Zheng, N.-C. Yen, C. C. Tung, H. H. Liu, Proc. Roy. Soc. Lond. A Mat. 454 (1998) 903-995.

[85] M. Bensellam, D. R. Laybutt, J. C. Jonas, Mol. Cell. Endocrinol. 364 (2012) 1-27.

[86] M. Gosak, C. Guibert, N. Billaud, E. Roux, M. Marhl, Exp. Physiol. 99 (2014) 272-285.

[87] R. Albert, H. Jeong, A.-L. Barabási, Nature 406 (2000) 378-82.

[88] P. Buchwald, Theor. Biol. Med. Model. 8 (2011) 20.

PRILOGE

Priloga 1

M Gosak, R Markovič, M Marhl, *The role of neural architecture and the speed of signal propagation in the process of synchronization of bursting neurons*, Physica A 391 (2012) 2764–2770.

Priloga 2

R Markovič, M Gosak, M Marhl, *The role of topological features of intercellular communication networks by the synchronization of cellular oscillators*, AIP Conference Proceedings, New York, USA (2012) 256–267.

Priloga 3

R Markovič, M Gosak, M Marhl, *How optimal synchronization of oscillators depends on the network structure and the individual dynamical properties of the oscillators*, J. Phys.: Conf. Ser. 410 (2013) 012044–4.

Priloga 4

R Markovič, M Gosak, M Marhl, *Broad-scale small-world network topology induces optimal synchronization of flexible oscillators*, Chaos Soliton. Fract. 69 (2014) 14-21.

Priloga 5

R Markovič, A Stožer, M Gosak, J Dolenšek, M Marhl, M Slak Rupnik, *Progressive glucose stimulation of islet beta cells reveals a transition from segregated to integrated modular functional connectivity patterns*, Sci. Rep. 5 (2015) 7845.

Physica A 391 (2012) 2764–2770

Contents lists available at SciVerse ScienceDirect

Physica A

journal homepage: www.elsevier.com/locate/physa

The role of neural architecture and the speed of signal propagation in the process of synchronization of bursting neurons

Marko Gosak*, Rene Markovič, Marko Marhl

Department of Physics, Faculty of Natural Sciences and Mathematics, University of Maribor, Koroška cesta 160, SI-2000 Maribor, Slovenia

ARTICLE INFO

Article history:
Received 16 September 2011
Received in revised form 24 November 2011
Available online 22 December 2011

Keywords:
Complex network
Chaotic oscillator
Bursting
Synchronization

ABSTRACT

Synchronized neuronal activity has been observed at all levels of human and any other nervous systems and was suggested as particularly relevant in information processing and coding. In the present paper we investigate the synchronization of bursting neuronal activity. Motivated by the fact that in neural systems the interplay between the network structure and the dynamics taking place on it is closely interrelated, we develop a spatial network representation of neural architecture in which we can tune the network organization between a scale-free network with dominating long-range connections and a homogeneous network with mostly adjacent neurons connected. Our results reveal that the most synchronized response is obtained for the intermediate regime where long- as well as short-range connections constitute the neural architecture. Moreover, the optimal response is additionally enhanced when the speed of signal propagation is optimized.

1. Introduction

Neural dynamics is a cooperative process of neurons and the existence of the synchronous rhythms is crucial for performing of the operational tasks in various specialized areas of the nervous system [1,2]. A particularly interesting type of a complex oscillatory rhythm of neurons is bursting, where the neural activity alternates, on a slow time scale, between a quiescent state and fast repetitive spiking [3]. Neural bursting has been identified in several processes and regions in the mammal brain [4] such as the olfactory system or the hippocampal region [5]. Remarkably, variations of rhythmic bursting activity are also believed to be involved in various clinical disorders and pathological conditions [6,7]. In order to explore the bursting synchronization mechanisms in ensembles of coupled neurons mathematical models have been utilized [8–10]. This is because the study of synchronization and desynchronization of neuronal bursting behaviours from biophysical models may help us to understand further the information processing and coding as well as disorders in the nervous system. Notably, in the last decade the focus of this interest has shifted to ensembles characterized with complex interaction topologies, as constituted by small-world or scale-free networks [11–16]. Motives are definitely related with the fact that such topological structures have been identified in the nervous system [17]. Moreover, Pontes et al. also took into account the spatial distance between coupled bursting neurons [18]. In their model the interaction strength decreased as a power law with increasing distance, thus enabling the emulation of the fractal nature of dendritic connections.

It is known that information flow in neural networks is not instantaneous. A finite signal transmission speed along the axons results in a space dependent time delay. Typical speed of signal conduction is on the order of m/s, leading to transmission times up to hundreds of milliseconds for information propagation through the cortical network [19]. Previous studies have already revealed that time delays can gradually affect the spatiotemporal dynamics in networks of coupled neurons [20]. Remarkably, Dhamala et al. [21] have shown that time-delayed coupling facilitates the existence of stable

* Corresponding author. Tel.: +386 2 2293893; fax: +386 2 2518180.
E-mail address: marko.gosak@uni-mb.si (M. Gosak).

0378-4371/$ – see front matter
doi:10.1016/j.physa.2011.12.027

synchronized states of two chaotic neurons, whereas Burić et al. [22] extended the concept to a pair of noisy bursting neurons. Furthermore, many interesting phenomena such as zigzag fronts of excitations and antiphase synchronization [23] as well as multiple stochastic resonances [24] were found in neuronal networks with constant delays. Wang et al. [25] investigated delay-induced synchronization transitions on neuronal network and their study has revealed that an enhanced synchronized response is observed if the delay equals a multiple of the inherent oscillation frequency of neurons. Special attention has also been devoted to different types of coupling mechanisms and transmission delays. Along these lines Wang et al. [26] studied synchronization transition of bursting neurons with respect to attractive and repulsive coupling, whereas Hao et al. [27] focused on the difference between electrical and chemical coupling. In Ref. [28] burst synchronization via delayed inhibitory synapses has been analysed. Nevertheless, the use of constant fixed delays provides a good approximation for simple circuits consisting of a small number of cells. However, realistic neural networks are embedded in metric space and hence the network topology and the transmission delays are also a function of the Euclidean distance between the neurons. In view of that, several studies tackled synchronization of neural networks with distributed and time-varying delays [29–32]. It has been shown that space-dependent delays can destabilize the synchronous states and induce the formation of waves [33]. Later on, Ko et al. [34] and Ko and Ermentrout [35] widened the idea of distance-dependent delays to complex interaction topologies by studying the synchronous behaviour and wave formation in sparsely coupled neuronal oscillators.

In the present study we extend the scope of research of synchronization of bursting activity on complex networks with the presence of signal transmission delays. For this purpose we develop a network representation of neural architecture, where vertices are bursting neurons embedded in three-dimensional metric space and links model electrical coupling between them. The employed network model allows us to smoothly alter the topology from a scale-free network with dominating long-range connections to a network where principally only adjacent neurons are connected. In our previous studies a similar network model has been used in order to determinate the topology leading to optimal stochastic and coherence resonance responses in an ensemble of excitable neurons [36,37]. Here we widen this idea to identify the most favourable interaction topology for the synchronization of bursting neurons. Additionally, we consider transmission delays, which are a consequence of finite signal propagation speeds and they depend on the Euclidean distances between coupled neurons. Therefore, when the topology is altered, the distribution and the rate of delays are simultaneously modified as well. In contrast to previous studies on small-world and scale-free networks [11–16], the employed model thus enables the identification of topological as well as dynamical conditions which ensure the most synchronized bursting activity, without choosing any specific network configuration.

2. Mathematical model

To mimic the characteristic bursting dynamics of neurons, we make use of the iterated map proposed by Rulkov [8], which captures succinctly the main features of more complex time-continuous neuronal models, but is numerically much more efficient. The temporal evolution of the i-th neuron along with delayed coupling is defined as follows:

$$x_i(t+1) = \frac{\alpha_i}{1+x_i(t)^2} + y_i(t) + D\sum_{j=1}^{N} \varepsilon_{ij}[x_j(t-\tau_{ij}) - x_i(t)], \tag{1}$$

$$y_i(t+1) = y_i(t) - \gamma x_i(t) - \sigma, \tag{2}$$

where $y_i(t)$ and $x_i(t)$ are the slow and fast variable of the map, respectively, and are considered as dimensionless variables, t is the discrete time index and α, γ and σ are systems parameters. By choosing $\gamma = \sigma = 0.001 \ll 1$ we ensure that the dynamics of $x_i(t)$ is much faster than that of $y_i(t)$. Furthermore, we consider values of α_i above 4.0, where the Rulkov map produces chaotic oscillations. In this case the slow variable $y_i(t)$ exhibits saw-tooth oscillations, whereas the fast variable $x_i(t)$ emulates the spiking–bursting behaviour. When the slow variable reaches a local maximum the fast variable begins its firing interval. After the slow variable reaches a local minimum the firing interval switches then into a quasi-steady state. In order to take into account the diversity of neurons, values of α_i are assumed to follow a power-law $P(\alpha) \sim \alpha^{-\beta}$ with a scaling exponent $\beta = 2.5$. Values of α_i are then confined within the interval [4.1, 4.4], whereby the characteristic of the distribution remains intact. This arrangement of α_i implies a small number of highly active oscillators with small time intervals between the bursts whereas the majority of neurons are less active. Namely, higher the values of α_i correspond to higher frequencies of bursting patterns. In this manner we presume the existence of a small fraction of leader (precursor) neurons, which endeavour to trigger the response of its neighbours and thus act as global initiators of the bursts [38].

The sum in Eq. (1) stands for the coupling, where the coupling strength is symbolized by D and ε_{ij} is the connectivity matrix which has a value of 1 if the i-th and j-th neuron are electrically coupled and 0 otherwise. The calculation of the network connectivity is based on the spatially embedded vertex fitness network model [39]. First, N neurons are randomly distributed according to a uniform distribution inside a unit cube. Then, the i-th and the j-th neuron are connected if the following condition is fulfilled:

$$\frac{\alpha_i \alpha_j}{I_{ij}^{\delta}} > \Theta, \tag{3}$$

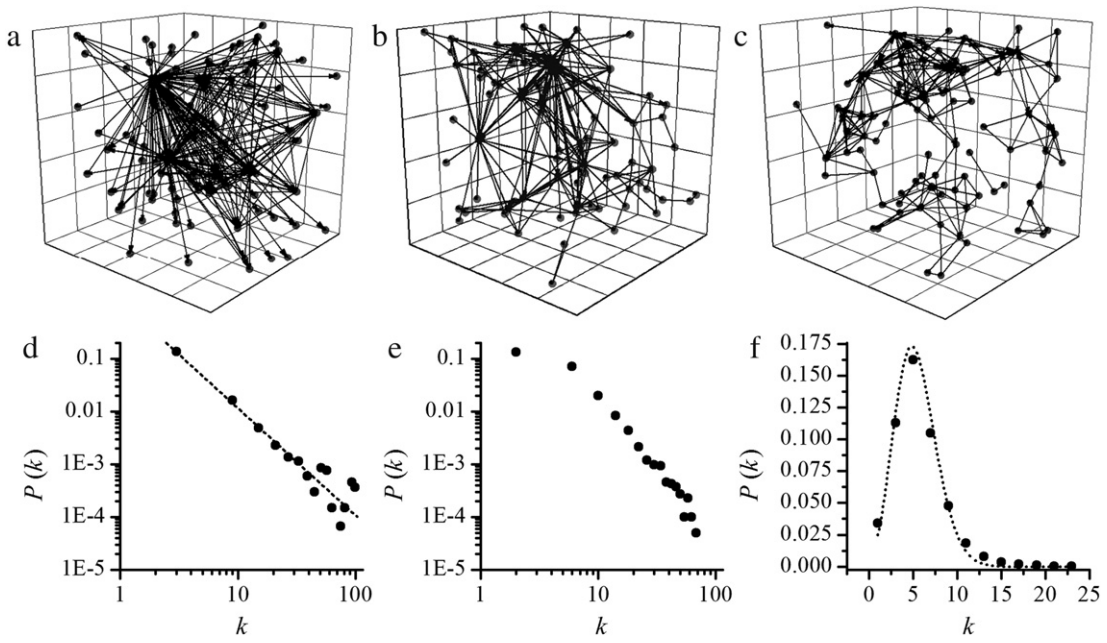

Fig. 1. Characteristic network structures and the corresponding degree distributions for $\delta = 0.1$ (a, d), $\delta = 1.7$ (b, e) and $\delta = 5.0$ (c, f). The number of neurons is $N = 100$ and mean vertex degree is $\langle k \rangle = 5$. The calculation of degree distributions is based on the average of ten independent network generations.

where Θ is a threshold that adjusts the mean vertex degree $\langle k \rangle$, I_{ij} is the Euclidean distance between the i-th and j-th neuron and δ is a control parameter that enables smooth alterations of the topology of the interaction network (see also our previous work [36,37]). The condition given in Eq. (3) entails that in general neurons with higher values of α_i, i.e. leader neurons, are more likely to be connected. The characteristic network configurations obtained for different values of δ along with the corresponding degree distributions are shown in Fig. 1.

It can be observed that for $\delta = 0.1$ (Fig. 1a) the network consist solely of long-range connections which originate mostly from a few leader neurons. In this case the creation of connections is not affected by the Euclidean distance and hence neurons with higher values of α_i have the highest vertex degree. The corresponding degree distribution (Fig. 1d) follows a power-law indicating a highly heterogeneous network structure. However, as δ is increased, the spatial distribution of neurons becomes more and more important and consequently short-range interactions emerge. For $\delta = 1.7$ (Fig. 1b) we have thus a mixture of long- and short-range link, whereas for $\delta = 5$ (Fig. 1c) only adjacent neurons are connected. It can also be noticed that for higher values of δ the degree distributions become more homogeneous, so that for $\delta \gg 1$ the degree distribution obeys a Poisson distribution (Fig. 1f), a typical feature of random geometric graphs.

The coupling term in Eq. (1) also involves a transmission delay τ_{ij}, which is, as announced in the Introduction, a consequence of finite speed of the action potential propagation. Accordingly, the transmission delay between the i-th and the j-th neuron is defined as follows:

$$\tau_{ij} = \frac{I_{ij}}{v}, \tag{4}$$

where v is the signal propagation speed. Since the model describing the bursting dynamics is discrete in time, the delays have to be converted into integer numbers. In particular, the value calculated in Eq. (4) is rounded down, i.e., only the integer part of the calculated value is considered. In our model the neurons are uniformly randomly distributed in a unit cube and hence the maximal possible distance between them is $\sqrt{3}$. Accordingly, $v = 2$ corresponds to instant communication with no delays, whereas v smaller then $\sqrt{3}$ give rise to finite delays τ_{ij}. It should be emphasized that the lengths of connections I_{ij} vary with δ and therefore the resulting delays are directly related to the topology of the network as well. To adjust the range of delays, v is used as a control parameter, whereby the resulting delays are always between 0 and the integer part of the fraction $\sqrt{3}/v$.

3. Results

We consider an ensemble of $N = 200$ neurons which form a network with a mean degree $\langle k \rangle = 5$ and are weakly coupled with a coupling strength $D = 0.003$. All presented results were averaged over at least 20 independent runs in order to assure the appropriate statistical accuracy. Our main interest is to examine the coherent behaviour in the system as a

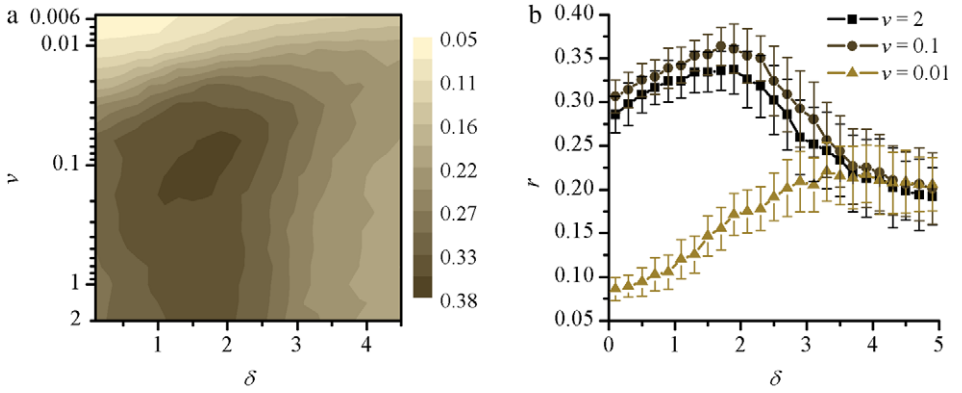

Fig. 2. The level of phase synchronization quantified via r as a function of network structure δ and transmission speed v (a) and the cross sections of the colour map at different values of v (b).

function of the network topology and the signal propagation speed. We focus mainly on the phase synchronization, which is a quite weak condition of synchronization, since it gives only an inside on how synchronous is the switching between the bursting and quasi-steady state phases of oscillators. For a given oscillator the phase increases for 2π at the beginning of each burst, i.e. each maximum of the slow variable $y_i(t)$. Between two bursts the phase increases linearly with the discrete time t. The phase $\varphi_j(t)$ for the j-th neuron is described by the following equation [12–14]:

$$\varphi_j(t) = 2\pi\left(n + \frac{t - t_j(n-1)}{t_j(n) - t_j(n-1)}\right), \quad t_j(n-1) \le t < t_j(n) \tag{5}$$

where the n-th burst of the j-th oscillator begins at time $t_j(n)$. Note that the duration of individual burst $t_j(n) - t_j(n-1)$ varies in an irregular fashion due to the chaotic dynamics. Furthermore, the neurons are heterogeneous and hence with the given coupling strength exact equality of bursting times cannot be realized. However, coupling gives rise to a more collective motion in terms of chaotic phase synchronization, where neurons try to harmonize their phases with each other, while the amplitude and spiking behaviour are in general poorly correlated. To capture the order of phase synchronization, we have to calculate the complex phase order parameter r_t at a given time t:

$$r_t = \frac{1}{N}\sum_{j=1}^{N} e^{i\varphi_j(t)}. \tag{6}$$

The phase order parameter in a system of completely synchronized oscillators equals one, whereas in the case of totally uncorrelated activity $r_t = 0$. In order to describe the average global collective motion we calculate the time averaged order parameter r:

$$r = \frac{1}{T}\sum_{t=1}^{T} r_t, \tag{7}$$

where $T = 10^5$ is the total number of iterations used in the calculations after $2 \cdot 10^4$ initial iterations were discarded as transients. In case of synchronization in a network of heterogeneous chaotic neurons, values of r are expected between 0 and 1, whereby higher values correspond to a greater extent of synchronization. Results showing r as a function of δ and v are presented in Fig. 2. It can be observed that as long as $v > 0.02$ the optimal phase synchronization is achieved for intermediate values of δ, at which the network is constituted by long- as well as by short-range connections. For lower propagation speeds the most synchronized response is obtained at larger values of δ, where the lengths of connections are lower. Furthermore, the best synchronization is at $v \approx 0.1$, which shows that delayed coupling gives rise to the collective behaviour in a network of heterogeneous neurons. Thus the plot in Fig. 2 shows that the collective dynamics of weakly coupled chaotic neurons is strongly influenced by both the network configuration and the propagation speed of the signals.

To get some additional insights into the dynamical behaviour we examine the correlations between individual neurons by calculating the correlation matrix R, whose ij-th element is defined as follows:

$$R_{ij} = \frac{\sum[\bar{x}_i - x_i(t)][\bar{x}_j - x_j(t)]}{s_{x_i} s_{x_j}} \tag{8}$$

where $\bar{x}_i$ and $\bar{x}_j$ are the mean values of the fast variables during all iterations and s_{x_i} and s_{x_j} the standard deviations of the time series $x_i(t)$ and $x_j(t)$, respectively. If $R_{ij} = 0$ no correlation between the i-th and j-th oscillator exist, whilst $R_{ij} = 1$ signifies

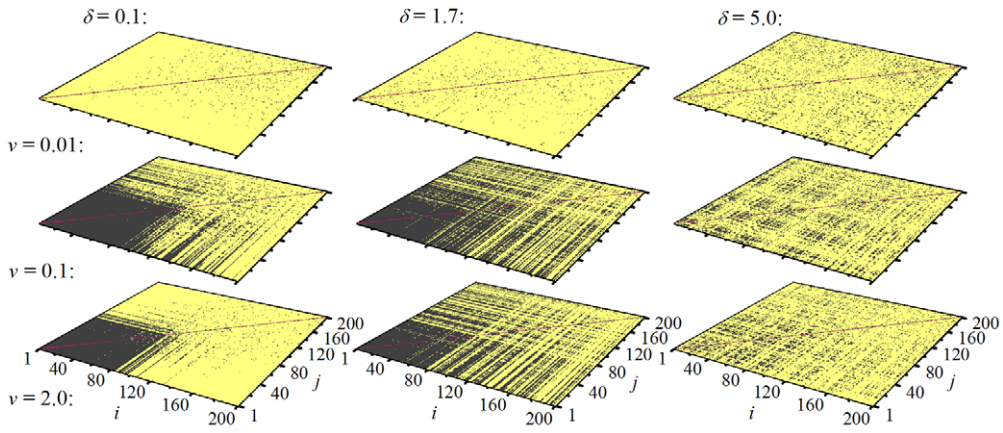

Fig. 3. Correlation matrices R_{ij} for different interaction topologies (columns) and different speeds of signal propagation (rows). If the correlation between the i-th and j-th neuron is more than 0.1, point (i, j) is marked black, otherwise it is yellow. Note that the neurons are indexed in descending order of α_i.

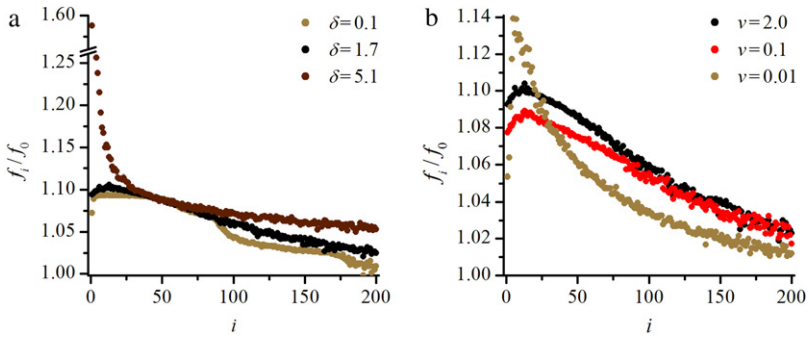

Fig. 4. Frequency of the i-th oscillator f_i at $v = 2$ (instantaneous communication) for different network structures (a) and for different propagation speeds at optimal network configuration, i.e. $\delta = 1.7$ (b). Note that the frequencies have been normalized to the minimal frequency $f_0 = 0.00291$.

completely synchronous motion. The correlation matrices for three characteristic network structures ($\delta = 0.1$, $\delta = 1.7$ and $\delta = 5$) and three different propagation speeds ($v = 2.0$, $v = 0.1$ and $v = 0.01$) are shown in Fig. 3. We can observe that in case of scale-free interaction topology ($\delta = 0.1$), a good correlation exists mainly between active neurons, which also have a high node degree, whereas the less active neurons are weakly correlated. On the other hand, in the network where short-range connections are dominative ($\delta = 5$), only some clusters of correlated neuronal activity exist, whose positions do not depend on the inherent dynamics of individual neurons. Notably, the biggest overall correlation is attained at intermediate values of δ, which once again confirms that the best synchronization is achieved if both long- and short-range interactions characterize the network. In this case the most active neurons function as "local" hubs that dictate the dynamics of the local interconnected neighbourhood and also communicate among themselves (Fig. 1b). Moreover, the optimal speed of signal transmission at $v = 0.1$ additionally improves the correlation among bursting neurons in comparison to $v = 2.0$, where no transmission delays are incorporated in the coupling.

To further investigate the impact of network topology and transmission speed on synchronized bursting, we examine the distribution of frequencies of individual neurons. The average bursting frequency of the i-th neuron f_i is defined as the total number of bursts n_i divided by the time interval in which they occur t_i:

$$f_i = \frac{n_i}{t_i}. \tag{9}$$

The system consists of a small number of very active oscillators with high intrinsic frequencies when they are uncoupled, and a large number of low-frequency oscillators. When they are coupled, the effect of different network configurations and different propagation speeds on the average frequency distribution are shown in Fig. 4. We use the standard deviation (SD) as a measure for dispersion of the frequencies. The results in Fig. 4a reveal that the frequency distribution is the most homogeneous for the optimal system constellation consisting of short- and long-range connections ($\delta = 1.7$). In particular, the SD's expressed as a percentage of the mean values for $\delta = 0.1$, $\delta = 1.7$ and $\delta = 5$ were 2.9%, 2.4% and 5.2%, respectively. Clearly, for intermediate network topology the coupled neurons maximally adopt their frequencies and try to unify their values. Moreover, in Fig. 4b we can observe that the optimal speed of signal transmission ($v = 0.1$) additionally unifies the frequencies. The SD's expressed as a percentage of the mean values for $v = 2.0$, $v = 0.1$ and $v = 0.01$ were 2.4%, 2.0% and

3.0%, respectively. It can be observed that the frequencies of more active neurons are considerably reduced, which reflects the fact that they have a higher node degree and hence have larger coupling fluxes. Remarkably, Yu et al. [14] who studied synchronization behaviour of bursting neurons in small-world networks also revealed that coupled neurons unify their bursting frequencies and that the more active neurons adopt the bursting frequencies of less active neurons. Furthermore, we found that this additional frequency lowering of leader neurons, or increasing their periods, corresponds to the average delay of the signal transduction. Of course, a threshold exist to which the oscillatory periods can be extended by these delays; when the threshold is exceeded, the oscillators cannot be delayed any further and the distribution of frequencies become again more heterogeneous (see the case for $v = 0.01$).

4. Discussion

We have studied synchronization of weakly coupled bursting neurons. Our results show that a highest level of synchronization is obtained when a proper ratio of long- and short-range connections exist in the network. Moreover, this optimal response is additionally enhanced when the speed of signal propagation is optimized. It is worth mentioning that the presented results are in agreement with our previous studies [36,37], where we studied the impact of the interaction topology on the regularity of noise induced oscillations in an ensemble of excitable neurons. The most coherent responses were also found in the intermediate regime between the scale-free network with dominating long-range connections and the strong geometric regime, thus indicating that this is the most favourable neural architecture for various types of dynamical behaviour. However, it should be noted that not in all dynamical regimes the intermediate network configuration ensures best synchronizability. We argue that the mechanism is similar and strongly related to the flexibility properties of the individual oscillators, which enables adopting of frequencies, as it has been discussed in Fig. 4 for the present case. Sensitivity and flexibility of oscillators and their relation to the frequency adaptation have been extensively discussed in our previous papers (for review see e.g. Ref. [40]). It has been shown that the oscillator's flexibility is in principle independent of its inherent dynamics, but in general oscillators are more adoptable in the proximity of bifurcation points (for example in an excitable steady state). For the model system under consideration, the system is more flexible in the region of chaotic bursting than in the region of periodic oscillations [41]. Therefore, reduction of the discrepancy of the frequencies leading to the most synchronized response (see Fig. 4), which is attained at the intermediate network configuration, can be achieved if the oscillators operate in the regime of chaotic bursting.

Our findings thus reveal that the both network structure as well as the speed of signal transmission are vital for assuring optimal conditions for synchronization of bursting neurons. Remarkably, alterations of exactly these factors have been found to be important and responsible for certain pathological conditions. Many neurodegenerative diseases such as multiple sclerosis are related to the process of demyelination in which the myelin shells that cover the neuron fibres vanishes and consequently the action potential propagation speed is significantly modified [42]. Moreover, a number of studies have established that several neuronal pathologies are associated with changes in efficiency of the intercellular coupling and neural network dysfunctions [7,43–45]. One kind of those dysfunctions is Parkinson's disease, which leads to movement disorders. A well established method to treat patients with Parkinson's disease is deep brain stimulation [46]. This treatment includes surgical implantation of electrodes in certain areas of the brain and connects them with an external current source of high frequency [47]. The synchronization/desynchronization of a neural network under external periodic forcing has already been studied from a theoretical point of view [16,18]. The authors investigated the ability of an external periodic signal to synchronize or desynchronize a neural network. They showed that the locking frequency interval width increases with the amplitude of the external signal. Hence to achieve desynchronization, the external frequency must be chosen outside the frequency looking interval. In the future it would be worth to investigate the impact of the joint effect of delayed transmissions between neurons, topology and external forcing.

We hope that further theoretical and experimental studies about the topology and dynamics of cellular networks will be conducted, and that the results will contribute to even better understanding of physiological and pathological conditions in biological tissues with direct applications in medicine. In particular, for diagnostic purposes it would be of much importance to detect and probably measure some relevant quantities in order to get indicators for (pathological) changes in the cellular network structure and the dynamical properties of signal transduction, where the speed of signal propagation is probably the most obvious element. Additional studies will be needed to understand the communicational links, the ways of cellular coupling, not only in a way of direct adjacent connections, like gap-junctions for example, but also long-range connections of cells at different locations in the tissue. This might have spectacular consequences in preventive diagnostic, like it has been indicated for chronic hypoxia in a very early study in this direction [48].

References

[1] F. Varela, J.P. Lachaux, E. Rodriguez, J. Martinerie, The brainweb: phase synchronization and large-scale integration, Nature Rev. Neurosci. 2 (2001) 229–239.
[2] T. Nowotny, R. Huerta, M.I. Rabinovich, Neuronal synchrony: peculiarity and generality, Chaos 18 (2008) 037119.
[3] R.C. Elson, A.I. Selverston, H.D. Abarbanel, M.I. Rabinovich, Inhibitory synchronization of bursting in biological neurons: dependence on synaptic time constant, J. Neurophysiol. 88 (2002) 1166–1176.
[4] D.A. McCormick, H.R. Feeser, Functional implications of bursting firing and single spike activity in lateral geniculate relay neurons, Neuroscience 39 (1990) 103–113.

[5] M.R. Mehta, A.K. Lee, M.A. Wilson, Role of experience and oscillations in transforming a rate code into a temporal code, Nature 417 (2002) 741–746.
[6] D.R. Weinberger, Implications of normal brain development for the pathogenesis of schizophrenia, Arch. Gen. Psychiatry. 44 (1987) 660–669.
[7] T.I. Netoff, R. Clewley, S. Arno, T. Keck, J.A. White, Epilepsy in small-world networks, J. Neurosci. 24 (2004) 8075–8083.
[8] N.F. Rulkov, Regularization of synchronized chaotic bursts, Phys. Rev. Lett. 86 (2001) 183–186.
[9] M. Dhamala, V.K. Jirsa, M. Ding, Transitions to synchrony in coupled bursting neurons, Phys. Rev. Lett. 92 (2004) 028101.
[10] T. Pereira, M.S. Baptista, J. Kurths, Multi-time-scale synchronization and information processing in bursting neuron networks, Eur. Phys. J. Special Topics 146 (2007) 155–168.
[11] I. Belykh, E. de Lange, M. Hasler, Synchronization of bursting neurons: what matters in the network topology, Phys. Rev. Lett. 94 (2005) 188101.
[12] C.A.S. Batista, A.M. Batista, J.A.C. de Pontes, R.L. Viana, S.R. Lopes, Chaotic phase synchronization in scale-free networks of bursting neurons, Phys. Rev. E 76 (2007) 016218.
[13] C.A.S. Batista, S.R. Lopes, R.L. Viana, A.M. Batista, Delayed feedback control of bursting synchronization in a scale-free neuronal network, Neural Netw. 23 (2010) 114–124.
[14] H. Yu, J. Wang, B. Deng, X. Wei, Y.K. Wong, W.L. Chan, K.M. Tsang, Z. Yu, Chaotic phase synchronization in small-world networks of bursting neurons, Chaos 21 (2011) 013127.
[15] E.J. Agnes, R. Erichsen Jr., L.G. Brunnet, Synchronization regimes in a map-based model neural network, Physica A 389 (2010) 651–658.
[16] C.A.S. Batista, A.M. Batista, J.C.A. De Pontes, S.R. Lopez, R.L. Viana, Bursting synchronization in scale-free networks, Chaos, Solition. Fract. 41 (2009) 2220–2225.
[17] E. Bullmore, O. Sporns, Complex brain networks: graph theoretical analysis of structural and functional systems, Nat. Rev. Neurosci. 10 (2009) 186–198.
[18] J.C.A. De Pontes, R.L. Viana, S.R. Lopez, C.A.S. Batista, A.M. Batista, Bursting synchronization in non-localy coupled maps, Physica A 387 (2008) 4417–4428.
[19] E.R. Kandel, J.H. Schwartz, T.M. Jessell, Principles of Neural Science, fourth ed., McGraw-Hill, New York, 2000.
[20] A. Roxin, N. Brunel, D. Hansel, Role of delays in shaping spatiotemporal dynamics of neuronal activity in large networks, Phys. Rev. Lett. 94 (2005) 238103.
[21] M. Dhamala, V.K. Jirsa, M. Ding, Enhancement of neural synchrony by time delay, Phys. Rev. Lett. 92 (2004) 074104.
[22] N. Burić, K. Todorović, N. Vasović, Exact synchronization of noisy bursting neurons with coupling delays, Chaos, Soliton. Fract. 40 (2009) 1127–1135.
[23] Q. Wang, Z. Duan, M. Perc, G. Chen, Synchronization transitions on small-world neuronal networks: effects of information transmission delay and rewiring probability, EPL 83 (2008) 50008.
[24] Q. Wang, M. Perc, Z. Duan, G. Chen, Delay-induced multiple stochastic resonances on scale-free neuronal networks, Chaos 19 (2009) 023112.
[25] Q. Wang, M. Perc, Z. Duan, G. Chen, Synchronization transitions on scale-free neuronal networks due to finite information transmission delays, Phys. Rev. E 80 (2009) 026206.
[26] Q. Wang, G. Chen, M. Perc, Synchronous bursts on scale-free neuronal networks with attractive and repulsive coupling, PLoS ONE 6 (2010) e15851.
[27] Y. Hao, Y. Gong, L. Wang, X. Ma, C. Yang, Single or multiple synchronization transitions in scale-free neuronal networks with electrical or chemical coupling, Chaos, Soliton. Fract. 44 (2011) 260–268.
[28] I. Franović, V. Miljković, Phase plane approach to cooperative rhythms in neuron motifs with delayed inhibitory synapses, EPL 92 (2010) 68007.
[29] A. Hutt, F.M. Atay, Effects of distributed transmission speeds on propagating activity in neural populations, Phys. Rev. E 73 (2006) 021906.
[30] T. Li, S. Fei, K. Zhang, Synchronization control of recurrent neural networks with distributed delays, Physica A 387 (2008) 982–996.
[31] Y. Sun, D. Zhao, J. Ruan, Consensus in noisy environments with switching topology and time-varying delays, Physica A 389 (2010) 4149–4161.
[32] K. Wang, Z. Teng, H. Jiang, Adaptive synchronization of neural networks with time-varying delay and distributed delay, Physica A 387 (2008) 631–642.
[33] P.C. Bressloff, S. Coombes, Synchrony in an array of integrate-and-fire neurons with dendritic structure, Phys. Rev. Lett. 78 (1997) 4665–4668.
[34] T.-W. Ko, S.-O. Jeong, H.-T. Moon, Wave formation by time delays in randomly coupled oscillators, Phys. Rev. E 69 (2004) 056106.
[35] T.-W. Ko, G.B. Ermentrout, Effects of axonal time delay on synchronization and wave formation in sparsely coupled neuronal oscillators, Phys. Rev. E 76 (2007) 056206.
[36] M. Gosak, D. Korošak, M. Marhl, Optimal network configuration for maximal coherence resonance in excitable systems, Phys. Rev. E 81 (2010) 056104.
[37] M. Gosak, D. Korošak, M. Marhl, Topologically determined optimal stochastic resonance responses of spatially embedded networks, New J. Phys. 13 (2011) 013012.
[38] J.-P. Eckmann, S. Jacobi, S. Marom, E. Moses, C. Zbinden, Leader neurons in population bursts of 2D living neural networks, New J. Phys. 10 (2008) 015011.
[39] S. Morita, Crossovers in scale-free networks on geographical space, Phys. Rev. E 73 (2006) 035104.
[40] M. Perc, M. Marhl, Local dissipation and coupling properties of cellular oscillators: A case study on calcium oscillations, Bioelectrochem. 62 (2004) 1–10.
[41] A.L. Shilnikov, N.F. Rulkov, The origin of chaos in a two-dimensional map modeling spiking-bursting neural activity, Int. J. Bifurcat. Chaos 13 (2003) 3325–3340.
[42] S. Reutskiy, E. Rossoni, B. Tirozzi, Conduction in bundles of demyelinated nerve fibers: computer simulation, Biol. Cybern. 89 (2003) 439–448.
[43] N. Rouach, et al., Gap junctions and connexin expression in the normal and pathological central nervous system, Biol. Cell. 94 (2002) 457–475.
[44] J.J. Palop, J. Chin, L. Mucke, A network dysfunction perspective on neurodegenerative diseases, Nature 443 (2006) 768–773.
[45] Y. He, et al., Impaired small-world efficiency in structural cortical networks in multiple sclerosis associated with white matter lesion load, Brain: J. Neurol. 132 (2009) 3366–3379.
[46] C.R. Buston, C.C. McIntyre, Current steering to control the volume of tissue activated during deep brain stimulation, Brain Stimul. 1 (2008) 7–15.
[47] W.M. Grill, A.N. Synder, Svjetlana Miocinovic, Deep brain stimulation creates an informational lesion of the stimulated nucleus, NeuroReport 15 (2004) 1137–1140.
[48] M. Gosak, M. Marhl, C. Guibert, M. Billaud, E. Roux, Pulmonary artery smooth muscle responses to KCl under normoxic and hypoxic conditions studied by means of a spatial network model, in: A. Zhang, M. Borodovsky, G. Özsoyoglu, A.R. Mikler (Eds.), Proceedings of the First ACM International Conference on Bioinformatics and Computational Biology, ACM New York, New York, 2010, pp. 475–477.

The role of topological features of intercellular communication networks by the synchronization of cellular oscillators

R. Markovič*, M. Gosak*,† and M. Marhl*,†

*Faculty of Natural Sciences and Mathematics, University of Maribor, Koroška cesta 160, SI-2000 Maribor, Slovenia
†Faculty of Education, University of Maribor, Koroška cesta 160, SI-2000 Maribor, Slovenia

Abstract. Because of the complexity of processes that govern the regulatory mechanisms which control the cellular functions and dynamic behavior, mathematical models and numerical simulations are needed to fully grasp the mechanisms and functions of biological rhythms. In the last decade the theory of complex networks is frequently applied to address those issues. In the present paper we investigate theoretically the role of the intercellular communication network structure by synchronization of cellular oscillators. Motivated by the fact that in biological systems the interplay between the network structure and the dynamics taking place on it is closely interrelated, we develop a spatial network representation of an ensemble of cells in which we can tune the network organization between a scale-free network with dominating long-range connections and a homogeneous network with mostly adjacent neurons connected. Our results reveal that for noise-induced oscillations in excitable cells and for chaotic bursting oscillations the most synchronized response is obtained for the intermediate regime where long- as well as short-range connections constitute the intercellular network. On the other hand, for periodic oscillations it is found than the scale-free network topology ensures the greatest collective response. We argue that those findings are related to flexibility properties of individual cells.

Keywords: cellular oscillations, intercellular communication, complex networks.
PACS: 05.45.Xt Q, 87.18.Sn, 05.45.Xt

1 INTRODUCTION

New insights gained over the past three decades in the fields of nonlinear dynamics and complex systems are nowadays frequently applied to analyze concrete problems in biology, such as the identification of general principles that underlie the cellular organization and the relation between dynamic behaviors and cellular functions [1]. It is nowadays clear that the functioning of tissues does not only depend on intrinsic rhythms of individual cells, but crucially relies also on collective activity of cell populations. Rhythms essential for life are thus a result of interactions of these cells with each other in terms of intercellular communication. The many efforts devoted to understand collective phenomena in biological systems take now advantage of the recent theory of complex networks [2]. This is definitely related with the fact that complex interaction topologies such as constituted by small-world or scale-free networks have been identified in a plethora of real-life systems. Recently, great attention is devoted to studies describing the functioning

Let's Face Chaos through Nonlinear Dynamics
AIP Conf. Proc. 1468, 256-267 (2012); doi: 10.1063/1.4745588

of biological systems by means of the complex network theory. Examples include intracellular metabolic networks [3], interconnectedness of human diseases [4], functional and anatomical connectivity in the nervous system [5], regulation of circadian rhythms [6], cytoarchitecture of Purkinje fiber networks [7], networks of beta cells in pancreatic islets [8], etc.

Nevertheless, the question arises which network topology ensures the optimal dynamical responses under given circumstances. Namely, cells in different parts of the body have different intrinsic properties and they exhibit diverse temporal patterns. In particular, periodic oscillations and spiking are the simplest cases of dynamical processes in complex biological systems and have been identified in several tissues and organisms. Many kinds of cells are known to generate periodic voltage spikes across their cell membranes, including neurons, cells from the pumpkin stem, tadpole skin, etc. [9]. Furthermore, several types of nerve and muscle cells are excitable [10], which means that by weak external stimulation they remain quiet, whereas a strong enough stimulus activates the cells in a strongly nonlinear way. Another particularly interesting type of a complex oscillatory rhythm is bursting, where the temporal activity alternates, on a slow time scale, between a quiescent state and fast repetitive spiking. This type of dynamical behavior has been identified in several processes and regions in the mammal brain such as the olfactory system and the hippocampal region [11] or in several types of secretory cells such as the insulin producing cells in the pancreas [12].

In order to explore the relation between the optimal topological features of the intercellular network and the nature of cellular signals we make use of a spatial network model in which nodes represent cellular oscillators and links signify intercellular communication pathways. In the model the topology can smoothly be changed from a scale-free network with dominating long-range connections to a homogeneous network with dominating short-range connections, where actually only adjacent cells are connected. In this manner, similarly to our previous studies [13, 14, 15] we are able to identify the optimal intercellular network topology leading to the most coherent global response, a desirable attribute of several biological systems, which ensures physiological tissue homeostasis. However, in this paper we additionally investigate how the most synchronizable network structure is related to inherent properties of the cells. We show that the flexibility of individual cells plays important role.

2 SINGLE CELL MODEL

To mimic the different types of physiological signals, we make use of the iterated map proposed by Rulkov [16], which captures succinctly the main features of more complex time-continuous neuronal models, but is numerically much more efficient. The two-dimensional map has the following form:

$$x(t+1) = \frac{\alpha}{1+x(t)^2} + y(t), \tag{1}$$

$$y(t+1) = y(t) - \beta x(t) - \gamma, \tag{2}$$

where $x(t)$ and $y(t)$ are the fast and slow dynamic variables representing the trans membrane voltage and the slow gating process. The parameter γ represents the external dc bias current and the parameter β is related with the frequency of the slow variable [17]. In all calculations both parameter values are set to $\beta = \gamma = 0.001$. Importantly, the parameter α is taken as the control parameter enabling us to switch between different dynamical regimes. However, before we proceed to the analysis of coupled oscillators we will first explain some fundamental properties of the map. For this purpose we computed the bifurcation diagram of the fast variable, which is shown in figure 1.

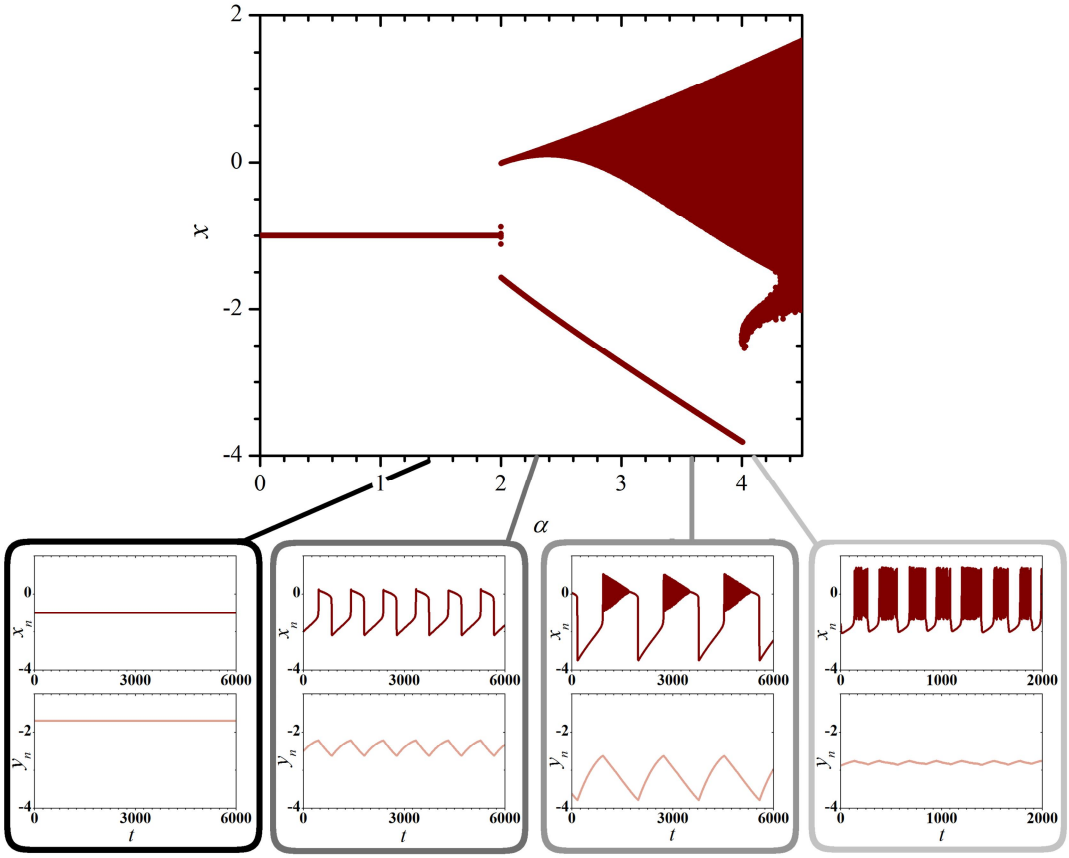

FIGURE 1. Bifurcation diagram for the fast variable of the Rulkov map and time traces for four different values of α (1.4, 2.3, 3.6 and 4.1).

For $\alpha < 2$, the system is in a steady state. If $\alpha < 1.55$ the steady state is stable, whereas for $\alpha > 1.55$ the steady state becomes excitable. The system in this region has one fixed point with the coordinates $(-1, -1 - \alpha/2)$. To analyze the stability

of this state, we have to derive the Jacobian matrix:

$$J_{(x_1^*,y_1^*)} = \begin{pmatrix} \frac{\alpha}{2} & 1 \\ -\beta & 1 \end{pmatrix}. \tag{3}$$

The eigenvalues for the fixed point (x_1^*, y_1^*) are $\Lambda_{1,2} = 1/4\left(2+\alpha \pm \sqrt{(\alpha-2)^2-16\beta}\right)$. In general, eigenvalues computed for a fixed point of a discrete system signify the stability of the fixed point to external perturbations. Adding a small perturbation to the fixed point, will cause the system to:

- move away from the fixed point if $|\Lambda| > 1$ (unstable),
- move back to the fixed point if $|\Lambda| < 1$ (stable),
- or conserves its location after the perturbation in the phase space if $|\Lambda| = 1$ (marginally stable).

The results showing the eigenvalues of the uncoupled Rulkov map and the absolute product of the eigenvalues are presented in figure 2. For $\alpha < 2$ both of the eigenvalues are $|\Lambda_{1,2}| < 1$, the solution is stable. Near the bifurcation at $\alpha = 2$ stable subthreshold oscillation with small amplitudes emerge [18]. At the bifurcation point the real part of the eigenvalues is equal to 1, the system is said to be marginally stable. After the bifurcation, the solution (x_1^*, y_1^*) becomes unstable and the system begins to oscillate. In particular, in the oscillatory region $2 \leq \alpha \leq 4$, the system alternates between two fixed points. The stability analysis from this point on is hard to tackle analytically. For this propose we make use of the Lyapunov exponents, that give us in inside on the rate of separation of infinitesimally close trajectories. We computed the Lyapunov spectrum using the Gram-Schmidt procedure [19]. The eigenvalues for any discrete systems are defined as exponential functions of the Lyapunov exponents. Furthermore, another interesting feature of a dynamical system is related to the eigenvalues – the dissipation rate. The dissipation rate is an indicator for the stability of an attractor. Discrete systems are dissipative if $|\Lambda_1 \Lambda_2| < 1$ [20].

We can conclude that the system has a stable trajectory in the phase space for all $\alpha \leq 4$. Small perturbation will on the long run not affect the systems dynamics. On the other hand, for $\alpha > 4$, the trajectories become unstable, meaning that small perturbations cause the system to diverge from its trajectory. In this region the system thus exhibits chaotic bursting. To further analyze the origins of this chaotic behavior for the uncoupled system we will treat the slow variable y_n in Eq. (1) as a parameter η [16, 21, 22]. With this simplification we can transform the Rulkov map into a 1D iterative map, which is much easier to analyze. This system can have one, two or three fixed points according to the value of η and α. From the return map of the fast variable in figure 3a, we can notice that the systems can have either two fixed points or one for low values of the parameter η. The reason for the observed phenomenon can be understood by investigating the role of the parameter η in more detail. The return map for this simplified system is shown in figure 3b. When $\eta = -2.9$, the map has three fixed points, one of the being

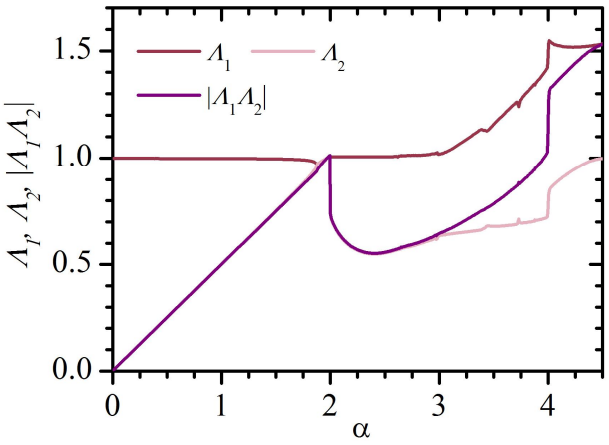

FIGURE 2. Eigenvalues Λ_1 and Λ_2 computed with the Gram-Schmidt procedure and the absolute product of the eigenvalues $|\Lambda_1\Lambda_2|$ as a function of the bifurcation parameter α.

unstable whereas the other two are stable (figure 3d). By increasing the value η the stable x_1^* and unstable x_2^* fixed points merge together at the critical value η_{sn} the point of the saddle-node bifurcation. When the slow variable exceeds this value $\eta > \eta_{sn}$ the fixed points x_1^* and x_2^* disappear and irregular bursts emerge. On the other hand, when the unstable branch crosses the minimal iterate line of the fast variable, another bifurcation occurs due to an external crisis, where the strange attractor disappears. For the 2D Rulkov map, the same mechanisms are involved (see figure 3c).

Another turning point is reached, when the fast variable reaches the value $x_n = -1$ in the region where the slow variable increases towards a local maximum and the stable and unstable solution of the map disappear. From this point on the slow variable begins to decreases till a local minimum is reached. When the slow variable starts to decrease from a local maximum towards a local minimum, bursting spikes emerge in the fast variable. The duration of the bursting is limited by the onset of the external crisis bifurcation. The saddle-node and the external crisis bifurcations are boundaries, which ensure that the system will always return to a stable branch after a perturbation.

In order to provide further insight to the subject we apply an external periodic signal to the fast variable of the Rulkov map with the aim to check how the map adopts to external driving in different dynamical regimes. The fast variable coupled with the periodic signal has the following form:

$$x(t+1) = \frac{\alpha}{1+x(t)^2} + y(t) + Asin\,(\omega t)\,, \tag{4}$$

where A and ω are the amplitude and frequency of the external signal, respectively. Results presented in figure 4 reveal that before the bifurcation at $\alpha = 2$ the systems adopts very well to external driving, whereas in the oscillatory region $(2 \leq \alpha \leq 4)$

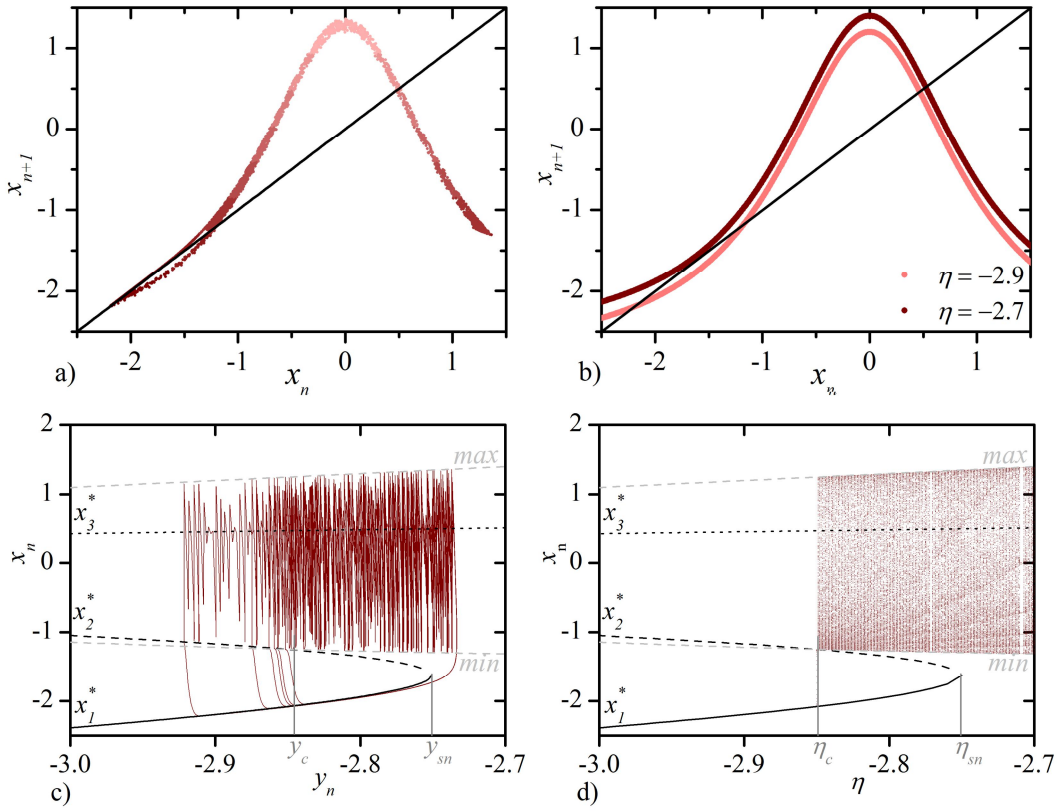

FIGURE 3. Return map for the fast variable of the Rulkov map (a) and simplified 1D Rulkov map (b) and the corresponding phase space plot for the 2D Rulkov map (c) and 1D Rulkov map (d). The *max* and *min* line represent the maximal and minimal iterate of the Rulkov map. The external bifurcation and saddle-node bifurcation are indexed as *c* and *sn*. The bifurcation parameter in all cases is $\alpha = 4.1$.

the map is very rigid and hard to entrain. However, in the regime of chaotic bursting the oscillator becomes again more susceptible to external driving, since there is a broad range of frequencies at which the system follows the driving. We argue that the mechanism is similar and strongly related to the flexibility properties of an individual oscillator, which enables adopting of frequencies [23]. To put in another way, the Rulkov map is more flexible in the excitable state and in the region of chaotic bursting than in the region of periodic oscillations [15, 18]. In the continuation we will examine how these properties are related with synchronization behavior in a network of coupled cells.

3 NETWORK OF COUPLED OSCILLATORS

The model of coupled cellular oscillators is composed of $N = 100$ Rulkov maps linked by a complex network of intercellular communication. The temporal evolu-

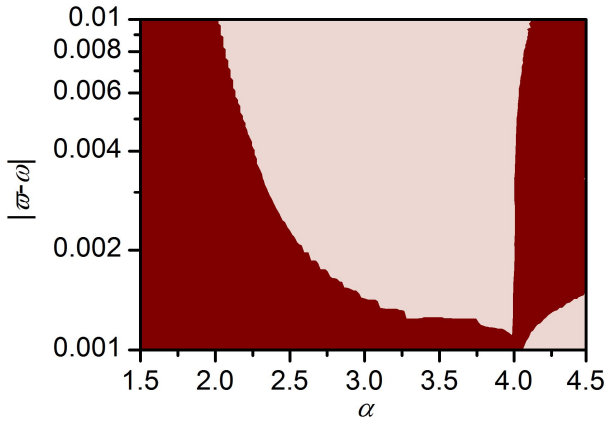

FIGURE 4. Area of synchronization of the fast variable with an external periodic signal as a function of α. The term $|\bar{\omega}-\omega|$ signifies the difference between the inherent frequency of the oscillator and the frequency of external driving. Synchronized regions are marked with a dark red color and the unsynchronized regions with a bright red color. The amplitude of the external signal is $A = 0.1$.

tion of the i-th oscillator is defined as follows:

$$x_i(t+1) = \frac{\alpha_i}{1+x_i(t)^2} + y_i(t) + \epsilon \sum_{j=1}^{N} d_{i,j}\left(x_j(t) - x_i(t)\right), \tag{5}$$

$$y_i(t+1) = y_i(t) - \beta x_i(t) - \gamma. \tag{6}$$

Each oscillator of the system is labeled with an integer i, hence $x_i(t)$ and $y_i(t)$ are the fast and slow variable for the i-th oscillator. The sum in Eq. (5) represents the coupling term with the coupling strength ϵ and the connectivity matrix $d_{i,j}$. The elements of the connectivity matrix are 1 if the i-th and j-th oscillator are connected and 0 otherwise. For the creation of the network we make us of the spatially embedded vertex fitness network model [13, 14, 15, 24]. First, N vertices are randomly distributed inside a unit square. Then, to vertices fitness values f_i are ascribed, which are assumed to follow a power law distribution. Two vertices are connected when the following condition is fulfilled:

$$\frac{f_i f_j}{I_{ij}^{\delta}} > \Theta, \tag{7}$$

where Θ is a threshold, which is used to adjust the mean degree $\langle k \rangle$. In our calculations the mean degree was set to 5. The parameter I_{ij} is the Euclidian distance between the i-th and j-th node. Furthermore, δ is the control parameter which enables changes of the network structure. Characteristic network structures for three different values of δ along with the global efficiency E of the network and the average clustering coefficient C as a function of δ are shown in figure 5.

For small values of the control parameter ($\delta << 1$), the spatial distribution of the networks units has almost no effect on the connection algorithm, and hence the network consists mainly of long-range connections. It can be noticed that for $\delta = 0.1$ we have a very efficient network with a relatively low clustering coefficient. Its degree distribution follows a power law [13, 24]. With increasing δ long-range connections become less likely to be accepted and accordingly also short-range link emerge. So, for $\delta = 1.3$ there is a combination of long- and short-range connections. Furthermore, the network is less efficient but has on the other hand a larger clustering coefficient. Evidently, for ($\delta >> 1$) the Euclidean distance becomes the key constraint defining the network connectivity and according only short-range connections can be established. For that reason for $\delta = 4.2$ we obtain a network that has properties of a random geometric network [13], which has a low efficiency.

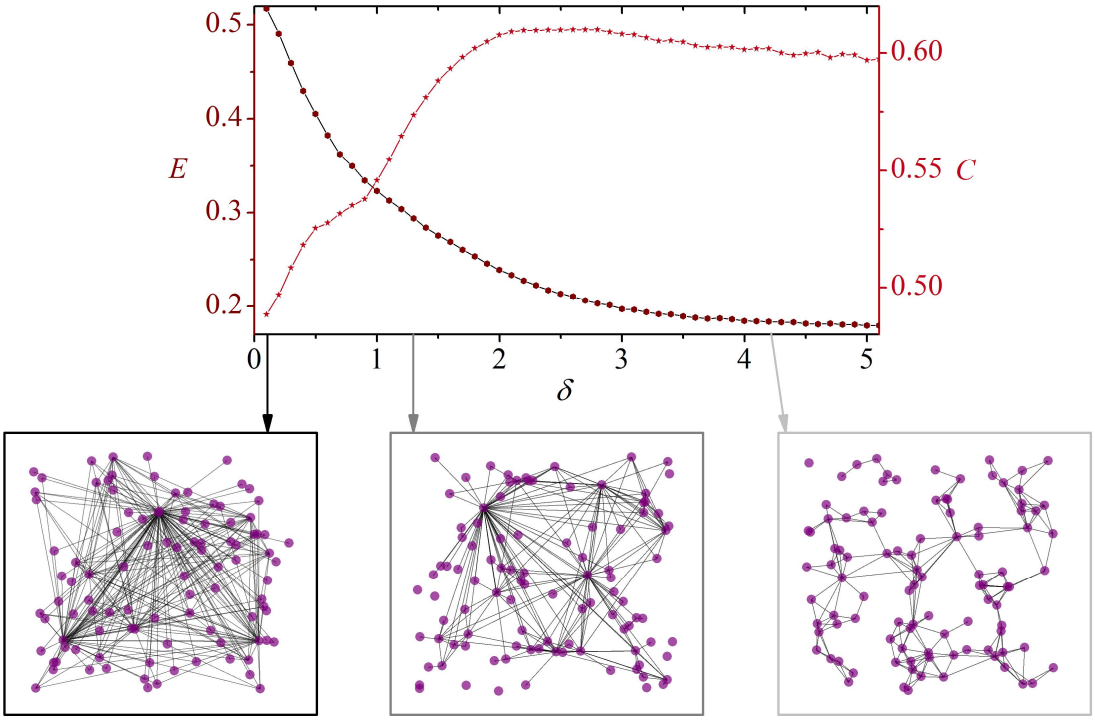

FIGURE 5. The average efficiency (left axes) and the average clustering coefficient (right axes) as a function of the topology parameter. In the insets characteristic network structures are shown for $\delta = 0.1$, $\delta = 1.3$ and $\delta = 4.2$.

4 RESULTS

We populate the given network with cellular oscillators whose dynamics is driven by the Rulkov map and systematically analyze the synchronization behavior. We give special attention to the role of the network structure and to synchronization of oscillators in different dynamical regimes. To quantify the degree of synchronization

in the system we compute the correlation between any pair of oscillator R_{ij}:

$$R_{ij} = \frac{1}{T} \frac{\sum [\bar{x}_i - x_i(t)] [\bar{x}_j - x_j(t)]}{S_i S_j}, \tag{8}$$

where $\bar{x}_i$ and $\bar{x}_j$ are the average value of the fast variable for the i-th and j-th oscillator, respectively, whereas S_i and S_j are the corresponding standard deviations of the time series. T signifies the number of iteration steps used in the calculation.

After computing the average correlation between all pairs of oscillators, we get an $N \times N$ correlation matrix whose ij-th element is R_{ij}. If $R_{ij} = 1$ then the dynamics of the i-th and j-th oscillator is completely synchronized, whilst $R_{ij} = 0$ means that the dynamics is completely uncorrelated. We characterize the global synchronization of the system by the average correlation coefficient:

$$\bar{R} = \frac{1}{N(N-1)} \sum_{i=1}^{N} \sum_{j \neq i} R_{ij}. \tag{9}$$

We focus on synchronization in three different dynamical regimes: i) noise induced dynamics in the excitable steady state ($\alpha = 1.95$), ii) periodic oscillations ($\alpha = 2.5$), iii) chaotic bursting ($\alpha = 4.1$). For $\alpha = 1.95$ we supplement Eq. (5) with the term $\sqrt{2D}\xi_i(t)$ which stands for random fluctuations, whereby D defines the strength of Gaussian noise with zero mean and autocorrelation $\langle \xi_i(t)\xi_i(t') \rangle = \delta_{ij}\delta(t - t')$. For a proper noise value ($D = 0.0005$) nearly periodic noise induced oscillations are attained, thereby signaling the coherence resonance phenomenon [13, 25].

The color-contour plots in figure 6a-c feature the average correlation coefficient $\bar{R}$ value as s a function of the network structure δ and coupling strength ϵ. We can notice that for $\alpha = 1.95$ the optimal synchronization is always attained for the intermediate network configuration ($\delta \approx 1.3$). Similarly, for the case of chaotic bursting ($\alpha = 4.1$) the intermediate network structure ensures the best synchrony except for strong coupling where the largest coherence is attained in the scale-free network. Remarkably, in the region of periodic oscillations ($\alpha = 2.5$) the situation is completely different. Namely, irrespective of the coupling strength value, the most synchronized response is always attained in the long-range dominated scale-free network. To further corroborate our findings we show in figure 6d-f cross-sections of the contour-plots at intermediate coupling strength $\epsilon = 0.005$. Obviously, for $\alpha = 1.95$ and $\alpha = 4.1$ we have a resonant response due to the change in topology, whereas for $\alpha = 2.5$ the average correlation coefficient monotonously decreases with increasing δ.

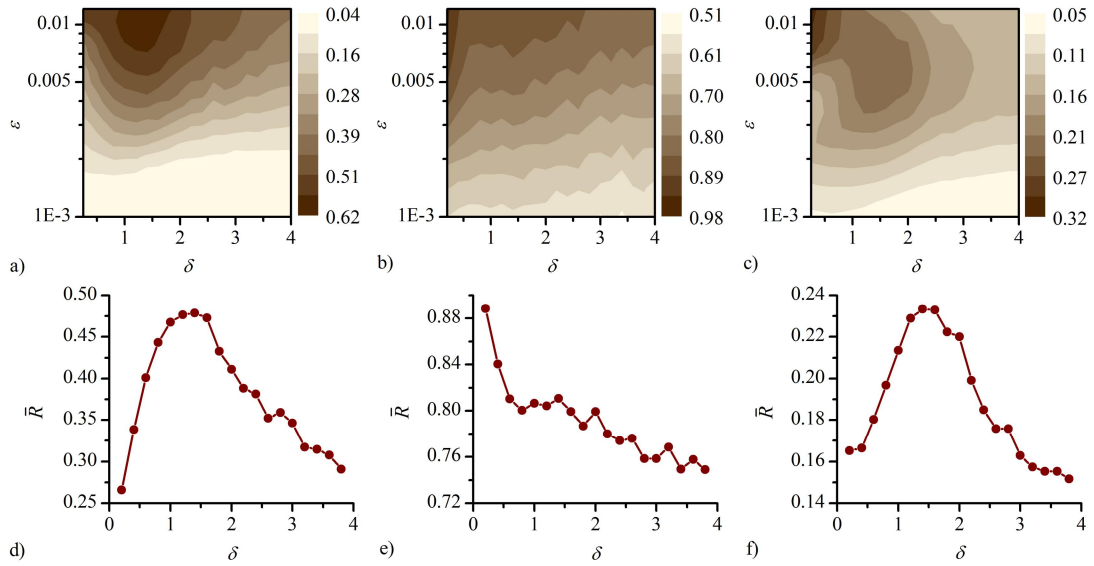

FIGURE 6. Contour plots of the average correlation $\bar{R}$ as a function of the coupling strength ϵ and the topology parameter δ for a) $\alpha = 1.95$, b) $\alpha = 2.5$ and c) $\alpha = 4.1$ and the corresponding cross sections at $\epsilon = 0.005$ (d-f).

In order to define the regions, where the optimal synchronization is achieved in the intermediate topology and where the scale-free network is the better option, we introduce the relative correlation quantity:

$$\kappa = 1 - \frac{\bar{R}(0.1)}{\bar{R}(1.3)}, \tag{10}$$

which denotes the ratio between the average correlation coefficient values at $\delta = 0.1$ and $\delta = 1.3$. If $\kappa < 0$, then the average correlation in a setup with a scale-free topology is higher than in the intermediate network structure. Results showing κ as a function of δ are shown in figure 7. We can observe that changes occur at the transition points between different dynamical regimes. It is now clear that in the case of periodic oscillations the scale-free topology ensures best synchrony, whereas for noise-induced oscillations in the excitable state and chaotic bursting the intermediate topology leads to the largest level of coherence. A comparison of figures 7 and 4 implies an incontestably relation between the ability of the oscillators to adapt to external forcing and the most synchronizable topology. It appears, as discussed more detailed later in the Discussion, that for rigid oscillators a scale-free network structure ensures the most synchronized response, but on the other hand, flexible oscillators exhibit the most synchronized motion in the intermediate regime where long- as well as short-range interactions are present in the network.

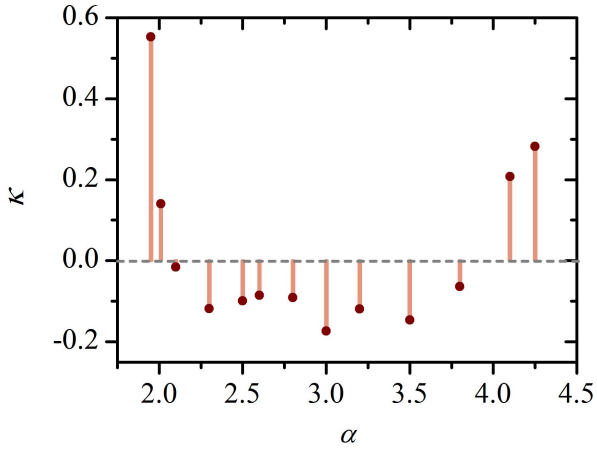

FIGURE 7. The relative correlation quantity κ as a function of the bifurcation parameter α.

5 DISCUSSION

Properties of complex networks have been reported in numerous biological systems [2, 3, 4, 5, 6, 7, 8]. It seems that the structural principles of complex networks indeed play a pivotal role by the functioning of living organisms. In the present study we focused on synchronization of cellular oscillators, which is an essential component by the regulation of many physiological tasks. Our results indicate that in case of noise-induced oscillations or chaotic bursting a highest level of synchronization is obtained when a proper ratio of long- and short-range connections exists in the network. On the other hand, in the case of periodic oscillations, the scale-free network structure with dominating long-range connections ensures the greatest degree of coherence. Furthermore, we relate the synchronization behavior in different dynamical regimes with the flexibility of individual oscillators. However, at this point it must be emphasized that in principle flexibility properties are independent of the inherent dynamics of the oscillators [26]. The oscillator model system under consideration is more flexible in the excitable state and in the region of chaotic bursting than in the region of periodic oscillations. But in general, oscillators are flexible in regimes with weak dissipation, which is not necessarily related with the nature or complexity of the signal [23, 26]. We hypothesize that many cellular oscillators are flexible in terms of being able to adapt to a broad range of entraining frequencies. Hence it follows that the most synhronizable network structure for such oscillators is constituted by both, long- as well as short-range connections (see figure 5). Remarkably, such topological features in general offer a good compromise between network efficiency, wiring economy, and robustness [13]. They have been found, for example, in anatomical neural networks, which are on the one hand connected in a heterogeneous and efficient network, but on the other hand they are sparsely connected, so that the physical distance between cells is relatively small [5]. In that way, an efficient information transport between nodes is achieved at low connectivity cost.

REFERENCES

1. L. Glass, *Nature* **410**, 277–284 (2001).
2. R. Albert, and A.-L. Barabási, *Rev. Mod. Phys.* **74**, 47–97 (2002).
3. H. Jeong, B. Tombor, R. Albert, Z. N. Oltvai, and A. L. Barabási, *Nature* **407**, 651–654 (2000).
4. K.-I. Goh, M. E. Cusick, D. Valle, B. Childs, M. Vidal, and A.-L. Barabási, *Proceedings of the National Academy of Sciences* **104**, 8685–8690 (2007).
5. E. Bullmore, and O. Sporns, *Nature Reviews Neuroscience* **10**, 186–198 (2009).
6. C. Vasalou, E. D. Herzog, and M. A. Henson, *Journal of Biological Rhythms* **24**, 243–254 (2009).
7. N. Ono, T. Yamaguchi, H. Ishikawa, M. Arakawa, N. Takahashi, T. Saikawa, and T. Shimada, *Archives of Histology and Cytology* **72**, 139–149 (2009).
8. D. Korošak, and M. Rupnik, *AIP Conference Proceedings* **1076**, 122–128 (2008).
9. K. Kruse, and F. Jülicher, *Current Opinion in Cell Biology* **17**, 20–26 (2005).
10. E. M. Izhikevich, *International Journal of Bifurcation & Chaos* **10**, 1171–1266 (2000).
11. D. McCormick, and H. Feeser, *Neuroscience* **39**, 103–113 (1990).
12. R. Bertram, A. Sherman, and L. S. Satin, "Electrical Bursting, Calcium Oscillations, and Synchronization of Pancreatic Islets," in *The Islets of Langerhans*, edited by M. S. Islam, Springer Netherlands, 2010, vol. 654 of *Advances in Experimental Medicine and Biology*, pp. 261–279.
13. M. Gosak, D. Korošak, and M. Marhl, *Phys. Rev. E* **81**, 056104 (2010).
14. M. Gosak, D. Korošak, and M. Marhl, *New Journal of Physics* **13**, 013012 (2011).
15. M. Gosak, R. Markovič, and M. Marhl, *Physica A: Statistical Mechanics and its Applications* **391**, 2764–2770 (2012).
16. N. F. Rulkov, *Phys. Rev. Lett.* **86**, 183–186 (2001).
17. B. Ibarz, H. Cao, and M. A. F. Sanjuán, *Phys. Rev. E* **77**, 051918 (2008).
18. A. L. Shilnikov, and N. F. Rulkov, *Physics Letters A* **328**, 177–184 (2004).
19. F. Christiansen, and H. H. Rugh, *Nonlinearity* **10**, 1063 (1997).
20. B.-H. Wang, *Commun. Theor. Phys.* **21**, 289–298 (1994).
21. B. Ibarz, J. Casado, and M. Sanjuán, *Physics Reports* **501**, 1–74 (2011), ISSN 0370-1573.
22. R. Viana, A. Batista, C. Batista, J. de Pontes, F. dos S. Silva, and S. Lopes, *Communications in Nonlinear Science and Numerical Simulation* **17**, 2924–2942 (2012).
23. M. Perc, and M. Marhl, *Bioelectrochemistry* **62**, 1–10 (2004).
24. S. Morita, *Phys. Rev. E* **73**, 035104 (2006).
25. A. S. Pikovsky, and J. Kurths, *Phys. Rev. Lett.* **78**, 775–778 (1997).
26. M. Perc, and M. Marhl, *Biophysical Chemistry* **104**, 509–522 (2003).

IC-MSQUARE 2012: International Conference on Mathematical Modelling in Physical Sciences IOP Publishing
Journal of Physics: Conference Series **410** (2013) 012044 doi:10.1088/1742-6596/410/1/012044

How optimal synchronization of oscillators depends on the network structure and the individual dynamical properties of the oscillators

R Markovič[1], M Gosak[1,2,3] and M Marhl[1,2]

1 Faculty of Natural Sciences and Mathematics, University of Maribor, Koroška cesta 160, SI-2000 Maribor, Slovenia
2 Faculty of Education, University of Maribor, Koroška cesta 160, SI-2000 Maribor, Slovenia
3 Faculty of Civil Engineering, University of Maribor, Smetanova ulica 17, SI-2000 Maribor, Slovenia

E-mail: rene.markovic@uni-mb.si

Abstract. The problem of making a network of dynamical systems synchronize onto a common evolution is the subject of much ongoing research in several scientific disciplines. It is nowadays a well-known fact that the synchronization processes are gradually influenced by the interaction topology between the dynamically interacting units. A complex coupling configuration can significantly affect the synchronization abilities of a networked system. However, the question arises what is the optimal network topology that provides enhancement of the synchronization features under given circumstances. In order to address this issue we make use of a network model in which we can smoothly tune the topology from a highly heterogeneous and efficient scale-free network to a homogeneous and less efficient network. The network is then populated with Poincaré oscillators, a paradigmatic model for limit-cycle oscillations. This oscillator model exhibits a parameter that enables changes of the limit cycle attraction and is thus immediately related to flexibility/rigidity properties of the oscillator. Our results reveal that for weak attractions of the limit cycle, intermediate homogeneous topology ensures maximal synchronization, whereas highly heterogeneous scale-free topology ensures maximal synchronization for strong attractions of the limit cycle. We argue that the flexibility/rigidity of individual nodes of the networks defines the topology, where maximal global coherence is achieved.

Complex networks are nowadays used for the description of several natural and artificial systems. Since topological features of interactions between individual units characterize the global properties of a given system, the research of structural properties is increasingly gaining on attention. To qualitatively analyze the local and global structural properties of a network, numerous techniques have been developed, which have been utilized in various disciplines and diverse circumstances [1]. One of the basic measures that describes the properties of a network is its degree distribution. Scale-free networks, for instance, are known to have a highly heterogeneous power-law degree distribution [1], which can foster the synchronization abilities of a network of coupled oscillators [2], especially due to their hight global efficiency. Furthermore, it has been shown that a high level of heterogeneity can suppress synchronization, even thought it also reduces the average distance between the nodes. Another importing network measure is the average clustering coefficient C characterizing the cliquishness of a

network. Remarkably, high clustering coefficients were detected in several real-life networks [1]. On the other hand, high clustering implies the existence of many transitive connections and can thus hinder global synchronization [3]. There are several other topological factors, such as for example the existence of a community structure [4], which also have an impact on synchronization processes. Nevertheless, even though the dynamical behavior of networks is inevitable and non-trivially connected with structural properties of the underlying networks, there are also several other important factors having an impact. With this in mind, in the present study we focus on the analysis of the role of dynamical properties of individual oscillators. In a previous theoretical study on cellular oscillators it has been argued that the local dissipation rate crucially determines the coupling ability of cellular oscillators [5]. Notably, the dissipation rate is directly correlated with flexibility/rigidity of an oscillator. A low dissipation rate stands for rigid oscillators whereas on the other hand, oscillators with a near zero dissipation rate have attractors that are very susceptible to external perturbations and are thus flexible. Therefore, the main goal of the present work is to explore how the relation between flexibility/rigidity properties of individual oscillators on one hand and the structure of the network topology that characterizes the connectivity patterns between them on the other hand impacts the synchronization of oscillators.

By applying the algorithm described previously [6, 7] we can generate networks whose topologies can smoothly be altered between a highly heterogeneous scale-free network and a more homogeneous network. First, N nodes are randomly distributed in a unit square and to each node a fitness value f_i is prescribed. Two nodes are connected if:

$$\theta < \frac{f_i f_j}{I_{ij}^{\delta}}, \tag{1}$$

where f_i and f_j are fitness values of the i-th and j-th node, I_{ij} is the Euclidean distance between them and the δ is used to alter the topology of the network. The parameter θ is used as a threshold to control the average node degree of the network $\langle k \rangle$. In order to quantify topological features of the network and its degree of heterogeneity, the standard deviation of the node degrees STD(k) (Fig. 1a), the standard deviation of the clustering coefficients STD(C) (Fig. 1b) and the average clustering coefficient C (Fig. 1c) are plotted as a function of δ. Both, STD (k) and STD(C) are decreasing monotonically with increasing values of the topology parameter δ. Higher values of STD(k) and STD(C) are indicators of diverse local topological properties indicating a high degree of network heterogeneity.

Characteristic examples of generated networks are shown in Fig. 1d-f. It can be observed that for low values of δ indeed very heterogeneous networks are generated, in which mostly long-range connections exist. On the other hand, if $\delta >> 1$ mostly nearby nodes are connected and, in addition, there are no expressive differences in individual node degrees. Finally, intermediate values of δ, i.e. $\delta = 1.1$, result in an intermediate heterogeneous network with both long- and short-range connections. In other words, Fig. 1d-f provide a visual assessment that the network heterogeneity indeed decreases with increasing values of δ.

The dynamics of individual nodes is driven by the paradigmatic Poincaré oscillator:

$$\dot{x}_i = -\gamma \left(r_i - A\right) x_i - \omega_i y_i - \epsilon \sum_{i=1}^{N} d_{ij} \left(x_i - x_j\right), \tag{2}$$

$$\dot{y}_i = -\gamma \left(r_i - A\right) y_i + \omega_i x_i - \epsilon \sum_{i=1}^{N} d_{ij} \left(y_i - y_j\right), \tag{3}$$

where x_i and y_i are the phase space coordinates of the i-th oscillator, A is the limit cycle radius, $r_i = \sqrt{x_i^2 + y_i^2}$ is the distance between the origin of the phase space and the position of the i-th

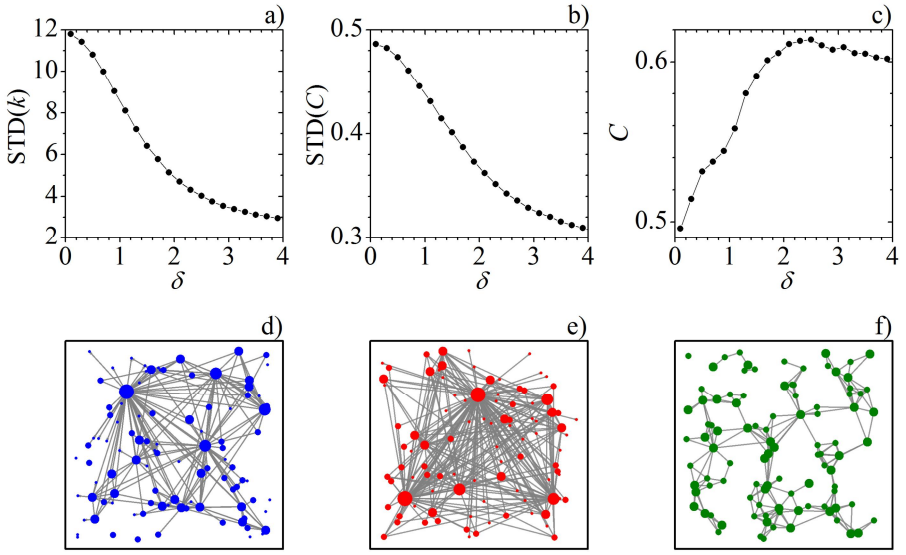

Figure 1. Standard deviation of node degrees (a), standard deviation of the local clustering coefficient (b), the average clustering coefficient (c) and characteristic network structures obtained for $\delta = 0.1$ (d), $\delta = 1.1$ (e) and $\delta = 4.0$ (f). Note that in lower panels the size of the nodes is proportional to their degrees. The number of nodes is $N = 100$ and the average node degree is $\langle k \rangle = 5.0$

node in the phase space, ω_i is the angular velocity of the i-th oscillator and ϵ is the coupling strength and d_{ij} is the connectivity matrix with values of 1 if the i-th and j-th node are connected and 0 otherwise. Angular velocities ω_i were distributed according to a normal distribution with mean angular velocity $\overline{\omega} = 1.0$ with standard deviation of 0.2. The limit cycle radius was set to $A = 1.0$ and the coupling strength to $\epsilon = 0.25$.

The parameter γ determines the relaxation towards the limit cycle and is immediately related with the dissipation rate of the oscillators [5, 8]. In order to investigate the interplay between structural and dynamical features of the network, we simulated how the overall synchronization in the systems changes according to the initial rigidity of the oscillators and structural properties of the network. For that purpose we analyze the synchronization behavior as a function of the relaxation rate γ and network topology parameter δ. For the quantification of the global network synchronization we calculate the average correlation coefficient $\overline{R}$. Accordingly, we have to construct the $N \times N$ correlation matrix, whose ij-th element is defined as:

$$R_{ij} = \frac{1}{M} \sum_{t=1}^{M} \frac{[x_i(t) - \overline{x_i}][x_j(t) - \overline{x_j}]}{S_i S_j}, \tag{4}$$

where M is the number of integration steps, $x_i(t)$ and $x_j(t)$ are the time series of the i-th and j-th oscillator, $\overline{x_i}$ and $\overline{x_j}$ are the average values of the time series and S_i and S_j the corresponding standard deviations. The average correlation coefficient $\overline{R}$ is then obtained as the average over all non-diagonal elements of the matrix. Its values range between 0 (uncorrelated dynamics) and 1 (complete synchronized motion).

Numerical simulations were carried out on a network of $N = 100$ Poincaré oscillators, with an average node degree $\langle k \rangle = 5.0$. Fig. 2a features the results showing the average correlation as a function of the dissipation rate γ and the network structure δ. It can be observed that both parameters mutually affect the synchronization behavior. For rigid oscillations where $\gamma > 100$, maximal synchronization is achieved in the highly heterogeneous scale-free network.

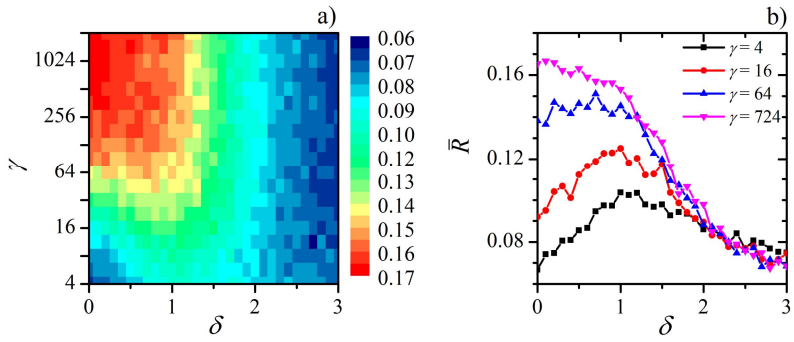

Figure 2. a) The average correlation $\overline{R}$ as a function of the topology parameter δ and flexibility parameter γ. b) Average correlation values for four different values of γ as a function of δ.

On the other hand, in case the network is populated with flexible oscillators ($\gamma < 100$), maximal synchronization is achieved for intermediate values of the topology parameter δ, where the network is less heterogeneous as the scale-free network and is constituted by long- as well as short-range links (see Fig. 1). Notably, for this intermediate values of δ the network exhibits a higher average clustering coefficient. Furthermore, in the homogeneous network ($\delta > 2$) with mostly short-range interactions, the degree of synchronization does not change by changing γ, thus indicating that in this case the synchronization does not depend on flexibility/rigidity properties of oscillators. In order to provide a better inside into the reported phenomena, we additionally plotted characteristic cross-sections of the color-contour plots for different values of γ. The results presented in Fig. 2b additionally confirm the existence of a resonant response due to changes in network topology for flexible oscillators, whereas for rigid oscillators the level of synchronization decreases monotonically with increasing δ.

In sum, we have shown that the network topology ensuring most synchronized response in an ensemble of coupled oscillators depends on individual oscillator properties. While rigid oscillators synchronize best in heterogeneous scale-free networks, flexible oscillator exhibit the most coherent collective response when they are connected in a less heterogeneous network. Our findings provide novel insights into synchronization behavior of coupled oscillators, which may be of importance especially from biological point of view. Signal transduction systems have to respond sensitively to weak external stimuli, thus indicating that cellular oscillators in general should behave like flexible oscillators. On the other hand it is known that different biological oscillators differ in their rigidity and, moreover, that the coupling influences the flexibility/rigidity properties of an oscillator [8]. Apparently, the optimal structural organization of the intercellular communication networks is determined also by characteristics of individual cells. Interestingly, the intermediate network structure that ensures best synchronizability of flexible oscillators is very economic, since it represents a good compromise between efficiency, wiring economy and robustness - a desirable attribute of several real-life systems.

References

[1] Albert R and Barabási A L 2002 *Rev. Mod. Phys.* **74**(1) 47–97
[2] Hong H, Kim B J, Choi M Y and Park H 2004 *Phys. Rev. E* **69**(6) 067105
[3] McGraw P N and Menzinger M 2005 *Phys. Rev. E* **72**(1) 015101
[4] McGraw P N and Menzinger M 2008 *Phys. Rev. E* **77**(3) 031102
[5] Perc M and Marhl M 2004 *Bioelectrochemistry* **62** 1–10
[6] Gosak M, Korošak D and Marhl M 2011 *New Journal of Physics* **13** 013012
[7] Gosak M, Markovič R and Marhl M 2012 *Physica A: Statistical Mechanics and its Applications* **391** 2764 – 2770 ISSN 0378-4371
[8] Abraham U, Granada A E, Westermark P O, Heine M, Kramer A and Herzel H 2010 *Molecular System Biology* **6** 13

Chaos, Solitons & Fractals 69 (2014) 14–21

Contents lists available at ScienceDirect

Chaos, Solitons & Fractals

Nonlinear Science, and Nonequilibrium and Complex Phenomena

journal homepage: www.elsevier.com/locate/chaos

Broad-scale small-world network topology induces optimal synchronization of flexible oscillators

Rene Markovič [a,*], Marko Gosak [a,b], Marko Marhl [a,b]

[a] Faculty of Natural Sciences and Mathematics, University of Maribor, Korošak cesta 160, Maribor SI-2000, Slovenia
[b] Faculty of Education, University of Maribor, Korošak cesta 160, Maribor SI-2000, Slovenia

ARTICLE INFO

Article history:
Received 15 October 2013
Accepted 24 August 2014
Available online 28 September 2014

ABSTRACT

The discovery of small-world and scale-free properties of many man-made and natural complex networks has attracted increasing attention. Of particular interest is how the structural properties of a network facilitate and constrain its dynamical behavior. In this paper we study the synchronization of weakly coupled limit-cycle oscillators in dependence on the network topology as well as the dynamical features of individual oscillators. We show that flexible oscillators, characterized by near zero values of divergence, express maximal correlation in broad-scale small-world networks, whereas the non-flexible (rigid) oscillators are best correlated in more heterogeneous scale-free networks. We found that the synchronization behavior is governed by the interplay between the networks global efficiency and the mutual frequency adaptation. The latter differs for flexible and rigid oscillators. The results are discussed in terms of evolutionary advantages of broad-scale small-world networks in biological systems.

1. Introduction

Complex networks have attracted a great deal of interest since the discoveries of the small-world [1] and scale-free [2] properties. Signatures of such exceptional topological features have been discovered in many natural and man-made systems, which represents the root of modern network science [3,4]. It is nowadays a well-known fact that many real-world networks display degree distributions that deviate from a Poisson distribution found for simple random graph models. Generally three classes of small-world networks have been identified [5]. Very abundant types are scale-free networks (SFNs), whose degree distribution follows a power law. However, in many real networks, especially the physically embedded ones, there are different constraints which hinder the development of extremely connected nodes in a network, which leads to a cutoff of the power law regime in the connectivity distribution or making it disappear altogether. As a result, the so-called broad-scale networks (BSNs) and single-scale networks emerge [5].

With the progress in the network science it has been pointed out that networks can be treated not just as abstract entities with the vertices or nodes as formless place-holders, but as oscillators or dynamical systems coupled in the geometry of the network. Perhaps one of the most studied phenomena in this context is the synchronization of dynamical nodes in a network. Synchronization in networks is a very common collective behavior in real systems and is manifested by the appearance of some forms of relations between the functions of different dynamical variables as a result of interactions [6,7].

It is known that structural properties of a network significantly affect synchronization behavior. Primal works have found that complex networks, due to their small network distances, are generally more synchronizable than

* Corresponding author.
E-mail addresses: rene.markovic@uni-mb.si (R. Markovič), marko.gosak@uni-mb.si (M. Gosak), marko.marhl@uni-mb.si (M. Marhl).

http://dx.doi.org/10.1016/j.chaos.2014.08.008
0960-0779/

regular networks [7–10]. However, especially SFNs are characterized by heterogeneity in the degree distribution, which on one hand tends to reduce the average network distance, but on the other hand in more heterogeneous networks synchronization is increasingly harder to achieve [11]. This issue has been further addressed by several authors. Motter et al. [12] have revealed that directed and weighed coupling can balance the heterogeneity in the degree distribution. Furthermore, Zhou and Kurths [13] reported that in heterogeneous complex networks individual oscillators exhibit different levels of synchronization with respect to the collective dynamics and they exhibit a hierarchical dependence on the connection degrees. Moreover, it has been shown that the path to synchronized behavior is in homogeneous networks different than in heterogeneous network [14,15]. McGraw and Menzinger [16,17] have shown that the existence of community structures inside the network can hinder the synchronization of oscillators.

In our previous study [18] we observed that synchronization of oscillators in a network depends on its heterogeneity. We studied synchronization of Rössler oscillators on a spatially embedded network, where the level of heterogeneity could be varied from a highly heterogeneous SFN to a rather homogeneous random geometric network. It turned out that the maximal synchronization was obtained in the intermediate heterogeneous regime, i.e. in the BSN. The same results of this optimal intermediate network configuration were also obtained for the Rulkov map, where we additionally found that the flexibility of individual oscillators in the network might play an important role [19]. We further studied this phenomenon and found that the flexibility of individual oscillators in a network influences correlation and synchronization of oscillators also in other systems [20,21]; however, we did not succeed to explain this phenomenon until now.

In this paper we provide a mathematical explanation why flexible oscillators, characterized by low values of divergence, express maximal correlation in BSNs, whereas the non-flexible (rigid) oscillators are best correlated in more heterogeneous SFNs. To this purpose we use a mathematical model (Section 2) in which the dynamics of each node in the network is governed by the dynamics of the Poincaré oscillator. The network model enables smooth changes of the topology from a highly heterogeneous SFN to a homogeneous network. This setup enables us to explore the relationship between the flexibility of individual oscillators and the connectivity pattern that leads to the most synchronized response. The results (Section 3) show that correlations are maximized for rigid oscillators in a highly heterogeneous SFN, and for flexible oscillators in a less heterogeneous BSN. These findings are discussed in Section 4 in terms of a trade-off between high efficiency and an increased fragility of the networked systems, which could have an important role in the evolution of biological systems.

2. Mathematical model

We consider a network of coupled oscillators where the structure of this network can be varied from a highly heterogeneous SFN to a homogeneous regular network. For this purpose we utilize the spatially embedded vertex fitness model [19,22,23]. Initially each node is labeled with an integer i and a fitness value f_i is prescribed to it, where the fitness values follow a power-law distribution with a scaling exponent $\beta = 2.5$ [23]. Afterwards all N nodes are randomly distributed in a unit square. A connection between the i-th and j-th node is established if the following conditions is satisfied:

$$\Theta < \frac{f_i f_j}{I_{ij}^{\delta}}, \tag{1}$$

where Θ is used as the connectivity threshold that defines the average node degree of the network $\langle k \rangle$, I_{ij} is the Euclidean distance between the i-th and j-th node and the parameter δ alters topological features of the network. Following this algorithm we constructed the connectivity matrix with ij-th element d_{ij} equal to 1 if those two nodes are connected and 0 otherwise. If δ is near zero the connections are accepted only according to the fitness values independently of the inter-nodal Euclidean distances. In this case a highly heterogeneous SFN is constructed with mainly long-range connections. By increasing the topology parameter δ, long-range connections become more rare. The network topology becomes less heterogeneous, yet the presence of a few long-range connections still make the network very efficient in terms of small-world topological features [24]. Remarkably, the resulting constrains which limit the lengths of connections cause a cut-off in the power-law regime, meaning that extremely connected nodes are missing. Such networks are thus classified as BSNs [5]. On the other hand, for high values of the topology parameter $(\delta \gg 1)$ only short-range connections are accepted and the network becomes very homogeneous and inefficient.

In the network, the dynamics of each node is governed by the paradigmatic Poincaré oscillator:

$$\dot{x}_i = \gamma(A - r_i)x_i - 2\pi\nu_i y_i + \epsilon\sum_{j=1}^{N} d_{ij}(x_j - x_i), \tag{2}$$

$$\dot{y}_i = \gamma(A - r_i)y_i + 2\pi\nu_i x_i + \epsilon\sum_{j=1}^{N} d_{ij}(y_j - y_i), \tag{3}$$

where $\dot{x}_i$ and $\dot{y}_i$ are time derivatives of the variables x_i and y_i of the i-th oscillator, A is the limit cycle radius, $r_i = \sqrt{x_i^2 + y_i^2}$ is the distance from the origin to the attractor in the phase space, ν_i is the frequency, ϵ is the coupling strength and d_{ij} is the ij-th element of the connectivity matrix. The parameter γ represents the dissipation rate for the uncoupled Poincaré oscillator which indicates the stability of the oscillator with respect to amplitude perturbations [25,26] (see Appendix). We refer to oscillators with low values of the dissipation parameter γ as flexible and oscillators with high values of the parameter γ as rigid oscillators. Namely, the dissipation rate is directly related to the oscillators frequency adaptation to an external periodic signal [26–29], as flexible oscillators are easier to entrain.

3. Results

Our network consists of $N = 100$ nodes. The average node degree is fixed to $\langle k\rangle = 5$, whereas the individual number of edges or links k_i is determined by the connectivity matrix. The coupling strength is set to $\epsilon = 0.25$ and frequencies follow a normal distribution with a mean value $\overline{\nu} = 1.0$ and a relative standard deviation of $0.2\overline{\nu}$. The results are averaged over 300 independent simulation runs in order to ensure statistical accuracy.

3.1. Correlation of node dynamics

The correlation of every ij-th element is calculated as follows:

$$R_{ij} = \frac{\sum[\langle x_i\rangle - x_i(t)]\left[\langle x_j\rangle - x_j(t)\right]}{s_{x_i}s_{x_j}}, \tag{4}$$

where $\langle x_i\rangle$ and $\langle x_j\rangle$ are the mean values of the numerically calculated discrete time series of the i-th and j-th oscillator, i.e. $x_i(t)$ and $x_j(t)$ and s_{x_i} and s_{x_i} are the corresponding standard deviations. The overall degree of correlation $\overline{R}$ is obtained by averaging the correlations of all pairs of oscillators in the system:

$$\overline{R} = \frac{1}{N(N-1)}\sum_{i\neq j} R_{ij}. \tag{5}$$

We calculated the average correlation coefficient $\overline{R}$ as a function of the topology parameter δ and dissipation parameter γ. The color-contour plot in Fig. 1(a) and the corresponding cross-sections in Fig. 1(b) feature the results. It can be observed that both, the network topology (characterized by δ) and the dissipation rate (characterized by γ) affect the overall synchronization of the system in a non-trivial way. When the network is populated with rigid oscillators ($\gamma > 100$) maximal synchronization is reached in a highly heterogeneous SFN, where the value of the topology parameter δ is near zero. Remarkably, for low dissipation rates (down to 4), which correspond to flexible oscillators, the most synchronized dynamics is attained at intermediate values of δ where the network topology is less heterogeneous, i.e. in the BSN.

We additionally tested the robustness of our observation to variations in system size N, average degree $\langle k\rangle$ and coupling strength ϵ. It turned out that qualitatively similar results are obtained for parameter variations within reasonable ranges. Increasing the system size only causes a slight decrease of the average correlation. On the other hand, increasing the average degree $\langle k\rangle$ of the network leads to higher correlations among oscillators. In case of flexible oscillators, an increase of $\langle k\rangle$ also causes a shift of the most synchronized state towards higher values of the topology parameter δ, whereas the dynamics of rigid oscillators is always best correlated in the most efficient SFN. Similarly, variations of the coupling strength ϵ do not considerably change the observations for synchronization behavior of rigid and flexible oscillators, except for high values of ϵ which could lead to oscillation death cf. [30].

3.2. Efficiency of communication and flexibility of oscillators

In several studies it has been shown that synchronization of dynamical units in a network crucially depends on the network's topological features, such as efficiency and heterogeneity [8–10,31]. In order to characterize the communication ability of our network model we computed the global efficiency E as a function of the topology parameter δ. The global efficiency E is defined as the inverse average over all average shortest path lengths between any node pair and is computed as [3]:

$$E = \frac{1}{N(N-1)}\sum_{i,j}\frac{1}{l(i,j)}. \tag{6}$$

In Eq. (6) $l(i,j)$ refers to the average shortest path length between the nodes i and j. Results in Fig. 2(a) reveal that the efficiency monotonically decreases with increasing δ, thus indicating that the SFN is the most effective structure from this point of view. The correlation between coupled oscillators does not depend solely on the efficiency of the node-to-node communication, but also on the ability of the oscillators to mutually adapt their frequencies [32]. To quantify the overall degree of frequency adaptation in the system we calculate the absolute frequency change in the system $|\overline{\Delta\nu}|$ with the following expression:

$$|\overline{\Delta\nu}| = \frac{1}{N}\sum_{i=1}^{N}\frac{1}{M_i}\sum_{m=1}^{M_i}|\nu_i - \nu_i^m|, \tag{7}$$

where M_i is the number of local maxima's of the i-th oscillator and $|\nu_i - \nu_i^m|$ defines the absolute difference between the initially prescribed frequency ν_i and the actual frequency ν_i^m at the m-th maximum, which is calculated as

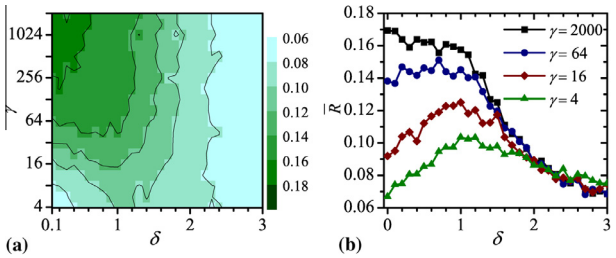

Fig. 1. Color-coded values of: (a) average correlation coefficient $\overline{R}$ as a function of the topology parameter δ and the dissipation parameter γ, and (b) the corresponding cross-sections of the color map at four dissipation rate values. (For interpretation of the references to colour in this figure legend, the reader is referred to the web version of this article.)

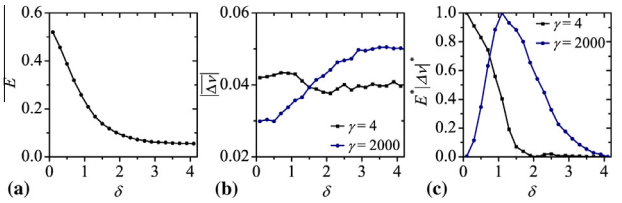

Fig. 2. Efficiency of the network and the flexibility of oscillators: (a) the efficiency E of the network as function of δ, (b) the absolute average change of the frequency $|\overline{\Delta v}|$ as function of δ, and (c) the product between the normalized values of the absolute average change in the frequency $|\overline{\Delta v}|^*$ and the networks efficiency E^*.

the inverse of the period between the m-th maximum and its first predecessor. In Fig. 2(b) the values of $|\overline{\Delta v}|$ are presented for rigid ($\gamma = 2000$) and flexible ($\gamma = 4$) oscillators. Notably, rigid oscillators adopt their frequencies better in the range of heterogeneous networks, whereas flexible oscillators achieve better frequency adaptation in a homogeneous network configuration.

The reported findings point out the importance of the interplay between the topology and dynamics. We argue that the network's communication ability and the ability of oscillators to unify their frequencies are the major features that define the synchronization behavior of the system. To take into account both effects, i.e. the network efficiency E and the ability of the oscillators to adapt their frequencies, we calculate the product of the normalized efficiency E^* and the normalized average change in the frequency $|\overline{\Delta v}|^*$. In this manner only a qualitative impact of both factors is attained. However, the maximal value of the product indicates the maximal mutual contributions of both terms, irrespective of the extent of contribution of individual factors to synchronization behavior. Results showing $E^*|\overline{\Delta v}|^*$ as a function of δ are presented in Fig. 2(c) and they indeed reflect nicely the synchronization behavior presented in Fig. 1. The product of the normalized network efficiency E^* and the normalized frequency adaptation level $|\overline{\Delta v}|^*$ monotonically decreases with increasing δ in case of rigid oscillators, whereas it exhibits a bell-shaped dependency for flexible oscillators, as it has been found for the average correlation coefficient. It remains of interest to explore the reasons for the different nature of frequency adaptation observed in both types of oscillators.

3.3. Dynamical flexibility of oscillators in the network

We focus on different responses of flexible ($\gamma = 4$) and rigid oscillators ($\gamma = 2000$), observed in Fig. 2(b). To understand the average values of frequency adaptation in Fig. 2(b), we compute the frequency adaptation of individual oscillators $|\overline{\Delta v_i}| = \frac{1}{M_i}\sum_{m=1}^{M_i}|v_i - v_i^m|$ (see Eq. (7)). In Figs. 3(a) and 3(b) the results are presented for flexible ($\gamma = 4$) and rigid oscillators ($\gamma = 2000$), respectively.

By comparing Fig. 3(a) and Fig. 3(b) we can see that the frequency adaptation of individual oscillators $|\overline{\Delta v_i}|$ in dependence on the network topology δ differs most considerably for the first 30 oscillators ($i \leqslant 30$). According to the network model (see Section 2) these oscillators represent nodes with highest node degrees k_i, which means that these oscillators are highly connected to other oscillators

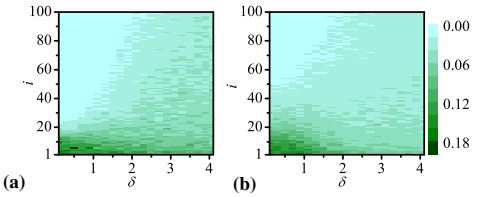

Fig. 3. Frequency adaptation of individual oscillators $|\overline{\Delta v_i}|$ as a function of the topology parameter δ for: (a) flexible oscillators ($\gamma = 4$), and (b) rigid oscillators ($\gamma = 2000$).

in the network, and also highly influenced by these oscillators. It was shown that coupling among oscillators changes their dynamical properties, e.g. causes faster relaxation times and makes the oscillators more rigid [26,33]. Here we take into account that this impact of coupling on the flexibility of oscillators also depends on the connectivity structure, and introduce the so-called dynamical flexibility, γ^i_{dyn}. For the model under consideration, the dynamical flexibility γ^i_{dyn} can be analytically determined (see Appendix):

$$\gamma^i_{dyn} = \gamma(2A - 3R_i) - 2\epsilon k_i. \tag{8}$$

Eq. (8) shows that with every additional connection the oscillator becomes more rigid. To get a more detailed picture about the behavior of individual oscillators in the network, we divide the oscillators into four groups. In the first group we have oscillators with indices $i \in [1, 15]$, in the second group $i \in [16, 30]$, in the third group $i \in [31, 60]$, and in the fourth group all the others, i.e. $i \in [61, 100]$. For every group of the oscillators we compute the average node degree $\langle k\rangle_{i-j}$ and the average dynamic dissipation rate $\langle\gamma_{dyn}\rangle_{i-j}$. The results are shown in Fig. 4. We analyze the results in Fig. 4 separately for two regimes: $\delta < 2$, where the network is heterogeneous, and $\delta > 2$, where the network structure is more compact with smaller differences node degrees k_i. For $\delta < 2$, the oscillators in the first group ($i \in [1, 15]$) have the highest node degrees (Fig. 4(a)). Consequently, the many neighboring oscillators significantly influence their dynamics, which means that these oscillators have a lower dynamical flexibility γ^i_{dyn} due to their higher degrees k_i (see Eq. (8)). Importantly, this decrease in the dynamical flexibility γ^i_{dyn} is relatively much more expressed for oscillators with a low dissipation rate ($\gamma = 4$) then for the rigid ones ($\gamma = 2000$) (see Fig. 4(b) and (c)). Fig. 4(b) shows that for ($\gamma = 4$) the first group of oscillators ($i \in [1, 15]$) is almost twice as rigid as the rest

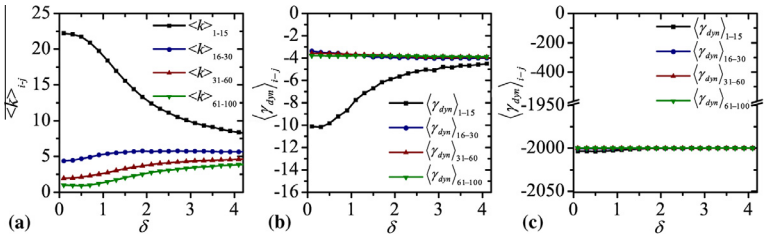

Fig. 4. Analysis of the four groups of oscillators: (a) the average node degree $\langle k\rangle_{i-j}$, and the corresponding average dynamic dissipation rate $\langle\gamma_{dyn}\rangle_{i-j}$ as a function of the network topology δ for: (b) $\gamma = 4$, and (c) $\gamma = 2000$.

of the system at lower values of δ, whereas for rigid oscillators ($\gamma = 2000$) the dynamical flexibility remains practically unchanged for all network configurations (Fig. 4(c)).

Next we examine the trade-off between the positive and negative effects that the neighboring oscillators have on the frequency adaptation. On one hand, many neighbors make the oscillators more rigid and suppress their ability for frequency adaptation. On the other hand, however, the many neighboring oscillators directly influence the dynamics of this oscillator and force it to change its frequency. Which one of these two effects is stronger depends on the basic oscillator's flexibility γ. Let us take rigid oscillators first ($\gamma = 2000$). They are easier to study because their dynamical flexibility is practically independent of the number of their neighbors ($\gamma^i_{dyn} \approx const.$, see Fig. 4(c)), and hence the frequency adaptation prevalently depends on the forcing effect of the neighborhood, which is directly related to the number of the neighboring oscillators. Therefore, rigid oscillators ($\gamma = 2000$) better adapt their frequencies if they are better connected. Since oscillators with $i \in [1, 15]$ in the networks with $\delta < 2$ are the most connected ones (note that at $\delta > 2$ the network is rather homogeneous), the rigid oscillators ($\gamma = 2000$), in particular the oscillators with lower values of i, better adapt their frequencies at $\delta < 2$ than at $\delta > 2$ (see Figs. 3(b), and 2(b)).

On the other hand, the flexible oscillators ($\gamma = 4$) with $i \in [1, 15]$ in heterogeneous networks ($\delta < 2$) change their dynamical flexibility γ^i_{dyn} significantly; they become relatively much more rigid due to many connections they have (see Fig. 4(b)). This effect of rigidity is stronger than the forcing effects from the surrounding (from many (k_i) neighbors). Therefore, these flexible oscillators ($\gamma = 4$) better adapt their frequencies in more homogeneous networks at ($\delta > 2$) (see Figs. 3(b) and 2(b)), which is exactly the opposite of the behavior observed for rigid oscillators ($\gamma = 2000$). Consequently, the synchronization behavior of flexible oscillators is determined by the interplay between network efficiency, which is the highest at $\delta \to 0$ (Fig. 2(a)), and the frequency adaptation, which is more effective at $\delta > 2$ (Fig. 2(b)). As a result, the most synchronized activity is observed between these two regimes, i.e., within the BSN ($\delta \approx 1.1$, see Fig. 1, cf. Fig. 2).

3.4. Generalization to other types of oscillators

To generalize our findings to other oscillator types we populate the network with Brusselator oscillators. The Brusselator is a two-dimensional system used as a paradigmatic theoretical model for autocatalytic reactions [34,35]. The dynamics of the i-th node together with the coupling term is governed by the following equations:

$$\dot{u}_i(t) = a_i + u_i(t)^2 v_i(t) - b u_i(t) - u_i(t) + \epsilon \sum_{j=1}^{N} d_{ij}\left[u_j(t) - u_i(t)\right], \tag{9}$$

$$\dot{v}_i(t) = b u_i(t) - u_i(t)^2 v_i(t) + \epsilon \sum_{j=1}^{N} d_{ij}\left[v_j(t) - v_i(t)\right]. \tag{10}$$

In our calculations we set the parameter b to 2.5 and the coupling strength ϵ to 0.05. The uncoupled oscillator has one fixed point $(a, b/a)$. The Hopf bifurcation announcing the turnover from stable limit cycle behavior to a stable steady point is present at $a_{\mathrm{HB}} = \sqrt{b-1}$. Remarkably, it has been shown that in the proximity of the bifurcation point, the system exhibits a near-zero dissipation and is thus very susceptible to external perturbations [28,29,36]. We compute the dissipation rate for the uncoupled Brusselator oscillator by numerically evaluating the Lyapunov spectrum as described in [37]. Afterwards, the dissipation rate $\left(\overline{\nabla \cdot f}\right)$ is obtained by summarizing both Lyapunov exponents. In Fig. 5(a) we show the dissipation rate for different values of parameter a, along with the bifurcation diagram. As expected, a near-zero dissipation rate is observed in the proximity of the bifurcation point a_{HB}, whereas its values become progressively more negative as the distance from the bifurcation point increases.

In order to explore the dynamic behavior of coupled Brusselator oscillators, we calculate the average correlation coefficient $\overline{R}$ for two different values of the parameter a, thereby reflecting different levels of dissipation. In particular, we define $a = 0.2$ and $a = 1.16$ for the cases of rigid and flexible oscillators, respectively. It should be noted that a slight dispersion of 3 % of the given mean value of parameter a was introduced in order to include the heterogeneity of oscillators. Results presented in Fig. 5(b) reveal that for flexible oscillators ($a = 1.16$, near-zero dissipation) best synchronization is achieved for intermediate values of the topology parameter δ, i.e., in the BSN. On the other hand, rigid oscillators ($a = 0.2$, high dissipation) exhibit maximal synchronization in the highly heterogeneous and efficient SFN. Apparently, the same mechanism as reported for the Poincaré oscillator governs the synchronization behavior in other oscillator models as well.

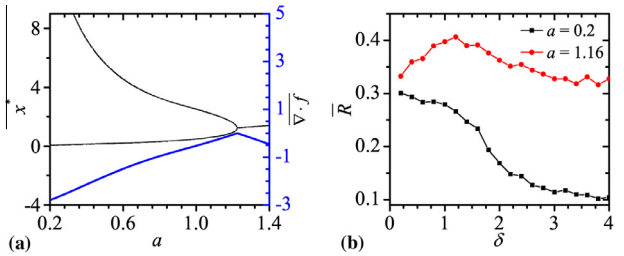

Fig. 5. The bifurcation diagram along with the corresponding dissipation rate for the Brusselator oscillator (a) and the average correlation coefficient as a function of the topology parameter δ for the coupled Brusselator model for rigid ($a = 0.2$) and flexible ($a = 1.16$) oscillators (b). The calculation was performed on networks with $N = 100$ oscillators and an average degree $\langle k \rangle = 5$.

4. Discussion

We investigated how the interplay between dynamical and topological features affects the overall degree of synchronization in a network of diffusively coupled Poincaré oscillators. The model also enabled us to alter the dissipation rate of individual oscillators with only one parameter. Our results show that flexible oscillators, characterized by low values of the dissipation rate, express maximal correlation in BSNs, whereas the non-flexible (rigid) oscillators are best correlated in more heterogeneous SFNs. By performing the same analysis with the Brusselator model, we have additionally shown that the reported phenomena can be generalized to other oscillator models as well. This also corresponds to our preliminary observations [18,20,21]. Furthermore, our results can also be used for explaining stochastic and coherence resonance phenomena in heterogeneous networks. We have previously shown that intermediate heterogeneous BSNs ensure the most coherent collective response in systems of coupled noisy excitable oscillators [24,38]. Notably, in these cases the oscillators operated in flexible regimes with weak dissipation.

To uncover precise mechanisms that govern synchronization behavior of rigid and flexible oscillators, we performed a stability analysis (see Appendix), which has revealed that the coupling of oscillators impacts flexible oscillators in a different manner than rigid oscillators. We have shown that the synchronization is governed mainly by the interplay between networks global efficiency and the ability of oscillators to unify their frequencies. Both of this factors have previously been proven to be important by the formation of the collective response of coupled oscillators [8,32]. Nevertheless, it has been shown that other quantities, such as the clustering and the presence of communities, can be of vital importance by synchronization in complex networks, especially due to partial synchronization in communities in the weak coupling regimes [16,17]. However, it turned out that in our system these processes are not deciding, because variations of the average clustering coefficient with respect to changes of the network parameter δ are minor. In particular, the average clustering coefficients for the SFN and the BSN are 0.48 and 0.57, respectively. Due to this rather insignificant changes of the networks cliquishness, the synchronization is mainly a result of the interplay between the networks efficiency and the capability of oscillators to unify their frequencies, which was shown to be related with the dynamical flexibility, a property that differs for rigid and flexible oscillators.

Our findings provide novel insights into synchronization behavior of coupled oscillators, which may be of particular importance especially from biological point of view. Numerous studies reported the presence of the small-world topological features in biological systems, e.g. metabolic networks [39], beta-cells [40], protein interaction networks, signal transduction pathway [41], neural networks [42], circadian rhythms [43,44] and others. Our results allow us to hypothesize the biological relevance of small-world networks and in particular the advantages of the BSNs in comparison to the SFNs. It seems that biological systems prefer a trade-off between the efficiency and the robustness. The BSNs are obviously efficient enough, and represent a setup which ensures synchronized activity of flexible oscillators. Perhaps the best solution would be having extreme rigid, well-determined oscillators in a pure scale-free network. However, these SFNs would be very fragile in terms of their extreme sensitivity to the external attacks [45,46]. Furthermore, very rigid oscillators would be very costly for biological systems because of permanent regulation, and no real variability would be allowed. Especially signal transduction systems have to respond sensitively to weak external stimuli, thus indicating that cellular oscillators should exhibit flexibility. Therefore, a reasonable trade-off between the flexibility of oscillators and the network robustness seems to be the best solution for multicellular oscillatory biological systems, which tend to consist of more flexible oscillators, which are organized in less heterogeneous but still very efficient broad-scale small-world networks.

Acknowledgment

The paper was produced within the framework of the operation entitled ‘Centre for Open Innovation and Research of the University of Maribor’. The operation is co-funded by the European Regional Development Fund and conducted within the framework of the operational Programme for Strengthening Regional Development Potentials for the period 2007–2013, development priority 1: ‘Competitiveness of companies and research excellence’, priority axis 1.1: ‘Encouraging competitive potential of enterprises and research excellence’.

Appendix A

We analyze the flexibility of a simple uncoupled oscillatory system and an oscillator coupled with other oscillators in a network. The uncoupled oscillator is given by the following equation:

$$\dot{\mathbf{z}} = F(\mathbf{z}), \tag{A.1}$$

where $\mathbf{z}$ is an l-dimensional state vector and $\dot{\mathbf{z}}$ is the corresponding time derivative. The flexibility of the oscillator can be estimated by the trace of the Jacobian matrix $\mathrm{Tr}(\mathbf{J})$ [47]:

$$\mathrm{Tr}(\mathbf{J}) = \sum_{j=1}^{l} \frac{\partial \dot{z}_j}{\partial z_j}. \tag{A.2}$$

For the Poincaré oscillators we obtain:

$$\mathrm{Tr}(\mathbf{J}) = \gamma(2A - 3r_i). \tag{A.3}$$

If the limit cycle radius is set to $A = 1$, under steady-state conditions ($r_i = A$) the flexibility of the uncoupled Poincaré oscillator is simply:

$$\mathrm{Tr}(\mathbf{J}) = -\gamma. \tag{A.4}$$

Larger values of γ refer to more rigid oscillators whereas values closer to zero express higher flexibility. In a system of N coupled oscillators the dynamics of the i-th oscillator is given by:

$$\dot{\mathbf{z}} = F(\mathbf{z_i}) - \epsilon \sum_{j=1}^{N} d_{ij}(\mathbf{z_j} - \mathbf{z_i}), \tag{A.5}$$

where ϵ is the coupling strength and d_{ij} is the connectivity matrix. The flexibility of the i-th oscillator depends on the influences of all the adjacent oscillators to which this oscillator is connected. We refer to this kind of flexibility as dynamical flexibility γ^i_{dyn}:

$$\gamma^i_{dyn} = \mathrm{Tr}(\mathbf{J_i}) = \sum_{j=1}^{l} \frac{\partial \dot{z}_{i,j}}{\partial z_{i,j}} = \sum_{j=1}^{l} \frac{\partial F(z_{i,j})}{\partial z_{i,j}} - l\epsilon k_i, \tag{A.6}$$

where k_i is the node degree of the i-th oscillator. For the mathematical model under consideration we obtain:

$$\gamma^i_{dyn} = -\gamma - 2\epsilon k_i. \tag{A.7}$$

Eq. (A.7) shows that flexibility of an oscillator decreases by the number of neighboring oscillators (k_i). The flexibility of an oscillator in the network is always lower than the flexibility of the uncoupled one ($k_i = 0$, see Eq. (A.4)). When the terms in equation Eq. (A.7) are comparable ($\gamma \approx 2\epsilon k_i$), the dispersion in γ^i_{dyn} is proportional to the heterogeneity of the networks. When on the other hand the ($\gamma \gg 2\epsilon k_i$) the topology causes only negligible changes in γ^i_{dyn}.

References

[1] Watts DJ, Strogatz SH. Collective dynamics of 'small-world' networks. Nature 1998;393:440–2. URL http://dx.doi.org/10.1038/30918.

[2] Barabási A-L, Albert R. Emergence of scaling in random networks. Science 1999;286:509–12. URL http://www.sciencemag.org/content/286/5439/509.short.

[3] Albert R, Barabási A-L. Statistical mechanics of complex networks. Rev Mod Phys 2002;74:47–97. URL http://link.aps.org/doi/10.1103/RevModPhys.74.47.

[4] Barabási A-L. The network takeover. Nat Phys 2012;8:14–6. URL http://www.nature.com/nphys/journal/v8/n1/full/nphys2188.html.

[5] Amaral LA, Scala A, Barthélémy M, Stanley HE. Proc Nat Acad Sci U S A 2000;97:11149–52. URL http://www.pnas.org/content/97/21/11149.short.

[6] Tyson JJ, Chen K, Novak B. Network dynamics and cell physiology. Nat Rev Mol Cell Biol 2001;2:908–16. URL http://www.nature.com/nrm/journal/v2/n12/full/nrm1201-908a.html.

[7] Arenas A, Díaz-Guilera A, Kurths J, Moreno Y, Zhou C. Synchronization in complex networks. Phys Rep 2008;469:93–153. URL http://www.sciencedirect.com/science/article/pii/S0370157308003384.

[8] Barahona M, Pecora LM. Synchronization in small-world systems. Phys Rev Lett 2002;89:054101–4. URL http://prl.aps.org/abstract/PRL/v89/i5/e054101.

[9] Wang XF, Chen G. Synchronization in small-world dynamical networks. Int J Bifurcation Chaos 2002;12:187–92. URL http://www.worldscientific.com/doi/abs/10.1142/S0218127402004292.

[10] Hong H, Kim BJ, Choi MY, Park H. Factors that predict better synchronizability on complex networks. Phys Rev E 2004;69.067105–4. URL http://pre.aps.org/abstract/PRE/v69/i6/e067105.

[11] Nishikawa T, Motter AE, Lai YC, Hoppensteadt FC. Heterogeneity in oscillator networks: are smaller worlds easier to synchronize? Phys Rev Lett 2003;91:014101–4. URL http://prl.aps.org/abstract/PRL/v91/i1/e014101.

[12] Motter AE, Zhou C, Kurths J. Network synchronization, diffusion, and the paradox of heterogeneity. Phys Rev E 2005;71:016116–9. URL http://pre.aps.org/abstract/PRE/v71/i1/e016116.

[13] Zhou C, Kurths J. Hierarchical synchronization in complex networks with heterogeneous degrees. Chaos 2006;16:015104–10. URL http://scitation.aip.org/content/aip/journal/chaos/16/1/10.1063/1.2150381.

[14] Gómez-Gardeñes J, Moreno Y, Arenas A. Paths to synchronization on complex networks. Phys Rev Lett 2007;98:034101–4. URL http://prl.aps.org/abstract/PRL/v98/i3/e034101.

[15] Gómez-Gardeñes J, Moreno Y, Arenas A. Synchronizability determined by coupling strengths and topology on complex networks. Phys Rev E 2007;75:066106–11. URL http://pre.aps.org/abstract/PRE/v75/i6/e066106.

[16] McGraw PN, Menzinger M. Clustering and the synchronization of oscillator networks. Phys Rev E 2005;72:015101–4. URL http://pre.aps.org/abstract/PRE/v72/i1/e015101.

[17] McGraw PN, Menzinger M. Analysis of nonlinear synchronization dynamics of oscillator networks by laplacian spectral methods. Phys Rev E 2007;75. 027104–4. URL http://pre.aps.org/abstract/PRE/v75/i2/e027104.

[18] Gosak M, Marhl M. Synchronization of Rössler oscillators on a spatially embedded network: the role of interaction topology. In: Assawinchaichote W, editor. Proceedings of the IASTED Technology and Management Conferences 2010. ACTA Press; 2010. p. 121–5. URL http://www.actapress.com/Abstract.aspx?paperId=42009.

[19] Gosak M, Markovič R, Marhl M. The role of neural architecture and the speed of signal propagation in the process of synchronization of bursting neurons. Phys A 2012;391:2764–70. URL http://www.sciencedirect.com/science/article/pii/S0378437111009435.

[20] Markovič R, Gosak M, Marhl M. The role of topological features of intercellular communication networks by the synchronization of cellular oscillators, In: Robnik M, Romanovski V.G. Editors, American Institute of Physics Conference Series, vol. 1468 of American Institute of Physics Conference Series, 2012, p. 256–267. URL http://scitation.aip.org/content/aip/proceeding/aipcp/10.1063/1.4745588.

[21] Markovič R, Gosak M, Marhl M. How optimal synchronization of oscillators depends on the network structure and the individual dynamical properties of the oscillators. J Phys Conf Ser 2013;410.012044–4. URL http://iopscience.iop.org/1742-6596/410/1/012044.

[22] Caldarelli G, Capocci A, De Los Rios P, Muñoz MA. Scale-free networks from varying vertex intrinsic fitness. Phys Rev Lett 2002;89:258702–4. URL http://prl.aps.org/abstract/PRL/v89/i25/e258702.

[23] Morita S. Crossovers in scale-free networks on geographical space. Phys Rev E 2006;73. 035104–4. URL http://pre.aps.org/abstract/PRE/v73/i3/e035104.

[24] Gosak M, Korošak D, Marhl M. Topologically determined optimal stochastic resonance responses of spatially embedded networks. New J Phys 2011;13:013012–6. URL http://iopscience.iop.org/1367-2630/13/1/013012.
[25] Perc M. Visualizing the attraction of strange attractors. Eur J Phys 2005;26:579–87. URL http://iopscience.iop.org/0143-0807/26/4/003/.
[26] Bordyugov G, Granada AE, Herzel H. How coupling determines the entrainment of circadian clocks. Eur Phys J B 2011;82:227–34. URL http://dx.doi.org/10.1140/epjb/e2011-20337-1.
[27] Marhl M, Schuster S. Under what conditions signal transduction pathways are highly flexible in response to external forcing? a case study on calcium oscillations. J Theor Biol 2003;224:491–500. URL http://www.sciencedirect.com/science/article/pii/S0022519303001991.
[28] Perc M, Marhl M. Sensitivity and flexibility of regular and chaotic calcium oscillations. Biophys Chem 2003;104:509–22. URL http://www.sciencedirect.com/science/article/pii/S0301462203000383.
[29] Perc M, Marhl M. Local dissipation and coupling properties of cellular oscillators: A case study on calcium oscillations. Bioelectrochemistry 2004;62:1–10. URL http://www.sciencedirect.com/science/article/pii/S1567539403001294.
[30] Suárez-Vargas JJ, González JA, Stefanovska A, McClintock PVE. Diverse routes to oscillation death in a coupled-oscillator system. Europhys Lett 2009;85. 38008–12. URL http://iopscience.iop.org/0295-5075/85/3/38008/.
[31] Lago-Fernández LF, Huerta R, Corbacho F, Sigüenza JA. Fast response and temporal coherent oscillations in small-world networks. Phys Rev Lett 2000;84:2758–61. URL http://link.aps.org/doi/10.1103/PhysRevLett.84.2758.
[32] Strogatz SH. From Kuramoto to Crawford: exploring the onset of synchronization in populations of coupled oscillators. Phys D 2000;143:1–20. URL http://www.sciencedirect.com/science/article/pii/S0167278900000944.
[33] Abraham U, Granada AE, Westermark PO, Heine M, Kramer A, Herzel H. Coupling governs entrainment range of circadian clocks. Mol Syst Biol 2010;6. 438–6. URL http://www.ncbi.nlm.nih.gov/pmc/articles/PMC3010105/.
[34] Auchmuty JFG, Nicolis G. Bifurcation analysis of nonlinear reaction-diffusion equationsI. Evolution equations and the steady state solutions. B Math Biol 1975;37:323–65. URL http://dx.doi.org/10.1007/BF02459519.
[35] You Y. Global Dynamics of the Brusselator Equations. Dyn Part Differ Equ 2007;4:167–96. URL http://dx.doi.org/10.4310/DPDE.2007.v4.n2.a4.
[36] Perc M, Marhl M. Frequency dependent stochastic resonance in a model for intracellular Ca2+ oscillations can be explained by local divergence. Phys A 2004;332:123–40. URL http://dx.doi.org/10.1016/j.physa.2003.09.046.
[37] Wolf A, Swift JB, Swinney HL, Vastano JA. Determining Lyapunov exponents from a time series. Phys D 1985;16:285–317. URL http://chaos.utexas.edu/manuscripts/1085774778.pdf.
[38] Gosak M, Korošak D, Marhl M. Optimal network configuration for maximal coherence resonance in excitable systems. Phys Rev E 2010;81:056104–7. URL http://pre.aps.org/abstract/PRE/v81/i5/e056104.
[39] Jeong H, Tombor B, Albert R, Oltvai ZN, Barábasi A-L. The large-scale organization of metabolic networks. Nature 2000;407:651–4. URL http://www.nature.com/nature/journal/v407/n6804/full/407651a0.html.
[40] Stožer A, Gosak M, Dolenšek J, Perc M, Marhl M, Rupnik MS, et al. Functional connectivity in islets of langerhans from mouse pancreas tissue slices. PLoS Comput Biol 2013;9. e1002923–13, URL http://dx.doi.org/10.1371/journal.pcbi.1002923.
[41] Albert R. Scale-free networks in cell biology. J Cell Sci 2005;118:4947–57. URL http://jcs.biologists.org/content/118/21/4947.long.
[42] Bullmore E, Sporns O. Complex brain networks: graph theoretical analysis of structural and functional systems. Nat Rev Neurosci 2009;10:186–98. URL http://www.nature.com/nrn/journal/v10/n3/full/nrn2575.html.
[43] Henson MA. Multicellular models of intercellular synchronization in circadian neural networks. Chaos Soliton Fract 2013;50:48–64. URL http://www.sciencedirect.com/science/article/pii/S0960077912002184.
[44] Hafner M, Koeppl H, Gonze D. Effect of network architecture on synchronization and entrainment properties of the circadian oscillations in the suprachiasmatic nucleus. PLoS Comput Biol 2012;8. e1002419–16. URL http://dx.doi.org/10.1371/journal.pcbi.1002419.
[45] Albert R, Jeong H, Barabási A-L. Error and attack tolerance of complex networks. Nature 2000;406:378–82. URL http://www.nature.com/nature/journal/v406/n6794/full/406378a0.html.
[46] Holme P, Kim BJ, Yoon CN, Han SK. Attack vulnerability of complex networks. Phys Rev E 2002;65:056109–14. URL http://pre.aps.org/abstract/PRE/v65/i5/e056109.
[47] Aronson DG, Ermentrout GB, Kopell N. Amplitude response of coupled oscillators. Phys D 1990;41:403–49. URL http://www.sciencedirect.com/science/article/pii/016727899090007C.

SCIENTIFIC REPORTS

OPEN

SUBJECT AREAS:
BIOLOGICAL PHYSICS
ENDOCRINOLOGY
CALCIUM SIGNALLING
COMPUTATIONAL BIOPHYSICS

Received
25 July 2014

Accepted
16 December 2014

Published
19 January 2015

Correspondence and requests for materials should be addressed to M.S.R. (marjan.rupnik@um.si)

* These authors contributed equally to this work.

Progressive glucose stimulation of islet beta cells reveals a transition from segregated to integrated modular functional connectivity patterns

Rene Markovič[1]*, Andraž Stožer[2,3]*, Marko Gosak[1,3,4]*, Jurij Dolenšek[2]*, Marko Marhl[1,3,4] & Marjan Slak Rupnik[2,3,5]

[1]Faculty of Natural Sciences and Mathematics, University of Maribor, Koroška cesta 160, 2000 Maribor, Slovenia, [2]Institute of Physiology, Faculty of Medicine, University of Maribor, Taborska ulica 8, 2000 Maribor, Slovenia, [3]Centre for Open Innovations and Research, University of Maribor, Slomškov trg 15, 2000 Maribor, Slovenia, [4]Faculty of Education, University of Maribor, Koroška cesta 160, 2000 Maribor, Slovenia, [5]Institute of Physiology, Center for Physiology and Pharmacology, Medical University of Vienna, Schwarzspanierstraβe 17, A-1090 Vienna, Austria.

Collective beta cell activity in islets of Langerhans is critical for the supply of insulin within an organism. Even though individual beta cells are intrinsically heterogeneous, the presence of intercellular coupling mechanisms ensures coordinated activity and a well-regulated exocytosis of insulin. In order to get a detailed insight into the functional organization of the syncytium, we applied advanced analytical tools from the realm of complex network theory to uncover the functional connectivity pattern among cells composing the intact islet. The procedure is based on the determination of correlations between long temporal traces obtained from confocal functional multicellular calcium imaging of beta cells stimulated in a stepwise manner with a range of physiological glucose concentrations. Our results revealed that the extracted connectivity networks are sparse for low glucose concentrations, whereas for higher stimulatory levels they become more densely connected. Most importantly, for all ranges of glucose concentration beta cells within the islets form locally clustered functional sub-compartments, thereby indicating that their collective activity profiles exhibit a modular nature. Moreover, we show that the observed non-linear functional relationship between different network metrics and glucose concentration represents a well-balanced setup that parallels physiological insulin release.

Beta cells secrete insulin in response to stimulation by energy rich molecules in a regulated manner and play a central role in whole-body energy homeostasis[1]. In vivo, beta cells are organized into microorgans called islets of Langerhans. All beta cells of an islet of Langerhans are coupled into a single functional unit by means of the gap junction protein Connexin 36 (Cx36) that allows for electrical coupling and exchange of small signaling molecules between physically adjacent cells. One of these small signaling molecules being calcium ions[2]. In this way, a coordinated activity in a large number of cells can be established, thereby leading to a regulated exocytosis of insulin[3,4].

The mechanisms that govern insulin secretion at the single-cell level have been studied extensively. An increase in extracellular glucose concentration leads to an increased entry of glucose into the beta cell, an increased metabolic production of ATP and a decrease in the open probability of ATP-sensitive potassium ion channels. Consequently, the beta cell depolarizes and the voltage-sensitive calcium ion channels open to increase the intracellular calcium concentration ($[Ca^{2+}]_i$) that triggers the calcium-sensitive exocytosis of insulin granules. This calcium-induced exocytosis is believed to be augmented via a less well known amplifying pathway[5]. The changes in membrane potential, $[Ca^{2+}]_i$ as well as exocytosis occur in the form of synchronous oscillations[6–10]. Insulin acting on different target cells in the body subsequently reduces glucose concentration to stop the stimulation of insulin release and prevent hypoglycemia by means of a negative feedback loop.

At the tissue level however, the relationship between the collective activity of cell populations and hormone release is not completely understood[11]. This is mainly due to the fact that until recently, our ability to study the physiology of many cells simultaneously had largely been limited by the existing experimental methods[12]. The investigations of the intercellular communication between beta cells had mostly relied on imaging changes in

$[Ca^{2+}]_i$ in isolated islets. These measurements, using either CCD cameras with limited temporal resolution and a height of the focal plane larger than a single cell[8,13] or confocal microscopy with limited uptake of $[Ca^{2+}]_i$-sensitive fluorescent dyes, constrained the number of simultaneously studied cells to a few cells from the mantle of the islet[14,15]. Recently, the drawbacks of the existing experimental techniques were circumvented by applying high spatial and temporal resolution confocal functional multicellular calcium (fMCI) and membrane potential imaging to the islets of Langerhans in tissue slices[7,16]. Additionally, two-photon confocal microscopy in combination with extracellular polar fluorescent dyes enables the study of exocytosis from all beta cells within a focal plane[17,18]. Therefore, from a technical point of view, it is now possible to study the collective behavior of cell populations, such as the islet of Langerhans, and more specifically the degree of coupling and residual heterogeneity in such populations.

The heterogeneity of beta cells is most pronounced when cells are dispersed or uncoupled, thereby completely or partially losing their social context within the functional syncytium of the islet[12,19]. Early studies proposed that such individual beta cells exhibit differences in glucose metabolism[20,21] and insulin secretion[22]. More recent works on the dynamics of $[Ca^{2+}]_i$ in isolated or uncoupled cells further confirmed heterogeneity of beta cells. In isolated beta cells, $[Ca^{2+}]_i$ responses were elicited at very different threshold concentrations of glucose, with a significant proportion of cells responding only to unphysiologically high concentrations of glucose or tolbutamide[23]. In uncoupled cells, $[Ca^{2+}]_i$ responses to a given concentration of glucose were unsynchronized[24,25].

In an intact islet, these heterogeneities are largely attenuated and the islet functions more homogeneously than isolated or uncoupled cells[12]. The cells within an islet respond metabolically over a more confined glucose concentration range[21,26] and the membrane potential and $[Ca^{2+}]_i$ oscillations of cells within an islet are, in contrast to single and uncoupled cells, in phase[6,10,15]. Finally, it has long been known that intact islets display a higher glucose stimulated insulin release than isolated and reaggregated, but not coupled beta cells[27].

However, the activity of beta cells within an islet is not completely synchronized and the islet shall not be regarded as a single large cell. Namely, the membrane potential and $[Ca^{2+}]_i$ changes spread over the islet in a wave-like manner[7,13,16]. Moreover, it was recently shown that in terms of exocytosis, upon stimulation with glucose, not all beta cells within an islet respond at the same time but are progressively recruited with increasing levels of stimulation[17]. Thus, in an islet there is a considerable degree of heterogeneity between individual beta cells.

It is important to focus on and quantify the level of heterogeneity among beta cells, since it was demonstrated that a larger-than-normal degree of heterogeneity, possibly due to disruptions to the normal intercellular communication, could play a role in type 2 diabetes mellitus[25,28–30]. Thus, studying how the activity of a large number of heterogeneous beta cells is aligned functionally, how the functional syncytium breaks down, and determining where the increasing heterogeneity results in disease, is of great importance.

However, before embarking on this journey, it is important to reevaluate the parameters on which our predictions about the heterogeneity of beta cells are based and assess a possibly present and physiologically important residual heterogeneity between beta cells in normal islets in a quantitative manner. We believe that such a reevaluation would make it possible to draw a line between normal and pathological function and predict or detect the development of diabetes mellitus.

From the analytical point of view, one possible way to better understand interactions between cells and the functioning of complex biological systems relies on the modern theory of complex networks[31]. Network concepts have been successfully applied on various scales of living organisms ranging from the organization of single cells[32] to that of entire ecosystems[33]. From the viewpoint of clinical applications, the greatest progress in this context has been done in the field of neuroscience[34]. The modern neuroimaging technologies allow the acquisition of comprehensive datasets of anatomical or functional connection patterns in the human brain, thereby providing new insights into the structure and functionality of healthy human brain as well as new insights into many brain disorders[35]. Impaired and disrupted complex brain networks were reported in autism[36], schizophrenia[37], and multiple sclerosis[38]. Moreover, recent investigations of functional network analysis exceed the stationary representation by focusing on dynamical tracking of the changes in brain activity associated with task performance. It has been shown that the brain's network organization reconfigures due to cognitive efforts[39], dynamic changes in the sensory environment[40], learning processes[41], and during stroke recovery processes[42].

While being well acknowledged in the field of neuroscience, the application of network concepts has not yet received very much attention at the tissue level, where individual cells represent the nodes of a network. Several tissues are often organized as networks, they evolve in time and their cells can be regarded as dynamic systems, which interact with each other. But they have not been studied as such, predominantly due to a lack of experimental techniques that would enable the necessary assessment of function in a large number of cells simultaneously, as noninvasively as possible, and over longer periods of time. First endeavors combining fMCI and graph-theoretical approaches were conducted on pituitary endocrine cells[43–45]. We and others succeeded in applying these methodologies to study the activity of beta cell populations[11,24,46]. In particular, in our previous study we showed that the functional connectivity extracted on the basis of $[Ca^{2+}]_i$ dynamics exhibits small-world topological features, which are most pronounced in the regime of high glucose stimulation[46]. This finding was later confirmed by Hodson and coworkers[11]. Recently, these techniques were also successfully applied at uncovering the functional cellular connectivity in a network of astrocytes[47].

In the present study, we continue our quest to explore functional heterogeneity in beta cells in islets of Langerhans *in situ* by applying advanced analytical tools from the realm of complex network theory. The tools have been applied on long temporal traces obtained by confocal fMCI of beta cells stimulated in a stepwise manner with a range of glucose concentrations from the substimulatory concentration of 6 mM to the above-physiological, but traditionally often used 12 mM glucose. Employing this experimental approach, we demonstrate a modular nature of mouse islets, revealing a multiunit organizational principle in a structure with an apparently homogeneous microanatomy and even largely synchronous activity in terms of traditional physiological measures.

Results

Confocal fMCI imaging was used to monitor $[Ca^{2+}]_i$ signals emanating from Oregon Green 488 BAPTA-1 (OGB-1)-loaded beta cells in acute tissue slices (see Methods). The temporal evolution of $[Ca^{2+}]_i$ in a typical beta cell under progressive stepwise stimulation with glucose from 6 mM to 12 mM is shown in Fig. 1. As expected, the frequency of oscillations $[Ca^{2+}]_i$ as well as the basal $[Ca^{2+}]_i$ level increase with increasing concentrations of glucose. The inset shows a segment of the $[Ca^{2+}]_i$ trace of the same cell $x(t)$ after subjecting it to ensemble empirical mode decomposition (EEMD) (see Methods).

We proceeded with the sliding window correlation analysis of beta cell dynamics in order to examine the temporal evolution of the average correlation coefficient R_{avg}. Results shown in Fig. 2 reveal that the level of correlation progressively increases with increasing concentrations of glucose. For the calculation of correlations and for the following network constructions we used, $[Ca^{2+}]_i$ traces that were subjected to EEMD in order to exclude baseline trends. These variations of the baseline activity are the so called slow $[Ca^{2+}]_i$ oscillations

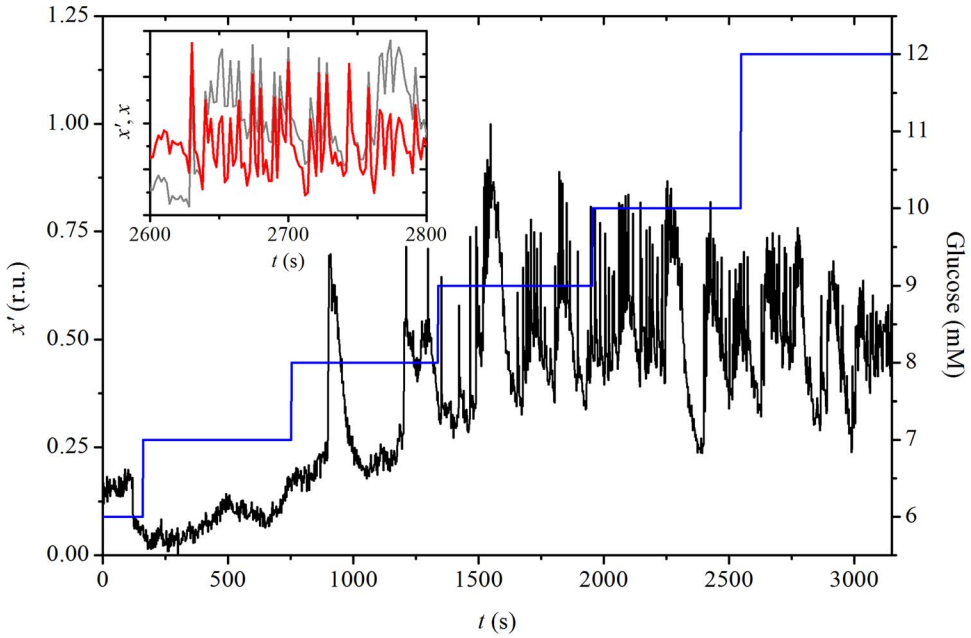

Figure 1 | Experimentally measured temporal evolution of $[Ca^{2+}]_i$ in a typical beta cell $x'(t)$ in response to different concentrations of glucose expressed in relative units (r.u., black line). The blue line denotes stepwise increases in glucose concentration with the respective axis located on the right. In the inset, a segment of the original signal (grey line) and the corresponding EEMD $x(t)$ (red line) are shown.

and most probably reflect glycolytic oscillations in some cells of the islet and not the rapid $[Ca^{2+}]_i$ oscillations that spread from cell to cell by means of depolarization waves and are the subject of this study[48]. In addition, fluctuations in baseline trends could be an experimental artefact due to drifts in the perifusion chamber. Furthermore, we verified if a similar behavior can be observed also in other islets, subjected to similar protocols. Indeed, results shown in Fig. S1 reveal that a very similar temporal evolution of the average correlation coefficient R_{avg} can be observed in three other islets as well, when the concentration of glucose is progressively increased.

Functional connectivity maps were constructed on the basis of pairwise correlations between $[Ca^{2+}]_i$ signals of individual cells. Two cells were considered to be connected if their Pearson product-moment correlation over a certain time interval $\Delta\tau$ exceeded a predetermined threshold value R_{th} (see Methods). Fig. 3 features the beta cell functional network architectures for different concentrations of glucose. We can observe that for low stimulation levels ($\leq$8 mM) only isolated and rarely synchronized activities are detected. With increasing concentrations of glucose, the network becomes denser, which reflects the increase of the average correlation coefficient shown in Fig. 2. Furthermore, it can be observed that the beta cell functional network is modular. Namely, well pronounced local communities are identified in which mostly interactions between nearest neighbors are present. It appears that the beta cell syncytium is structured in several sub-networks in each of which the degree of synchronization between the cells is very high. These sub-compartments are strongly segregated at lower concentrations of glucose, whereas for high concentrations they become more integral, yet still well expressed and localized. Thus, it appears that for different levels of stimulation the synchronization activity of beta cells is regulated in segregated local clusters. Furthermore, this localized organization suggests that physical constraints drive the structure of the beta cell functional network. A more precise tracking of the temporal evolution of the beta cell functional network by progressively increasing concentrations of glucose can be observed in the Supplementary video S1. In order to further corroborate our findings, we show in Fig. S2 beta cell functional networks of three additional islets (the same as in Fig. S1) subjected to similar protocols, under 8 mM and 12 mM glucose stimulation. Evidently, in all three cases the networks are sparse and very segregated in 8 mM glucose, whereas in 12 mM glucose they are much more dense and interconnected, but with well-expressed localized communities.

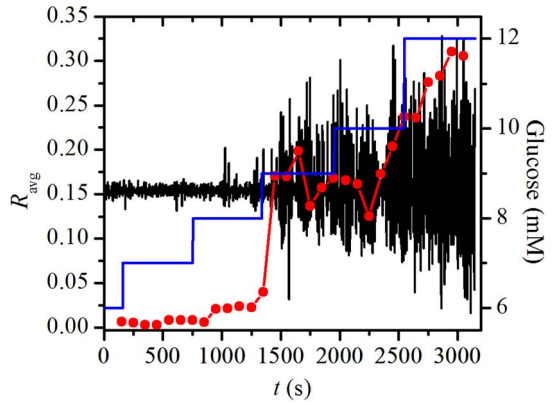

Figure 2 | The temporal evolution of the average correlation coefficient (red line with symbols) and the mean-field signal of EEMD processed $[Ca^{2+}]_i$ activity of beta cells (black line). The blue line denotes the concentration of glucose. In the calculation of the sliding window correlation analysis (see Methods), $\Delta\tau$ was set to 300 s and step Δn to 100 s.

It remains of interest to identify the reasons for the segmentation into functional sub-compartments. For this purpose we calculated the frequencies in five largest communities in the network, the corresponding EEMD-processed $[Ca^{2+}]_i$ mean-field signals within individual communities x_i^{com}, and the mean-field signal of the whole network x^{net}, at 9 mM and 12 mM glucose. The results for the islet analyzed and shown in Figs. 2 and 3 are presented in Fig. 4. It can be observed that the average frequencies under both stimulation levels are not completely unified. These discrepancies in the frequencies are principally not a consequence of uncoordinated intercellular activity, but rather a result of unexecuted oscillations in particular groups of cells, as it can be seen from the courses of individual mean-field

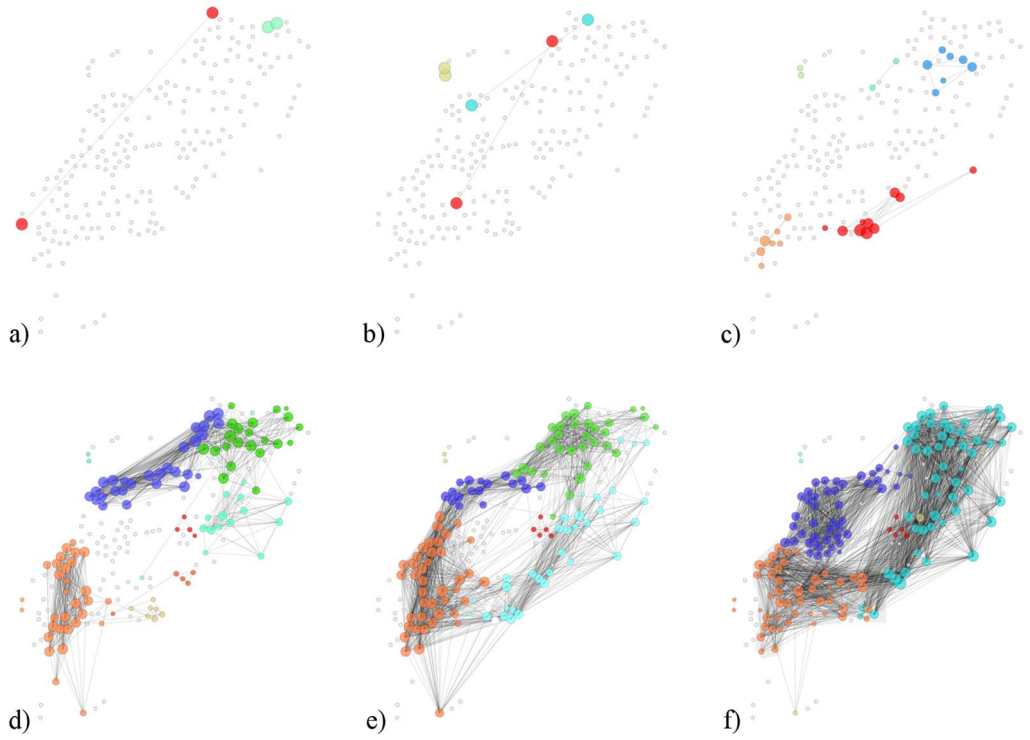

Figure 3 | Functional networks of beta cells at different concentrations of glucose: a) 6 mM, b) 7 mM, c) 8 mM, d) 9 mM, e) 10 mM, f) 12 mM. Colors of circles denote the modularity classes (communities). Grey circles signify unconnected cells. The threshold for functional connectivity R_{th} was set to 0.7. The number of cells in the examined slice was 200. The positions of nodes correspond to physical positions of cells within the examined islet of Langerhans.

signals. Furthermore, an inspection of the mean-field signals (Figs. 4(b) and 4(d)) reveals, that the amplitude of x^{net} is for the most of the time noticeably lower than the amplitude of signals in individual communities x_i^{com}, thereby indicating that the $[Ca^{2+}]_i$ dynamics among communities is not completely phase synchronized. To conclude, the existence of communities in the beta cell functional network can be attributed to a more simultaneous activity as well as to a better phase synchronization within other three individual groups of cells. The same behavior is observed also in the three other islets.

To further analyze the organization of interconnected modules of beta cells, we computed the average correlation coefficient between cell pairs within each of the communities, $R_{avg}^{c_i}$. The overall average correlation in communities R_{avg}^{cum} was then defined as the average $R_{avg}^{c_i}$ for all communities. The results presented in Fig. 5 feature the values of R_{avg}^{cum} for different concentrations of glucose. For comparison, we additionally calculate the average correlation between all cell pairs in the network, R_{avg}^{net}. The values of R_{avg}^{cum} and R_{avg}^{net} represent the averages of four different functional networks having altogether 722 nodes (slices shown in Figs. 3 and S2). Evidently, the correlations between cell pairs in individual communities are much higher than the correlation at the level of the whole slice, which further supports the idea of segregated synchronization activities in the islet. These findings are qualitatively independent of the choice of the connectivity threshold R_{th} (see Fig. S3).

To describe the temporal evolution of the network characteristics more quantitatively, we calculated several network measures (see Methods) at different concentrations of glucose. For a more precise and reliable quantification, the calculations were performed for four different islets (the same as shown in Figs. 3 and S2). In Fig. 6 we present the results showing the network measures for each concentration of glucose. The light grey lines with symbols denote values in individual islets and the thick red line with symbols signifies the average over all four functional networks. Quite considerable discrepancies in absolute values of network metrics can be observed, which reflect the inter-islet variability, whereas most notably, the functional relationship between different network metrics and glucose concentration is very similar in all four islets.

In Fig. 6(a), the average degree of cells k_{avg} is shown as a function of glucose concentrations. Its increase at higher concentrations of glucose is related to a greater level of synchronization between beta cells (see Fig. 2), as the correlation coefficient between more and more cell pairs exceeded the threshold and consequently the network became denser. We believe that the higher network degree is a result of a more pronounced communication via electrical synapses and possibly also other more long-range-oriented communication mechanisms. The average clustering coefficient C_{avg} is a measure for the network's functional segregation and is indicative of small-worldness of the network[49]. Results in Fig. 6(b) show that in the beta cell network a prevalence of clustered connectivity around individual cells was detected, but only for high enough stimulation levels reaching a plateau value at a glucose concentration of >9 mM. Another measure of interest is the global efficiency E, which reflects the functional integration of the tissue such as the traffic capacity of a network in the form of signal-propagation speed and degree of synchronizability. Fig. 6(c) features the results for different glucose concentrations. It can be noticed that for high stimulation levels ($\geq$10 mM) an efficient information exchange throughout the entire network was achieved.

We also focused on the evolution of the modular structure of the beta cell network. Figs. 6(d) and (e) show the number N_c and average size n_c of communities that change with increasing concentrations of glucose. Notably, for glucose concentrations >8 mM the networks are in average composed of around 7 densely interconnected groups of cells. The size of these communities increases markedly with increasing concentrations of glucose, but reaches a plateau at 10 mM. Finally, we examined the average length of functional connections I_{avg} as a function of glucose concentration. This parameter reflects either prevalent adjacent cell-to-cell communication in case

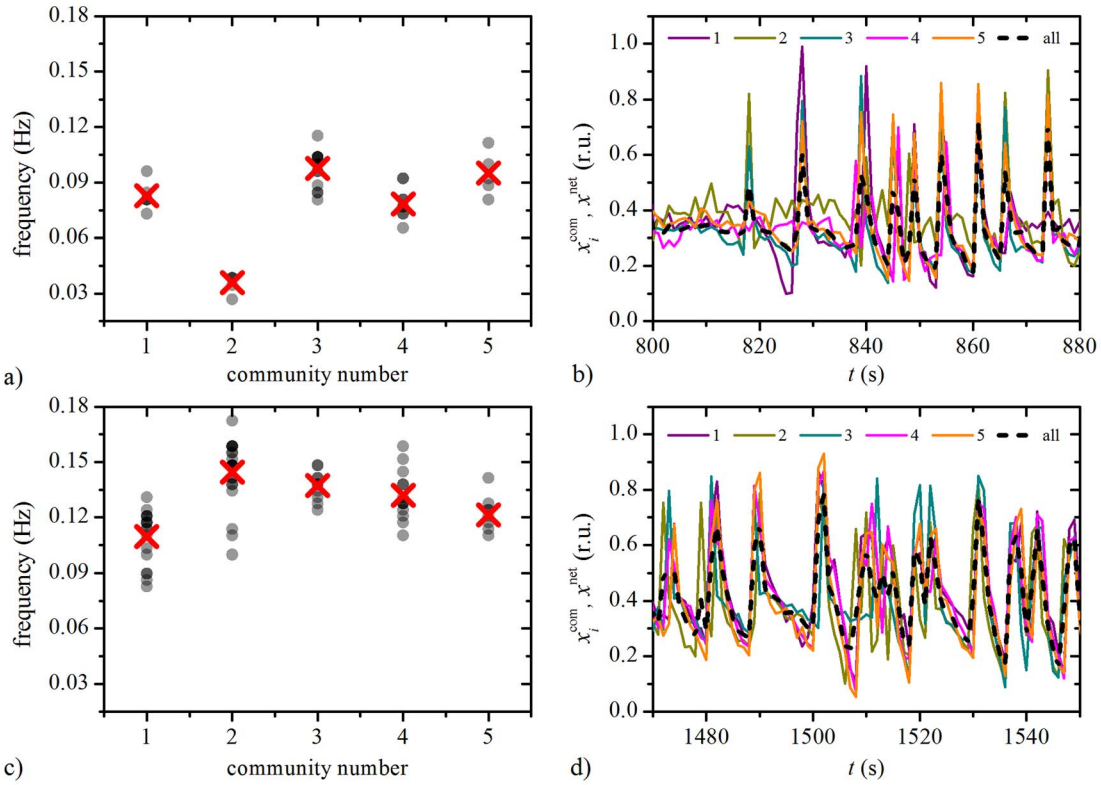

Figure 4 | Frequency distributions within 5 largest communities under 9 mM (a) and 12 mM (c) glucose. Grey dots denote frequencies of individual cells and the red crosses signify the average frequency in the given community. It can be observed that the frequencies are in average higher under 12 mM glucose stimulation, and that the average values in different communities are not exactly the same. The corresponding mean-field signals of individual communities x_i^{com} (colored lines) and of the whole network x^{net} (black dotted line) under 9 mM and 12 mM glucose are shown in panels (b) and (d), respectively. The amplitude of the whole-network mean-field signal x^{net} is lower than the amplitude in individual communities, thereby indicating that individual signals are not completely phase synchronized.

of short distances or, alternatively, cell-to-cell communication spanning over several cells that is mediated either by postganglionic nerve axons within islet or diffusible paracrine factors such as NO. Fig. 6(f) reveals that I_{avg}, similarly to other network metrics, rises between 7 mM and 10 mM glucose, while for concentrations >10 mM the average link length remained more or less constant. Notably, at high levels of stimulation, the average range of interactions between beta cells is around 45 μm.

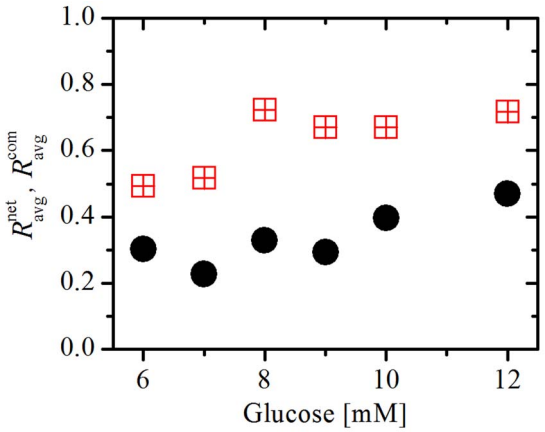

Figure 5 | **Average correlation between cell pairs in individual communities R_{avg}^{com} (red squares) and between all connected cells in the network R_{avg}^{net} (black circles) at different concentrations of glucose.** In the calculation the connectivity threshold R_{th} was set to 0.7. The results are based on the average of four different functional networks (slices presented in Figs. 3 and S2) having altogether 722 nodes.

Finally, to be able to ascribe the observed effects upon network metrics to increasing concentrations of glucose, we had to assess whether there are any time-dependent increases in parameter values in constant glucose. For this purpose, we analyzed eight additional islets. Four of them were stimulated with 8 mM and four of them with 12 mM of glucose for the entire period of stimulation. For all of them we calculated the temporal evolution of the same network metrics as presented in Fig. 6. Results in Fig. S4 reveal that the values obtained during constant stimulation with 8 mM and 12 mM glucose were comparable with the values obtained for the respective concentrations during stepwise stimulation. Additionally, with the exception of N_c, on average all parameters displayed lower values in 8 mM glucose than in 12 mM glucose throughout the entire period of stimulation. Finally, although beyond the scope of this paper, a clear trend toward decreasing parameter values with time was detected for constant long-term stimulation with 12 mM glucose.

Discussion

Individual or uncoupled beta cells have been found to be intrinsically heterogeneous and as such incapable of collectively adjusting their insulin secretion rates in accordance with blood glucose levels. Intercellular communication via gap junctions attenuates the heterogeneous nature of beta cells by synchronizing their activity and suppressing any subtreshold responses as well as recruiting high glucose responders of individual beta cells, thereby representing the fundamental mechanism ensuring whole body energy homeostasis[25,26,50,65]. In this study we obtained additional insight into these issues by analysing how the functional network of beta cells changes

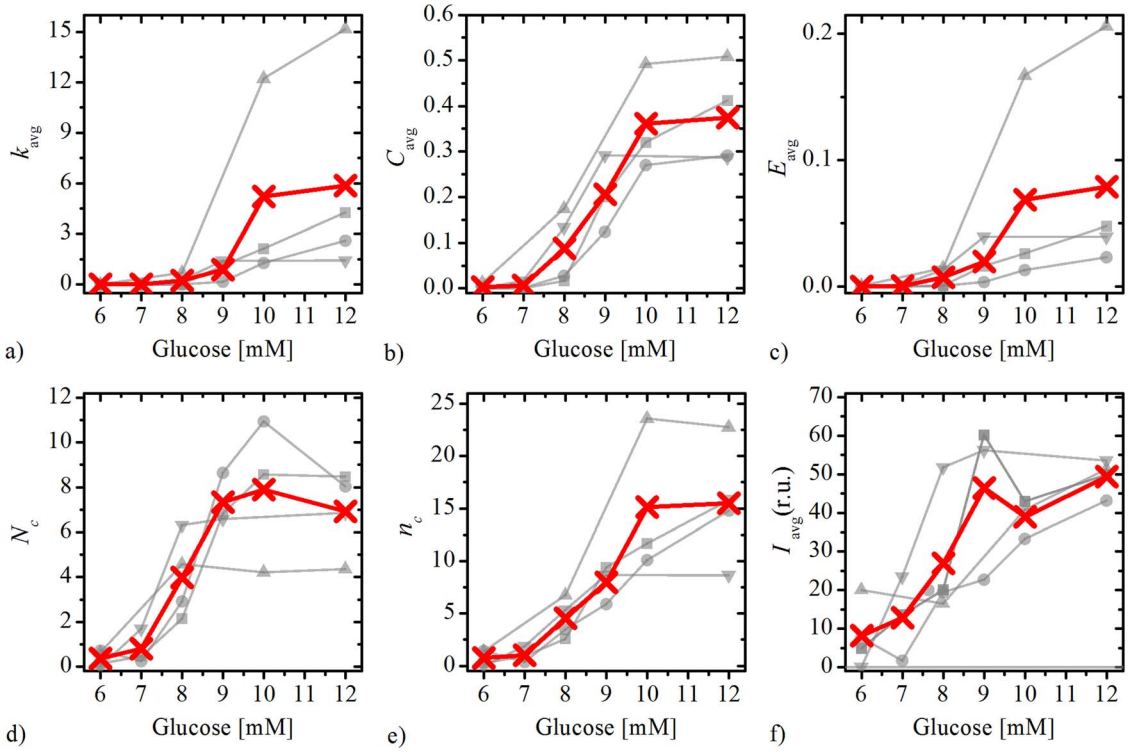

Figure 6 | Different network measures at different concentrations of glucose for four islets (the same as shown in Figs. 3 and S2). a) average degree, b) average clustering coefficient, c) global efficiency, d) average number of communities, e) average size of communities, f) average length of functional connections. Light grey line with symbols denote the values in individual islets, whereas the thick red lines with crosses indicates the average. In all calculations the connectivity threshold R_{th} was set to 0.7.

during step-wise elevations of stimulatory glucose levels, ranging from 6 mM (basal) to 12 mM (high). We showed that for basal glucose levels the collective dynamics is poorly synchronized resulting in a sparsely connected functional network. With increasingly stimulatory glucose levels, the multicellular system gets more synchronized and evolves into a more densely connected network with increasingly expressed small-world topological features, characterized by high global efficiency (short internodal distances) and a highly clustered organization[49]. This is in agreement with our previous study where we found that the functional network of beta cells, when exposed to high glucose levels, exhibits small-worldness[46]. In terms of the real network of an islet of Langerhans, the degree of small worldness probably contributes to the robustness of the network in terms of its secretory response and determines its resilience to metabolic and immune perturbations occurring during onset of diabetes mellitus. Furthermore, for glucose values above 10 mM, the network characteristics seem to saturate. This could be caused by spatial constraints which prohibit the establishment of too long connections and hence hinder additional improvements of the evolving functional network. The origin of the spatial constraints could be similar to those discussed in neuronal networks. In the brain it is believed that its small-world functional network is the outcome of an optimization mechanism based on minimizing wiring cost and maximizing efficiency[34]. Since long-range connections are related to higher cost, this causes spatial constraints. Since in our study, the connectedness of two cells depends on the similarity of their signals, which in turn conceivably depends on the degree of their electrophysiological coupling that is expected to be high at low membrane and high gap junctional conductance, the abovementioned spatial constraint could have its mechanistic substrate in the fact that at a certain level of stimulation, in this case at 10 mM glucose, the membrane conductance reaches its minimum or the junctional conductance its maximum.

Through the process of stimulus-secretion coupling in beta cells, membrane potential changes in the form of bursts of depolarizations are translated to oscillations of $[Ca^{2+}]_i$ and finally to pulses of insulin secretion. To assess beta cell activity, all three parameters can be used. Thus, we need to justify the choice of $[Ca^{2+}]_i$ as a proxy for beta cell function in our study and comment briefly on the generalizability of our findings. First, from the technical point of view, due to the commercial availability of $[Ca^{2+}]_i$ sensitive fluorescent dyes, their ease of use and high signal-to-noise ratio, especially as compared to currently available voltage sensitive fluorescent dyes, $[Ca^{2+}]_i$ seems a logical choice. Second, $[Ca^{2+}]_i$ is a trigger for exocytosis also in other tissues, where an increase in $[Ca^{2+}]_i$ is not brought about by electrical activity and influx of $[Ca^{2+}]_i$, but by secretagogue induced release of Ca^{2+} from internal stores. Some of these tissues are accessible to fMCI and the use of $[Ca^{2+}]_i$ in our case facilitates comparison between different tissues. Finally and most importantly, in previous studies by us and other groups employing a wide array of experimental approaches, it was demonstrated that in islets of Langerhans, the relationship between the changes in membrane potential and changes in $[Ca^{2+}]_i$[7,8,10] as well as between changes in $[Ca^{2+}]_i$ and pulses of insulin secretion[6,9,17,18] are straightforward. Thus, we are confident that changes in $[Ca^{2+}]_i$ are a representative measure of beta cell activity.

In addition, the binding of Ca^{2+} to $[Ca^{2+}]_i$ sensitive dyes with different affinities could influence the nature of the observed changes in $[Ca^{2+}]_i$ to depart from the ones occurring in vivo or even lead to cell death. Employing an armamentarium of $[Ca^{2+}]_i$ sensitive fluorescent dyes with different affinities, we and others have shown largely comparable $[Ca^{2+}]_i$ changes, even after prolonged periods of recording[6–10,15,16,46].

In general, in all four analyzed islets, all the network measures obeyed a similar response with respect to increasing concentrations

of glucose; a steep increase occurred between 8 mM and 10 mM, whereas above these values a saturation of the network properties was detected. It seems that within these physiological ranges of glucose, the beta cell network exhibits a high level of plasticity, reflected by gradual adjustments of the global efficiency and local organization with respect to the external stimulus. This is in an agreement with the role of beta cells as primary glucose sensors matching their dynamic range with normal physiological fluctuations of plasma glucose. For high concentrations of glucose (10 mM and above), on the other hand, a saturation of the network characteristics occurs, thereby indicating the realization of the maximal operating ability. A similar non-linear behavior within the same physiological range of stimulatory glucose concentrations was experimentally observed from dynamic glucose stimulated insulin release perifusion studies with isolated islets[51]. In our experimental setup, it is currently impossible to study insulin secretion simultaneously with $[Ca^{2+}]_i$ signals due to the exceedingly small amount of insulin released by an islet within tissue slice in the physiological glucose range.

One of our most important findings is the modular nature of the extracted functional networks, which indicates that beta cells inside the islet of Langerhans form functional sub-compartments. Cells within sub-compartments are clustered and their activity is much more correlated in comparison to the islet as a whole. For low levels of glucose, only completely segregated local areas occasionally responded to stimulation. With increasing levels of the stimuli, a higher number of communities were recruited which got more and more interconnected, thereby making the whole functional network more efficient. The modular behavior of the beta cell functional syncytium was predicted by previous experimental data[46]. Stepwise glucose stimulation progressively recruited cells that were organized in multicellular groups. Recruitment was shown on the level of glucose metabolism[52], insulin synthesis[53] and insulin secretion[17]. Since the global efficiency indicates shorter path lengths among nodes, it is also referred to as a measure of functional integration[35]. This suggests that the islet of Langerhans is capable to continuously improve from a highly segregated into a more integrated functional network. Since cell-to-cell communication coordinates the activities of individual cells, the modular nature of the islets could represent an additional spatially regulated insulin secretion mechanism.

Our control experiments with constant stimulation confirmed that the effects upon network metrics observed during stepwise stimulation can indeed be ascribed to increasing concentrations of glucose. In 8 mM glucose, the parameter values continued to increase after the initial 500 seconds (this was the time period used for each concentration of glucose during stepwise stimulation), but this additional increase was clearly insufficient to raise the parameter values to levels attained in 12 mM glucose. The trend toward a decrease in parameter values in 12 mM glucose warrants further investigation, since it might be a network correlate of glucotoxicity, previously observed in concentrations of glucose higher than 10 mM[54]. Exploring the effects of constant stimulation with high concentrations of glucose upon network metrics seems especially compelling in the light of a recent study demonstrating that lipotoxicity can target beta cell connectivity[24].

Recent studies analyzing mouse and human islets with a complex network approach, that have produced largely compatible results regarding the general connectivity patterns in mouse islets, have not explicitly detected any communities[11,16,24]. First, this might be due the fact that these studies have not specifically looked for the presence of communities analytically in a way we did in our present study. One of the reasons that communities have not been detected before might be that glucose concentration of 11 mM[11,24] or 12 mM[16] has been used to evoke $[Ca^{2+}]_i$ responses. As demonstrated in the present study, at this high concentrations of glucose, the activity of cells belonging to different communities is most aligned, i.e. the networks are quite dense, and this might have caused that the functional compartmentalization has escaped our attention.

It was shown that rodent islets are of polyclonal origin and that the cells stemming from the same progenitor remain spatially clustered[55]. Thus, it is tempting to speculate that the functional subunits of an islet of Langerhans might overlap with the embryological subunits defined by a common progenitor. This awaits further elucidation, possibly involving human tissue, since recently, a polyclonal origin of beta cells was also demonstrated for human islets of Langerhans[56].

It was pointed out that a balanced combination of segregated and integrated information processing, established via efficient small-word topological features, ensures normal brain functioning[57]. Disruptions to this balance can lead for instance to autism, in case of predominantly segregated information processing[58], or schizophrenia in case of predominantly integrated information processing[37]. It is reasonable to speculate that anomalies in the functional connectivity could results in pathological conditions of islets, leading to diabetes mellitus. Hence, additional experimental and theoretical studies are needed in order to gain knowledge about how this multicellular system regulates its functioning through cell-to-cell communication in disease states.

Finally, in our study beta cells exhibited greatest responsiveness at a range of glucose concentrations commonly experienced by animals *in vivo* and significantly below the ones traditionally used in electrophysiological, $[Ca^{2+}]_i$ imaging and insulin secretion experiments, where in our hands, the network parameters typically reached their maxima and stabilized. Perhaps, the supraphysiological concentrations were classically used due to lower inter-specimen variability and greater reproducibility of results. This study suggests, however, that in order to learn more about the physiology of beta cells and their heterogeneity, in future work, lower, more physiological stimulatory concentrations of glucose should be used.

Methods

Ethics statement. All methods and animal protocols were performed in strict accordance with all national regulations and ethical guidelines approved by the Ministry of Agriculture and Environment, Republic of Slovenia (Permit Number: 34401-61-2009/2).

Experimental protocol. Experimental protocols for preparation of acute pancreas tissue slices and confocal $[Ca^{2+}]_i$ imaging were described in detail previously[16]. In brief, tissue slices were cut from pancreata of 10–20 week old NMRI mice of either sex. After sacrificing the animals by cervical dislocation, low-melting point 1.9% agarose in extracellular solution (ECS, consisting of (in mM) 125 NaCl, 26 $NaHCO_3$, 6 glucose, 6 lactic acid, 3 myoinositol, 2.5 KCl, 2 Na pyruvate, 2 $CaCl_2$, 1.25 NaH_2PO_4, 1 $MgCl_2$, 0.5 ascorbic acid) at 40°C was injected into the proximal common bile duct clamped at the papilla of Vater. Small blocks of tissue from the agarose-injected pancreas were cut with vibratome (Leica vt1000) into 140 μm-thick slices in an ice-cold ECS continuously bubbled with a gas mixture (95% O_2 and 5% CO_2, pH of 7.4). Slices were incubated in a calcium dye loading solution composed of 6 μM Oregon Green 488 BAPTA-1 AM, 0.03% Pluronic F-127 (w/v) and 0.12% dimethylsulphoxide (DMSO, v/v) in HEPES-buffered saline (HBS, consisting of (in mM) 150 NaCl, 10 HEPES, 6 glucose, 5 KCl, 2 $CaCl_2$, 1 $MgCl_2$; titrated to pH = 7.4 using 1 M NaOH) for 50 minutes at room temperature and protected from light.

Confocal $[Ca^{2+}]_i$ imaging using OGB-1 was performed on a Leica TCS SP5 AOBS Tandem II upright confocal system using a Leica HCX APO L 20× water immersion objective (NA = 1.0). The dye was excited by an argon 488 nm laser. The emitted fluorescence in the range of 500–700 nm was collected by Leica HyD detector. Individual slices were imaged in a temperature-controlled bath chamber at 37°C (TC05, Luigs & Neumann) mounted on the microscope and continuously perifused with ECS. Sampling rate was 0.5–1 Hz at 512 × 512 pixels. The $[Ca^{2+}]_i$ oscillations were analyzed off-line employing custom-made scripts.

Analysis of time series. *Ensemble empirical mode decomposition.* The recorded time series were subject to Huang-Hilbert type empirical model decomposition[59] in order to retrieve baseline trends. In this manner, we were able to extract undistorted $[Ca^{2+}]_i$ dynamics of individual cells. In particular, we used the upgraded ensemble empirical mode decomposition (EEMD) proposed by Torres et al.[60]. The recorded time series $x'(t)$ were decomposed into the so called intrinsic mode functions (IMFs). Initially, white noise $w_i(t)$ in the range $w_i(t) \in [-0.1,0.1]$ is added to the original time series: $x'_i(t) = x'(t) + w_i(t)$, where i refers to the i-th realization of white noise at time t. Then, local maxima and minima are detected in the signal $x'_i(t)$. We separately interpolated

cubic spline lines through the detected maxima and minima and created an upper and lower envelope through them. Their mean value $m_1(t)$ and the difference $h_1(t)$ between the time series $x_i'(t)$ and the mean $m_1(t)$ was calculated. The process was repeated to ensure more symmetric wave profiles[58]. In the next repetition $h_1(t)$ was treated as the input. Again the upper and lower envelopes were constructed on the basis of the detected minima and maxima, and the difference $h_{11}(t)$ was calculated between the mean of the envelopes $m_{11}(t)$ and $h_1(t)$. In general, the process was defined as follows:

$$h_{1k} = m_{1k} - h_{1(k-1)}, \tag{1}$$

where k stands for the k-th repetition of the procedure described above. The process was repeated until the standard deviation (SD) in the difference between h_{1k} and $h_{1(k-1)}$ was above a predefined threshold (in our case 0.0001). Afterwards, h_{1k} became the first intrinsic mode during the i-th generation of white noise IMF_1^i. This mode contained the fastest time scale. In order to calculate other intrinsic modes of the signal, we took the signal $x_i'(t)$ and calculated the residue $r_i(t) = x_i'(t) - IMF_1^i$. Since IMF_1^i was excluded from $r_i(t)$ we repeated the process described above on the signal $r_i(t)$ and generated the second mode IMF_2^i. One can continue the process of decomposition until the residual becomes a monotonic function $r_{i,n}(t)$. Hence the signal $x_i'(t)$ can be expressed as:

$$x_i'(t) = \sum_{j=1}^{n} IMF_j^i + r_{j,n}(t) \tag{2}$$

The true IMFs of the signal $x'(t)$ were than calculated as the average over all m realizations of white noise as:

$$\overline{IMF}_j(t) = \frac{1}{m}\sum_t \sum_{i=1}^{m} IMF_j^i(t). \tag{3}$$

The true monotonic characteristics $\overline{r_n}(t)$ of the signal $x'(t)$ were calculated in the same manner:

$$\bar{r}_n(t) = \frac{1}{m}\sum_t \sum_{i=1}^{m} r_{i,n}(t). \tag{4}$$

Once all the true IMFs and monotonic characteristics of the original signal were determined, we excluded all the modes except the modes that possessed relevant dynamical features. Thus, the time series used for subsequent analysis $x(t)$ was calculated as:

$$x(t) = x'(t) - \bar{r}_n(t) - \sum_{i<8} \overline{IMF}_i(t). \tag{5}$$

Analysis of time series correlations. For the characterization of dynamical correlations between beta cells we calculated the correlation coefficient between the signals of the i-th and j-th cell, defined as follows:

$$R_{ij} = \frac{\sum [\bar{x}_i - x_i(t)][\bar{x}_j - x_j(t)]}{s_{x_i} s_{x_j}}, \tag{6}$$

where $\overline{x_i}$ and $\overline{x_j}$ are the mean values of the time series $x_i(t)$ and $x_j(t)$, and s_{x_i} and s_{x_j} the corresponding standard deviations. The correlation coefficient R_{ij} indicates the linear relationship between the dynamics of the i-th and the j-th cell. Values of R_{ij} are bounded within $[-1,1]$, whereby -1, 0 and 1 signify anti-correlation, no-correlation and complete correlation, respectively. In order to describe the level of global correlation in the whole slice, we calculated the average correlation coefficient:

$$R_{\text{avg}} = \frac{1}{N(N-1)}\sum_{i\neq j}^{N} R_{ij} \tag{7}$$

For the visualization of the temporal evolution of the average correlation coefficient, we made use of the sliding window correlation analysis. In particular, we calculated the average correlation coefficient between all pairs of cells in the interval $\Delta\tau$ and shifted it throughout the time series with a step Δn.

Construction and characterization of functional beta cell networks. *Extraction of functional networks from Ca^{2+} signals.* The adjacency matrix $d(t)$ of the evolving functional network was constructed according to the correlation coefficients $R_{ij}(t)$ between cells pairs. Two cells i and j were regarded as connected in a given time interval $\Delta\tau$ if the correlation coefficient $R_{ij}(t)$ exceeded or equaled a threshold value R_{th}. The value of R_{th} was selected in accordance to the corresponding R^2, in such a way, that at least 50% of the variation in system, can be explained with a linear relationship among a cell pair (we use $R_{\text{th}} = 0.7$ in the most of the calculations). These thresholding of the correlation matrix leads to a time-dependent connectivity matrix, whose ij-th element $d_{ij}(t)$ equals 1 if the nodes i and j are connected in the interval $\Delta\tau$ and 0 otherwise. A similar methodology was used for extraction of the functional connectivity patterns elsewhere[34,46].

Node degree and average degree. In an undirected network the degree of a node k_i equals the number of direct edges connecting it to its neighbors. By knowing the individual node degrees we computed the overall degree k_{avg} of the network as the average over all k_i.

$$k_{\text{avg}} = \frac{1}{N}\sum_{i=1}^{N} k_i. \tag{8}$$

Edges among individual nodal pairs reflect well synchronized mutual dynamical behavior. Therefore, the degree of a cell k_i corresponds to the number of cells with similar time courses. Higher average degree signifies a more synchronized collective behavior of the system.

Clustering coefficient. Functional segregation occurs within highly interconnected groups of nodes. A common way to find such groups is to compute the local clustering coefficient C_i of individual nodes. We implemented the method introduced by Watts and Strogatz[61]. The local clustering coefficient C_i of the i-th node is defined as:

$$C_i = \frac{2n_e}{k_i(k_i-1)}, \tag{9}$$

whereby n_e stands for the number of existing edges between the neighbors of the i-th node and the term $k_i(k_i-1)/2$ reflects the maximal number of possible edges between all its neighbors. The average clustering coefficient C_{avg} was then computed as the mean value of all C_i.

Global efficiency. A commonly used measure to characterize a network's integration of individual nodes is the network's global efficiency E_{avg}. In order to compute E_{avg}, one shall compute all the shortest paths lengths l_{ij} between all pairs of nodes in the network. Afterwards, E_{avg} is computed as follows[49]:

$$E_{avg} = \frac{1}{N(N-1)}\sum_{i\neq j}^{N}\frac{1}{l_{ij}}. \tag{10}$$

Community structure. A community is a partition of a network or a sub-graph in which the nodes are more densely interconnected as in the rest of the network. We will refer to the i-th community of the network as c_i. We implemented the algorithm introduced in ref. 62 to arrange nodes into partitions that maximized a measure called modularity Q. Modularity Q is commonly used as a measure that quantifies how successful the partitioning of a network was refs. 63, 64 and is defined as:

$$Q = \frac{1}{2m}\sum_{i,j}\left[d_{ij}(t) - \frac{k_i(t)k_j(t)}{2m}\right]\delta(c_i,c_j), \tag{11}$$

where $m = \frac{1}{2}\sum_{ij} d_{ij}(t)$, $\delta(c_i,c_j)$ is 1 if $c_i = c_j$ and 0 otherwise and $k_i(t)$ is the i-th node degree at time t. The aim of the algorithm is to maximize the modularity by continuously reshaping the community structure of the network. A new configuration is accepted if the gain in modularity ΔQ is positive. The process is repeated until no further improvement in ΔQ is achieved and the most likely community structure of the network is found.

1. Henquin, J. C. Regulation of insulin secretion: a matter of phase control and amplitude modulation. *Diabetologia* **52**, 739–751 (2009).
2. Cigliola, V., Chellakudam, V., Arabieter, W. & Meda, P. Connexins and β-cell functions. *Diabetes Res. Clin. Pr.* **99**, 250–259 (2013).
3. Rorsman, P., Braun, M. & Zhang, Q. Regulation of calcium in pancreatic α- and β-cells in health and disease. *Cell Calcium* **51**, 300–308 (2012).
4. Berridge, M. J., Lipp, P. & Bootman, M. D. The versatility and universality of calcium signalling. *Nat. Rev. Mol. Cell Biol.* **1**, 11–21 (2000).
5. Henquin, J.-C. The dual control of insulin secretion by glucose involves triggering and amplifying pathways in β-cells. *Diabetes Res. Clin. Pract.* **93**, S27–S31 (2011).
6. Bergsten, P., Grapengiesser, E., Gylfe, E., Tengholm, A. & Hellman, B. Synchronous oscillations of cytoplasmic Ca^{2+} and insulin release in glucose-stimulated pancreatic islets. *J. Biol. Chem.* **269**, 8749–8753 (1994).
7. Dolenšek, J., Stožer, A., Skelin Klemen, M., Miller, E. W. & Slak Rupnik, M. The Relationship between Membrane Potential and Calcium Dynamics in Glucose-Stimulated Beta Cell Syncytium in Acute Mouse Pancreas Tissue Slices. *PLoS ONE* **8**, e82374 (2013).
8. Gilon, P. & Henquin, J. C. Influence of membrane potential changes on cytoplasmic Ca^{2+} concentration in an electrically excitable cell, the insulin-secreting pancreatic β-cell. *J. Biol. Chem.* **267**, 20713–20720 (1992).
9. Gilon, P., Shepherd, R. M. & Henquin, J. C. Oscillations of secretion driven by oscillations of cytoplasmic Ca^{2+} as evidenced in single pancreatic islets. *J. Biol. Chem.* **268**, 22265–22268 (1993).
10. Santos, R. M. *et al.* Widespread synchronous Ca oscillations due to bursting electrical activity in single pancreatic islets. *Pflug. Arch. Eur. J. Phy.* **418**, 417–422 (1991).

11. Rutter, G. A. & Hodson, D. J. Minireview: Intraislet Regulation of Insulin Secretion in Humans. *Mol. Endocrinol.* **27**, 1984–1995 (2013).
12. Benninger, R. K. P. & Piston, D. W. Cellular communication and heterogeneity in pancreatic islet insulin secretion dynamics. *Trends Endocrin. Met.* **25**, 399–406 (2014).
13. Benninger, R. K. P., Zhang, M., Head, W. S., Satin, L. S. & Piston, D. W. Gap junction coupling and calcium waves in the pancreatic islet. *Biophys. J.* **95**, 5048–5061 (2008).
14. Liu, Y.-J., Tengholm, A., Grapengiesser, E., Hellman, B. & Gylfe, E. Origin of slow and fast oscillations of Ca^{2+} in mouse pancreatic islets. *J. Physiol.* **508**, 471–481 (1998).
15. Nadal, A., Quesada, I. & Soria, B. Homologous and heterologous asynchronicity between identified α-, β- and δ-cells within intact islets of Langerhans in the mouse. *J. Physiol.* **517**, 85–93 (1999).
16. Stožer, A., Dolenšek, J. & Rupnik, M. S. Glucose-stimulated calcium dynamics in islets of Langerhans in acute mouse pancreas tissue slices. *PloS ONE* **8**, e54638 (2013).
17. Low, J. *et al.* Glucose principally regulates insulin secretion in mouse islets by controlling the numbers of granule fusion events per cell. *Diabetologia* **56**, 2629–2637 (2013).
18. Takahashi, N., Kishimoto, T., Nemoto, T., Kadowaki, T. & Kasai, H. Fusion Pore Dynamics and Insulin Granule Exocytosis in the Pancreatic Islet. *Science* **297**, 1349–1352 (2002).
19. Pipeleers, D., Kiekens, R., Ling, Z., Wilikens, A. & Schuit, F. Physiologic relevance of heterogeneity in the pancreatic beta-cell population. *Diabetologia* **37**, S57–S64 (1994).
20. Heimberg, H. *et al.* Heterogeneity in Glucose Sensitivity among Pancreatic Beta-Cells Is Correlated to Differences in Glucose Phosphorylation Rather Than Glucose-Transport. *Embo. J.* **12**, 2873–2879 (1993).
21. Bennett, B. D., Jetton, T. L., Ying, G., Magnuson, M. A. & Piston, D. W. Quantitative Subcellular Imaging of Glucose Metabolism within Intact Pancreatic Islets. *J. Biol. Chem.* **271**, 3647–3651 (1996).
22. Van Schravendijk, C. F., Kiekens, R. & Pipeleers, D. G. Pancreatic beta cell heterogeneity in glucose-induced insulin secretion. *J. Biol. Chem.* **267**, 21344–21352 (1992).
23. Jonkers, F. C. & Henquin, J.-C. Measurements of Cytoplasmic Ca^{2+} in Islet Cell Clusters Show That Glucose Rapidly Recruits β-Cells and Gradually Increases the Individual Cell Response. *Diabetes* **50**, 540–550 (2001).
24. Hodson, D. J. *et al.* Lipotoxicity disrupts incretin-regulated human β cell connectivity. *J. Clin. Invest.* **123**, 4182–4194 (2013).
25. Ravier, M. A. *et al.* Loss of connexin36 channels alters beta-cell coupling, islet synchronization of glucoseinduced Ca^{2+} and insulin oscillations, and basal insulin release. *Diabetes* **54**, 1798–1807 (2005).
26. Speier, S., Gjinovci, A., Charollais, A., Meda, P. & Rupnik, M. Cx36-Mediated Coupling Reduces β-Cell Heterogeneity, Confines the Stimulating Glucose Concentration Range, and Affects Insulin Release Kinetics. *Diabetes* **56**, 1078–1086 (2007).
27. Halban, P. A. *et al.* The Possible Importance of Contact between Pancreatic-Islet Cells for the Control of Insulin Release. *Endocrinology* **111**, 86–94 (1982).
28. Bavamian, S. *et al.* Islet-cell-to-cell communication as basis for normal insulin secretion. *Diabetes Obes. Metab.* **9**, 118–132 (2007).
29. Do, O. H., Low, J. T., Gaisano, H. Y. & Thorn, P. The secretory deficit in islets from db/db mice is mainly due to a loss of responding beta cells. *Diabetologia* **57**, 1400–9 (2014).
30. Head, W. S. *et al.* Connexin-36 gap junctions regulate in vivo first- and second-phase insulin secretion dynamics and glucose tolerance in the conscious mouse. *Diabetes* **61**, 1700–1707 (2012).
31. Barabási, A. L. The network takeover. *Nat. Phys.* **8**, 14 (2011).
32. Barabási, A. L. & Oltvai, Z. N. Network biology: understanding the cell's functional organization. *Nat. Rev. Genet.* **5**, 101–111 (2004).
33. Green, D. G. & Sadedin, S. Interactions matter—complexity in landscapes and ecosystems. *Ecol. Complex.* **2**, 117–130 (2005).
34. Bullmore, E. & Sporns, O. Complex brain networks: graph theoretical analysis of structural and functional systems. *Nat. Rev. Neurosci.* **10**, 186–198 (2009).
35. Rubinov, M. & Sporns, O. Complex network measures of brain connectivity: uses and interpretations. *NeuroImage* **52**, 1059–1069 (2010).
36. Belmonte, M. K. *et al.* Autism and abnormal development of brain connectivity. *J. Neurosci.* **24**, 9228–9231 (2004).
37. Liu, Y. *et al.* Disrupted small-world networks in schizophrenia. *Brain* **131**, 945–961 (2008).
38. He, Y. *et al.* Impaired small-world efficiency in structural cortical networks in multiple sclerosis associated with white matter lesion load. *Brain* **132**, 3366–3379 (2009).
39. Kitzbichler, M. G., Henson, R. N. A., Smith, M. L., Nathan, P. J. & Bullmore, E. T. Cognitive effort drives workspace configuration of human brain functional networks. *J. Neurosci.* **31**, 8259–8270 (2011).
40. Nicol, R. M. *et al.* Fast reconfiguration of high frequency brain networks in response to surprising changes in auditory input. *J. Neurophysiol.* **107**, 1421–1430 (2012).
41. Bassett, D. S. *et al.* Dynamic reconfiguration of human brain networks during learning. *Proc. Natl. Acad. Sci. U S A* **108**, 7641–7646 (2011).
42. Wang, L. *et al.* Dynamic functional reorganization of the motor execution network after stroke. *Brain* **133**, 1224–38 (2010).
43. Hodson, D. J., Molino, F., Fontanaud, P., Bonnefont, X. & Mollard, P. Investigating and Modelling Pituitary Endocrine Network Function. *J. Neuroendocrinol.* **22**, 1217–1225 (2010).
44. Hodson, D. J. *et al.* Coordination of calcium signals by pituitary endocrine cells in situ. *Cell Calcium.* **51**, 222–230 (2012).
45. Hodson, D. J. *et al.* Existence of long-lasting experience-dependent plasticity in endocrine cell networks. *Nat. Commun.* **3**, 605 (2012).
46. Stožer, A. *et al.* Functional Connectivity in Islets of Langerhans from Mouse Pancreas Tissue Slices. *PLoS Comput. Biol.* **9**, e1002923 (2013).
47. Pires, M. *et al.* Modeling the functional network of primary intercellular Ca^{2+} wave Propagation in astrocytes and its application to study drug effects. *J. Theor. Biol.* **356**, 201–212 (2014).
48. Bertram, R., Sherman, A. & Satin, L. S. Metabolic and electrical oscillations: partners in controlling pulsatile insulin secretion. *Am. J. Physiol. Endocrinol. Metab.* **293**, E890–E900 (2007).
49. Boccaletti, S., Latora, V., Moreno, Y., Chavez, M. & Hwang, D. U. Complex networks: Structure and dynamics. *Phys. Rep.* **424**, 175–308 (2006).
50. Benninger, R. K. P., Head, W. S., Zhang, M., Satin, L. S. & Piston, D. W. Gap junctions and other mechanisms of cell–cell communication regulate basal insulin secretion in the pancreatic islet. *J. Physiol.* **22**, 5453–5466 (2011).
51. Buchwald, P. A local glucose-and oxygen concentration-based insulin secretion model for pancreatic islets. *Theor. Biol. Med. Model* **8**, 20 (2011).
52. Kiekens, R. *et al.* Differences in glucose recognition by individual rat pancreatic β-cells are associated with intercellular differences in glucose-induced biosynthetic activity. *J. Clin. Invest.* **89**, 117–25 (1992).
53. Schuit, F. C., In't Veld, P. A. & Pipeleers, D. G. Glucose stimulates proinsulin biosynthesis by a dose-dependent recruitment of pancreatic beta cells. *Proc. Natl. Acad. Sci. U S A* **85**, 3865–9 (1988).
54. Bensellam, M., Laybutt, D. R. & Jonas, J. C. The molecular mechanisms of pancreatic β-cell glucotoxicity: recent findings and future research directions. *Mol. Cell Endocrinol.* **364**, 1–27 (2012).
55. Deltour, L. *et al.* Polyclonal origin of pancreatic islets in aggregation mouse chimaeras. *Development* **112**, 1115–1121 (1991).
56. Scharfmann, R., Xiao, X., Heimberg, H., Mallet, J. & Ravassard, P. Beta Cells within Single Human Islets Originate from Multiple Progenitors. *PLoS ONE* **3**, e3559 (2008)
57. Russo, R., Herrmann, H. J. & de Arcangelis, L. Brain modularity controls the critical behavior of spontaneous activity. *Sci. Rep.* **4**, 4312 (2014).
58. Just, M. A., Cherkassky, V. L., Keller, T. A., Kana, R. K. & Minshew, N. J. Functional and Anatomical Cortical Underconnectivity in Autism: Evidence from an fMRI Study of an Executive Function Task and Corpus Callosum Morphometry. *Cereb. Cortex.* **12**, 951–961 (2007).
59. Huang, N. E. *et al.* The empirical mode decomposition and the Hilbert spectrum for nonlinear and non-stationary time series analysis. *Proc. Roy. Soc. Lond. A Mat.* **454**, 903–995 (1998).
60. Torres, M. E., Colominas, M. A., Schlotthauer, G. & Flandrin, P. A complete ensemble empirical mode decomposition with adaptive noise. Paper presented at Acoustics, Speech and Signal Processing (ICASSP): 2011 IEEE International Conference on, (Czech Republic) Prague (2011, May 22–27). doi: 10.1109/ICASSP.2011.5947265.
61. Watts, D. J. & Strogatz, S. H. Collective dynamics of 'small-world' networks. *Nature* **393**, 440–442 (1998).
62. Blondel, V. D., Guillaume, J.-L., Lambiotte, R. & Lefebvre, E. Fast unfolding of communities in large networks. *J. Stat. Mech.* **2008**, P10008 (2008).
63. Girvan, M. & Newman, M. E. Community structure in social and biological networks. *Proc. Natl. Acad. Sci. U S A* **99**, 7821–7826 (2002).
64. Newman, M. E. J. Finding community structure in networks using the eigenvectors of matrices. *Phys. Rev. E* **74**, 036104 (2006).
65. Hraha *et al.* Phase transition in the multi-cellular regulatory behavior of pancreatic islet excitability. *PLoS Comput. Biol.* **10**, e1003819 (2014).

Acknowledgments

This work was produced within the framework of the operation entitled Centre of Open Innovation and Research UM. The operation is co-funded by the European Regional Development Fund and conducted within the framework of the Operational Programme for Strengthening Regional Development Potentials for the period 2007–2013, Development priority 1: Competitiveness of companies and research excellence, Priority axis 1.1: Encouraging competitive potential of enterprises and research excellence.

Author contributions

A.S., J.D. and M.S.R. conceived and designed the experiments. A.S. and J.D. performed the experiments. R.M., M.G. and M.M. designed analysis tools and performed the calculations. R.M., A.S. and M.G. wrote the main manuscript text and prepared the figures. All authors reviewed the manuscript.

Additional information

Supplementary information accompanies this paper at http://www.nature.com/scientificreports

Competing financial interests: The authors declare no competing financial interests.

How to cite this article: Markovič, R. *et al*. Progressive glucose stimulation of islet beta cells reveals a transition from segregated to integrated modular functional connectivity patterns. *Sci. Rep.* **5**, 7845; DOI:10.1038/srep07845 (2015).

Delovni življenjepis

Osebni podatki:	Rene Markovič Rojen: 22. 6. 1985 Stanujoč: Prežihova Ulica 2A, 2331 Pragersko
Izobraževanje:	1992- 2000: OŠ Tabor II, Maribor 2000-2004: Elektrotehnik-elektronik, Srednja elektro-računalniška šola, Maribor 2004-2005: Maturitetni tečaj, Srednja elektro-računalniška šola, Maribor 2005-2011: Univerzitetni študij – smer enopredmetna fizika, Oddelek za fiziko, Pedagoška fakulteta, Univerza v Mariboru; pridobljen naziv: profesor fizike. 2011: vpis na doktorski študij.
Habilitacija	2012: Prva izvolitev v naziv »asistent za fiziko«.
Zaposlitev:	2011-: mladi raziskovalec, Fakulteta za naravoslovje in matematiko, Univerza v Mariboru.
Raziskovalno področje:	Nelinearni dinamični sistemi, kompleksni sistemi, kompleksne mreže, sinhronizacija kolektivne dinamike, funkcionalne mreže.

UNIVERZA V MARIBORU

FAKULTETA ZA NARAVOSLOVJE IN MATEMATIKO

IZJAVA DOKTORSKEGA KANDIDATA

Podpisani Rene Markovič, vpisna številka N3000508

izjavljam,

da je doktorska disertacija z naslovom

VPLIV TOPOLOŠKIH LASTNOSTI KOMPLEKSNIH MREŽ IN DINAMIČNIH LASTNOSTI SKLOPLJENIH CELIČNIH OSCILATORJEV NA KOLEKTIVNO DINAMIKO

- rezultat lastnega raziskovalnega dela,
- da predložena disertacija v celoti ali v delih ni bila predložena za pridobitev kakršnekoli izobrazbe po študijskem programu druge fakultete ali univerze,
- da so rezultati korektno navedeni in
- da nisem kršil avtorskih pravic in intelektualne lastnine drugih.

Podpis doktorskega kandidata:

_____